Twenty-fifth
Engineering Mechanics
Symposium

Twenty-fifth Engineering Mechanics Symposium

October 25 - October 26, 2022
Hotel Papendal, Arnhem

Contents

Preface

The Graduate School on Engineering Mechanics, a joint initiative of the Eindhoven and Delft Universities of Technology, University of Twente and the University of Groningen, organizes on an annual basis the Engineering Mechanics Symposium. The aim of this symposium is to stimulate the communication and exchange of information pertaining to recent developments and ongoing research in the field of Engineering Mechanics. To achieve this, the program presents the Koiter lecture by a leading expert in the field of Engineering Mechanics, and topical sessions in relation to selected research programs of the research school.

The Twenty-fifth Engineering Mechanics Symposium takes place October 25 - October 26, 2022 at Hotel Papendal in Arnhem. In the opening session, Prof. M. Ortiz will present a Koiter lecture entitled:
"Model-Free Data-Driven Computing"

Furthermore, four workshops are organized that partly run plenary and partly run in parallel.
Topics of this year's workshops are:

Trends and challenges in "Machine learning"
Organized by dr.ir. Iuri Rocha (TUD, main organizer), dr.ir. Michael Abedlmalik (TU/e), dr. Hongyang Cheng (UT),
dr. Francesca Maresca (RUG)
Trends and challenges in "Molecular and particle-based mechanics"
Organized by dr. Andrea Giuntoli (RUG, main organizer), dr. Igor Ostanin (UT), dr.ing. Saullo Castro (TUD),
dr. Azahara Luna Triguero
Trends and challenges in "Additive manufacturing"
Organized by dr.ir. Hans van Dommelen (TU/e, main organizer), dr. Can Ayas (TUD), dr.ir. Ton Bor (UT)
Trends and challenges in "Material and structural health monitoring"
Organized by dr.ir. Richard Loendersloot (UT), dr. Eliz-Mari Lourens (TUD), dr.ir. Johan Hoefnagels (TU/e)

The workshop organizers provide plenary introductions on the trends and challenges of the workshops. Two of those plenary introductions have been included in the morning program on the first symposium day, whereas the other two have been included in the morning program of the second symposium day. Next, two of the actual workshops have been scheduled to run in parallel on the first symposium day, whereas the other two have been scheduled to run in parallel on the second symposium day. Each workshop consists of two parts, separated by a break. Each part consists of 2 presentations by AIOs/postdocs. The duration of each of the AIO/postdoc presentations is 20 minutes and followed by 10 minutes of discussion.

For the best AIO-presentation within each workshop a prize will be awarded. Winners will be announced directly before the closing of the symposium on Wednesday, October 26, 2022.

Additionally, there are two poster discussion sessions in which PhD-students and postdocs participating in the Graduate School on Engineering Mechanics present their current research project. In relation to these presentations a contest is organized in which a jury selects the best four contributions.

This year's members of the jury are: dr.ir. O. Rokos (TU/e), prof.dr. Maryam GhandchiTehrani (RUG),
dr.ir. Jurnan Schilder (UT), dr.ir. Frits de Prenter (TUD).

Winners will be announced directly before the closing of the symposium on Wednesday, October 26, 2022.
On Wednesday, October 26 a meeting of the senior academic staff participating in Engineering Mechanics takes place.

This report contains more detailed information on the Twenty-fifh Engineering Mechanics Symposium. Included are the following sections:
- **Section 1:** Detailed program of the symposium
- **Section 2:** Abstracts of the koiter lecture and introduction to the workshops
- **Section 3:** Abstracts of presentations in the workshops and a short introduction of the presenters
- **Section 4:** Survey of poster presentations

1

PROGRAM

Tuesday, 25 October 2022		
10.00-10.30	Registration and Informal get-together	Foyer 3
10.30-12.40	Opening Session	Room 8-9
10.30-10.40	Opening of the Symposium by prof.dr.ir. Harald van Brummelen	
10.40-11.40	Koiter lecture by Prof. Michael Ortiz	
11.40-12.10	Trends and challenges in "Machine learning" by dr.ir. Iuri Rocha (TUD)	
12.10-12.40	Trends and challenges in "Molecular and particle-based mechanics" by dr.ir. Andrea Giuntoli (RUG)	
12.45-13.45	Lunch	Sydney Room
13.50-14.50	Workshops 1 and 2, part A	

Workshop 1: Room 4-5 Machine learning	Workshop 2: Room 8-9 Molecular and particle-based mechanics
13.50-14.10 Bas Kessels (TU/e) *Parameter Updating in Nonlinear Dynamics Models using Machine Learning-Based Inverse Mappings*	**13.50-14.10 Juan E. Alvarez (UT)** *Multi-scale thermo-viscoelastic modelling of powder-based processes*
14.20-14.40 Retief Lubbe (UT) *Bayesian inference of granular mesostructures: the identifiability and interplay with grain properties*	**14.20-14.40 Leon Thijs (TU/e)** *Investigation of single iron paricle combustion in the Knudsen transition regime*

14.50-15.50	**Poster Discussion Session I:** Room 6-7 Presentation of current research projects, carried out by PhD students and Postdocs participating in Engineering Mechanics	
15.50-16.20	Break	Foyer 3
16.20-17.20	Workshops 1 and 2, part B	

Workshop 1, cont'd Room 4-5 Machine learning	Workshop 2, cont'd: Room 8-9 Molecular and particle-based mechanics
16.20-16.40 Lei Zhang (RUG) *Atomistic fracture in bcc iron revealed by active training of machine learning potential*	**16.20-16.40 Sam van Elsloo (TUD)** *Application of the Immersed Interface Method to the Lattice Boltzmann Method*
16.50-17.10 Prakash Thakolkaran (TUD) *Learning hyperelasticity without stress data*	**16.50-17.10 Varun Shah (RUG)** *Unravelling the atomic scale interaction of H with dislocations in iron*

17.30-18.30	**Poster Discussion Session II:** Room 6-7 Presentation of current research projects, carried out by PhD students and Postdocs participating in Engineering Mechanics	
18.30-19.00	Informal reception	Sydney Room
19.00-22.00	Dinner	Sydney Room
22.00-24.00	Bar	Dug Out

Wednesday, 26 October 2022		

08.45-9.45	**Plenary Session**	**Room 8-9**

08.45-09.15	Trends and challenges in "Additive manufacturing" by Dr. ir. Hans van Dommelen (TUe)
09.15-09.45	Trends and challenges in "Material and structural health monitoring" by Dr.ir. Richard Loendersloot (UT)

09.45-10.45	**Workshops 3 and 4, part A**

Workshop 3: Room 6-7 Additive manufacturing	**Workshop 4:** Room 8-9 Material and structural health monitoring:
09.45-10.05 Mohammad Sattari (UT) *Thermo-Fluidic Behavior To Solidification Microstructure Texture Evolution During Laser-assisted Powder-based Direct Energy Deposition – An Integrated Approach*	**09.45-10.05 Arno Huijer (TUD)** *Monitoring of dynamic loads and acoustic emissions in composite marine propellers using embedded piezoelectric sensors*
10.15-10.35 Luca Palmeira Belotti (TU/e) *On the anisotropy of wire arc additively manufactured parts*	**10.15-10.35 Tijmen Vermeij (TU/e)** *Unraveling plasticity and damage in multi-phase steels through dedicated integrated "2D" experimental-numerical testing*

10.45 -11.15	**Break**	**Foyer 3**

11.15-12.15	**Workshops 3 and 4, part B**

Workshop3, cont'd: Room 6-7 Additive manufacturing	Workshop 4, cont'd: Room 8-9 Material and structural health monitoring
11.15-11.35 Vibhas Mishra (TUD) *Computational Design for Wire Arc Additive Manufacturing*	**11.15-11.35 Natáli Marinho (UT)** *Dynamic-based impact identifaction method for composite structures*
11.45-12.05 Zhaohang Zhang (RUG) *Additive Manufacturing of Metamaterials*	**11.45-12.05 Aleks Vrcek (UT-ET)** *Newly developed Cam-Roller follower Tester (CRT) with self-aligning mechanism in a line contact configuration and ways of simulating, detecting, and measuring surface initiated RCF cracks*

12.20- 12.50	**Biezeno lecture**	**Room 8-9**

12.50-13.15	- **Announcement of winning contributions in the AIO/Postdoc Presentation contest and in the Poster contest** - **Closure**

13.15-14.00	**Lunch**	**Sydney Room**

14.00-15.00	**Assembly of Project Leaders EM**	**Room 6-7**

16.00-20.00	Meeting of EM Advisory Board

2

KOITER LECTURE

The Koiter lecture at the Twenty-fifth Engineering Mechanics symposium will be given by:

Michael Ortiz

Previous distinguished keynote speakers at the Engineering Mechanics symposia were:

2021 Katia Bertoldi
2020 Ellen Kuhl
2019 Marco Amabili
2018 William Curtin
2017 Zhigang Suo
2016 Kurt Maute
2015 Stefanie Reese
2014 Anja Boisen
2013 Wolfgang Wall
2012 Roger Owen
2011 Oded Gottlieb
2010 Herbert Mang
2009 Charbel Farhat
2008 Gerhard Holzapfel
2007 Bernard Schrefler
2006 Alan Needleman
2005 Peter Wriggers
2004 Alan Grodzinsky
2003 Ole Sigmund
2002 Norman Fleck
2001 Edwin Kreuzer
2000 Ekkehard Ramm
1999 John Hutchinson
1998 Pieter Zandbergen,
Werner Schiehlen

Koiter Lecture

Model-Free Data-Driven Computing

Prof. Michael Ortiz

California Institute of Technology

I will present a model-free Data-Driven computing framework for multiscale analysis of inelastic materials. The aim of the framework is to enable predictions of structural response directly from material data, without the intermediate step of modeling the data by means of constitutive relations. A distinguishing aspect of the formulation is that it is internal-variable free, i.e., it does not require the identification of actual or ad hoc (learned) internal variables. Instead, the inelastic macroscopic response and its evolution are characterized by defining a dissipation connection in macroscopic phase space. We show how the phase field can be sampled, and the dissipation connection identified, directly from micromechanical calculations on representative-volume elements (RVEs). The data is reusable over a broad range of boundary-value problems and loading conditions involving the same material. Solutions to specific boundary-value problems are obtained by minimizing a distance from the material sample to the set of equilibrium and compatible states and, in a time-discrete setting, by simultaneously minimizing the incremental dissipation. We demonstrate the framework by means of an application concerned with the prediction of the behavior of sand, a prototypical complex historydependent material.

3

INTRODUCTION TO THE WORKSHOPS

Workshop 1
Trends and Challenges in
"Machine Learning"

<u>Iuri Rocha</u>[1], Michael Abdelmalik[2], Hongyang Cheng[3], Francesco Maresca[4]

[1]Delft University of Technology, Faculty of Civil Engineering and Geosciences
[2]Eindhoven University of Technology, Department of Mechanical Engineering
[3]University of Twente, Faculty of Engineering Technology
[4]University of Groningen, Faculty of Science and Engineering

Machine learning is permeating virtually every field of research at an unprecedented pace, and engineering mechanics is of course no exception. Challenges we have been tackling with traditional tools — *e.g.* accelerating expensive multiscale/multiphysics simulations, solving inverse problems for model calibration, assimilating experimental data, optimizing material design and performance — can now be approached from the perspective of machine learning and its impressive toolbox of models. At the same time, advanced machine learning systems are often portrayed in the news and popular culture as quasi-sentient entities of mystical, mysterious and sometimes insidious nature. Are these models as inscrutable and unpredictable as they sometimes seem? Can we safely let go of some of our trusted physics knowledge in exchange for speed and flexibility?

In this workshop, we take you on a journey across the vast landscape of machine learning techniques used to construct new solutions to engineering mechanics problems. We start in true EM spirit by placing a complicated deep learning model under the microscope, observing its internal structure across the scales, and discussing the blessing and the curse of working with models of virtually unlimited flexibility. We illustrate the classic tradeoff between bias and variance when constructing machine learning models and explore several strategies to build trustworthy models with an optimum balance between physics and data. Our speakers will showcase a number of exciting research avenues currently being explored by the EM community at the interface between machine learning and engineering mechanics, including experimental and numerical challenges at multiple spatial and time scales.

Workshop 2
Trends and Challenges in
"Molecular and Particle-based Mechanics"

Andrea Giuntoli[1], Igor Ostanin[2], Saullo Castro[3], Francesco Maresca[4]

[1] University of Groningen, in the micromechanics unit of the Zernike Institute for Advanced Materials, [2] University of Twente, [3] Delft University of Technology, [4]Eindhoven University of Technology

Particle-based simulations constitute a powerful alternative to continuum methods like FEM to investigate the mechanics of complex materials. The key to these methods is the choice of what the 'particle' is, and what are the physical laws that govern the interaction among particles. From single hydrogen atoms to grains of sand or larger, the extreme flexibility in the nature of the particle allows this class of models to investigate almost ten decades of spatiotemporal scales. From all-atom molecular dynamics simulations to macroscale discrete elements methods, particle-based algorithms excel at accurately investigating phenomena at a scale of 2-3 orders of magnitude larger than the size of their discrete constituents, easily incorporating structural heterogeneity.

The main drawbacks of particle-based methods are usually the high computational cost and the limitations in size and timescale that can be simulated, which are limited by the fastest timescales of the system. The incorporation of elements of very different sizes is then not efficient, nor is the investigation of multiscale phenomena like fracture, where emergent phenomena are of critical importance and the macroscale mechanics behavior is not easily predicted by the nano- or micro-scale particle interactions.

To overcome these limitations one can (i) develop multiscale simulation frameworks where particles of different resolutions are seamlessly coupled together, efficiently simulating multiple scales, and (ii) establish general and accurate coarse-graining techniques to extract and move information across models of increasing size, with the goal of capturing the key microscopic properties that are predictive of the macroscale material mechanics.

In this talk, we will discuss the current trends and challenges in particle-based mechanics simulations across the scales, with a focus on emerging strategies to tackle multiscale problems and ongoing efforts by the research community in the Netherlands and abroad.

UNIVERSITY OF TWENTE.   TUDelft Delft University of Technology   university of groningen   TU/e EINDHOVEN UNIVERSITY OF TECHNOLOGY

Workshop 3
Trends and Challenges in
"Additive Manufacturing"

Hans van Dommelen[1], Can Ayas[2], Ton Bor[3]

[1]*Eindhoven University of Technology, Department of Mechanical Engineering*
[2]*Delft University of Technology, Faculty of Mechanical, Maritime and Materials Engineering*
[3]*University of Twente, Department of Mechanics of Solids, Surfaces & Systems*

Whereas many classical manufacturing methods are based on deforming or removing material, such as rolling or milling, additive manufacturing is based on repeatedly adding material to a build to obtain the near net shape layer-by-layer in an automated manner. Many different additive manufacturing methods have been developed, including stereolithography, powder bed fusion, and deposition methods, each with their own advantages and challenges for a wide range of materials, including polymers, metals, ceramics, concrete and even food. These new production methods enable realisation of geometrically complex product geometries. For example, complex designs with internal cavities and structures, such as in metamaterials, or intricate designs obtained with topology optimization methods can be manufactured, increasing design freedom. Also, these techniques allow for small series production, part integration and customization of individual products.

Initial research focused on the technological development of additive manufacturing equipment, but this technology has now reached the stage where more fundamental research will lead to further advancements, and this creates many opportunities for cool new science that can impact the industry. This research covers the entire path from the additive production process, modelling of the process, the specific microstructures created by this process, the resulting material properties and performance, and design based on these properties and process constraints. All these aspects are covered by the research within the Engineering Mechanics graduate school, such as in the various projects of the AiM2XL programme that focuses on direct energy deposition methods for manufacturing large components. In this workshop, current research and future challenges in research on additive manufacturing will be presented.

Workshop 4
Trends and Challenges in
"Material & Structural Health Monitoring"

Richard Loendersloot[1], Eliz-Mari Lourens[2], Johan Hoefnagels[3]

[1] University of Twente, Faculty of Engineering Technology
[2] Delft University of Technology, Department of Mechanical Engineering
[3] Eindhoven University of Technology, Department of Mechanical Engineering

Mechanical Engineering is the discipline that can be referred to as the art to get things to work. The discipline stretches multiple length scales, from tuning, describing and controlling the microstructure of materials to optimize their performance in macro scale structures to describing and modelling the behaviour of large scale structures. The Mechanical Engineer as the ultimate enabler, turning laws of physic into working systems and machines, who's creations engineers are nested deeply in the pores of the industrial society; Astonishing accomplishments.

Yet, the story does not end with "creation of", but continues into the operational life of the structure or system that is created. Objects are subjected to a variety of loads – mechanical, electrical, chemical, and so on – affecting their performance, affecting their functionality. Again it is the engineer's fundamental knowledge that can answer the questions to get a better grip on the damage, degradation and wear of structures over time. Understanding material behaviour and the interaction between materials reveals on the one hand the ways in which structures can fail, while on the other hand understanding of the way structural deterioration affects the mechanical, in particular dynamic behaviour of the structure provides the tools for state monitoring. Although this principle is already applied to a large variety of applications, the creation of more complex, more sophisticated and larger structures and the urge for sustainable use of materials and resources keeps driving the research in this field of material and structural health monitoring.

The tango material and structural health monitoring dance is one of a mutual understanding of dependency. Certainly, a flirt with data science enriches the relation; artificial intelligence, machine learning, Industry 4.0, IIoT – to just name a few of the dance partners – can nor should be ignored in particular due to the developments in these areas over the past years, but the Mechanical Engineering will always find a foundation in the physical laws allowing to formulate not just an observation, but also an explanation thereof.

All four presenters, each from their own perspective, work in this broad field between material and structural health monitoring. The connection is found in the changing state of the material during and due to usage: what happens, why and how does it happen, how can it be monitored? Doing so, they contribute to the entanglement of Mechanical Engineering beyond the design and realisation, into the operational phase, thus further shaping the world of tomorrow.

4

INTRODUCTION PRESENTERS

AND

ABSTRACTS OF PRESENTATIONS

Workshop 1

"Machine learning"

Parameter Updating in Nonlinear Dynamics Models using Machine Learning-Based Inverse Mappings

B.M. Kessels, R.H.B. Fey, N. van de Wouw

Eindhoven University of Technology, Department of Mechanical Engineering,
Dynamics and Control, P.O. Box 513, 5600MB Eindhoven
phone +31-402474817, e-mail b.m.kessels@tue.nl

Introduction

A digital twin of a (controlled) physical system allows engineers to efficiently optimize the design of the physical system and both optimize its performance and monitor its health in real-time. Since a model (i.e., a digital twin) is typically not an exact representation of a measured physical system, the digital twin cannot be exploited to its full potential. Therefore, model (parameter) updating is employed such that the mismatch between the model and the measured system is minimized. To make model parameter updating generally applicable in an online, digital twin context, the updating method should be: 1) computationally fast, 2) applicable to nonlinear models, and 3) physically interpretable.

Methodology

In this presentation, we propose to use Inverse Mapping Models (IMMs), based on Artificial Neural Networks (ANNs) or Gaussian Processes (GPs), to update parameter values of a first-principles model of a nonlinear dynamic system with a fixed model structure. This methodology is referred to by the authors as the Inverse Mapping Parameter Updating (IMPU) method.

In an online setting, an IMM rapidly maps a set of time-domain output features, extracted from data measured at a physical system, to a set of physically interpretable parameter values of the first-principles (or forward) model. This is enabled by training the IMM offline using simulated data consisting of various sets of parameter values and their corresponding output features. Parameterizing the first-principles model with the inferred (or updated) parameter values results in an updated model that, when used in a simulation, yields a set of output features close in similarity to the original, measured features. Additionally, in contrast to ANNs, the use of GPs as IMMs also enables uncertainty quantification of the inferred parameter values.

Application

To illustrate the capability of these IMM types to update parameter values with high computational efficiency (and, in the case of GPs, to extract corresponding uncertainty measures), the proposed methodology is applied to a (simulated) nonlinear multibody model. To mimic a physical experiment, noisy data is used in both the offline and online phase. In this application, it is shown that the IMPU method enables fast estimation of parameter values with high accuracy.

Abstract title: Parameter Updating in Nonlinear Dynamics Models using Machine Learning-Based Inverse Mappings

Workshop: Machine Learning

Kessels, B.M. (Bas)

Eindhoven University of Technology, Department of Mechanical Engineering, Dynamics & Control

Advisor: Prof.dr.ir. N. (Nathan) van de Wouw
Co-advisor: Dr.ir. R.H.B. (Rob) Fey

Portrait photo by Angeline Swinkels

Biography and description of research:
Bas Kessels (1996) obtained his BSc-degree (with great appreciation) and MSc-degree (with honours) in Mechanical Engineering from the Eindhoven University of Technology (TU/e), Eindhoven, the Netherlands, in 2017 and 2020, respectively. In 2018, he did an internship at the Leibniz Universität in Hannover, Germany. Here, Kessels researched model reduction for models describing dynamic buckling of composite panels. Subsequently, he wrote his master's thesis in cooperation with the company ASML about an alternative, more efficient model order reduction method for models consisting of multiple components by using frequency-based substructuring techniques. Since 2020, Kessels works as a doctoral candidate at the TU/e where he focuses on the autonomous model updating of mechanical systems in (near) real-time within a Digital Twin context. His current research interests are structural dynamics, (combined) model parameter and structure updating, machine learning techniques, and flexible multibody dynamics.

Bayesian inference of granular mesostructures: the identifiability and interplay with grain properties

UNIVERSITY OF TWENTE.

R. Lubbe

Chair of Soil MicroMechanics, Department of Civil Engineering, Faculty of Engineering Technology, P.O. Box 217, e-mail r.lubbe@utwente.nl

Abstract

Granular materials exhibit scale-dependent properties. The interplay between the structure of a representative volume element (or mesostructure) and the particle properties determine the macroscopic response of granular materials. The discrete element method (DEM) predicts complex macroscopic constitutive behavior from interparticle contacts and the mesostructure evolution. The identification of contact parameters is often treated as an inverse problem. However, uncertainties on the mesostructure are rarely considered, due to the high computational cost. We use Sequential Monte Carlo (SMC) filtering to quantify uncertainties on the contact parameters and mesostructure and train machine learning models to effectively learn and sample from contact-mesostructure correlations.

In this talk, we revisit the multi-level Bayesian calibration approach that is used to identify DEM parameters [1]. We class the inference algorithm into two processes namely the filtering phase and the sampling phase. At the core of the filtering phase is the iterative Sequential Monte Carlo (SMC) which learns a proposal distribution by minimizing the associate uncertainty. Compared to conventional SMC, where random perturbations are used to evolve a system in time, a sampling phase is employed, moving from a discrete distribution (of simulated data) to a continuous distribution (of parameters), by training a Gaussian Mixture Model (GMM). Next, we show how the Bayesian calibration algorithm is used to extend the parameter identification problem to also include the particle size distribution (PSD) and solid volume fraction as parameters [2]. The result is a set of multi-mode distributions of contact and mesostructure parameters which are iteratively approximated and sampled until convergence. The Bayesian calibration process of the mesostructure is studied using a synthesized triaxial response as the ground truth. Satisfactory macro responses are achieved for dense and loose samples, but due to the interdependence between parameters, dense samples are more prone to converge to local minima. Finally, my current research involves granular systems moving from solid to fluid and back. An overview will be given on how Bayesian statistics will be used to quantify the uncertainty between various continuum methods.

References

[1] Cheng, Hongyang, et al. "An iterative Bayesian filtering framework for fast and automated calibration of DEM models." *Computer methods in applied mechanics and engineering* 350 (2019): 268-294.
[2] Lubbe, Retief, et al. "Bayesian Calibration of GPU–based DEM meso-mechanics Part II: Calibration of the granular meso-structure." *Powder Technology* 407 (2022): 117666.

Abstract title: Bayesian inference of granular mesostructures: the identifiability and interplay with grain properties.

Workshop: Machine Learning

Name: Retief Lubbe

Affiliation: Department of Civil Engineering, Faculty of Engineering Technology, University of Twente

Advisors: Prof.dr. Vanessa Magnanimo, Prof dr. Stefan Luding
Co-advisor: Dr. Hongyang Cheng

Biography and description of research:

Retief Lubbe was born in Pretoria, South Africa in 1992. After finishing High School, he worked at the Earth Observation department of the Council for Scientific and Industrial Research (CSIR). He received his bachelor's in physics at the University of South Africa (UNISA), and an honour's in Physics at the University of Pretoria (UP) in 2019. During his studies at UP he developed high performance spatial partitioning algorithms for GPU Discrete Element Method (DEM). He later moved to Beijing, China and graduated from Tsinghua University in 2021 with a master's degree in Geotechnical Engineering. During his master's he worked on applying GPU DEM at a representative volume element (RVE) for high performance multi-scale analysis and calibration of geomaterials.

Currently, Retief Lubbe is pursuing his doctoral degree at the University of Twente. His main research is about developing an industrial scale continuum solver to model the fluid-solid transition of granular materials. His PhD is part of the TUSAIL (Training in Upscaling particle Systems: Advancing Industry across Length-scale) ITN funded by Marie Sklodowska-Curie Actions Horizon 2020.

Atomistic fracture in bcc iron revealed by active training of machine learning potential

L. Zhang

University of Groningen, Faculty of Science and Engineering,
Computational Mechanics and Materials Engineering, P.O. Box 800, 9700 AV Groningen
phone +31-(0)653139704, e-mail lei.zhang@rug.nl

Brittle fracture is a key failure mechanism of body-centred cubic (bcc) transition metals, which limits their application and can jeopardize the safety of infrastructures. The competition between thermally activated dislocation mobility and atomistic crack-tip deformation mechanisms controls the fracture process. However, existing atomistic simulations of the crack-tip under mode-I loading based on classical interatomic potentials yield contradicting mechanisms[1].

To predict fracture with quantum accuracy, we developed an active learning algorithm based on Gaussian approximation potential (GAP) framework[2] (Fig. 1). We applied the active learning algorithm to crack systems (100)[011](crack plane/crack front) and (110)[001]. During the learning, the GAP predicted error converges to 8 meV/atom over a broad range of stress intensity factors (SIFs) in 4 iterations. The obtained model (referred to as GAP22) can predict the fracture process of crack systems (100)[010] and (110)[1-10]. The simulations reveal that cleavage along the original crack plane is the crack tip mechanism for {100} and {110} crack planes at T=0K under mode-I loading, thus settling a long-standing dispute.

Based on GAP22, we computed the critical SIFs at T=0K to 300K under high loading rates. The results are compared with Griffith and Rice theories. We found that the fracture mechanism remains unchanged at T=0K to 300K under high loading rates. Our work highlights the need for a multiscale approach to predicting fracture and intrinsic ductility, whereby finite temperature, finite loading rate effects and pre-existing defects (e.g. nanovoids, dislocations) should be taken explicitly into account.
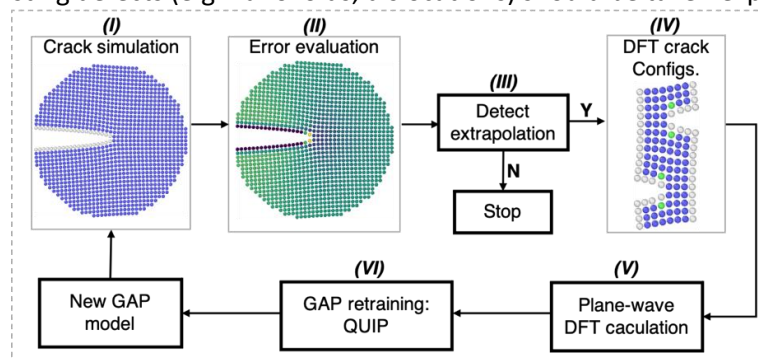
Fig. 1 Workflow of the active learning algorithm.

[1]. Möller, J. J., & Bitzek, E. (2014). Modelling and Simulation in Materials Science and Engineering, 22(4), 045002.
[2]. Dragoni, D., Daff, T. D., Csányi, G., & Marzari, N. (2018). Physical Review Materials, 2(1), 013.
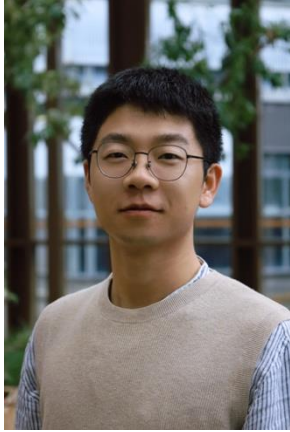
Abstract title: Atomistic fracture in bcc iron revealed by active training of machine learning potential.

Workshop: Machine Learning

Zhang, L. (Lei)

University of Groningen, Faculty of Science and Engineering, Engineering and Technology Institute, Computational mechanics and materials engineering.

Advisor: Dr. Francesco Maresca
Co-advisor: Prof.dr. Erik van der Giessen, Prof.dr. Gábor Csányi (University of Cambridge)

Biography and description of research:
Lei Zhang obtained his BSc degree in Mechanical Engineering from Sichuan University, Sichuan, China, in 2017. After finishing his BSc, he continued his education at Xian Jiaotong University, Shaanxi, China. He graduated with distinction and obtained his MSc in Solid Mechanics in 2020. During his MSc, he focused on the atomistic simulation of grain boundaries and interfaces in metals/ceramics.

He started his PhD in 2020 in the Multi-Scale Mechanics (MSM) group led by Dr. Francesco Maresca at the University of Groningen. The first stage of his PhD research focuses on developing quantum-accurate machine learning potential for predicting fracture in iron and its alloys. The second stage will focus on transferring the information from atomic-scale to microscale to enable connection with experimental results. A multiscale approach for predicting fracture will be developed.

Learning hyperelasticity without stress data

P. Thakolkaran[*], A. Joshi, Y. Zheng, M. Flaschel, L. De Lorenzis, S. Kumar

Delft University of Technology, Department of Materials Science and Engineering,
Section Materials, Mechanics & Computing, 2628 CD, Delft
phone , +41 (0)78 653 37 51, P.Thakolkaran@tudelft.nl

Abstract

We propose a new approach for unsupervised learning of hyperelastic constitutive laws with physics-consistent deep neural networks. In contrast to supervised learning, which assumes the availability of stress-strain pairs, the approach only uses realistically measurable full-field displacement and global reaction force data, thus it lies within the scope of our recent framework for Efficient Unsupervised Constitutive Law Identification and Discovery (EUCLID) and we denote it as NN-EUCLID [1]. The absence of stress labels is compensated for by leveraging a physics-motivated loss function based on the conservation of linear momentum to guide the learning process. The constitutive model is based on input-convex neural networks, which are capable of learning a function that is convex with respect to its inputs. By employing a specially designed neural network architecture, multiple physical and thermodynamic constraints for hyperelastic constitutive laws, such as material frame indifference, material stability, and stress-free reference configuration are automatically satisfied. We demonstrate the ability of the approach to accurately learn several hidden isotropic and anisotropic hyperelastic constitutive laws – including e.g., Mooney-Rivlin, Arruda-Boyce, Ogden, and Holzapfel models -- without using stress data. For anisotropic hyperelasticity, the unknown anisotropic fiber directions are automatically discovered jointly with the constitutive model. The neural network-based constitutive models show good generalization capability beyond the strain states observed during training and are readily deployable in a general finite element framework for simulating complex mechanical boundary value problems with good accuracy.

Reference

[1] Thakolkaran, P., Joshi, A., Zheng, Y., Flaschel, M., De Lorenzis, L., & Kumar, S. (2022). NN-EUCLID: deep-learning hyperelasticity without stress data. arXiv preprint arXiv:2205.06664.
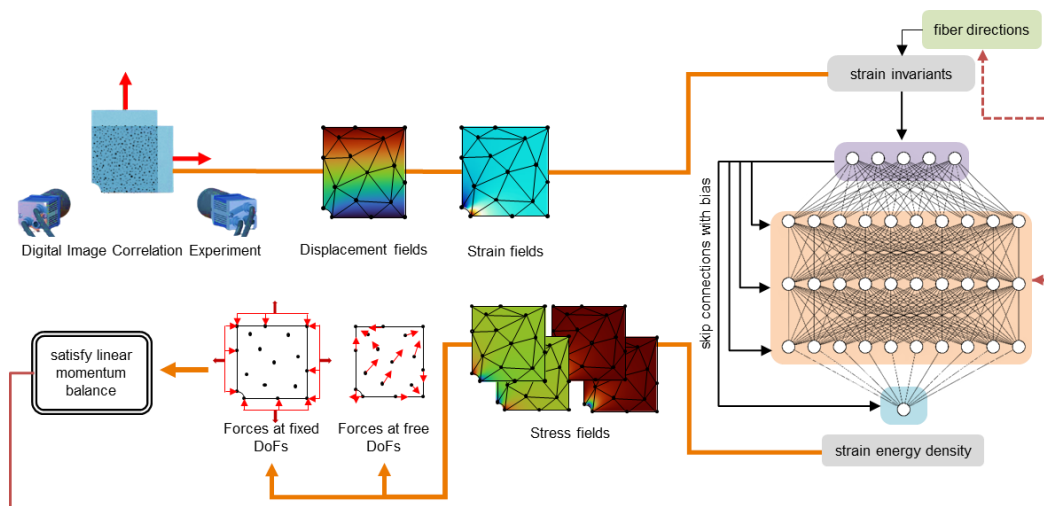
Unsupervised deep-learning of hyperelastic constitutive laws.

Abstract title: Learning hyperelasticity without stress data

Workshop: Machine learning

Thakolkaran, P. (Prakash)

Delft University of Technology, Department of Materials Science and Engineering

Advisor: Prof. Dr. Marcel Sluiter
Co-advisor: Dr. Siddhant Kumar

Biography and description of research:
Prakash is a second year PhD candidate at the Department of Materials Science and Engineering at Delft University of Technology. He received his B.Sc. (2018) and M.Sc. (2021) from ETH Zurich in Mechanical Engineering with a focus in design optimization and artificial intelligence.

Since September 2021 Prakash is a PhD candidate in the Mechanics, Materials & Computing group. His doctoral research focuses on the development of data-driven methods to learn hidden representations for materials design and modeling. In the design stream, he identifies classes of materials which lack a simple design parameterization and implements deep learning methods to create seamless and efficient design spaces. Whereas in the modeling stream, he aims to learn material models purely from full-field displacement and global reaction force data from a mechanical experiment.

Workshop 2
"Molecular and particle-based mechanics"

Multi-scale thermo-viscoelastic modelling of powder-based processes

Juan E. Alvarez

University of Twente, Faculty of Engineering and Technology,
Multi-scale Mechanics, Mesa+, P.O. Box 217, 7500 AE Enschede
phone: +31-(05)-34898416, email: j.e.alvareznaranjo@utwente.nl

Accurate modelling of powder processes requires capturing multi-physical phenomena at the particle scale. However, simulations at this size are demanding due to the high computational cost of modelling the high number of degrees of freedom represented by the discrete elements. Even though the computational analysis at the particle-particle level unveils the heterogeneity and multi-physics behaviour of powder materials, it is still prohibited the simulation of powder processes on a single high-resolution scale. This work presents a multi-scale thermal modelling approach to couple particulate-based systems with solid media using the discrete element method (DEM) and the finite element method (FEM). The implementation is built into two open-source packages, MercuryDPM[1] and oomph-lib [2], for discrete and continuum simulations, respectively. The implementation requires mapping the response of discrete particles onto a smooth, differentiable field satisfying the continuum equation of motion and energy balance. To achieve this, a bridging approach is utilized within an overlapping thermal interface that maps responses between particles and finite elements via volume coupling enriched by a micro-macro transition technique called coarse-graining [3]. The coupled approach is validated against the analytical solutions of both unsteady heat transfer and the propagation of elastic waves through the media. As a result, advanced powder technologies can be modelled using the proposed bridging methodology, enabling efficient modelling of micro-macro scale transitions.
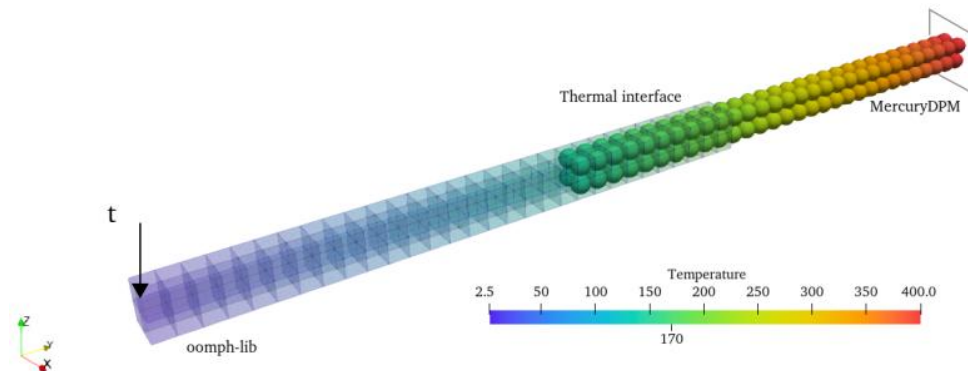
Fig. Thermal multi-scale approach from granular sub-model to continuum sub-model.

References

[1] Weinhart, T., et al., *Fast, flexible particle simulations – an introduction to MercuryDPM*, Computer physics communications 2020, vol. 249, 107129.

[2] Heil, M., and Hazel, A.L., *oomph-lib an object-oriented multi-physics finite element library,* Fluid-structure interaction. Springer, Berlin, Heidelberg 2006. pp.19-49.

[3] Weinhart, T., et al., *Coarse-grained local and objective continuum description of three-dimensional granular flows down an inclined surface,* Physics of fluids 2013, vol. 25, no. 7, 070605.

Biography
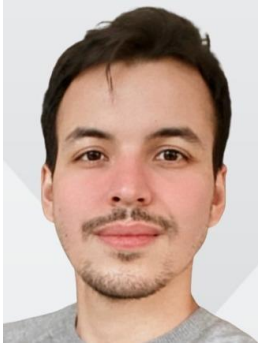
Juan Esteban Alvarez is a PhD candidate in the Multi-Scale Mechanics group of Prof. Stefan Luding at the University of Twente (Netherlands). Juan's research focuses on multi-scale thermo-viscoelastic modelling of powder-based processes using the Discrete Element Method, Finite Element Method and coarse-graining coupling technique. His work also focuses on numerical and experimental characterization of visco-elastic sintering kinetics of virgin and aged polymer powders. During the PhD research phase, he has also been a visiting researcher at the Department of Mathematics of University of Manchester (United Kingdom). Juan's previous research focused on a fully dynamic multi-scale approach for modelling intergranular failure mechanisms in 2D polycrystalline materials using the Boundary Element Method, at the University of Campinas (Brazil).

Investigation of single iron particle combustion in the Knudsen transition regime

L.C. Thijs

Eindhoven University of Technology, Department of Mechanical Engineering,
Power and Flow
e-mail l.c.thijs@tue.nl

Metal fuels, powders of micron-sized metal particles are gaining attention as promising energy carriers [1]. Most of them have high energy densities, are inherently carbon free, recyclable and compact. Iron is considered as a promising metal fuel since it is widely available, cheap and has the possibility to burn heterogeneously, without the formation of nano-sized iron-oxide products [1,2].

Understanding the burning process of a single iron particle is of key importance to be able to use iron as a metal fuel. In our previous work [2,3], it is shown that when assuming the conversion of Fe to FeO is the relevant conversion up to the maximum temperature, and neglecting internal transport, good agreement with experimental data is obtained. However, in this work, only particles of 40 μm and 50 μm are investigated. If the size of the particle becomes too small (Knudsen larger than 0.01), modelling the heat and mass transfer using the continuum approach becomes invalid.

In order to accurately describe the heat and mass transfer in the free-molecular regime, the thermal (TAC) and mass accommodation coefficients (MAC) should be known. In this work, molecular dynamics simulations are used to determine the TAC and MAC in the case of iron and air. Subsequently, the TAC and MAC values will be used to investigate the effect of the Knudsen layer on the combustion behavior of single iron particles.

References
[1] J. Bergthorson et al., "Direct combustion of recyclable metal fuels for zero-carbon heat and power," Appl. Energy, vol. 160, pp. 368–382, 2015.
[2] L. C. Thijs, C. E. A. G. van Gool, W. J. S. Ramaekers, J. A. van Oijen, and L. P. H. de Goey, "Resolved simulations of single iron particle combustion and the release of nanoparticles," Proc Combust Inst, 2022.
[3] L. C. Thijs, C. E. A. G van Gool, W. J. S. Ramaekers, J. G. M. Kuerten, J. A. van Oijen & L. P. H. de Goey. "Improvement of heat- and mass transfer modeling for single iron particles combustion using resolved simulations,", Combust Sci Technol., 2022

Abstract title: Investigation of single iron particle combustion in the Knudsen transition regime.

Workshop: Molecular and particle-based mechanics

Thijs, L.C. (Leon)

Eindhoven University of Technology, Department of Mechanical Engineering, Power and Flow **Advisor:** Prof.dr.L.P.H de Goey

Co-advisor: Prof.dr.J.A. van Oijen

Biography and description of research:
Leon Thijs obtained his BSc degree in Mechanical Engineering at Eindhoven University of Technology (TU/e) in 2017. He obtained his MSc double degree in Mechanical Engineering (Power & Flow group) and Applied Physics (Fluids & Flow group) in 2020. His master thesis is called "Honeycomb wake turbulence and particle dynamics in a magnetic density separation system". Directly after graduation, Leon joined the Power and Flow group as a Doctoral Candidate. In this position, he is now working on model development of single metal particle combustion

Under the supervision of full professor Philip de Goey and full professor Jeroen van Oijen, he researches numerical techniques for the simulation of single metal particle combustion. Metal powders are very promising high-energy-density fuels that are entirely carbon-free and recyclable. The metal powders can be oxidized to metal oxides while producing heat. These metal oxides can be reduced back to metal powders with green electricity to enable a cyclic process of oxidation and reduction which can be repeated over and over again.

Application of the Immersed Interface Method to the Lattice Boltzmann Method

S.J. van Elsloo

Delft University of Technology, Faculty of Aerospace Engineering, Kluyverweg 1, 2629 HS Delft
phone: +31-(06)-81158580, email: s.j.vanelsloo@tudelft.nl

The lattice Boltzmann method (LBM) is a popular technique to model unsteady, incompressible, low Reynolds number flow such as blood flow through artery systems. It boasts a number of advantages over classical fluid simulation frameworks. In particular, its simplicity and scalability using parallelism whilst fully (approximating) the Navier-Stokes equations in the limit of incompressibility for Newtonian fluids is appealing. In the LBM, the fluid flow is solved on a mesoscopic scale, which models the average motion of particles on a microscopic scale, to construct the velocity and density field at a macroscopic scale. Through repeated collision and streaming of populations, an unsteady flow simulation may be performed.

Boundary conditions require special attention in the LBM due to the need for a non-conforming, Cartesian fluid grid and the solution space being mesoscopic instead of macroscopic. The diffusive immersed boundary method (IBM) is a boundary treatment that can be readily applied to the LBM, by placing a feedback force along boundaries and diffusing this forcing to the fluid. Its extension to moving boundaries is trivial, making it a logical candidate for problems involving fluid-structure interaction. However, the IBM is troubled by spurious oscillations in its boundary force field [1].

The immersed interface method (IIM) [2] is a derivative of the IBM, in which discontinuities across boundaries are directly incorporated in finite-difference schemes, rather than through diffusion of an external forcing term. Although the IIM has been previously applied to fluid problems [3], it had yet to be successfully applied to LBM. It has been shown that the framework of the IIM allows for a reformulation of the way the boundary force is incorporated in the LBM. Rather than applying the boundary forcing during the collision step of the LBM, the boundary forcing is accounted for in population jumps during streaming. In turn, this results in a significant damping of the numerical oscillations compared to the classical diffusive IBM.

Figure 1: Multiscale description of LBM
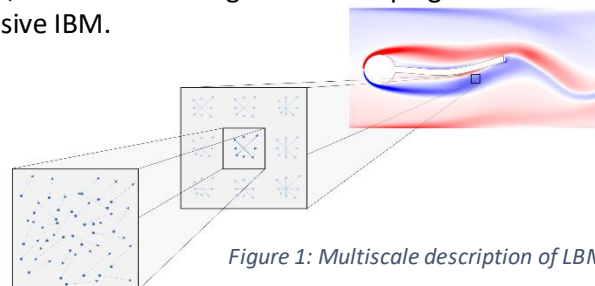
References

[1] Yang, X., Zhang, X., Li, Z., and He, G.. *A Smoothing Technique for Discrete Delta Functions with Application to Immersed Boundary Method in Moving Boundary Simulations*, Journal of Computational Physics, 2009, vol. 2289, no. 20, pp. 7821-7836.

[2] Leveque, R.J. and Li., Z., *The Immersed Interface Method for Elliptic Equations with Discontinuous Coefficients and Singular Sources*, SIAM Journal on Numerical Analysis, 1994, vol. 31, no. 4, pp. 1019-1044.

[3] Lee, L., and LeVeque, R.J., *An Immersed Interface Method for Incompressible Navier-Stokes Equations*, SIAM Journal on Scientific Computing, 2003, vol. 25, no. 3, pp. 832-856.

Biography and description of research:

Sam obtained his Bachelor of Aerospace Engineering at Delft of University in 2018, after which he completed his Master of Aerospace Engineering in 2022. During his MSc. Thesis, he worked on developing a simulation framework suitable for the simulation of flapping wing micro aerial vehicles, which included development of a lattice Boltzmann-based fluid solver that accounts for the presence of solid boundaries through diffusive immersed boundary-based methods.

Currently, Sam is a PhD candidate at the Department of Aerospace Structures and Materials at the Faculty of Aerospace Engineering, Delft University of Technology. His PhD research focusses on the development of a mid-fidelity model suitable for the simulation of the deployment and retrieval of morphing wing UAVs that are deployed from larger transport aircraft. This includes modelling of aeroservoelastic effects associated with the relative motion of aerodynamic surface. This project is a collaboration between the TU Delft and the NLDA (Netherlands Defence Academy).

Unravelling the atomic scale interactions of H with dislocations in iron

V. Shah[1], G. Csyani[2], E. van der Giessen[1], F. Maresca[1]
[1]University of Groningen, the Netherlands
[2]University of Cambridge, United Kingdom
phone: +31-(0)50-3638047, e-mail: v.d.shah@rug.nl

Hydrogen (H) is deemed as the leading candidate to aid the energy transition problem due to its clean and sustainable makeup. Yet, one of the major obstacles for an efficient hydrogen economy is material compatibility since it leads to metal embrittlement. Over the last decades, following several experimental and numerical investigations at different time and length scales, several embrittlement mechanisms have been presented [1]. However, the physics behind these mechanisms are often contradictory, with no amass consent on the fundamental role of hydrogen, especially the influence of local concentration on the motion of the dislocation, which governs plasticity and fracture toughness.

In this work, we study the nano/macro-scale interaction of H atoms with dislocations in iron and how this interplay ultimately dictates the glide behaviour. To this purpose, firstly we perform DFT calculations to predict the H-lattice defect interaction using the open-source code Quantum Espresso. Based on this DFT database, we develop new DFT-accurate machine learning (GAP [2]) based Fe-H potentials. Secondly, we perform molecular statics and dynamics simulations of bcc edge dislocations using the empirical EAM potentials [3], serving as the validation case for our newly developed GAP potentials. These simulations are performed using the open-source LAMMPS code. The influence of edge dislocation line length, and varying distribution and concentration of H atoms around the dislocation core is systematically investigated.

The critical Peierls stress for dislocation glide in presence of H is computed and compared with the reference case i.e., of pure iron, revealing H assisted pinning of dislocation glide. Additionally, for a given H concentration the extent of pinning is observed to be larger for higher temperatures due to rapid diffusion of H to the dislocation core. The discovered H assisted dislocation pinning mechanism is in contradiction with the well-established theory of hydrogen enhanced localized plasticity (implying hydrogen enhanced dislocation mobility) and is supported by the observation that the H-dislocation interaction energy is caused by strong elastic interaction of H with the dislocation core, ultimately increasing the Peierls stress. Moreover, considering the physical mechanism of dislocation pinning, an analytical model to predict the finite temperature critical resolved shear stress for varying local H concentration is currently being developed, which will be used to make predictions corresponding to experimental conditions.

References
[1] Li, X., *et al. Acta Metallurgica Sinica* 33(6), 759 (2020).
[2] Bartók, A. *et al. Physical review letters*, *104*(13), 136403 (2010).
[3] Ramasubramaniam, A. *et al. Physical Review B*, 79(17), 174101 (2009).

Abstract title: Unravelling the atomic-scale interactions of H with dislocations in iron

Workshop: Molecular and particle-based mechanics

Varun Shah University of Groningen, Faculty of Science and Engineering

Supervisors: Dr. Francesco Maresca, Prof. Erik van der Giessen

Biography:

Varun Shah obtained his bachelors degree in metallurgical and materials engineering from Gujarat University, India followed by a masters degree in materials science from the Technical University of Darmstadt, Germany. Subsequently, he received his PhD in mechanical engineering from the Eindhoven University of Technology, the Netherlands. His PhD research dealt with predicting the microstructure evolution of tungsten under extreme nuclear fusion conditions. Currently, he is working as a postdoctoral researcher on atomistic modelling of hydrogen embrittlement in iron with Dr. Francesco Maresca and Prof. Erik Van der Giessen at the University of Groningen.

Workshop 3

"Additive manufacturing"

Thermo-Fluidic Behavior To Solidification Microstructure Texture Evolution During Laser-assisted Powder-based Direct Energy Deposition – An Integrated Approach

UNIVERSITY OF TWENTE.

Mohammad Sattari[1*], Martin Luckabauer[1], G.R.B.E. (Gert-Willem) Römer[1]

[1] Department of Mechanics of Solids, Surfaces & Systems, Faculty of Engineering Technology, University of Twente
*Phone: +31- 534899352, e-mail m.sattari@utwente.nl

Abstract

In laser-based metal processing techniques, the intensity profile of the laser beam plays an essential role in the cyclic temperature evolution of the process. On the other hand, the microstructure and the resulting mechanical properties of the part follow the temperature profile during solidification. One way to control the microstructure and mechanical properties of a part, is the manipulation of the laser beam intensity profile using the so-called laser beam shaping method. Since finding a suitable laser beam intensity profile based on the required microstructure and mechanical properties is an expensive iterative trial and error process, the use of high-fidelity models is preferable to experiments.

In this research, a thermo-fluid model is developed for the Laser-assisted powder-based Direct Energy Deposition (L-DED) process based on the Computational Fluid Dynamics (CFD) method, where the powder particle flow is simulated using the Discrete Element Method (DEM) and the governing equations are solved using the Finite Volume Method (FVM). Also the Volume of Fluid (VOF) method is used to track the metal and gas interface.
With high accuracy, this model includes arbitrary laser beam intensity profiles, powder particle stream and particle size distribution, powder particle and laser beam interaction, addition of powder particles to the molten pool, temperature- and incident angle- dependent laser beam absorption, Marangoni effects due to surface tension, buoyancy flow, evaporation, solidification, shrinkage, and heat transfer in the substance and to the surroundings. On the other hand, a solidification microstructure texture model is developed and one-way coupled to the thermo-fluid model. The microstructure model is based on the Cellular Automata (CA) method and includes the grain nucleation and columnar-equiaxed grain growth competition to simulate the crystallographic texture changes of 316L austenitic stainless steel. In this model, the crystallographic orientation of the nuclei is selected randomly, but the grain growth with the preferred crystallographic orientation is followed based on a dendrite growth kinetics model. With the aid of experiments, both the thermo-fluid and the solidification microstructure models are validated. The thermo-fluid model has a high agreement with the experiments in terms of the geometry of the molten pool and clad. The microstructure model also predicts the size and crystallographic orientation of the grains after solidification in excellent agreement with the EBSD results.

Abstract title: Thermo-Fluidic Behavior To Solidification Microstructure Texture Evolution During Laser-assisted Powder-based Direct Energy Deposition – An Integrated Approach

Workshop: Additive Manufacturing

Sattari, M. (Mohammad)

University of Twente, Faculty of Engineering Technology, Department of Mechanics of Solids, Surfaces and Systems, Chair of Laser Processing

Advisor: Prof.dr.ir. G.R.B.E. Römer (Gert-Willem)
Co-advisor: Dr. M. Luckabauer (Martin)

Biography and description of research:
Mohammad Sattari is a last-year PhD student at the Laser Processing Chair at the University of Twente. Mohammad's research focuses on the effect of the laser beam intensity profile on the thermo-fluidic behavior of the resulting melt pool and solidification microstructure texture through the numerical modeling of the Laser-assisted powder-based Direct Energy Deposition (L-DED) process of 316L austenitic stainless steel. In the framework of Computational Fluid Dynamics (CFD) modeling, he uses Discrete Element (DEM), Finite Volume (FVM) and Volume of Fluid (VOF) methods, while using a Cellular Automaton (CA) for microstructure modeling. His modeling chain can help tailor the microstructure and mechanical properties by optimizing the laser beam intensity profile, i.e. laser beam shaping.

Mohammad received his MSc in Mechanical Engineering from Brest National School of Engineering (ENIB) in France, where he studied the functional fatigue behavior of Ni-Ti shape memory alloys. prior going to France, Mohammad received his first master's degree from Isfahan University of Technology in Iran, where he studied the wear behavior of the same alloy.

On the anisotropy of wire arc additively manufactured parts

L. Palmeira Belotti, T.F.W. van Nuland, M.G.D. Geers, J.P.M. Hoefnagels, J.A.W. van Dommelen

Eindhoven University of Technology, Department of Mechanical Engineering, P.O. Box 513, 5600 MB Eindhoven, The Netherlands
e-mail: l.palmeira.belotti@tue.nl

Wire arc additive manufacturing (WAAM) is an emerging group of methods for producing large parts with complex geometries, such as varying wall thicknesses. These parts usually exhibit anisotropic material behavior due to their intrinsic heterogeneous microstructure. To fully exploit the versatility of WAAM, a rigorous understanding of the relationship between microstructure and mechanical response of WAAM parts is necessary. Here, the structure-property relationship for thick-walled austenitic stainless steel WAAM parts is investigated using experiments and a mean-field crystal plasticity model. The major microstructural features are studied using optical microscopy and electron backscattered diffraction. A representative microstructure volume element is obtained with averaged features to study spatial variations in the microstructure across the WAAM part [1]. Uniaxial tensile tests assisted with Digital Image Correlation at different loading directions, along the horizontal (transverse direction), diagonal (45° from the transverse direction), and vertical (building direction), within the transverse direction-building direction plane, are used to study the mechanical properties and deformation fields of the part. The results reveal a heterogeneous microstructure [2] with periodically alternating microstructural features that lead to anisotropic material behavior. Furthermore, distinct plastic deformation patterns for different loading directions arise from the spatially varying microstructure [3]. The proposed crystal plasticity model describes the orientation-dependent material behavior trend regarding yield strength.

References

[1] L. Palmeira Belotti, J. P. M. Hoefnagels, M. G. D. Geers, and J. A. W. van Dommelen, "A modular framework to obtain representative microstructural cells of additively manufactured parts," *J Mater Res Technol*, 2022, doi: 10.1016/j.jmrt.2022.08.110.

[2] L. Palmeira Belotti, J. A. W. van Dommelen, M. G. D. Geers, C. Goulas, W. Ya, and J. P. M. Hoefnagels, "Microstructural characterisation of thick-walled wire arc additively manufactured stainless steel," *J Mater Process Technol*, 2022, 299:117373, doi:10.1016/J.JMATPROTEC.2021.117373.

[3] T. F. W. van Nuland, L. Palmeira Belotti, J. P. M. Hoefnagels, J. A. W. van Dommelen, and M. G. D. Geers, "Microstructural modeling and measurements of anisotropic plasticity in large scale additively manufactured 316L stainless steel," *Eur J Mech A Solids*, 2022, 96:104710, doi: 10.1016/J.EUROMECHSOL.2022.104710.

Abstract title: On the anisotropy of wire arc additively manufactured parts

Workshop: Additive Manufacturing

Palmeira Belotti, L. (Luca)

Eindhoven University of Technology, Department of Mechanical Engineering

Advisor: dr. ir. J.A.W. van Dommelen
Co-advisor: dr. ir. J.P.M. Hoefnagels

Biography and description of research:
Luca received his Bachelor's degree in Mechanical Engineering at the Federal University of Paraná, Brazil. He received his Master's in Mechanical Engineering with an emphasis in Tribology at Luleå University of Technology, Sweden, where he investigated the effect of hygrothermal aging on the tribological behavior of UHMWPE (Ultra-high-molecular-weight polyethylene). Currently, he is a doctoral candidate at the Eindhoven University of Technology, working at the Mechanics of Materials group. His research focuses on understanding the structure-property relationship for Wire Arc Additively Manufactured (WAAM) stainless steel parts.

Computational Design for Wire Arc Additive Manufacturing

V. Mishra, C. Ayas, M. Langelaar, F. van Keulen

Delft University of Technology, Faculty of Mechanical, Maritime and Materials Engineering,
Mekelweg 2, 2628 CD Delft, The Netherlands
phone +31-628658915, e-mail v.mishra@tudelft.nl

Abstract

Wire and Arc Additive Manufacturing (WAAM) is an upcoming manufacturing process to manufacture large engineering structures such as ship propellers and pedestrian bridges. In WAAM, the metal wire is melted by an electric arc and deposited simultaneously along a predefined path using a robotic arm. Materials with excellent weldability and high applicability such as austenitic stainless steel are used for the WAAM process. Austenitic stainless steel plates manufactured by WAAM show remarkable elastic anisotropy. The anisotropy arises due to textured microstructure development [1]. The texture is observed at an angle of $45°$ from the deposition direction. The stiffness along the direction of textured microstructure is 50% more than the deposition direction. The elastic anisotropy can be fully utilized by aligning the maximum stiffness direction along the load path directions of a WAAM manufactured structure. It opens up the possibility of optimizing the deposition directions. Topology Optimization (TO), a popular computational design tool, is used to optimize structural design layouts. In TO, continuous density-based design variables vary between 0 and 1 where extremum represents the void and material, respectively [2]. In this work, WAAM-related elastic anisotropic considerations are included in TO. A cubic crystal material model is presented to capture the elastic anisotropy exhibited by the WAAM-manufactured stainless steel plates. The deposition directions are considered as additional design variables. The cubic material model represents the local elastic properties in conjunction with deposition direction. The material properties become the function of two design variables: density and deposition directions. Both sets of design variables are optimized simultaneously to obtain an optimized design layout with corresponding optimized deposition directions for various structural problems. The results show that the optimized deposition directions are at an angle of $45°$ from the load path directions. The maximum stiffness directions are aligned with the load path directions.

References

[1]   P. Kyvelou, H. Slack, D. D. Mountanou, M. A. Wadee, T. B. Britton, C. Buchanan, L. Gardner, Mechanical and microstructural testing of wire and arc additively manufactured sheet material, Materials & Design 192 (2020) 108675.

[2]   M. P. Bendsoe, O. Sigmund, Topology optimization: theory, methods, and applications, Springer Science & Business Media, 2013.
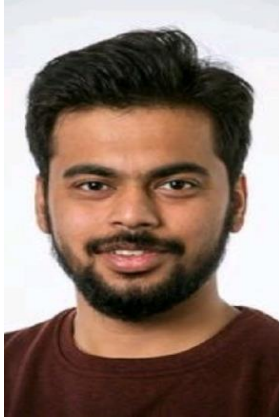
Abstract title: Computational Design for Wire Arc Additive Manufacturing.

Workshop: Additive Manufacturing

Mishra, V. (Vibhas)

Delft University of Technology, Faculty of Mechanical, Maritime and Materials Engineering, Mekelweg 2, 2628 CD Delft, The Netherlands

Advisor: Prof. dr. Fred van Keulen
Co-advisor: Dr. Matthijs Langelaar, Dr. Can Ayas

Biography and description of research:
Vibhas Mishra completed his bachelor's in Mechanical Engineering in India. Then he moved to the Netherlands and completed his master's in Aerospace Engineering at Delft University of Technology (TU Delft). Post his M.Sc. graduation, he joined the Structural Optimization and Mechanics group at TU Delft as a doctoral candidate. His field of research is Metal Additive Manufacturing (AM) processes and Topology Optimization (TO).

His research focuses on developing the structure-process-properties relation for a large-scale AM process, Wire and Arc Additive Manufacturing (WAAM), and using these relations in the TO framework for design optimization. He has developed 2D and 3D experimentally validated AM thermal process models. These process models, predict mechanical properties which are later validated through experiments. He has also developed novel TO methods to improve the mechanical performance and manufacturability of AM parts.

Additive Manufacturing of Metamaterials

Z. Zhang, P. Zieliński, M.K. Włodarczyk-Biegun, A. O. Krushynska

ENTEG & ZIAM, Faculty of Science and Engineering, University of Groningen
Nijenborgh 4, 9747 AG, Groningen, the Netherlands
phone +31-0644532966, z.h.zhang@rug.nl

The rapid advances in additive manufacturing (AM) have greatly promoted the development of advanced materials — metamaterials — rationally designed materials that gain unprecedented properties mainly from their structures. AM as a rapid prototyping technology can be utilized to fabricate most metamaterials with unconventional architectures in relatively low costs. Nowadays, various AM technologies are becoming more mature and widely used, e.g., stereolithography (SLA), fused deposition modeling (FDM), selective laser sintering (SLS), multi jet fusion (MJF), melt electrowriting (MEW). In this talk, we will focus on the additive manufacturing techniques and share our experience on fabricating different metamaterials using SLA, FDM, MJF, MEW, etc.
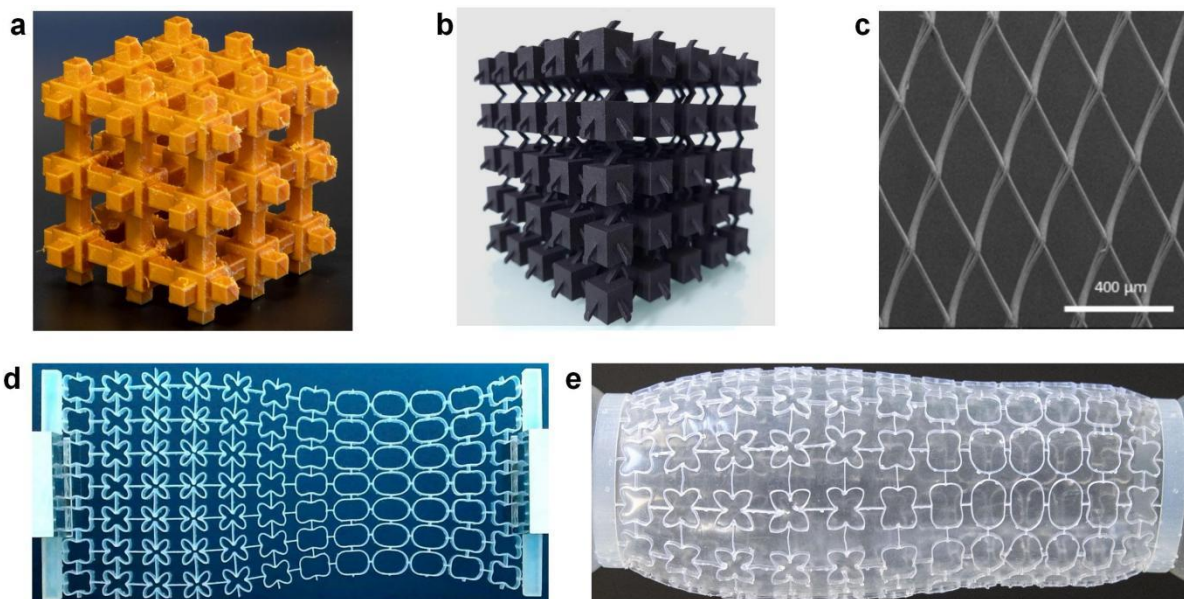
Figure 1. Metamaterial samples produced by additive manufacturing techniques: (a) PLA phononic structure by FDM (lab sample), (b) Nylon phononic structure by MJF/SLS[1], (c) PCL scaffold by MEW[2], (d) durable resin flat structure by SLA[3], (e) durable resin tubular structure by SLA[4].

Reference

[1] Krushynska, A. O., et al. (2021). Materials & Design, doi: 10.1016/j.matdes.2021.109714.
[2] Włodarczyk-Biegun, M.K., et al. (2022). ECB conference, "3D printing of hybrid gradient scaffolds for native tissues reconstruction".
[3] Zhang, Z.; Krushynska, A. O. (2022). APL Materials 10, doi: 10.1063/5.0099323.
[4] Zhang, Z.; Krushynska, A. O. (2022), "Programmable shape-morphing of tubular structures", submitted.

Abstract title: Additive Manufacturing of Metamaterials

Workshop: Additive manufacturing

Zhaohang Zhang

University of Groningen, Faculty of Science and Engineering

Advisor: Dr. Anastasiia Krushynska
Promotors: Prof. dr. Antonis Vakis, Prof. dr. Francesco Picchioni

Biography and description of research:

Zhaohang Zhang is a Ph.D. student in the Meta Mechanics Group of Computational Mechanical and Materials Engineering at the University of Groningen. He received his bachelor's degree in Aircraft Manufacture Engineering from Tongji University (Shanghai, China) in 2017, and obtained his master's degree in Solid Mechanics from Beihang University (Beijing, China) in 2020. In his bachelor thesis, he studied the compression failure behavior of laminate composites experimentally by manufacturing and testing carbon fiber reinforced polymer (CFRP) composites. During his master's period, he initially worked on the defects of C/SiC weave composites, then got interested in the unique properties and functionalities of mechanical metamaterials, so he studied the shape morphing behaviors of auxetic honeycomb structures in his master thesis.

Currently, his research interests lie primarily in the design, optimization, manufacture, and application development of metamaterials. In 2020, he started his Ph.D. research on "Programmable design of active cellular metamaterials". This project focuses on exploring the relationship between mechanical properties and geometric architecture, and developing mechanical and acoustic metamaterials in a programmable manner. This is achieved by a combination of theoretical analyses, numerical simulations, and experiments.

Workshop 4
"Material and structural health monitoring"

Monitoring of dynamic loads and acoustic emissions in composite marine propellers using embedded piezoelectric sensors

A. Huijer[1]*, C. Kassapoglou[2], L. Pahlavan[1]

[1]Delft University of Technology, Faculty of Mechanical, Maritime and Materials Engineering,
Section of Ship and Offshore Structures, Mekelweg 2, 2628CD Delft
[2]Delft University of Technology, Faculty of Aerospace Engineering,
Section of Aerospace Structures and Computational Mechanics, Kluyverweg 1, 2629 HS Delft
*phone +31-152786190, e-mail a.j.huijer@tudelft.nl

Flexible composite marine propellers have the potential to reduce the electromagnetic and acoustic signatures of maritime vehicles, as well as reducing their carbon emissions [1], [2]. There are however large uncertainties in the material properties and damage progression in composite materials. In-service monitoring of loads and damage to the blades may provide useful input for improved operation and estimation of the remaining lifetime [3].

This presentation will highlight current progress on the measurement and analysis of vibrations and acoustic emissions (AE) in composite marine propeller blades using a network of embedded piezoelectric sensors. In this regard, a framework is shown for the reconstruction of vibrations, together with preliminary measurements on blade in dry condition. Further, the measurement and processing of AE signals is outlined. This is aimed at damage localization and characterization. Considerations concerning the non-homogeneity and anisotropy of the propeller blade are explained. Initial results on AE measurements from the blade are also displayed.

References
[1]   Young, Y. L., Motley, M. R., Barber, R., Chae, E. J., and Garg, N., (Nov 2016), "Adaptive composite marine propulsors and turbines: Progress and challenges," Appl. Mech. Rev., vol. 68, no. 6
[2]   Maljaars, P., Bronswijk, L., Windt, J., Grasso, N., and Kaminski, M., (2018), "Experimental validation of fluid-structure interaction computations of flexible composite propellers in open water conditions using BEM-FEM and RANS-FEM methods," J. Mar. Sci. Eng., vol. 6, no. 2
[3]   Huijer, A., Zhang, X., Kassapoglou, C., and Pahlavan, L., (Jul 2022), "Feasibility evaluation for development of composite propellers with embedded piezoelectric sensors," Mar. Struct., vol. 84, p. 103231

Abstract title: Monitoring of dynamic loads and acoustic emissions in composite marine propellers using embedded piezoelectric sensors.

Workshop: Materials and Structural Health Monitoring

Huijer, A.J. (Arnaud)

Delft University of Technology, Department of Mechanical Engineering

Daily supervisor: Dr. L. (Pooria) Pahlavan
Promotor: Prof. dr. C. (Christos) Kassapoglou

Biography and description of research:
Arnaud (Arno) Huijer works as a PhD candidate since 2020 under the supervision of dr. Pooria Pahlavan and prof. dr. Christos Kassapoglou. In his research he assesses the feasibility of composite marine propellers with embedded piezoelectric sensors for in-service structural health monitoring.

Early on, Arno became acquainted with shipping and shipbuilding. These experiences let him to pursue his studies in Marine Technology at TU Delft. Starting in 2013, he received his Bachelor's degree in 2016 and his Master's degree in 2019.

In his graduation thesis, Arno researched the embedding of piezoelectric sensors in carbon fibre reinforced plastic composites. During experiments he demonstrated that the embedded sensors were able to measure low-frequency vibrations and acoustic emissions caused by the development of damage within the composite material.

Arno has so far throughout his PhD published 2 journal papers and 1 conference paper on the topic of embedded sensors for structural health monitoring of composites.

Unraveling plasticity and damage in multi-phase steels through dedicated integrated "2D" experimental-numerical testing

T. Vermeij, J. Wijnen, R.H.J. Peerlings, M.G.D. Geers, J.P.M. Hoefnagels

Eindhoven University of Technology, Department of Mechanical Engineering, P.O. Box 513, 5600 MB 4 Eindhoven, The Netherlands
e-mail: t.vermeij@tue.nl

Recent years saw advancement in simulations of plasticity, localizations and damage of various alloys and steels, using crystal plasticity or more advanced models. However, experimental validation of these simulation frameworks, particularly at the micro- and nanoscale, remains notoriously challenging due to (i) the unknown 3D subsurface microstructure, (ii) proper matching of boundary conditions and stress states, and (iii) the intricacy of damage mechanisms. Here, we aim to circumvent these problems by characterizing and testing "2D" (multi-phase) steel specimens, which have a micrometer thin through-thickness microstructure over a rather large area, thereby allowing direct comparison to a full 3D micromechanical crystal plasticity model. Such a dedicated methodology allows direct comparisons of plastic deformation fields between experiments and simulations, which have almost exactly the same 2D/3D microstructure. We will show at the EM symposium that the discrete slip activity at ferrite-ferrite grain boundaries is very well captured, in a statistical sense, by the 3D model with a novel discrete-slip plane crystal plasticity model, thereby validating the elaborate integrated experimental-numerical approach. Additionally, more complex multi-phase (ferrite-martensite) microstructures deform in a highly anisotropic manner, only yielding a good experimental-numerical agreement when applying a dedicated substructure-enriched martensite model. Further investigations are focused on damage, which requires even more advanced modelling approaches.

Abstract title: Unraveling plasticity and damage in multi-phase steels through dedicated integrated "2D" experimental-numerical testing

Workshop: Material and structural health monitoring

Vermeij, T. (Tijmen)

Eindhoven University of Technology, Department of Mechanical Engineering

Advisor: dr. ir. J.P.M. Hoefnagels
Co-advisors: prof. dr. ir. M.G.D. Geers & dr. ir. R.H.J. Peerlings

Biography and description of research:
Tijmen Vermeij was born in Haarlemmermeer, The Netherlands in 1991. After finishing secondary school in 2010, he travelled the world for a while and then started his BSc in Mechanical Engineering at TU/e. For his MSc internship, he visited the research group of Prof. Cem Tasan at the Massachusetts Institute of Technology (MIT), Boston, USA for a period of four months. For his MSc final project, he worked on the development of state-of-the-art 3D residuals stress measurements, which resulted in two journal publications, the prize for the best MSc thesis in the year 2018 at the Eindhoven University of Technology and the Acta Student Paper award, all of which was celebrated with a decent number of beers.

Tijmen is currently a PhD Candidate in the Mechanics of Materials group at Mechanical Engineering. His PhD project, supervised by Johan Hoefnagels, focuses on experimental investigations of micromechanical deformation and damage mechanisms in Dual-Phase Steels. This research is primarily conducted by combining advanced microscopic techniques on micromechanical deformation tests, through which the full chain of deformation and damage events can be tracked. Other research interests involve the development of state-of-the-art Electron Backscatter Diffraction (EBSD) and Digital Image Correlation (DIC) methods.

DYNAMICS-BASED IMPACT IDENTIFICATION METHOD FOR COMPOSITE STRUCTURES

UNIVERSITY OF TWENTE.

N.R. Marinho[1,*], R. Loendersloot[1], T. Tinga[1], and F. Grooteman[2]

[1] University of Twente, Faculty of Engineering Technology, Department of Mechanics of Solids, Surfaces & Systems, Dynamics Based Maintenance Group, P.O. Box 217, 7500AE Enschede, The Netherlands
[2] National Aerospace Laboratory (NLR), P.O. Box 153, 8300AD Emmeloord, The Netherlands
phone +31 (0) 53 – 489 4440 , e-mail n.ribeiromarinho@utwente.nl

Modern aircraft design acknowledges integrity, superior strength-to-weight ratio, and safety as critical priorities, which has led to the development of monitoring and maintenance techniques for composite structures. However, composite materials pose the risk of introducing damage that cannot be identified visually, namely barely visible impact damage (BVID). If not detected and repaired in time, damage to the structure can compromise its performance and integrity. Therefore, structural health monitoring (SHM) is an emerging technology that can enhance BVID detection in composite structures. Using ultrasonic waves to locate and characterize an impacted region in composite materials is one of the most promising SHM techniques for quantitative impact identification. Although previous studies use guided waves to assess impact in composite materials, few have addressed in-service inspection, and still, few have attempted to quantify impact severity information from the measured signals to full-scale engineering structures. The present investigation addresses these challenges by developing measures of impact identification based on features extracted from ultrasonic waves. Hence, the research aims to develop a monitoring method using combined sensing technologies to gather data from the system and then translate it into predictions about its health. It requires research across multiple disciplines, such as signal processing, data analysis, damage modeling, dynamics, and sensing technologies. This work proposes to combine the building block (B.B.) approach and the design of experiments (DOE) for guided wave-based structural health monitoring (GWSHM). This practical and systematic approach minimizes the number of tests needed for realistic and large structures by building data from lower-level to higher-level systems. Researchers have conducted low-energy impact tests on a square (1x1m) aluminum and composite plates in the current research phase. Several sensor signal features and the effect of signal response for various energy levels have been examined using the impact response data generated from three different sensor types: Fiber Bragg Grating (FBG), Piezoelectric Patch Transducer (PZT), and Optical Acoustic Emission (OptimAE). Therefore, the present work compares the performance and reliability of FBGs and OptimAE sensors using PZT-based sensors as a reference. In addition, this study describes a systematic experimental approach and analyzes preliminary results over a range of energy levels below the damage onset. The results showed that the distance from sensors and the directivity effect (for FBG) affect the sensitivity and signal strength. Furthermore, considering the requirements of SHM sensors, the performance also varies with different sensing technologies. In the next stage, SHM analysis will address the effect of structural elements with added complexity (i.e., stiffeners and variable thickness).

*corresponding author

Abstract title: DYNAMICS-BASED IMPACT IDENTIFICATION METHOD FOR COMPOSITE STRUCTURES

Workshop: Material and structural health monitoring

Marinho, N.R. (Natália)

University of Twente, Faculty of Engineering Technology, Department of Mechanics of Solids, Surfaces & Systems, Dynamics-Based Maintenance Group

Advisor: Prof. dr. Tiedo Tinga
Co-advisor: Dr. ir. Richard Loendersloot

Biography and description of research:

Natália Ribeiro Marinho graduated in Civil Engineering from the Federal University of Bahia (UFBA), Brazil, with a sandwich year at Swansea University, Wales, UK, specializing in structural design. As part of the Laboratory of New Concepts in Aeronautics (LNCA), she received her Master of Science degree from the Aeronautics Institute of Technology (ITA), São Paulo, Brazil, with a research project on the fracture characterization of advanced composite materials under cyclic loading. She also was an active member of the Brazil-Netherlands initiative on Research and Innovation in Thermoplastic Composites (SPIRIT) during this period. Upon graduating from the ITA, she joined the Hydro-mechanical Systems Design team at Mitsubishi Aircraft Corporation (MITAC), Nagoya, Japan. In her role, she performed structural integrity analyses of landing gear systems, applying damage prediction methods to demonstrate compliance with airworthiness directives. In 2020, she worked at the Innovation Institute for Integrated Solutions in Applied Mechanics (ISI SIM). Her Senior Mechanical Design researcher responsibilities included developing, integrating, and validating Proofs of Concepts (POCs) for computational vision systems and sensing technologies. She is currently a Ph.D. candidate at the University of Twente, part of the Department of Mechanics of Solids, Surfaces & Systems, integrating the Dynamics-Based Maintenance Group in Enschede, the Netherlands.

A key objective of this Ph.D. project is to develop a monitoring method that utilizes combined sensing technologies for impact characterization in a full-scale aircraft composite structure. Achieving this aim requires detecting and understanding impact-induced traveling waves generated in complex structures with typical features, such as thickness variations and stiffeners. A multidisciplinary approach is therefore needed, including signal processing, data analysis, damage modeling, dynamics, and sensor installation. As a result, the researcher works on a novel method for localizing an impact event and estimating the energy level from measured signals with high accuracy. The approach includes a combination of numerical analysis and experimental work to answer the research questions and reach the objectives.

The described Ph.D. project is part of the Predictive Maintenance for Very Effective Asset Management (PrimaVera) research program. This project, funded by the Dutch National Research Agenda (NWA), is executed by the University of Twente (UT) and the Netherlands Aerospace Center (NLR). The research will contribute to Data Processing and Diagnosis (WP2), one of the six technical work packages in PrimaVera. This work package aims to convert raw sensor data into actionable information relevant to predictive maintenance.

Newly developed Cam-Roller follower Tester (CRT) with self-aligning mechanism in a line contact configuration and ways of simulating, detecting, and measuring surface initiated RCF cracks

A. Vrček

University of Technology, Department of Mechanical Engineering,
Section, P.O. Box 217
phone +31-534899042, a.vrcek@utwente.nl

Rolling contact fatigue damage represents the end life of all rotating machinery e.g. rolling bearings, gears, camshaft-roller followers, rail wheels etc. Typically, such components can operate under wide operating conditions from full film lubrication to boundary lubrication, depending on the application. For this study, focus is given on boundary conditions, where load is caried mainly via asperity-asperity interaction and less via lubricant. As such, two damage modes are competing with each other e.g. wear and surface/subsurface initiated rolling contact fatigue. In order to understand and predict these two complex damage/failure mechanisms, firstly a cam-roller follower tester was developed to experimentally reproduce such damages under laboratory controlled conditions. The newly developed tester is unique as it utilizes self-aligning mechanism in a line contact configuration and it truly resembles the dynamics of most rotating machinery i.e. one specimen is driven and the other one is follower. The main feature of the tester is to measure traction force under very low partial slip conditions. Secondly, two non-destructive testing (NDA) techniques are selected to detect and measure initiation (Electromagnetic Testing - ET) and propagation (Computed Tomography – CT) of surface initiated rolling contact fatigue cracks. Finally, the results from NDAs will be used to validate undergoing semi-analytical model being under development to simulate the synergetic effect of wear and rolling contact fatigue on the end life of the component.

Abstract title: Newly developed Cam-Roller follower Tester (CRT) with self-aligning mechanism in a line contact configuration and ways of simulating, detecting, and measuring surface initiated RCF cracks.

Workshop: Material and structural health monitoring

Vrček, A. (Aleks)

University of Twente, Department of Mechanisms of Solids, Surfaces & Systems, Surface Technology and Tribology group (STT)

Advisor: Prof.dr. Matthijn de Rooij

Biography and description of research:

Aleks Vrček works as a postdoc since October 2021 under the supervision of prof. dr. Matthijn de Rooij. In his research he experimentally investigates wear and rolling contact fatigue (RCF) damage of various steels in rolling/sliding contact under boundary lubrication conditions. In particular, he investigates on ways to detect and measure RCF cracks. The research focuses on cold rolling application together with Tata steels.

Earlier, Aleks obtained his PhD degree in 2020 at Lulea University of Technology in Sweden under supervision of prof. dr. Par Marklund and prof. dr. Roland Larsson in Machine elements group. His research work with his PhD thesis entitled "*Tribology of rolling/sliding contacts under mixed lubrication: With the focus on a crankshaft roller bearing application*" contributed to a better-dimensioned tribological system in general and rolling element bearings in motor environment in particular. The work was together with Volvo Cars and partially with SKF.

Prior to that, Aleks graduated from Tribos Erasmus+ program in 2015, which is a joint European master in tribology of surfaces and interfaces. The program took place at 4 different European universities; University of Leeds (UK), University of Ljubljana (Slovenia), Lulea University of Technology (Sweden) and University of Coimbra (Portugal).

Aleks has so far throughout his studies and research published 12 journal papers on the topic of wear, RCF and EHL lubrication.

5

SURVEY

of

POSTER PRESENTATIONS

This section contains a survey of poster presentations of actual PhD-projects within the Graduate School Engineering Mechanics. Furthermore, poster presentations are available through: **http://www.engineering.mechanics.nl**

Survey of Poster Presentations Twenty-fifth EM Symposium

	Name	Univ	Title Poster
1	Adly, M.A.	TUD	A Physics Based Traction Separation Law for Metal Crashworthiness in Shell Elements
2	Ai, X.	TUD	C1 Floating Node Method for the Modelling of Composites Damage and Failure
3	Akhtar, M.	TUe	Assembling nano/micro-structured ceramic-based composites into complex shapes
4	Alvarez, J.E.	UT	Multi-scale thermo-viscoelastic modelling of powder-based processes
5	Alves Maia, M.A.	TUD	Neural networks with embedded physics-based material models to accelerate FE^2 simulations of path-dependent heterogeneous materials
6	Anselmucci, F.	UT	Quantifying hydro-mechanical properties of vegetated soil
7	Asijee, T.J.	UT	Towards Robust Laser Assisted Fibre Placement Adapting the process to the incoming material properties
8	Atzampou, P.	TUD	Contactless Position Control of Offshore Wind Turbines during the Installation
9	Babbepalli, P.R.	TUe	Comparison of data-based and physics-based Model order reduction
10	Bechlenberg, A.	RuG	Simulating the power extraction of a dense wave energy converter array with different levels of power take-off adaptability
11	Bentalib, S.	UT	Microstructure evolution during fusion bonding processes of thermoplastic composites
12	Berghuis, M.W.	UT	Life after the Constant Curvature assumption
13	Bertens, T.	TUe	Towards understanding wear particle generation on silicon wafers
14	Bhattarai, S.	TUD	Modelling combined necking/cracking interaction
15	Bieleman, G.	UT	Fibre-matrix Distribution Evolution of Thermoplastic Composites Fusion Bonding Interfaces
16	Brands, D.	UT	Forming simulations for unidirectional thermoplastic composites: Improvements in characterizing, modelling and validating in-plane shear
17	Bruinsma, S.	UT	Feature Selection for Failure Recognition: Comparing Vibration Analysis and Motor Current Signature Analysis
18	Brunner, F.	RuG	Predictive modelling of liquid metal induced fracture in Fe-based alloys
19	Buser, Y. M.	UT	Inducttion Heating of UD c/PAEK. What thermography can teach us about eddy currents
20	Chidambaram, N.	UT	Estimation of the shape and size of interaction volume for non-collinear wave mixing inspections in PVC
21	Cordewener, B.	TUe	A numerical framework for the electro-mechanical analysis of conductive tracks in printed electronics
22	Cupertino, A.	TUD	Extreme high aspect ratio mechanical resonators with low mechanical dissipation
23	Delissen, A.	TUD	GPU-accelerated matrix-free topology optimization
24	Dijk, van D.	UT	Generalized Kalman Filtering for Nonlinear Dynamic Problems using Machine Learning
25	Dorussen, B. J. A.	TUe	A hybrid ray tracing and Discrete Element Method framework for the simulation of particle based Additive Manufacturing processes
26	Fărăgău, A.B.	TUD	Drivability of piles under vibratory driving: small scale experiments

27	Fioravanti, D.	RuG	Multiscale modelling of plasticity in HCP metals
28	Gartner, T.	TUD	Comparison of the Nonlinear Elastic Behavior of Auxetic Lattice Architectures
29	Giele, R.	TUD	Topology optimization with cleanability requirements
30	Gödde, T.	UT	Physically constrained machine learning: Simulating battery deformation
31	Gülmez, D.E.	TUD	Computational Modelling of Discontinuous Tape Thermoplastic Composites
32	Gurian, M.	UT	Residual stresses in fusion-bonded thermoplastic composites
33	Haasjes, R.	UT	Active noise control in anechoic chambers using an efficient scheme incorporating frequency-domain derived filters
34	Han, Z.	TUD	Computational Micromechanics Modeling of Failure in Composites
35	He, Z. H.	TUe	A dynamic homogenization framework towards analysis of acoustic-structure coupling for metamaterials
36	Heerink, N.A.	UT	Predictive Maintenance Models for Military Aircraft Systems
37	Hendriks, F.	Tue	Graph Neural Networks for computational homogenization
38	Hermann, N.	TUD	A level set eXtended IsoGeometric Analysis approach for finite strains
39	Hofman, P.	TUD	Computational Modeling of Fatigue Failure in Composite Laminates
40	Hoksbergen, T. H.	UT	Modeling of rain erosion damage and lifetime of wind turbine blades
41	Huijer, A.	TUD	Monitoring of dynamic strain and acoustic emissions of composite marine propellers using embedded piezoelectric sensors
42	Jalalimoghadas, F.	UT	Multi-scale friction model for Aluminum sheet metal forming
43	Janssen, L.A.L.	TUe	Error Bounds in Model Reduction of Interconnected Systems: A Robust Performance Approach
44	Jong, de M.H.J.	TUD	Mechanical overtone frequency combs
45	Joseph, S.	UT	Noise and Vibration in Wet Soil: Micromechanical modelling for smart mitigation strategies
46	Karaseva, E.	UT	Multiscale analysis of polymer composite materials filled with nanofiller using multigrid method
47	Keizers, L. S.	UT	Atmospheric Corrosion Prognostics: Predicting the Unpredictable?
48	Kessels, B.M.	TUe	Model Parameter Updating for Digital Twins using Gaussian Process Regression as Inverse Mapping Model
49	König, D.	TUe	Micromechanical characterization of Zinc coatings and high entropy alloys (Next-Coat)
50	Koppen, S.	TUD	Topology optimization of multi-DOF comp
51	Kousemaker, T.M.	RuG	Numerical Investigation of Supercritical CO2 Extrusion Using the Level Set Method
52	Kovacevic, D.	TUD	unidirectional composites undergoing finite strains
53	Kuci, X.	TUe	Acoustic metasurface for Enhanced reflectivity and Redirection of ultrasound waves
54	La Rosa, L.	RuG	Atomistic simulations of twin boundaries in Ni-Ti Shape-Memory Alloys
55	Lenders, T.	TUe	Predicting the rate-dependent behaviour of polyvinylidene fluoride (PVDF) using an elasto-viscoplastic constitutive model
56	Li, A.	TUe	Continuous fiber reinforced woven composites : geometry, meshing and homogenization
57	Liu, L.	TUe	Computational homogenization of martensite/ferrite interface microstructures towards enhanced cohesive interfaces

58	Liupekevicius, R.	TUe	Computational Homogenisation of Locally-Resonant Poroelastic Medium
59	Livani, M.A.	TUe	Homogenization of hygro-mechanical response of oak wood based on 3D micro-CT images and finite cell method
60	Lubbe, R.	UT	Continuum-DEM modelling of fluid-solid transition in weakly compacted systems of polydisperse particles of varying shapes
61	Madabhushi, S.	TUD	Optimization of Laminated Composites
62	Martens, R.F.M.	TUe	Building aMulti-Layer Stress Depth Profiler
63	Meijers, P.C.	TUD	Controlling the motion of a pendulum with mag
64	Mishra, V .	TUD	Computational Design for Wire Arc Additive Manufacturing
65	Mudunuru, S.N.R.	TUe	Time-dependent Anisotropic Behavior of Fibre Reinforced Thermoplastics.
66	Munzone, F.	UT	A data-driven model updating approach for robust optimization of (multi-stage) production processes
67	Nazemzadeh, N.	UT	Modelling of Recycled Fibre-Reinforced Polymer Composites
68	Nienhuis, R.M.	RuG	Quantifying the Round-trip Efficiency of a Novel Offshore Pumped Hydro Energy Storage System
69	Palmeira Belotti, L.	TUe	Process-structure-properties of wire arc additively manufactured stainless steels
70	Parsa Sadr, A.	TUe	A multi-physics and multi-scale model for the degradation of historical paper
71	Pierik, E.R.	UT	From no-slip to full slip in the matrix-fiber interface: a state-rate approach
72	Pirmoradi, P.	TUe	Multi-Scale Modeling of Fiber-Reinforced Concrete using Granular Micromechanics Approach
73	Poort, L.	TUe	Passivity Preserving Reduction of Interconnected Linear Models of Dynamic Systems
74	Poot, A.	TUD	A Novel Bayesian Finite Element Method
75	Rathore, S.	UT	Modelling the Battery-can manufacturing process for cylindrical batteries
76	Reales, G	TUD	Thermocouple Design for Cooling Purposes Through Non-Convex Topology Optimization with Power Allocation Constraints
77	Rezaeinejad, S.S.	UT	A feasibility study on friction screw extrusion additive manufacturing of AA6060
78	Ribeiro Marinho, N.R.	UT	Impact identification method for composite structures
79	Riccioli, F.	TUD	Predictive digital twin for offshore structures
80	Riccius, L.F.	TUD	Bayesian Machine Learning for Multiscale Modeling of 3D-printed Materials
81	Saghafian Larijani, R.	UT	Meso-scale description of wet powders for industrial-scale modelling
82	Sanchez Martinez, N.M.	TUe	Efficient tools for the analysis of 4D printing processes
83	Scheeren, B.	TUD	Assessment of Natural Degradation in a Low-speed Roller Bearing using Acoustic Emission Monitoring
84	Shaban, M.	TUe	Photopolymerization Kinetics in Stereolithography Modeling and Simulation
85	Shah, V.	RuG	Does H strengthen iron?: Insights from atomic-scale H-dislocation interaction

86	Shi, H.	TUe	Modelling the thermomechanical behaviour of functional ceramic membranes
87	Suryanarayanan M. S.	TUD	Searching for designs in a neural network's parameter space may be more rewarding!
88	Storm, J.	TUD	Mesh-based surrogate for FE2 microstructure simulations
89	Sulollari, E.	TUD	Vibration-Induced Friction Force Modulation
90	Thakolkaran, P.	TUD	Learning hyperelasticity without stress data
91	Theulings, M.J.B.	TUD	Towards improved porous models for solid/fluid topology optimization
92	Tosti Balducci, G.	TUD	Predicting composite structures failure with the help of quantum neural networks
93	Traff, E.A.	TUD	Simple and Efficient GPU accelerated Topology Optimization
94	Tsetas, A.	TUD	Vibratory pile installation in layered soil media: numerical modelling and field tests
95	Valappil, S.V.	TUD	Phononic structures to mitigate crosstalk in clamp-on ultrasonic flowmeters
96	Vermeij, T.	TUe	Experiments vs Simulations: Episode IV - A New Hope
97	Vonk, N.	TUe	Understanding the hygro-expansion magnitude of freely and restrained dried handsheets
98	Voorthuizen, K. van	UT	Additive manufacturing of concrete: a dynamic analysis
99	Wadadar, D.	TUd	Gaussian Process Simulation of Nonlinear History Dependent Material Model D.Wadadar1
100	Wang, C.	TUD	Computational Fluid Dynamics of Flows Around Rigid Cylinders: a Comparative Study
101	Weg, B.P. van de	UT	Auto-Adapting Multi-Element Polynomial Chaos Expansion
102	Wijnen, J.	TUe	How to gain insights into the failure behavior of advanced metals: Comparing simulations with experiments
103	Willems, R.	TUe	Isogeometric Analysis of an Electromechanical Bi-Ventricular Heart Model
104	Winkelmann, M.	UT	From particles to continuous fields: Upscaling towards micropolar theory based on structure and rotation
105	Wong, W.J.	TUD	Effect of strain hardening on the bending capacity of welded I-section highstrength steel beams
106	Wu, K.	TUD	Space-time Topology Optimization Considering Material Anisotropy
107	Wulff, A.	TUD	Quantum and machine learning methods for stacking retrieval of laminated composite materials
108	Xu, X.	TUD	Multiscale Extended Finite Element Method for the Simulation of Cracks Propagation in Fractured Geological Formations
109	Xu, Q.	TUe	Implementation of a pyrolysis model in two-way coupled fire-structure simulations
110	Yan, C.	TUe	Nanoindentation creep behavior of supercrystalline nanocomposites
111	Yan, Y.	TUD	Computational Analysis of Origami Structures for Vibration Isolation
112	Yang, Y.	TUD	Laser Scanning Strategy Effects on Phase Distribution in Ti–6Al–4V Multi-Laser Powder Bed Fusion Process
113	Zhang, J.	TUe	Toughening Bio-inspired Ceramics via the Tetragonal-to-Monoclinic Phase Transformation
114	Zhang, L.	RuG	Atomistic Fracture in bcc Iron Revealed by Active Training of Machine Learning Potential

115	Zhang, X.	TUD	Size effect on the mechanical properties of 3D printing
116	Zhang, Z.	RuG	Programmable Shape-morphing of Rose-shaped Mechanical Metamaterials
117	Zwet, van der J.M.	TUD	Multi-material topology optimization with crisp material interface
0	Asiikkis, A.T.	RuG	CFD Simulations of Breaking Wave Impacts on a Recurved Seawall
0	Vasconcelos, A.C.A.	TUD	Design Optimization of Acoustic/Elastic Metamaterial-Based Structures for Underwater Noise Mitigation

A Physics Based Traction Separation Law for Metal Crashworthiness in Shell Elements

M.A. Adly, C.L. Walters

*Department of Maritime and Transport Technology,
Faculty of Mechanical, Maritime and Materials Engineering,
Delft University of Technology*

Background

Simulating the failure behavior of thin-walled structures at sea is usually done through using shell elements. Current computational power capabilities allow the utilization of elements with dimensions of around five times the thickness. At such a scale, the apparent failure behavior can be strongly influenced by localization phenomena, such as necking. The application of a traction-separation law (TSL) in shell elements should offer the desired balance between computational cost and accuracy. This TSL should therefore reflect the force-separation behavior of such elements from the moment of its initiation.

Objective

In order for the TSL implementation to be more realistic in practice, the TSL should be developed *a priori* rather than *a posteriori*. This mean that the TSL should be derived solely based on material properties, states of stress and constraints rather than relying heavily on experiments of relevant scale and complexity to the application. Furthermore, as the mesh sensitivity usually starts at the onset of necking, the TSL should therefore reflect the behaviour from the onset of necking to the onset of shear localization. This is illustrated for the uniaxial tension case as an example in figure 1.
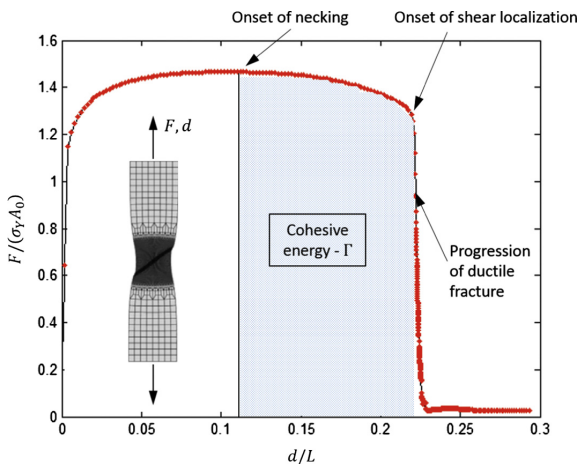
Figure 1: TSL activation zone [1]

Methodology

A modular framework for obtaining the TSL *a priori* was developed and is presented in figure 2. The primary inputs for this framework are the biaxial strain ratio (currently ratios between -0.5 (uniaxial tension) and 1 (equibiaxial tension) are being considered) and the material model including both plasticity and damage models. The numbered blocks indicate the areas of research interest that would result in a satisfactory TSL *a priori*. Therefore, obtaining better answers for some of those research questions is essential for the current framework.
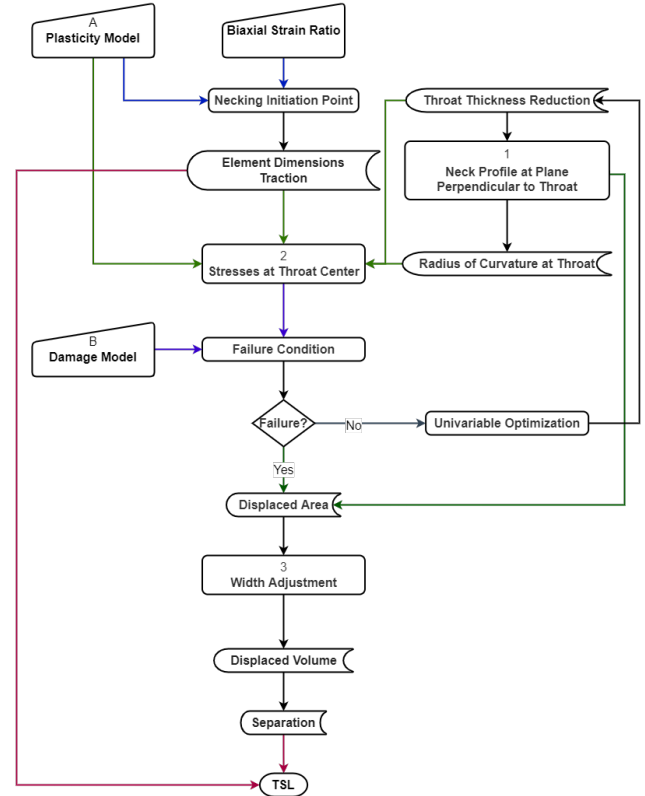
Figure 2: TSL framework

Focal Research Points

Currently, most of the focus is on three areas. First, there is a literature gap in obtaining an analytical description of the neck profile at the plane perpendicular to the throat. Second, even though works by [2] and [3] already offer ways to estimate the stresses at the throat center, more accurate methods are desired. Finally, the effect of the width of the structure on the localization needs to be better understood. The neck profile varies along the width and this variation is not only dependent on the material but the specimen size as well.

Future Work

Validation experiments of varying scale are to be conducted to ensure the framework is working as expected. Furthermore, the framework is to be extended to include more cases relevant in practice such as a wider range of biaxial strain ratios and strain rates

References

[1] P.B. Woelke, M.D. Shields, J.W. Hutchinson, Cohesive zone modeling and calibration for mode I tearing of large ductile plates, Engineering Fracture Mechanics. 147 (2015) 293–305.

[2] P.W. Bridgman, Studies in Large Plastic Flow and Fracture, 2nd ed., Harvard University Press, Cambridge, Massachusetts, 1952.

[3] R.C. Dragt, J. Kraus, C.L. Walters, Calculation of Shell Element Failure Based on the State of Stress Inside of a Neck, in: Volume 3: Structures, Safety and Reliability, American Society of Mechanical Engineers, 2015.

PhD progress

1 2 3 4

C1 Floating Node Method for the Modelling of Composites Damage and Failure

Xiaopeng Ai, Boyang Chen

Aerospace Structures and Computational Mechanics,
Delft University of Technology

Introduction

Damage and failure predictions are indispensable for the design of composite structures. Floating Node Method (FNM) has demonstrated superior performance in capturing the complex crack networks that are developed during the progressive failure of composites. However, the high density of mesh needed to resolve the cohesive zone length for delamination prediction using cohesive elements makes the method computationally expensive.

C1 cubic ply element

This work aims to develop a new version of the FNM, where the plies and interfaces would be modelled with C1-continous triangular Kirchhoff-Love shell and cohesive elements, respectively. The triangular shape is chosen for its flexibility of modelling arbitrary (sub-)domain geometries. The ply element in this structural element is selected as a C1 cubic shell element. This shell element is built by a cubic plate element (Figure 2) and a membrane element.
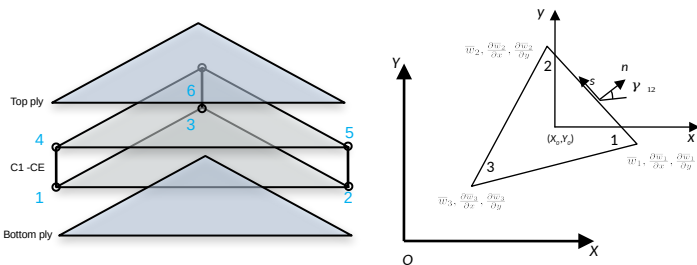
Figure 1: C1 Structural element & cubic plate element

C1 cubic cohesive element

The compatible cohesive element is built based on the cubic shell element. Turon's mixed-mode cohesive law is chosen in this work. The simple verification of C1 Cubic-CE was verified by two elements test and compared with the analytical results by using Abaqus UEL. In addition, the sub-domain integration technique is also considered in this work.
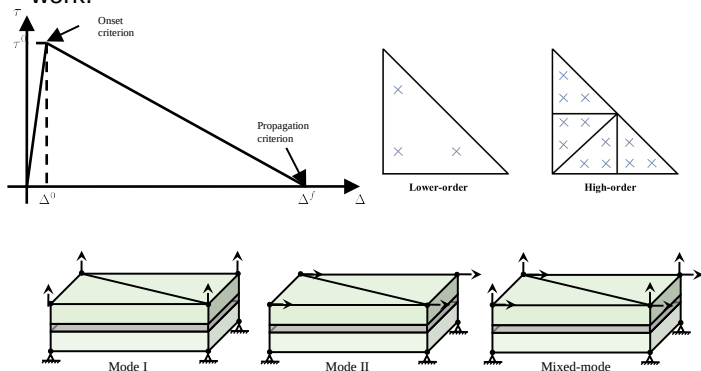
Figure 2: C1 cubic cohesive element

Conclusions

After the verification of benchmarks (Figure 4), the new CE has been shown to be able to overcome the cohesive zone limit, which enabled the use of CEs four times larger than the current CE size.
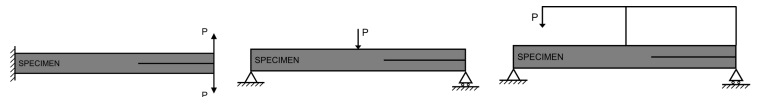
Figure 3: Benchmark of verification
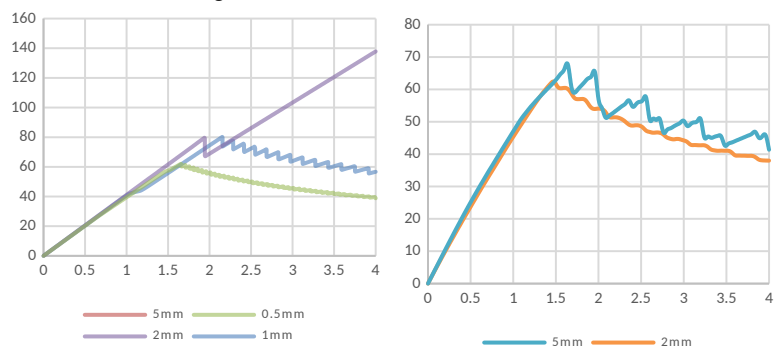
Figure 4: DCB load-displacement curves predicted with linear CEs (left) and C1 structural CEs (right)
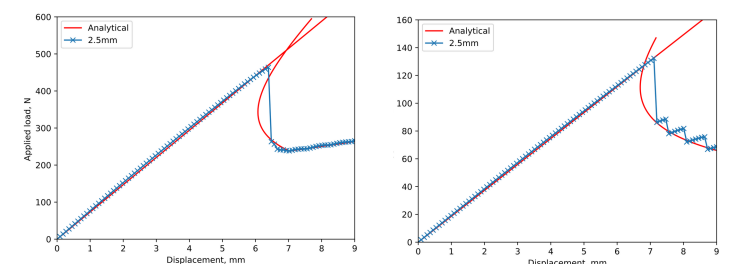
Figure 5: ENF load-displacement curves (left) and MMB (right) predicted with C1 structural CEs

Future work

In the future, this work will combine this structural element with Floating Node Method (FNM) to simulate matrix and fiber cracks.
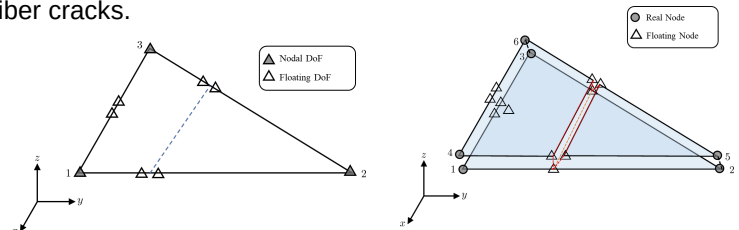
Figure 6: Applying FNM into both C1 ply element and CEs

References

[1] Turon, A., et al. "A damage model for the simulation of delamination in advanced composites under variable-mode loading." Mechanics of materials 38.11 (2006): 1072-1089.

Assembling nano/micro-structured ceramic-based composites into complex shapes

Moeen Akhtar, Diletta Giuntini

[1]Eindhoven University of Technology
[2]Graduate School Engineering Mechanics

Introduction

The biggest challenge in ceramics processing is enhancing their fracture toughness. Natural microstructures such as nacre, tooth, wood, etc. possess complex hierarchical structural arrangements and thus excellent properties. By successful transfer of technology from nature to engineering, these hierarchical microstructures can be a big aid in property enhancement for ceramics.

Scale-bridging and forming into complex shapes are other problems associated with the processing of ceramic materials, which can be addressed by using 3D printing technologies. Furthermore, the utilization of ultrafast sintering refines the nano/microstructure of the printed part resulting in further improvement of properties e.g., density, strength, toughness, etc.

Nature Inspired

Biomimicking has been a motivation for a long to develop sustainable and profitable technologies. Nature-inspired people have already developed ultrafast trains, sustainable buildings, self-cleaning glasses, and much more. Nacre possesses a brick-and-mortar structure and is best known for its fracture toughness. The fracture toughness of synthetic materials can also be improved by mimicking the structural arrangements (brick and mortar) of the nacre.
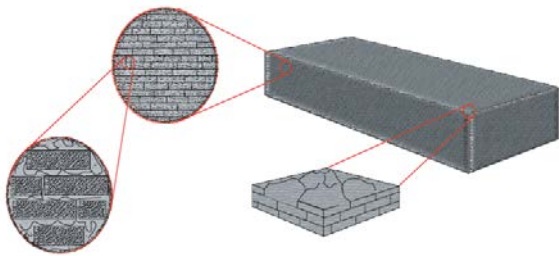
Objective

Direct ink writing of nature-inspired microstructures

Tailor the fabrication synthesis routes

Fracture toughness – Nature-mimetic structure

Complex shapes – 3D printing
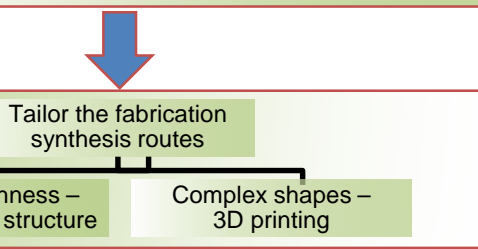
- Boost the mechanical properties of ceramics, especially fracture toughness.
- Improve the processability of ceramics into complex shapes.

Building Bridges

The combination of manufacturing technologies; 3D Printing, biomimicry, and ultrafast sintering will not only help us in improving the fracture toughness of the ceramics but also produce larger/ready-to-use products with specific microstructures in complex shapes.

Methodology

AL_2O_3 powder

3D printing slurry/ink

Direct Ink Writing (DIW) System
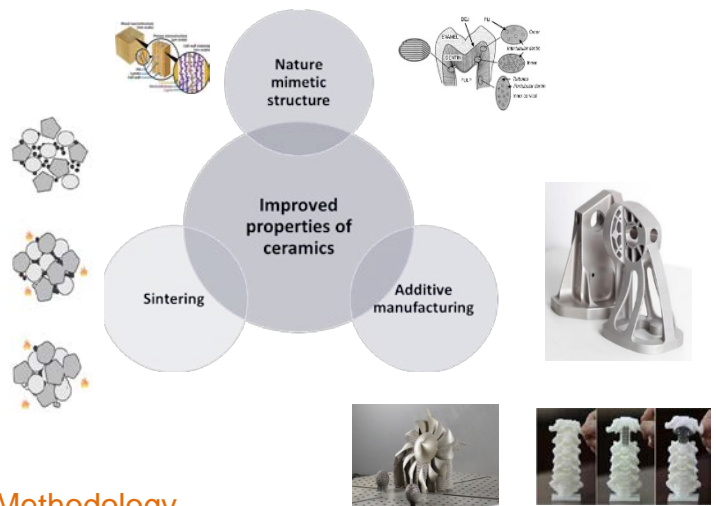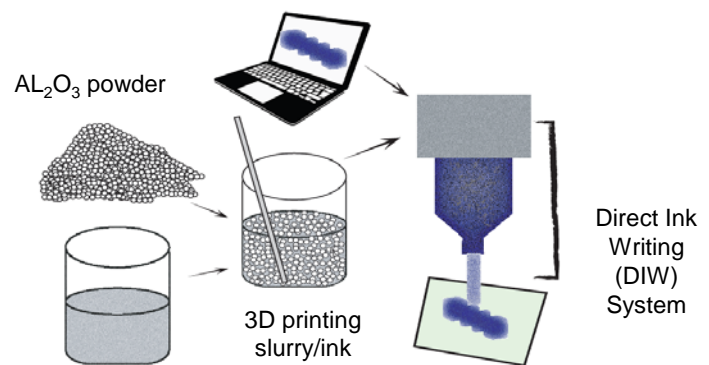
The aqueous solution with binders and other additives

Outlook

This project aims to develop specific nature-inspired microstructures to improve the fracture toughness of ceramics materials. The combined effect of different technologies would also contribute to overall microstructural refinement, material property improvement, and process flexibility/simplification. Our developed structures/materials would have enormous applications in the chemical industry, machinery, electronics, aerospace, and biomedical engineering.

References

[1] Wegst, U., Bai, H., Saiz, E. *et al.* Bioinspired structural materials. *Nature Mater* **14,** 23–36 (2015).

Technische Universiteit
Eindhoven
University of Technology

Multi-scale thermo-viscoelastic modelling of powder-based processes

J. E. Alvarez, H. Cheng, S. Luding, T. Weinhart

Multi-scale Mechanics, Thermal and Fluid Engineering, ET/Mesa+

UNIVERSITY OF TWENTE.

INTRODUCTION

This is a multi-scale framework to analyse powder-based multi-physics processes, e.g., **3D printing**. It computes particle-particle interactions at the microscopic scale (**DEM**) and large deformations at the macroscopic scale (**FEM**).

Heat transfer from granular sub-model to continuum sub-model

DEM   VC   FEM
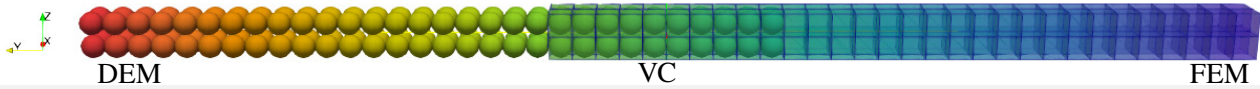
DEM: Discrete Element Method

Motion:
$$\frac{d\mathbf{v}_\alpha}{dt} = \frac{1}{m_\alpha}\left(\sum_{\beta=1}^{N}\mathbf{f}_{\alpha\beta} + \sum_{\gamma=1}^{N_W}\mathbf{f}_{\alpha\gamma}^{w} + \mathbf{f}_\alpha^b\right)$$

Heat transfer:
$$\rho_\alpha c_{p,\alpha}\frac{d\theta_\alpha}{dt} + \sum_{\beta=1}^{n_\alpha} k_\alpha(\theta_\beta - \theta_\alpha)\frac{a_{\alpha\beta}}{l_{\alpha\beta}} = \mathbf{Q}_\alpha$$
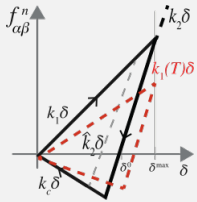
m_α : particle mass
v_α : particle velocity
$\mathbf{f}$: interaction force
ρ_α : particle density
$c_{p,\alpha}$: heat capacity
k_α : conductivity
θ_α : particle temperature
$a_{\alpha\beta}$: contact area
$l_{\alpha\beta}$: interacting distance
$\mathbf{Q}$: heat flux

k_1, k_2, k_c : loading, unloading, cohesive stiffness
δ : overalp, t : time

VC: Volume Coupling

Temperature diffuses from granular medium to solid medium.
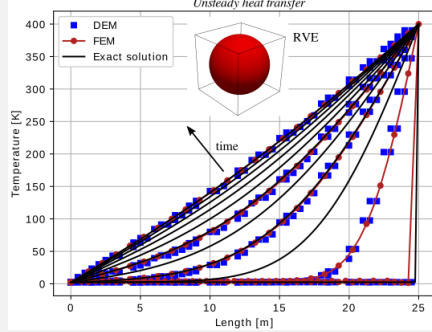
RVE: representative volume element.

FEM: Finite Element Method

Motion:
$$\int_V\left\{\sigma:\delta\varepsilon - \left(\mathbf{b} - \rho\frac{\partial^2\mathbf{X}}{\partial t^2}\right)\cdot\delta\mathbf{X}\right\}dV - \int_A\mathbf{t}\delta\mathbf{X}dA = 0$$

Heat transfer:
$$\int_V\left\{\rho c\frac{\partial T}{\partial t} - \mathbf{q}\delta\mathbf{X} - \mathbf{Q}\right\}\delta T dV + \int_A k\frac{\partial T}{\partial x}\mathbf{n}\delta T dA = 0$$
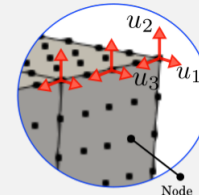
σ : stress tensor
ε : strain tensor
$\mathbf{b}$: body force
ρ : density
$\mathbf{X}$: local position vector
$\mathbf{t}$: traction
A : area
V : volume
c : heat capacity
k : conductivity
T : temperature
$\mathbf{n}$: normal vector
$\mathbf{Q}$: heat flux

u_i : nodal displacement

The heat flux balance and equilibrium equation of motion are solved simultaneously, and the volume coupling technique (**VC**) bridges the scales by satisfying energy, mass and momentum conservation.

MICROSCOPIC SCALE

Thermo-viscoelastic analysis - **MercuryDPM** [1].
Study: sintering rheology of polymers.
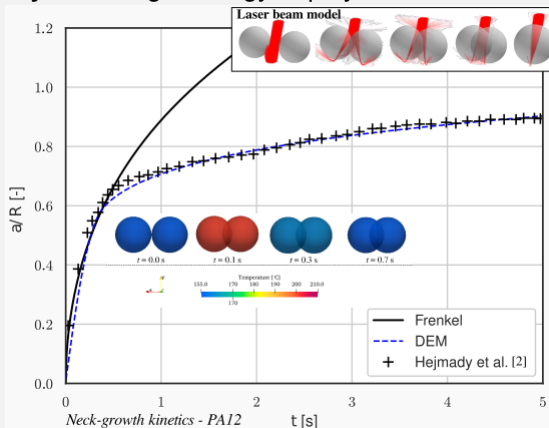
[1] T. Weinhart, et al. (2020) - MercuryDPM. COMPUT PHYS COMMUN.

[2] P. Hejmady, et al. (2022) - Laser sintering of PA12 particle pairs. ADDIT MANUFACT.

MACROSCOPIC SCALE

Thermo-viscoelastoplastic analysis - **oomph-lib** [3].
Study: deformation due to thermal expansion α.
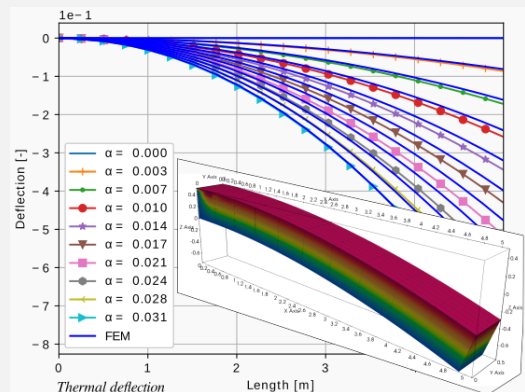
[3] Heil, M.,et al. (2006). - oomph-lib. SPRINGER.

CONCLUSIONS

- A Multiscale thermo-mechanical framework.
- Analysis of sintering kinetics at micro-scale.
- Study of large deformations at macro-scale.

UNIVERSITY OF TWENTE.   msm   PhD progress 1 2 3 4   MESA+ INSTITUTE FOR NANOTECHNOLOGY   MERCURYDPM

Neural networks with embedded physics-based material models to accelerate FE^2 simulations of path-dependent heterogeneous materials

M.A. Maia, I.B.C.M. Rocha, F.P. van der Meer

Delft University of Technology

Background

FE^2 is a powerful tool to model multiscale problems. However, the computational cost associated with the concurrent simulations is often prohibitive. Machine learning (ML) techniques can play a key role to help accelerating and thus enabling multiscale simulations for real-life applications [1].
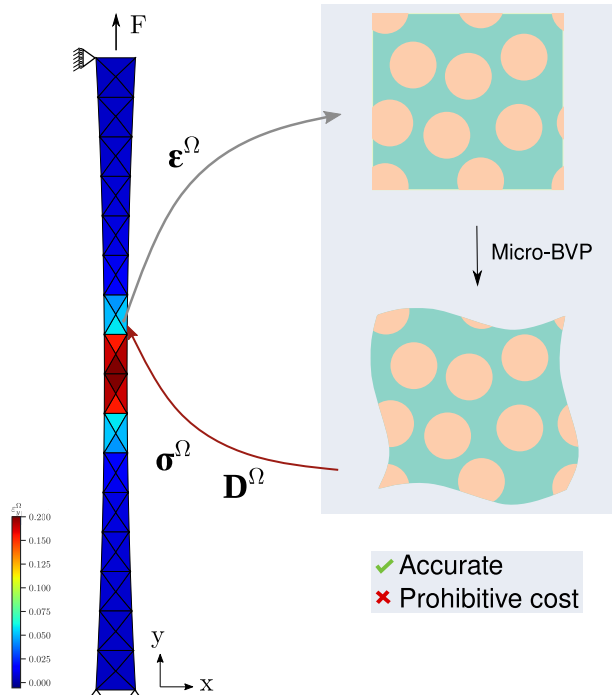
Figure 1: Schematic representation of FE^2

Neural Networks are among the most popular ML-based surrogate models. However, several issues related to their data-driven nature impede the reliable use of these models:
- Unique mapping between inputs and outputs
- Poor performance in extrapolation

Training data

In this work, the strain paths used for training the NN are sampled from Gaussian Processes (GPs).

Apply strain path & solve micro-BVP

$N_{samples}$

Compute stress

Each curve contains 60 pairs of ε^Ω - σ^Ω
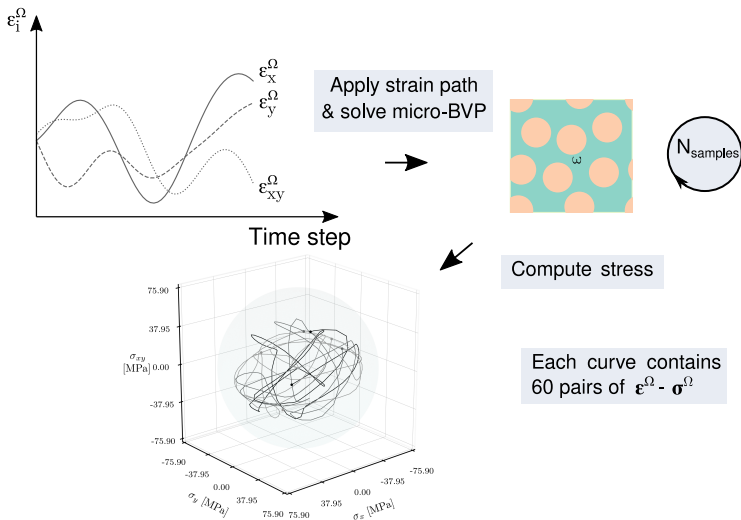
Figure 2: Generation of random loading paths using GPs

Present approach

An NN that learns **how to dehomogenize the macroscopic strains into a small set of representative (fictitious) material points and how to dehomogenize their responses to obtain the macroscopic stresses** is presented (Fig. 3). Since each material point keeps track of its own internal variables (α), path-dependence arises naturally.
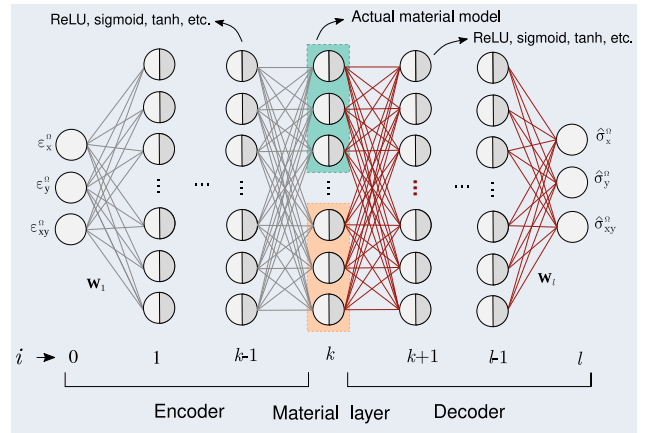
Figure 3: Proposed architecture

This feature also allows **networks trained on small datasets to capture complex path-dependent behavior** (see comparison with RNNs in Fig. 4).
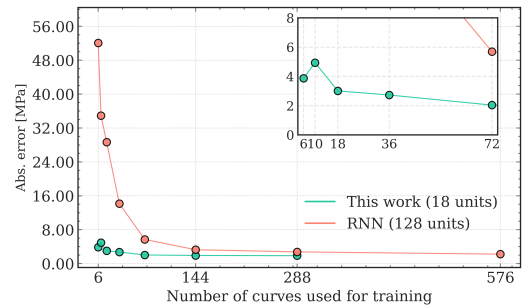
Figure 4: Average RMSE over test set with 100 unseen curves

Results

The tapered composite bar shown in Fig. 1 is solved using the presented NN. The training comprises 36 curves. The encoder and decoder are linear and the material layer consists of 6 fictitious material points. The matrix is described by an elastoplastic model and the fibers by an elastic model. **A speed-up of about 26000 is obtained with respect to the full-order FE^2 at limited loss of accuracy**.

RMSE: 8.47 N
Rel. RMSE: 4.8%

Full-order FE^2: 6 h
This work: 1 s
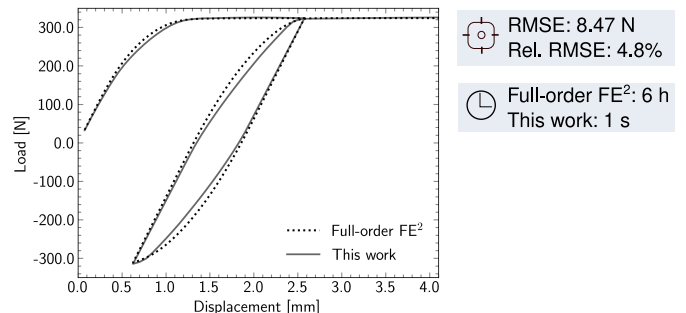
Figure 5: Load-displacement curve using full-order and proposed network

References

[1] I.B.C.M Rocha, P. Kerfriden, F.P. van der Meer. European Journal of Mechanics/A Solids, 2020.

PhD progress
1 2 3 4

SLIM MLAB LABS

Quantifying hydro-mechanical properties of vegetated soil

F. Anselmucci[1], H. Cheng[1], Y. Zeng[2], V. Magnanimo[1]

[1]*Soil MicroMechanics – Faculty of Engineering Technology, University of Twente*
[2]*Faculty of Geo-Information Science and Earth Observation (ITC), University of Twente*

Problem Background

Ground water table highly fluctuates during the seasons of the year. The presence of vegetation in soil has a key role on the in-situ instabilities. Hence, quantitative analyses need to be conducted to asses the influence of vegetation on the soil hydro-mechanical properties.

Problem Decompositions: How(s)

How can we understand in-situ root-soil-water interaction?
By separating the different phenomena involved in the process, and reproducing them at the laboratory scale?

- How do roots occupy pore space structure?
  How does water flow in the pore network?
  (**x-ray CT**)
- How can we relate leaves growth with root development? (**ASD-RLD-RMF-LAI**)
- How does root change the soil retention properties? (**SWRC**)

Goal

Obtain the link between laboratory measurements and estimating methods to quantify the evolution of 4D soil properties when a living inclusion is growing and changing the pores microstructure.
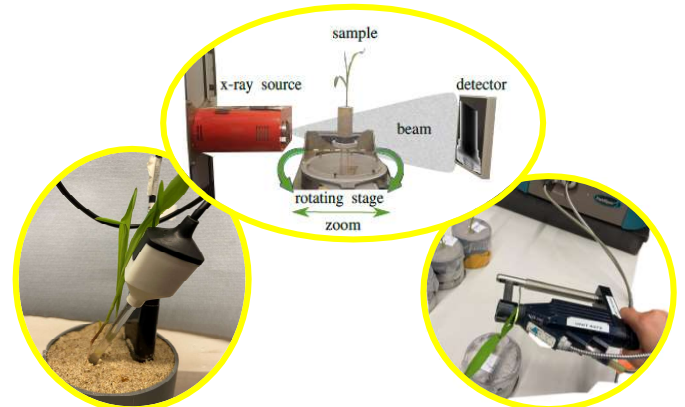
Figure 1: Tensiometer and moisture sensor installed in a vegetated sample (on the left), X-Ray scan setup (center), spectrometer (on the right).

Findings on the root-soil interactions, obtained so far…

From the x-ray CT, we can obtain:

a. Root System 4D growth

b. Soil Structure evolution

c. Pore Network Saturation Degree

d. Bulk Retention properties

3,5cm
5cm
10mm

Root Diameter[mm] <0,1 >0,8
Particle displacement[mm] <0,24 >1,2
Volumetric Strain[%] <-4 >4
Shear Strain[%] <0,05 >10
Saturation Degree[%] 0 >80
Root Length Density[cm/cm³] 0,1 1,6

Saturation Degree[%]
Suction [kPa]
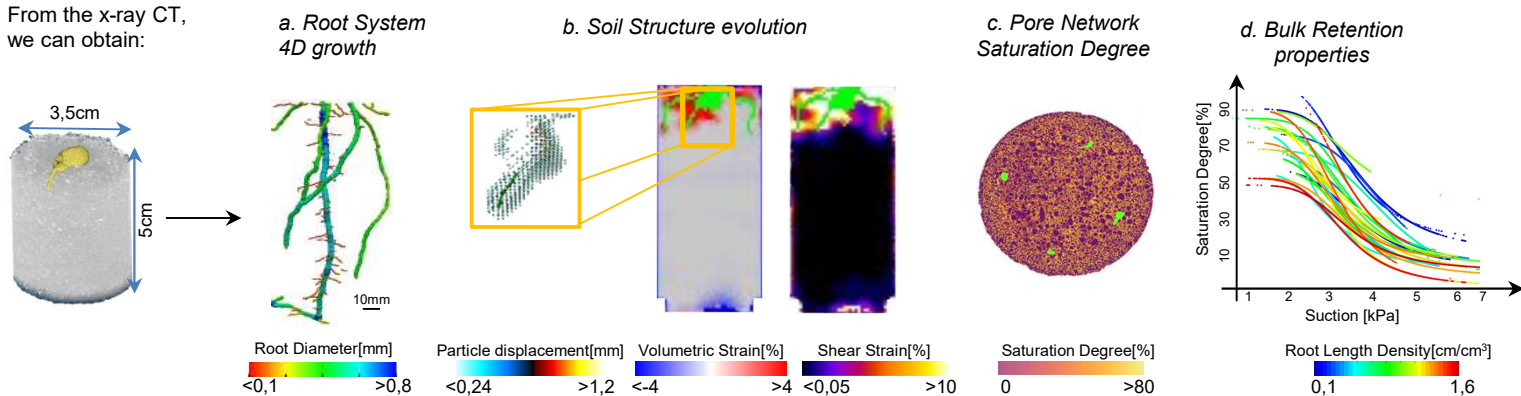
Take home messages

Exact identification of root quantity and position allow the understanding of the evolution of soil properties:
- At the Microscale, root shears soil and this induces a Volumetric soil Deformation in the spatial vicinity.
- The Saturation Degree detected at the pixel scale, matches the global Volumetric Water content detected through sensor.
- At the Macroscale, the retention properties of the soil depend on the root length density within the volume.

What's next?

- Quantify the effect that seasonal wet-dry cycles has on pore structure. Understanding this phenomenon at the microscale, will help the understanding of in-situ behavior when the seasonal water-ground level fluctuation occurs.
- Apply the experimental investigation to the development of a constitutive model able to predict the hydro-mechanical response of rooted soil.

References

[1] Cheng,H., *et al.,* 2022. Down to the root of vegetated soil: challenges and state-of-the-art. *Papers in Physics*, Accepted.
[2] Anselmucci, F., *et al.,* 2021. Imaging local soil kinematics during the first days of maize root growth in sand. *Scientific reports*, *11*(1), pp.1-13.
[3] Anselmucci, F., *et al., 2021.* Use of X-ray tomography to investigate soil deformation around growing roots. *Géotechnique Letters* 11, no. 1, 96-102.

UNIVERSITY OF TWENTE.

PostDoc progress
1 2 3

Towards Robust Laser Assisted Fibre Placement
Adapting the process to the incoming material properties

T.J. Asijee[1,2], W.J.B. Grouve[2], E.T.M. Krämer[1], M.I. Abdul Rasheed[3]

[1]ThermopPlastic composites Research Center, [2]UT - Production Technology, [3]UT - Applied Mechanics and Data Analysis
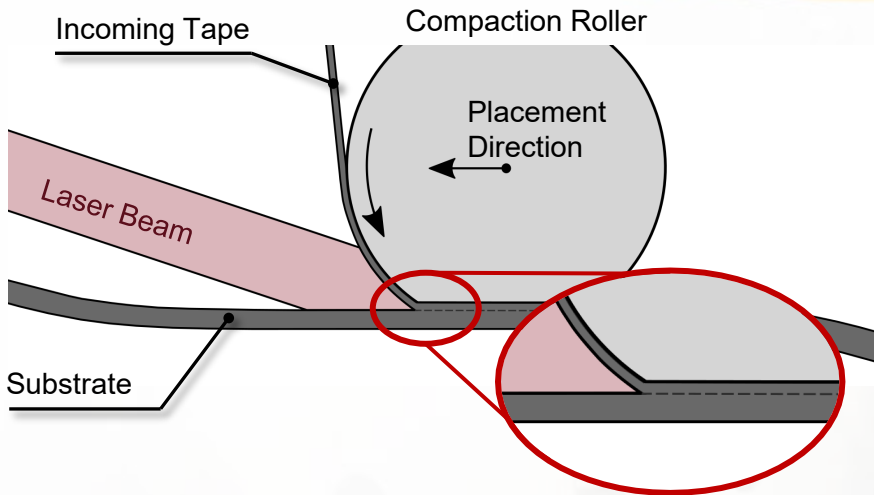
Research Goals

➢ Investigating **material** and **process variability**

➢ Maintaining **nip-point process temperature**

➢ Robust process with **temperature control** (material based)

Motivation: Towards In-Situ Consolidation

Laser assisted fibre placement (LAFP) and laser assisted tape winding (LATW) pose unique opportunities for the aerospace and automotive industry to manufacture **thermoplastic composite** (TPC) structures at large scale. LAFP technologies provide a high degree of automation, offering a scalable solution to meet the increasing demand for lightweight structures. Moreover, **in-situ consolidation** during LAFP has the potential to serve as a **cost-effective** single step manufacturing process for thermoplastic composites.

Process Temperature Measurements

Uniform nip-point temperature is desired (~380°C) but is challenging to maintain due to material variation.
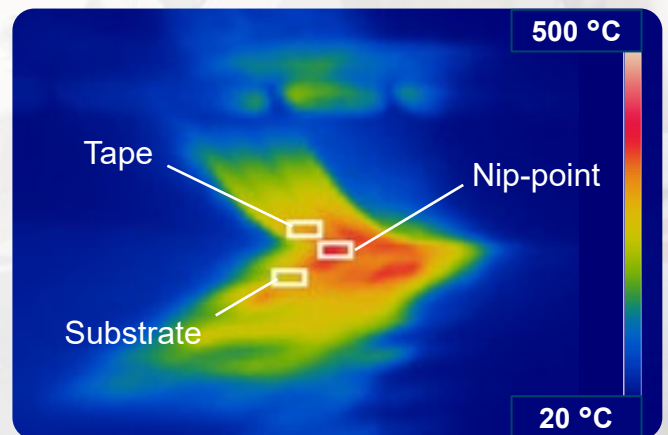
Figure 2: Measured temperature distribution during fibre placement, with temperature variations in the tape

Research Approach
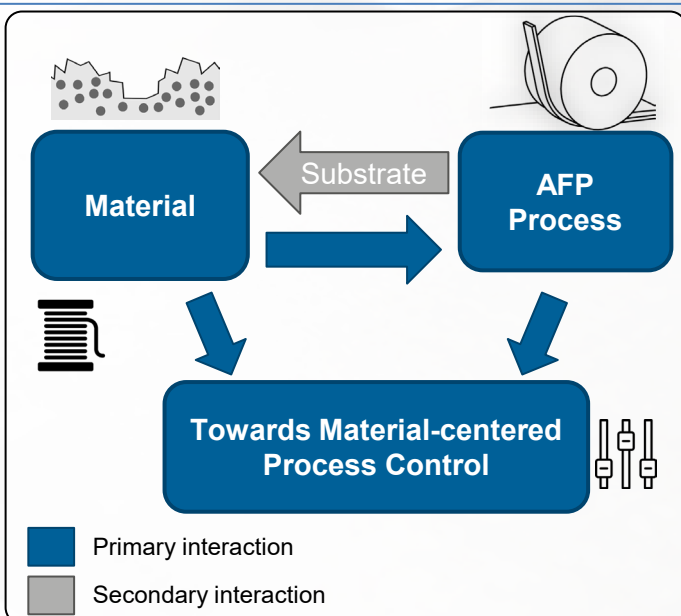
Figure 1: Flowchart depicting the research domains considered, with the interactions between them

Next Research Steps

More research is needed into the **material properties** relevant for laser heating (e.g., optical reflectance, roughness, etc.)

Once the material variation is quantified, **opto-thermal models** will be used to predict the expected variation in temperature

With the results of the previous steps, a surrogate model will be used to **connect** the **material & process** while observing variations in the material properties with an **in-line monitoring system**

THERMOPLASTIC COMPOSITES RESEARCH CENTER

PhD progress
| 1 | 2 | 3 | 4 |

UNIVERSITY OF TWENTE.

More information?

Visit the project page

Contactless Position Control of Offshore Wind Turbines during the Installation

P. Atzampou, A. Metrikine, A. Tsouvalas, P.C. Meijers
Delft University of Technology

Introduction:

In order to develop a contactless technique for control and positioning purposes, the design and modelling is initiated from the excitation of a hanging payload through a contactless magnetic interaction.

Dynamic System:

The characteristics of the dynamic system studied are the following:

- 1DOF Point mass pendulum (Model & Experiment).
- Permanent magnet-Electromagnet actuator interaction.
- Fixed reference and small angle approximation.
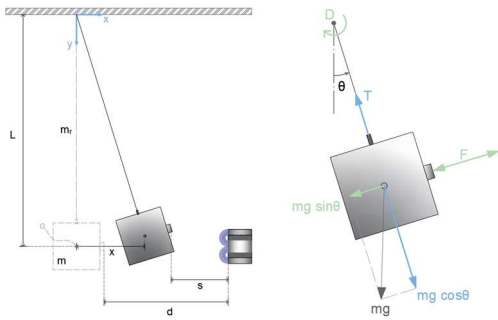
Figure 1: a. Simulation Set-Up, b. Free Body Diagram

Equation of Motion:

$$\left(mL^2 + \frac{m_r L^2}{3}\right)\ddot{\theta} + \left(mgL + \frac{m_r}{2}gL\right)\theta = D\,L + F\,L$$

where:

$$D(N) = sign(\dot{\theta})\,\mu_T \qquad \textit{Damping Force}$$

$$F(N) = \frac{\alpha\,V(t)}{(L\theta(t) - d)^3} \qquad \textit{Electromagnetic Force}$$

$$d(mm) \in [25, 75] \qquad \textit{Initial Separation}$$

Free Vibrations:

These data sets resulted in the determination of the natural frequency (ω_n) of the system and the damping calibration of the numerical model.

D: Coulomb Friction [1]
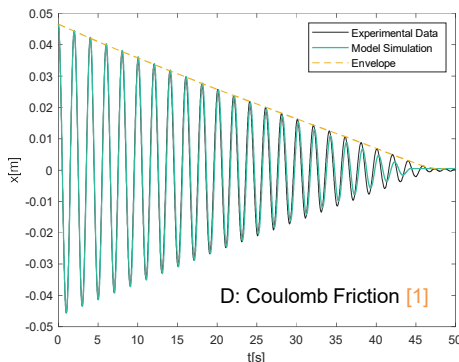
Figure 2: Dissipation of the Free Vibrations

Forced Vibrations:

The system is subjected to an external excitation force F of a harmonic oscillating V(t), while different cases of forcing amplitudes and frequencies are studied as well as the experimental and numerical data are juxtaposed.
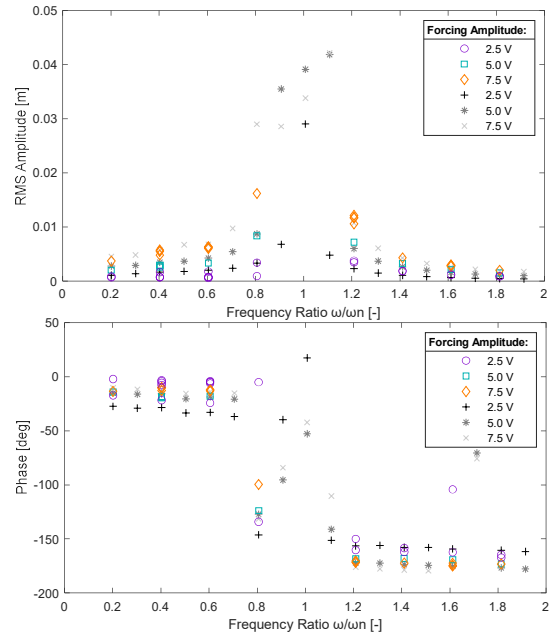
Figure 3: Response & Phase Spectrum of the Experimental (colour) and Modelled (greyscale) data

Results:

- ✓ Validation of one natural frequency for a 1DOF system.
- ✓ Characteristic phase shift π in the response after resonance.
- ✓ Lowest deviation between model and experiments for higher amplitudes of excitation.
- ✓ Both simulations predicted instability when $\omega/\omega_n \approx 1$.

Excitation (V): 7.5 sin(2 π 0.4 t)
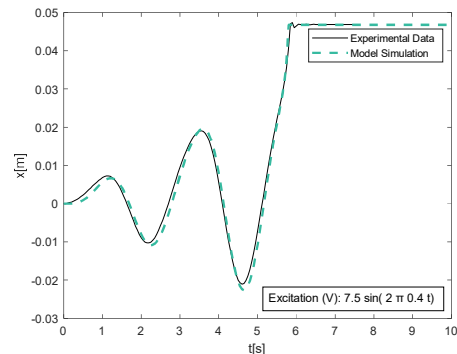
Figure 4: Displacement Time Series for ω/ω_n =0.80 & A=7.5V

References:

[1] Giacomo, T., & Peranzoni, P. (2009) The Real Pendulum: Theory, Simulation, Experiment. Lat. Am. J. Phys. Educ. Vol. 3, (2).

PhD progress

| 1 | 2 | 3 | 4 |

Comparison of data-based and physics-based Model order reduction

Phani Ram Babbepalli [1], Olaf van der Sluis [1,2], Joris J.C Remmers [1]

[1] Eindhoven University of Technology
[2] Philips Research Laboratories

Introduction

The pan-European ITEA3 Project UPSIM aims to accelerate innovation and reduce development costs by generating credible digital twins. One use case is to generate a digital twin of the medical imaging catheter. To this extent, efficient model order reduction techniques are being developed.
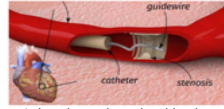
Figure 1: Imaging catheter in a blood vessel [1]

Model Order Reduction

Model order reduction (MOR) is a technique to construct a simpler model from a more complex one. In solid mechanics, projection-based model order reduction is widely used [2], where a lower-order representation of the displacement is assumed to be available through a projection function.

$$\vec{u} \approx \boldsymbol{\Psi} \vec{q} \quad \boldsymbol{\Psi} : \mathbb{R}^N \to \mathbb{R}^n ; n << N \tag{1}$$

Two linear projection-based MOR approaches are considered, one data-based (POD-based MOR) [2] and the other being the physics-based approach (Linear Manifold) [3].

Offline Phase

Data based Method

Generation of Training data
$X_{N \times p} := [\vec{u}_1 \ \dots \ \vec{u}_i \ \dots \ \vec{u}_p]$

Dimensionality reduction technique
SVD
$X_{N \times p} \approx U_{N \times r} \Sigma_{r \times r} V_{r \times p}^T$

Left singular matrix as the projection matrix
$\boldsymbol{\Psi} := U_{N \times r}$

Physics based Method

Eigen value analysis
$[\mathbf{K_0} - \omega_i^2 \mathbf{M}] \vec{\phi_i} = 0 \ \mathbf{K_0} = \left. \frac{\partial \vec{f}_{int}}{\partial \vec{u}} \right|_{\vec{u}=0}$

Enhancing the vibration modes by Modal derivatives
$\mathbf{K_0} \frac{\partial \vec{\phi_i}}{\partial q_j} = -\frac{\partial \mathbf{K_0}}{\partial q_j} \vec{\phi_i} ; \vec{\theta}_{ij} = \frac{\partial \vec{\phi_i}}{\partial q_j}$

Inserting the modal derivatives to form the projection matrix
$\boldsymbol{\Psi} := [\cdots \ \vec{\phi_i} \ \cdots \ \vec{\phi_n} \ \cdots \ \vec{\theta}_{ij} \ \cdots]$

Online Phase

Estimating displacement
$\vec{u} = \boldsymbol{\Psi} \vec{q}$

Projecting the equation onto reduced space
$\boldsymbol{\Psi}^T (\vec{f}_{int} - \vec{f}_{ext}) = \vec{0} ; \mathbf{K} = \frac{\partial \vec{f}_{int}}{\partial \vec{u}}$

Iterative Procedure to Solve for $\Delta \vec{q}_j$
$[\boldsymbol{\Psi}^T \mathbf{K} \boldsymbol{\Psi}] \Delta \vec{q}_j = \boldsymbol{\Psi}^T \Delta \vec{f}_j$
$\tilde{\mathbf{K}} \Delta \vec{q}_j = \Delta \vec{\zeta}_j$

Reconstruction to original space
$\Delta \vec{u}_j = \boldsymbol{\Psi} \Delta \vec{q}_j$
$\vec{u}_j = \vec{u}_{j-1} + \Delta \vec{u}_j$

Figure 2: Flow chart for projection-based MOR

MOR example
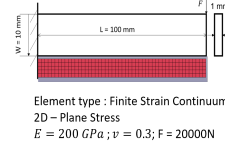
Element type : Finite Strain Continuum
2D – Plane Stress
$E = 200 \ GPa ; v = 0.3; F = 20000N$

A geometric nonlinear cantilever beam is used for comparing data-based and physics-based MOR. In the offline phase, modes in POD-based MOR and the modal derivatives in LM are calculated. In both LM and POD based MOR, the mode/modal derivatives are added in a sequential order to increase the size of $\boldsymbol{\Psi}$. For example, LM4 represents use of 4 modal derivatives and the 1st eigen mode and in P0D4, the first 4 modes from SVD are used.
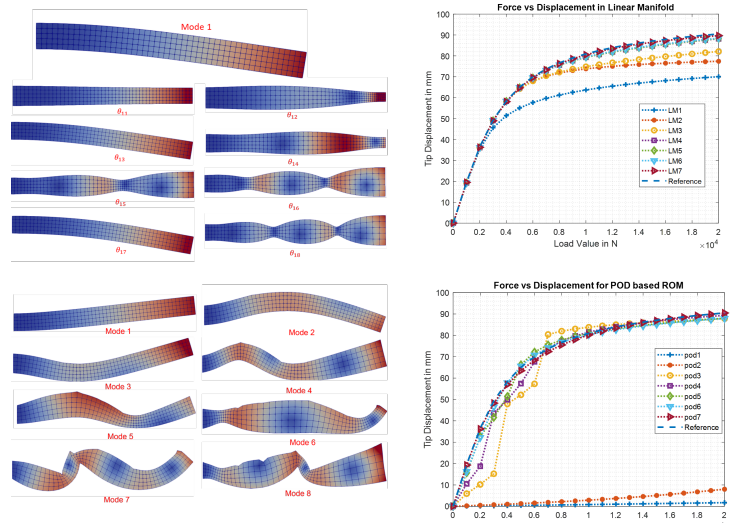
Figure 3: Force displacement curve for different LMs and POD-based MORs
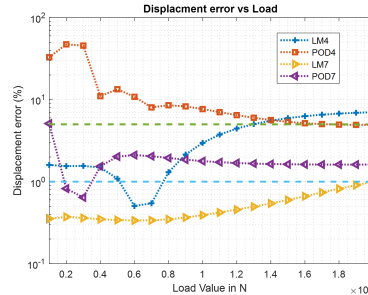
Figure 4: Displacement error vs load for different MORs

ROM	Projection Function	e_d
LM4	$\boldsymbol{\Psi}: \mathbb{R}^{612} \to \mathbb{R}^5$	7.08
POD4	$\boldsymbol{\Psi}: \mathbb{R}^{612} \to \mathbb{R}^4$	4.95
LM7	$\boldsymbol{\Psi}: \mathbb{R}^{612} \to \mathbb{R}^8$	0.95
POD7	$\boldsymbol{\Psi}: \mathbb{R}^{612} \to \mathbb{R}^7$	1.62

Conclusions and Future Outlook

Linear manifold works better in comparison to POD-based MOR for problems involving geometric nonlinearity. In POD-based MOR, the solution does not match at every load step and the final error is also more in comparison to the linear manifold with the same number of modes. The next steps would be

- To develop a reliable mode participation parameter for both MORs
- To develop an efficient data set for POD-based MOR

References

[1] Stoute, R., et al (2016), Procedia Engineering, 168, 1563–1567.
[2] Hernández, J. A., et al (2017), Computer Methods in Applied Mechanics and Engineering, 313, 687–722.
[3] Jain, S., et al (2017), Computers & Structures, 188, 80–94.

PhD progress
| 1 | 2 | 3 | 4 |

Simulating the power extraction of a dense wave energy converter array with different levels of power take-off adaptability

A. Bechlenberg[1], Y. Wei[2], B. Jayawardhana[3], A.I. Vakis[1]

[1]CMME, ENTEG, FSE, University of Groningen
[2]Eastern Institute of Technology, Ningbo, China
[3]DTPA, ENTEG, FSE, University of Groningen

The Ocean Grazer

Increasing renewable energy generation is a necessity more than a luxury for the short- and long-term future. Herein, we study a concept complementary to other commercially available renewable energy generation systems to determine how much power it can contribute to an offshore energy farm.

The Ocean Grazer is a hybrid wind-wave-storage device for the offshore environment. This research focuses on the wave energy subsystem of the device. Wave energy is captured by **a dense wave energy converter (WEC) array** structured as shown in Fig.2. All WECs are connected to hydraulic power take-off (PTO) systems (Fig.3) which translate the heave motion of the floaters into potential energy [1].
To maximize the power output of the array through adaptability, a **transmission ratio (α)** is placed between the WEC and PTO. Different levels of adaptability are compared in 3 cases.

Figure 2: WEC array configuration [2]

Figure 3: Floater and PTO system of the OG [2]

Methodology – Mixed Frequency/Time Domain Model

To study the power extraction of the WEC array in more realistic **sea states**, a model is created that includes irregular forces from the excitation forces, the radiation effects between the floaters and the nonlinear forces of the PTO system.

This mixed frequency/ time domain (MFT) [2,3] model's main functions are depicted in Fig.4: **Step 1** – Generation of matrix form equations of motion of the system for each time window of the total simulation
Step 2 – Division of time windows into time steps for which the equations of motion are solved with MFT
Step 3 – Computation of the PTO forces in time domain
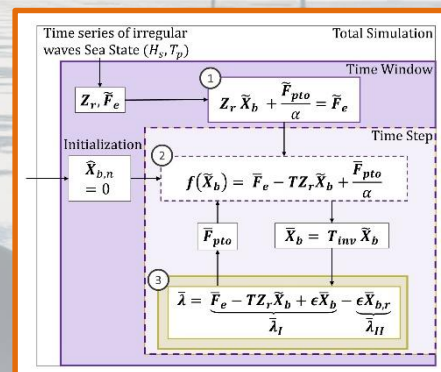
Figure 4: Flowchart of Model applied to simulate the nonlinear forces acting on the WEC array in irregular sea states

Figure 1: Artistic interpretation of the Ocean Grazer 3.0

Results – Performance captured through the Capture Factor

The WEC array performance is studied in a range of sea conditions and summarized in a power matrix which can be combined with the scatter diagram of a location to calculate the annual energy production of the device in a chosen ocean location [4]. In the same format, the **capture factor** can be depicted (seen in the Figure 5 below): this describes **how much of the potential energy (of the incoming wave) is absorbed by the WEC array.**

Case 1 – the transmission ratio stays **constant** for the entire sea state simulation

Case 2 – the transmission ratio adapts for each time windows of the simulation **with a restriction**

Case 3 – the transmission ratio **adapts without restriction** in each time window of the simulation
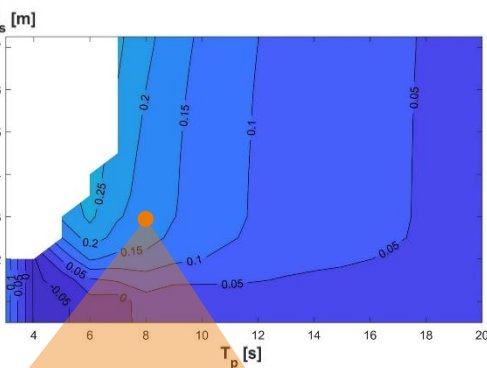
In the selected Sea State, the power extraction percentage per floater within the array is depicted here
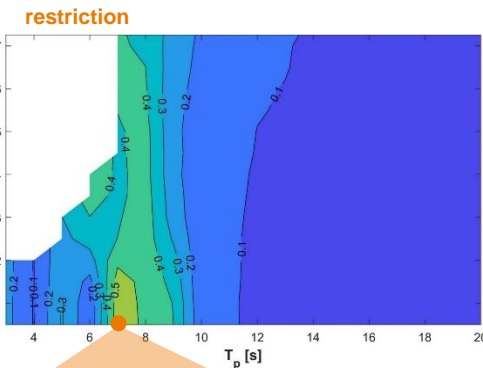
With higher adaptability, the power absorption becomes more evenly distributed throughout the array
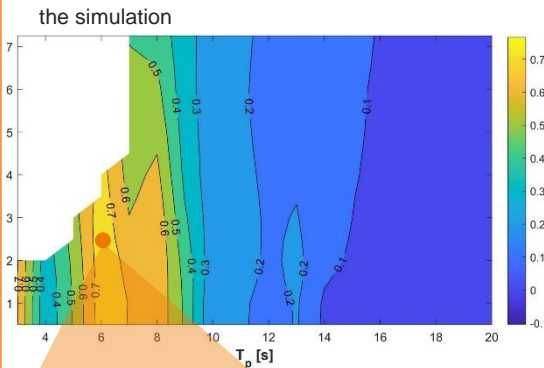
Scan the QR codes to see how this percentage changes with different α values (Case 1) and in consecutive time windows (Case 2 & 3)

Figure 5: (a) Capture Factor and distribution of power extracted within one sea state with constant α= 2,0 for Case 1

(b) Capture Factor and distribution of power extracted within one sea state for Case 2

(c) Capture Factor and distribution of power extracted within one sea state for Case 3

Conclusions and Future Steps

Adapting the PTO force with the transmission ratio shows increase in total power extraction and an even distribution of power extraction within the array. This can be improved further: at the moment, the transmission ratio is constant for all floaters in the array, while with additional complexity to the model, it would be possible to apply different transmission ratios for each floater to enhance the above mentioned advantages.

References

[1] Wei Y., Barradas-Berglind J.J., Van Rooij M., Prins W.A., Jayawardhana B., Vakis A.I. Investigating the adaptability of the multi-pump multi-piston power take-off system for a novel wave energy converter. Renewable Energy 111, 598–610 (2017). http://doi.org/10.1016/j.renene.2017.04.042

[2] Wei Y., Bechlenberg A., Van Rooij M., Jayawardhana B., Vakis A.I. Modelling of a wave energy converter array with a nonlinear power take-off system in the frequency domain. Applied Ocean Research 90, 101824 (2019). http://doi.org/10.1016/j.apor.2019.05.009

[3] Wei Y, Bechlenberg A, Jayawardhana B, Vakis AI. Modelling of a wave energy converter array with non-linear power take-off using a mixed time-domain/frequency-domain method. IET Renew. Power Gener. 2021;1–12. https://doi.org/10.1049/rpg2.12231

[4] Bechlenberg, A., Wei, Y., Jayawardhana, B., & Vakis, A. I. (2022). Analysing the influence of power take-off adaptability on the power extraction of dense wave energy converter arrays. arXiv preprint arXiv:2207.07525. https://doi.org/10.48550/arXiv.2207.07525

PhD progress
1 2 3 4

Microstructure evolution during fusion bonding processes of thermoplastic composites

S. Bentalib[1,2], M. van Drongelen[1], E. T. J. Klompen[2], L.E. Govaert[1,3]

[1] *Production Technology, University of Twente, 7522 NB Enschede*
[2] *Thermoplastic Research Center, 7521 PN Enschede*
[3] *Eindhoven University of Technology*

Motivation

Improving vehicles fuel efficiency through mass reduction, is one method to reduce greenhouse emissions. An appropriate material choice is the first step toward this transition, and thermoplastic composites (TPC) are excellent candidates. The preferred joining method involves local melting of the pre-fabricated substrates, consolidation, with dissolution of the interface, and finally cooling. Different phenomena, such as fibres migration, crystallization and build-up of stresses, will significantly influence the resulting joint mechanical performance. A holistic multiscale approach, connecting all of the aforementioned events, is still absent, and its definition would allow for TPC large-scale implementation.

Research objective

This research aims to contribute, to the general goal, by modelling the melting and crystallization kinetics in presence of a high fibre content, within the processing window of a semi-crystalline polymer. The evolving rheological properties will be also characterized: to predict non-isothermal multiphase flow in a porous medium, and to assess the time needed to fully heal the interface. Three processing methods will be considered, namely overmoulding, induction welding and ultrasonic welding.

Approach

Firstly, differential scanning calorimetry is used to investigate the effects of different processing parameters, such as cooling rates and dwell temperatures. The most evident consequences are cold-crystallization occurrence, shown in figure 1, and higher crystallization temperatures, linked to melt-memory effects, as shown in figure 2. Secondly, polarized optical microscopy is chosen to monitor crystal growth and to inspect the morphological features.
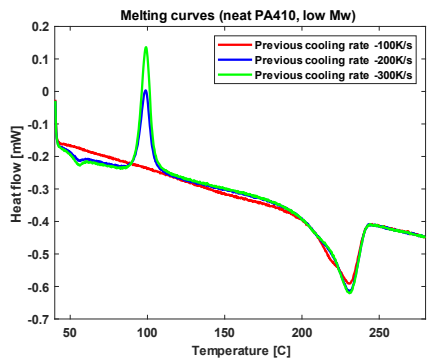
Figure 1: melting curves after cooling at different rates (from Flash DSC).
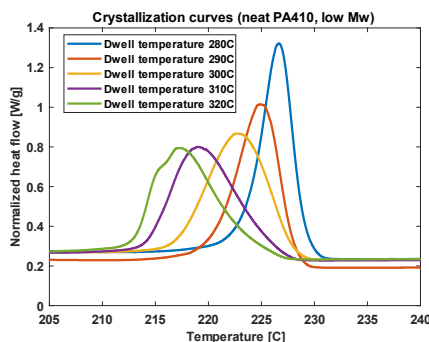
Figure 2: crystallization curves for different dwell temperatures (from regular DSC).

Schematic representation of the induction welding process with some insights on a micro-scale.
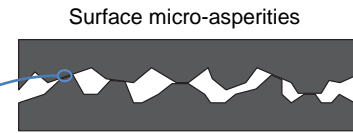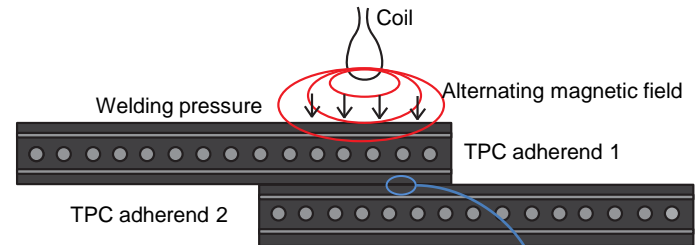
Heating

$$t_{ic} \propto \frac{\eta(T)}{P}$$

Time needed for full contact is directly proportional to the matrix viscosity.

Macromolecules diffuse across the interface.

Entanglements
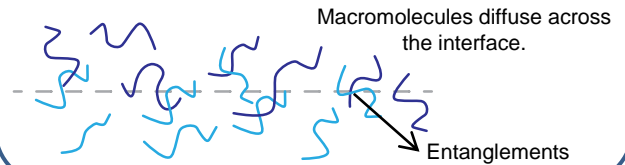
Cooling

The resulting crystalline structure depends on multiple factors: thermomechanical history, molecular weight of the polymer etc.
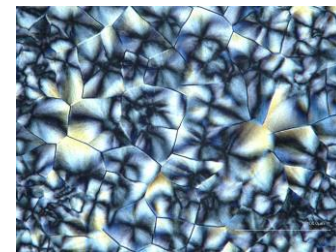
Crystalline phase of PA410 neat resin.

Future work

Enhanced material characterization to describe in detail solidification and melting behaviours:

- Melt-memory effects via DSC;
- Structural characterization via X-ray techniques;
- Determination of viscoelastic material behaviour via rheology.

UNIVERSITY OF TWENTE.

PhD progress
1 2 3 4

TPRC   NWO   m2i

Soft actuator modelling
Life after the Constant Curvature assumption

M.W. Berghuis[1], A. Stanic[1], A. Sadeghi[2], B. Rosić[1]

[1]Chair of Applied Mechanics & Data Analysis, University of Twente
[2]Department of Biomechanical Engineering, University of Twente

What's missing?

Tendons **+** Fiber reinforced pneumatic chambers **+** Silicone body **+** **?** **=** Antagonistic segment
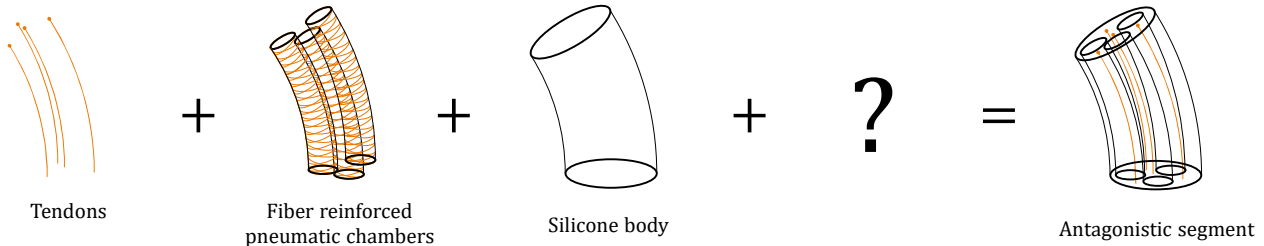
Microcontinua: model foundations

MICROMORPHIC
Deformable directors

→

MICROPOLAR
(Cosserat)
Rigid directors

→

CLASSICAL
No directors

Slender geometry, rigid cross sections

Projection onto finite basis
e.g. constant curvature (CC)

Weak formulation

Projection onto finite basis
e.g. piecewise linear

Discrete Cosserat rod model

Finite element model
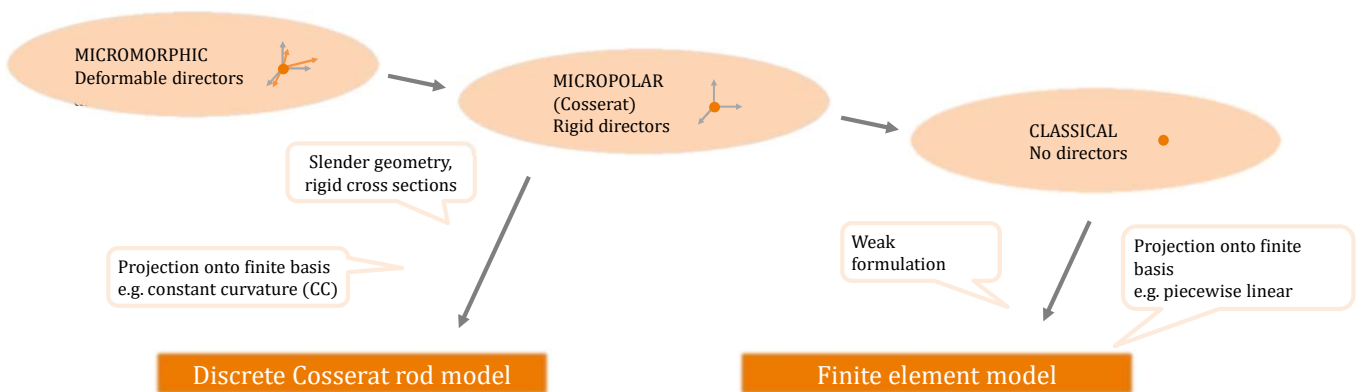
Excellent for fast modelling of **rods, cables, reinforcement fibers** …

… but very limited in modelling complex geometries, multibody structures, nonlinear material laws, volumetric deformations …
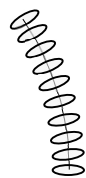
If the classical continuum is a special case of the micropolar continuum…
… can we 'couple' these models?

Excellent for high fidelity modelling **complex geometries, multibody structures, nonlinear material laws, volumetric deformations** …

… but too expensive in modelling simple rods, cables, reinforcement fibers …

Current work

- High fidelity FEM in Abaqus SIMULIA™ by Dassault Systèmes®
- Individual actuator / sensor / body models
- Tendons and fibers: slender beams and custom connectors
- Mesh dependence studies

Tendon actuator – soft silicone matrix interaction

Fiber reinforcement – soft silicone matrix interaction
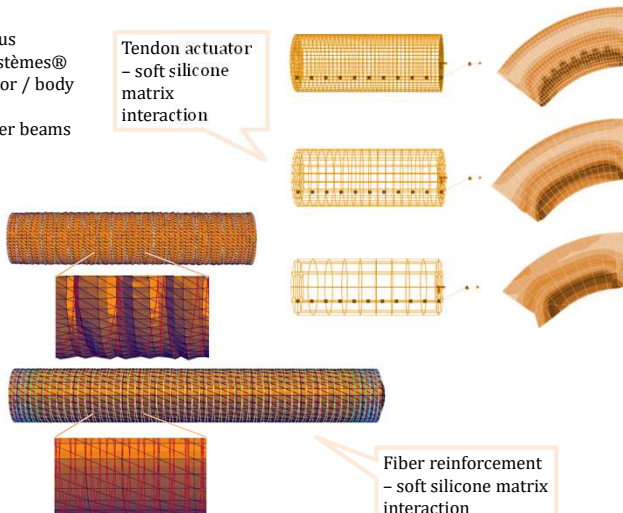
Future work

- Merge FEM actuators to antagonistic segment
- Define parametric (Cosserat) model
- Cast parametric model problem in stochastic setting
- Update the model parameters with a Bayesian approach

- Experimental validation high fidelity model
- Multiple segments in series

Contact details
m.w.berghuis@utwente.nl
www.linkedin.com/in/minke-berghuis

UNIVERSITY OF TWENTE.

PhD progress

| 1 | 2 | 3 | 4 |

Towards understanding wear particle generation on silicon wafers

T. Bertens[1], K. van den Broek[2] and J.P.M. Hoefnagels[1]

[1]Eindhoven University of Technology
[2]VDL Enabling Technologies Group

Introduction and problem statement

Particle driven contamination hampers the manufacturability of semiconductors. The interaction between the wafer material (silicon Si) and the manufacturing equipment instigates wear and generates wear particles, illustrated in Figure 1.

The instigation of wear is thought to originate from the phase transformations present in silicon during indentation and scratch loading. The how, when and where of these phase transformations is relatively poorly understood. Hence, experimental testing is employed to increase the understanding on the phase transformations of Si under changing loading conditions.

Figure 2: AFM scan ($A = 100 \ \mu m^2$) of DLC coating, height of asperity $h \approx 0.8 \ \mu m$.

Phase transformation

In-situ quasi-static indents, using a Bruker PI-89 Pico-indenter equipped with a Berkovich tip, were performed under varying loading conditions to determine when 'Pop-out', discontinuity in load-displacement curve attributed to phase transformation, occurs [3]. Initial scratch tests resulted in plastically deformed Si chips, see Figure 4. Formation of these chips is the following research inquiry.
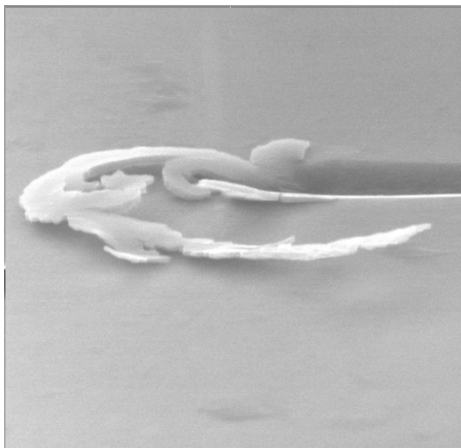
Figure 4: Plastically deformed silicon under lateral and normal load. Field of view is $10x10 \ \mu m^2$.

Figure 1: Wear particle formation on silicon wafer. Nominal contact area $D \approx 43 \ \mu m$.

Contact surface measurements

From literature [1-3] it is known that the phase transformations in Si are highly dependent on the loading conditions, and geometry of the contacting surface. An Atomic Force Microscopy (AFM) scan of the diamond-like-carbon (DLC) coating is shown in Figure 2. Statistical analysis of two DLC samples led to a characteristic value for roughness and asperity tip radius.

Figure 3: Indentation unloading curves on Si (100), where from right to left P_{max} and $\dot{P}_{unload}$ decreases. Occurrence of pop-out as a function of P_{max} and $\dot{P}_{unload}$.

References

[1] J. Jang et al., (2005), DOI: 10.1016/j.actamat.2004.12.025
[2] H. Huang, J. Yan, (2015), DOI: 10.1016/j.scriptamat.2015.02.008
[3] S. Ruffel et al., (2007), DOI: 10.1063/1.2781394

Modelling combined necking/cracking interaction

S. Bhattarai, L.J. Sluys

Faculty of Civil Engineering and Geosciences, Delft University of Technology

Introduction

Thin structures subjected to extreme loading undergo large inelastic deformation, leading to the formation of high-strain localized zones. Scenarios in which necking and cracking are present and interact are modelled. Also, the effect of the traction separation law on the evolution of necking and crack propagation is studied.

Methodology
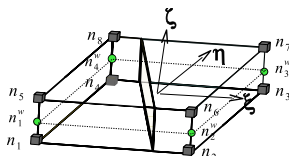
Figure 1: *Solid-like shell element with discontinuity[1]*

A traction separation law (TSL) based on a mixed-mode damage law is implemented with a shift to mimic the rigid behavior and equilibrium between bulk stress and traction in a cohesive surface [2]. XFEM is used with a solid-like shell element (Figure 1) to model cracking and the through thickness deformation.

Results

DCB test:

The numerical results of Mode I tearing of a plate, simulated by Woelke et al. [3], show good resemblance with experimental results (Figure 2) in terms of the peak load. As the crack propagates through the width of the plate, a neck evolves ahead of the crack tip (Figure 3). The accumulation of deformation in the necking region ahead of the crack tip is mesh dependent.
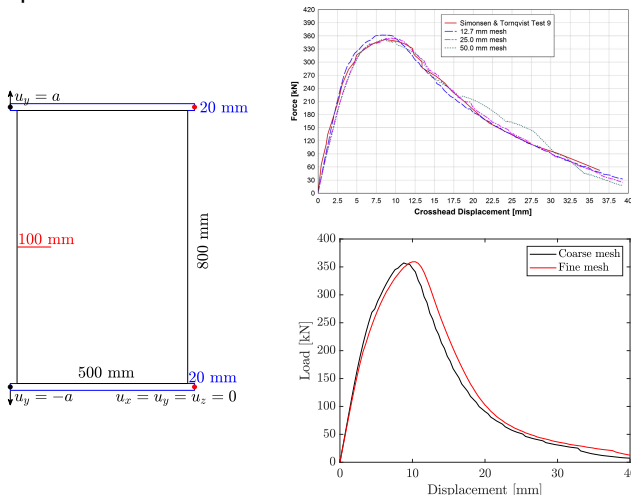
Figure 2: *Mode I fracture test of an aluminum plate and comparison with results from Woelke et al. [3]*
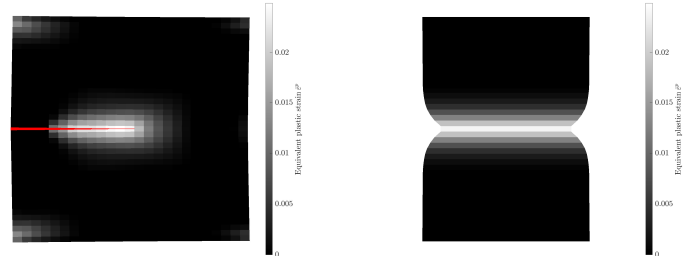
Figure 3: *Deformed cross-section (y-z) at mid-width (right) for coarse mesh when crack reaches this section (left)*

Results of varying the shape of the TSL (Figure 4) highlight the importance of proper coupling between bulk and cohesive surface as it affects the evolution of necking and subsequent crack propagation.
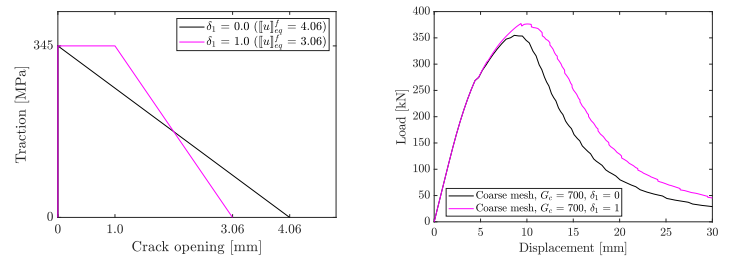
Figure 4: *Effect of using TSL with additional shape parameter* (δ_1)

Tensile test:

The results of a tensile test show mesh dependency at crack initiation as the critical equivalent plastic strain depends on the element size during necking (Figure 5).
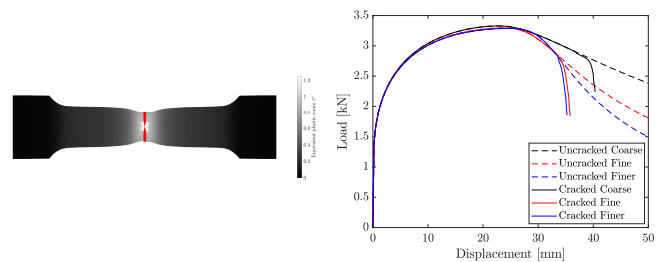
Figure 5: *Necking in a tensile test of an aluminum thin sheet with and without crack propagation*

Future work

Different crack initiation/propagation criteria and direction algorithms dependent on a range of stress states and failure behavior will be studied.

References

[1] A Ahmed et al. *Comput Methods Appl Mech Eng*, 201:191–207, 2012.

[2] FP van der Meer et al. *J. Compos. Mater.*, 46(5):603–623, 2011.

[3] PB Woelke et al. *Eng Fract Mech*, 147:293–305, 2015.

PhD progress

| 1 | 2 | 3 | 4 |

Fibre-matrix Distribution Evolution of Thermoplastic Composites Fusion Bonding Interfaces

G. Bieleman[1,2], W.J.B. Grouve[1,2], E.T.J. Klompen[2]

[1]Production Technology, University of Twente
[2]ThermoPlastic Composites Research Center

Motivation

Weight reduction of air and road transport vehicles is vital for the reduction of greenhouse gasses emitted by the transportation sector. Thermoplastic composite (TPC) materials are ideal for achieving this weight reduction. Furthermore, TPC materials can be produced in large volumes, and recycled in a cost and energy-efficient manner. Moreover, TPC's parts can be assembled into larger structures using techniques such as fusion bonding, providing an attractive alternative to fasteners and adhesives. These fusion bonding techniques largely exclude the weight of foreign material at the bonding interface and the processes can be highly automated.

Problem statement

The performance of these fusion bonded structures is governed by the interface performance, which is affected by the fibre-matrix distribution. Hence, performance predictions of the fusion bonded thermoplastic composite structures require extensive knowledge of the development of the fibre-matrix structure as a result of processing.

Research aim

Develop a model to predict the process-structure relationship of uni-directional thermoplastic composite welding interfaces, by means of non-isothermal multiphase flow of saturated and non-saturated thermoplastic polymer in a compressible, pre-stressed and or deconsolidated porous medium.

One-step overmoulding

The initially conducted research focuses on the evolution of the fibre-matrix distribution of one-step overmoulding, as this bonding method shows a significant evolution in fibre-matrix distribution.
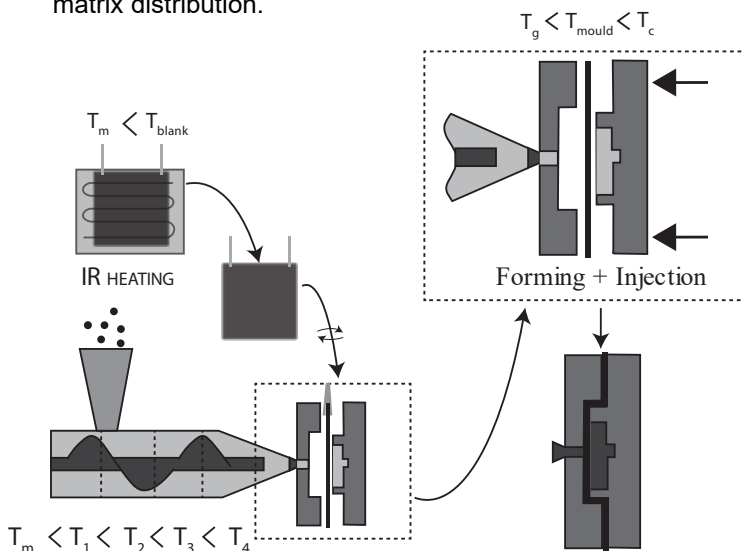
References

[1] Akkerman R. et al., Analysis of the Thermoplastic Composite Overmolding Process: Interface Strength, 2020

Overmouded rib structure fibre-matrix distribution

- Blank and rib in melt
- Fiber migration into the cavity [1]
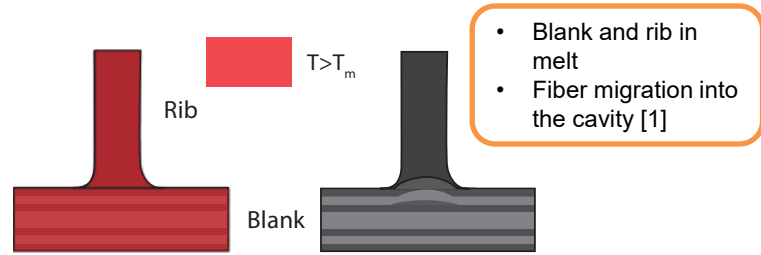
Overmoulding multiphase flow

- Blank: Flow of polymer through a deformable porous medium and squeeze flow
- Injection compound: Containing reinforcement in polymer, Poiseuille flow

$\downarrow$ Pressure injection

$\downarrow$ Pressure mould

$\downarrow$ Hydrostatic pressure blank
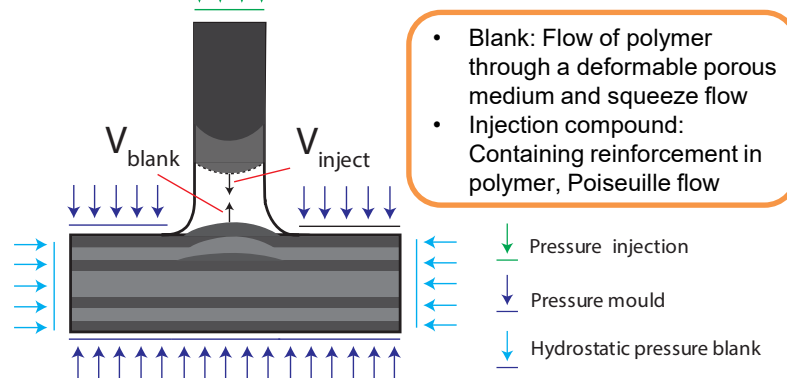
Preliminary results
Fibre migration of GF-PA410 S-rib geometry
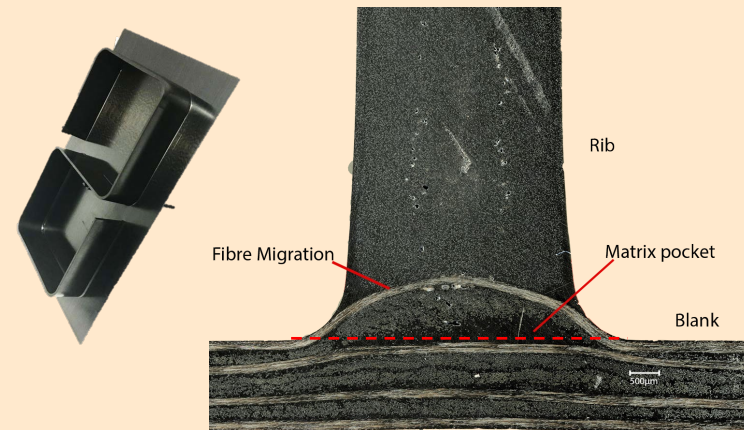
Observations

- Fibre migration into cavity 0,9mm – 12mm
- Matrix rich pockets
- Demonstrator shape distortion

Future work

- Fibre migration study one step overmoulding without injection
- Permeability and compaction stress measurement of uni-directional fibre bed
- Porous media flow simulations

Forming simulations for unidirectional thermoplastic composites: Improvements in characterizing, modelling and validating in-plane shear

D. Brands[1,2], W.J.B. Grouve[1], S. Wijskamp[2], R. Akkerman[1]

[1]University of Twente, Group of Production Technology
[2]ThermoPlastic composites Research Center (TPRC), Enschede

Introduction

Unidirectional (UD) carbon fibre reinforced thermoplastic composites material are of interest to the aerospace industry to enable automated manufacturing of low-weight, structurally loaded components. However, challenges with complex part geometry and (tailored) layups can easily lead to defects during production. Composite forming simulation tools offer virtual process modelling to aid engineers during initial design or problem solving. This research aims to advance forming simulations for UD materials through improved material characterization and modelling.

In-plane shear characterization

The bias extension method was developed for use on cross-ply laminates from unidirectional material. This method is already established for in-plane shear characterization of woven composites. Datasets for two materials were generated with varying rates and temperatures. See [1].

Figure 1: Bias extension test specimens and schematic deformation

The measured response is strongly dependent on rate and moderately dependent on temperature in molten condition. The non-linear force/shear angle curves are classified with start-up, steady state and large deformation regimes.

Figure 2: Bias extension experimental results and model

Bias Extension model

The trellis shear deformation is dominant during bias extension testing. For small deformation it is the same as simple shear, but a planar extensional flow transverse to the fibre occurs at larger deformation due to inextensibility and incompressibility.

$$\boldsymbol{D} = \dot{\varphi} \begin{bmatrix} 0 & -1 & 0 \\ -1 & \dfrac{2}{\tan(2\varphi)} & 0 \\ 0 & 0 & \dfrac{-2}{\tan(2\varphi)} \end{bmatrix}$$
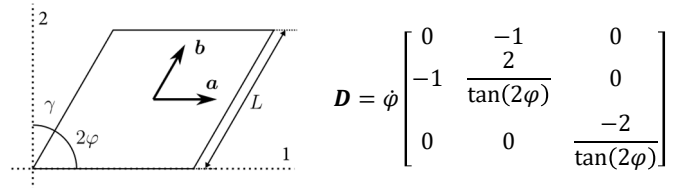
Power equilibrium is considered to model an analytical force response, with contributions from extra stresses in two distinct deformation regions.

$$F\dot{u} = \int_V \boldsymbol{\sigma}:\boldsymbol{D}\ dV = V_I(\tau_I:D_I) + 4V_{II}(\tau_{II}:D_{II})$$

Material model

In-plane shear is modelled with a 1D Maxwell model and utilizes a power law longitudinal viscosity. A power law transverse viscosity models the deformation perpendicular to the fibres.

$$\eta_L = k_L|2D_{12}|^{n_L-1}$$
$$\tau_{12} = G \cdot \varepsilon_s \quad \dot{\varepsilon}_s = 2D_{12} - \frac{G\varepsilon_s}{\eta_L}$$

$$\eta_T = k_T \cdot |2D_{22}|^{n_T-1}$$
$$\tau_{22} = 2\eta_T D_{22}$$
$$\tau_{33} = 2\eta_T D_{33}$$
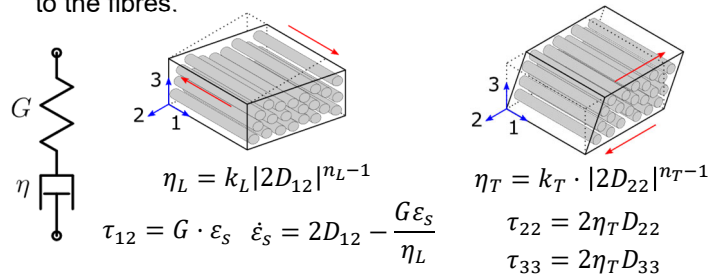
Validating simulations

Formed parts with pre-applied dot patterns are analysed to measure the experimental in-plane shear deformation and can be employed as validation cases for simulation models.
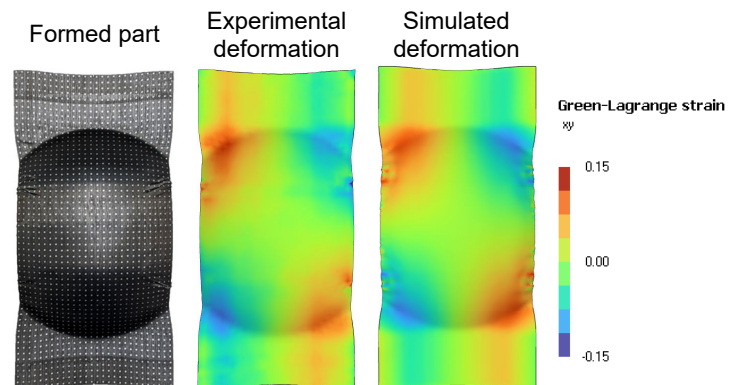
Figure 3: Dome validation geometry. Comparison of in-plane shear deformation.

References

[1] Brands et al. Front. Mater. 9:863952 doi: 10.3389/fmats.2022.863952

UNIVERSITY OF TWENTE.

PhD progress
1 2 3 4

TPRC

NWO

Project page →

Feature Selection for Failure Recognition:
Comparing Vibration Analysis and Motor Current Signature Analysis

S. Bruinsma[1,2], T. Tinga[1,3], R. Geertsma[3], R. Loendersloot[1]

[1]University of Twente
[2]Royal Netherlands Navy
[3]Netherlands Defence Academy

Introduction

- Continuous **condition monitoring** for increased availability
- Spectrum analysis requires **knowledge and experience**
- **Large amounts of data** from online measurements
- **Automation** of analysis is necessary
- High **information density** in high frequency sampled data
- Focus on Vibration Analysis **(VA)** and Motor Current Signature Analysis **(MCSA)**
- **Black box** models **not appropriate** towards implementation

Aim

Identify features best suited for fault recognition, based on literature, verified with novel dataset.

Overall Method overview

Spectrum

Step 1: Feature selection
- Domain knowledge
- Physical relation between feature and failure
- Measurement method

1X	1,94
2X	2,53
…	…

Features

Step 2: Automate analysis
- Machine Learning vs. Rule Based
- Anomaly detection
- Data limitations

Algorithm

Step 3: Algorithm implementation
- Identify failures
- Diagnosis of severity
- Explainable results

Warning

Step 4: Implementation on field data

Experimental dataset

- Electric motor – pump setup
- Individual failures
- VA and MCSA measured simultaneously
- Comparable preprocessing

Table 1: List of simulated failures

Failures
Bearing damage (5X)
Misalignment (3X)
Unbalance (2X)
Loose foot (2X)
Impeller damage
Winding short
Broken rotor bar
Soft foot
Cavitation (2X)
Bent shaft
Coupling damage (4X)

Overall value approach

- Not always logical
- Not sufficiently distinctive
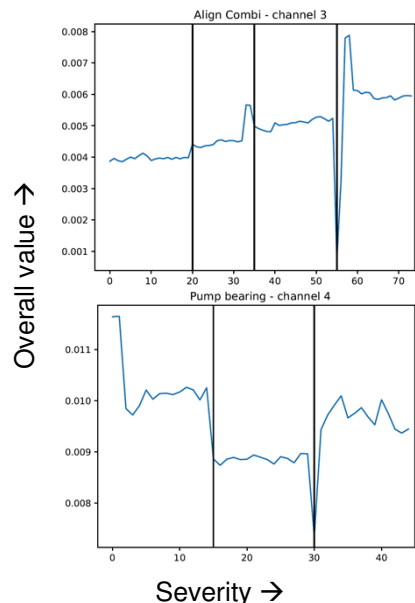
Figure 1: VA Overall value for different severities

Features: VA vs MCSA

- Comparing sensitivity of measurement methods
- Combination of methods could be key to success
- Severity dependent features
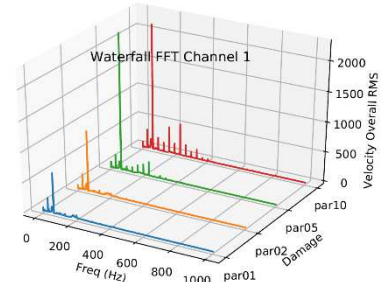
Figure 2: VA Waterfall plot of four misalignment severities
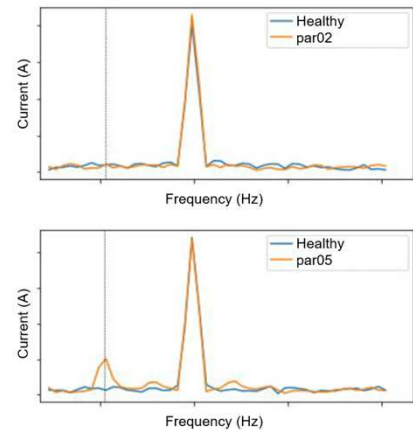
Figure 3: MCSA plots of two misalignment severities

Next steps

- Develop approach to measurement method comparison
- Establish complete list of features VA & MCSA per failure
- Verify feature list with experimental data

Contact

sj.bruinsma.01@mindef.nl
s.j.bruinsma@utwente.nl

Presenter:
Sietze Bruinsma

Predictive modelling of liquid metal induced fracture in Fe-based alloys

F. Brunner and F. Maresca

Computational Mechanical and Materials Engineering,
University of Groningen

f.brunner@rug.nl

Introduction & Motivation

- **What is liquid metal embrittlement (LME)?**
  Reduction in ductility and toughness of a solid metal in contact with a liquid metal (see Fig. 1 left).

- **LME is crucial for multiple applications** in the automotive and nuclear power industry, soldering, brazing and welding.
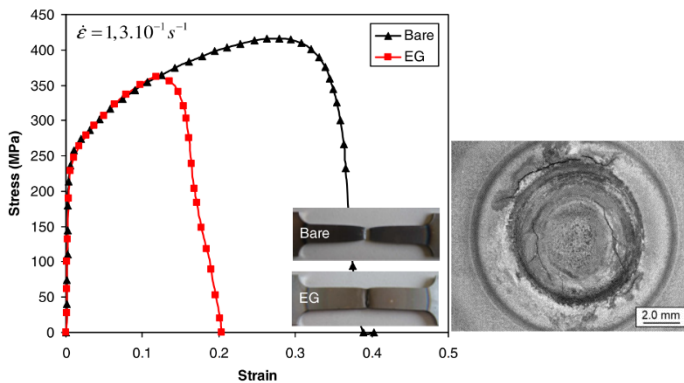
Figure 1: Left: Tensile curves of bare and electrogalvanized (EG) TWIP steel specimens at 700°C [1] Right: Spot weld with surface cracks due to LME [2]

- **Automotive Industry:** Advanced high strength steels (AHSS) have a good combination of strength and ductility. For corrosion protection they are Zn-coated. AHSS parts are joined via spot welds (several thousand in each car body), which can exhibit LME [2] (see Figure 1 right)

  → **great interest in understanding and preventing LME**
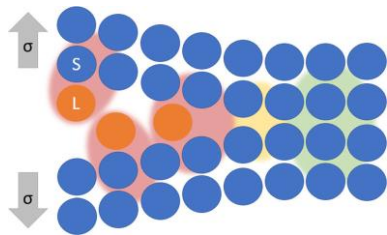
Figure 2: Schematic model of a crack tip in contact with liquid metal [3]

Project Description & Goals

- **Project aim:** Development of a predictive LME model for steels, with main focus on Zn-induced fracture.

- **LME can manifest** through e.g. interatomic bond weakening, micro-plasticity, grain boundary penetration or a combination thereof in the vicinity of crack tips [3] (see Fig. 2)
  → **LME predictions must account for atomistic processes** like crack tip plasticity and:
  - composition and phase of the solid metal
  - grain boundaries (GB's)
  - environmental factors: temperature, strain-rate, stress

- **Goals:** Contributing to the development of LME-free AHSS and the elucidation of LME in general

Methodology & Challenges

Challenges:

- LME is a multi-scale problem
- Multitude of disparate/contradictory experimental results
- High number of influencing factors to consider and account for

Methodology:

- Study of the intrinsic brittleness/ductility of the solid metal with a combination of molecular dynamics (MD) and linear elastic fracture mechanics (LEFM)

- Simulation of dislocation motion and crack propagation with a combination of MD and density functional theory (DFT)
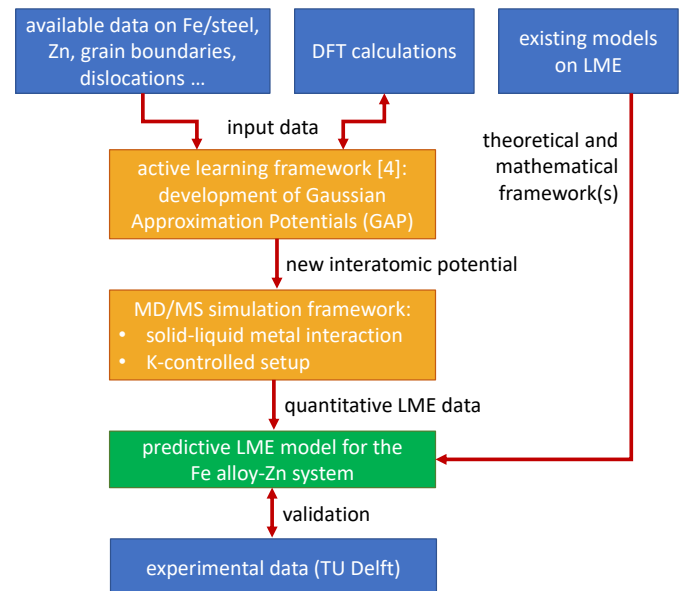
Figure 3: Flow diagram of intended project methodology

Research Questions

The following research questions shall be answered to systematically approach the final project goals:

- What is the intrinsic ductility/brittleness of Fe and fcc and bcc Fe dilute alloys (Zn, Mg, Si, Al, Mn)? To which degree is it altered due to the presence of a liquid metal?

- Which GB's in fcc and bcc Fe-alloys are most susceptible to LME and why?

- What are the main (nano-scale) criteria for design of LME-resistant steels?

References

[1] C. Beal, X. Kleber, D. Fabreguea, M. Bouzekrib. Scr. Mater. **66**, 1030-1033
[2] WorldAutoSteel. *Combined reports - AHSS implementation solution: liquid metal embrittlement study.* 2020
[3] X. Gong. *Liquid Metal Embrittlement of a 9Cr-1Mo Ferritic-martensitic Steel in Lead-bismuth Eutectic Environment under Low Cycle Fatigue.* PhD thesis. 2015
[4] J.E. Norkett, M.D: Dickey, V.M. Miller. Metall. Mater. Trans. A **52**, 2158–2172
[5] L. Zhang, G. Csanyi, E. van der Giessen, F. Maresca. *Atomistic Fracture in bcc Iron Revealed by Active Learning of Gaussian Approximation Potential.* under review (arXiv:2208.05912)

Induction Heating of UD C/PAEK
What thermography can teach us about eddy currents

Y. M. Buser[1,2], W.J.B. Grouve[2], S. Wijskamp[1], R. Akkerman[1,2]

[1]ThermoPlastic composites Research Center (TPRC)

[2]University of Twente

Introduction

Induction welding is an attractive technology for the fusion bonding of carbon fibre reinforced thermoplastic composites. In this process, **eddy currents** are induced in the conductive carbon fibre network by an alternating electromagnetic field, which heats up the parts (Fig. 1 →). In **unidirectional ply-based composites**, the formation of eddy currents relies on the ply interfaces where changes in the fibre orientation facilitate closed-loop conductive paths. A deeper understanding of how this fibrous architecture governs heat generation is required to improve control and/or predictability for large scale application of the welding process.

Induction heating thermography

Thin 300×300 mm^2 laminates of AS4/PEEK from Toray were induction heated with a stationary hairpin coil ( ) while monitoring the rapid temperature increase with a thermal camera. The thermograms (Fig. 2 ↘) highlight that:

1. Eddy currents are dominantly induced along the different fibre directions present in the lay-up.
2. The eddy current distribution is distorted for $[45/-45]_s$ and $[45/0]_s$ laminates. These lay-ups are the most reliant on interfacial junctions to form a closed-loop conductive path.

DC Joule heating experiments

300×50 mm^2 tapes were consolidated at their crossover while forcing a strong direct current (DC) of 10 A through the cross-ply interface. Resulting thermograms confirm the hypothesis that the ply interface plays an important role in the (re)distribution of electric current within a unidirectional reinforcement (Fig 3. ↓).
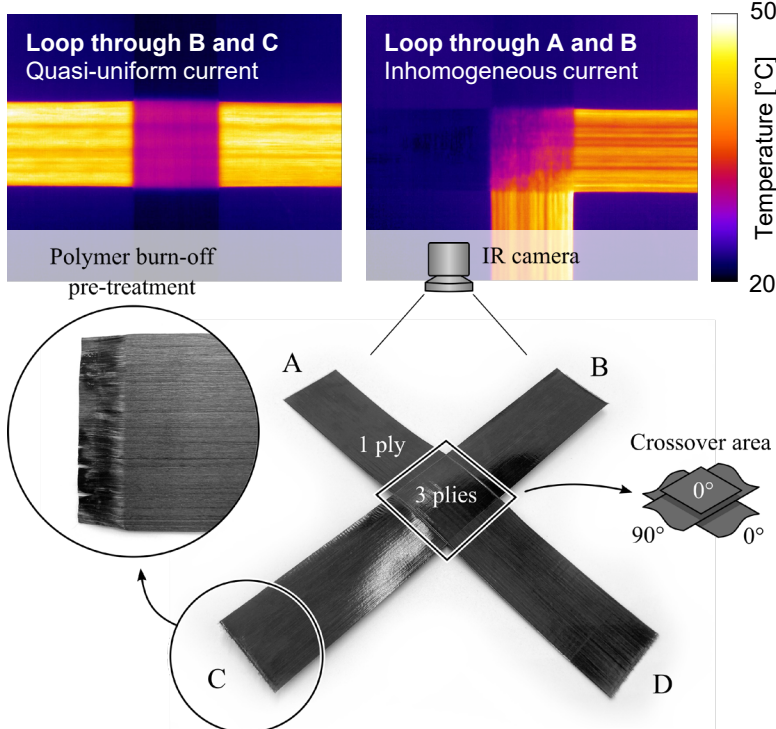
Fig. 3: DC Joule heating experiments on cross-shaped specimens
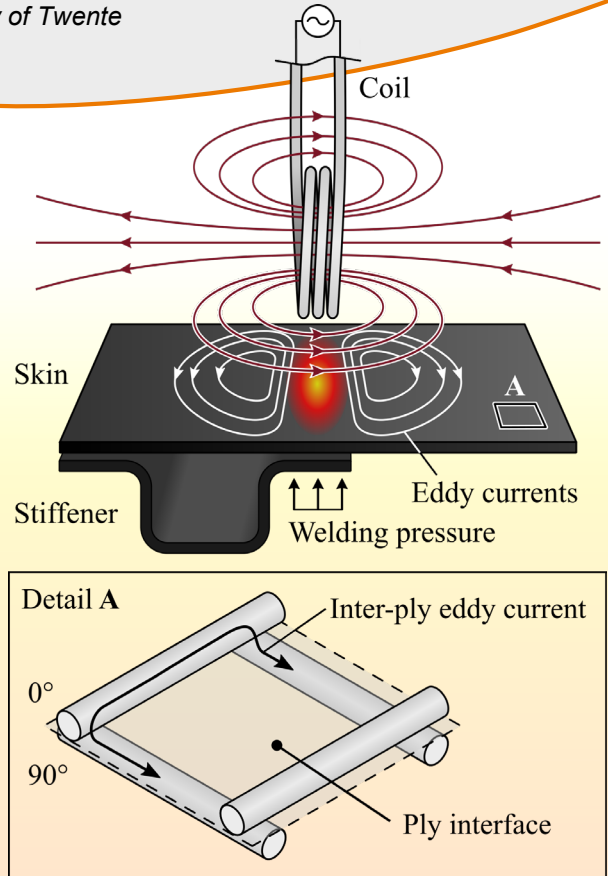
Fig. 1: Illustration of induction welding of UD-based TPCs

(a) After 0.33 seconds — $[0/90]_s$

(b) After 0.40 seconds — $[45/90]_s$

(c) After 0.43 seconds — $[45/-45]_s$

(d) After 0.87 seconds — $[45/0]_s$
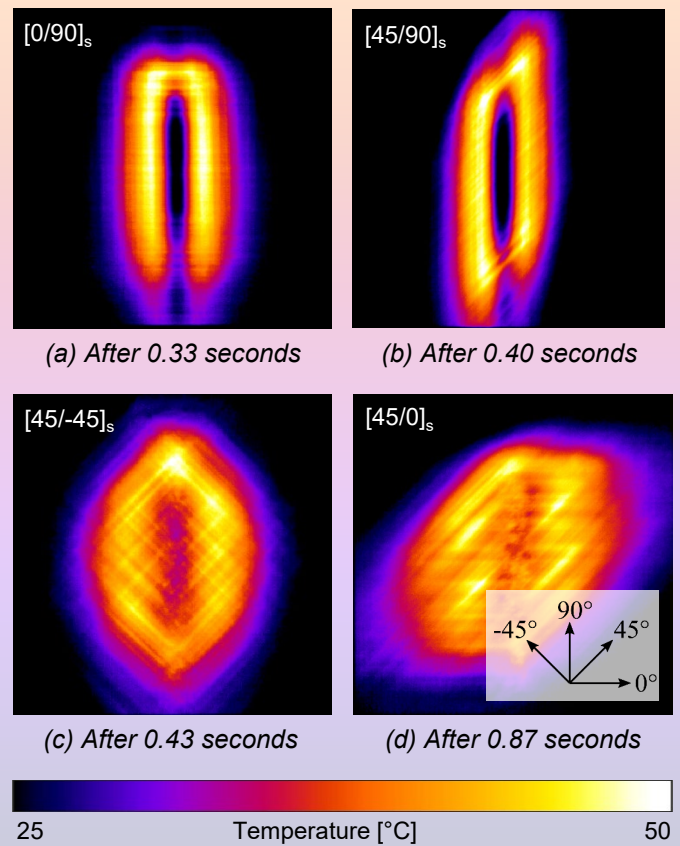
Fig. 2: Induction heating thermograms of 4-ply laminates at the onset of reaching 50 °C

Estimation of the shape and size of interaction volume for non-collinear wave mixing inspections in PVC

N. Chidambaram[1,2], R. Loendersloot[1], D. Yntema[2], T.Tinga[1]

[1]University of Twente. Faculty of Engineering Technology (ET)
[2]Wetsus European Centre of Excellence for Sustainable Water Technology

Motivation

For ultrasonic non-collinear wave mixing (NCWM) inspections, the shape and size of the interaction region (IR) in the material is unknown. In literature, it is assumed to be circular for the sake of mathematical simplicity but it is not experimentally proven [1]. It is crucial to understand if the material properties are obtained from a point or a finite volume in the test material.

Method

- NCWM experiment on two PVC samples of thickness 3mm and 12mm respectively.
- Horizontal movement of phased array in one direction to record signals from multiple points.
- Arrival time estimation of generated wave from received time signal at each point using (1) digital signal processing (2) energy criterion algorithm [2].
- 5 measurements per point for standard deviation.
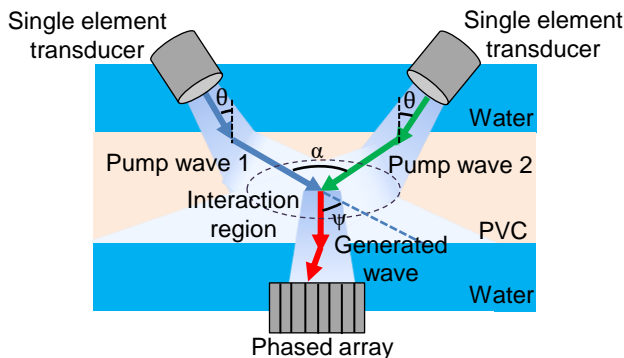
Figure 1: Experimental setup with 10mm wide SE transducers and phased array with 8 elements

Results

- Arrival time patterns are different in thick and thin sample i.e. inverted U shape and logarithmic decrease respectively (Figure 2).
- Shows that IR is a sphere or oval that fits exactly in the width of thick PVC and only a part of IR lies in the width of thin PVC.
- Horizontal width of IR is determined from distance between reference element in first point and last point ~14 mm.
- IR is oval in shape as horizontal width of IR > thickness of thick PVC.
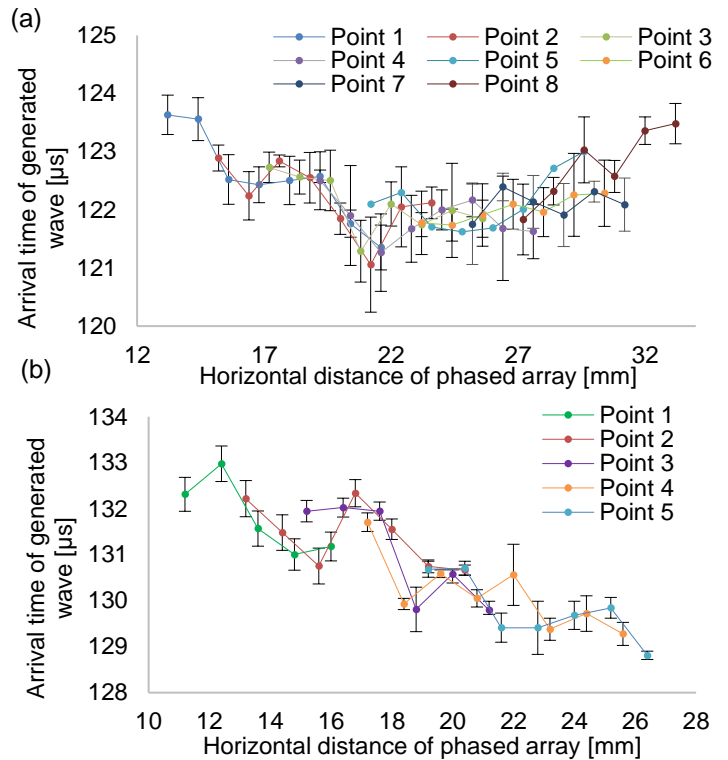
Figure 2: (a) Arrival time with respect to horizontal movement of phased array for (a) thick (b) thin sample

- Generated wave travels ~ 11mm more than near field distance to IR.
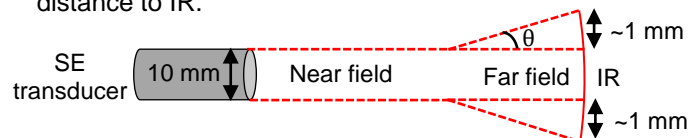
Figure 3: Near field and beam divergence of SE transducer

Conclusion

- The IR fits exactly in the width of thick PVC sample.
- The shape of IR is oval with horizontal width ~ 14mm and vertical width ~ 12mm.
- Horizontal width of IR is roughly higher than diameter of the single element transducers – divergence in far field.

References

[1] V A Korneev, A Demčenko, ' Possible second-order nonlinear interactions of plane waves in an elastic solid', The Journal of the Acoustical Society of America Vol 135, pp 591-598, 2014.
[2] L Chaparro, 'Discrete time Signals and Systems Signals and Systems using MATLAB (Second Edition)', pp 535-602, 2015.

A numerical framework for the electro-mechanical analysis of conductive tracks in printed electronics

Britt Cordewener, Marc Geers, Joris Remmers

Eindhoven University of Technology

Print cavaties | Place components | Print groove circuit | Fill groove circuit | Repeat & Finish
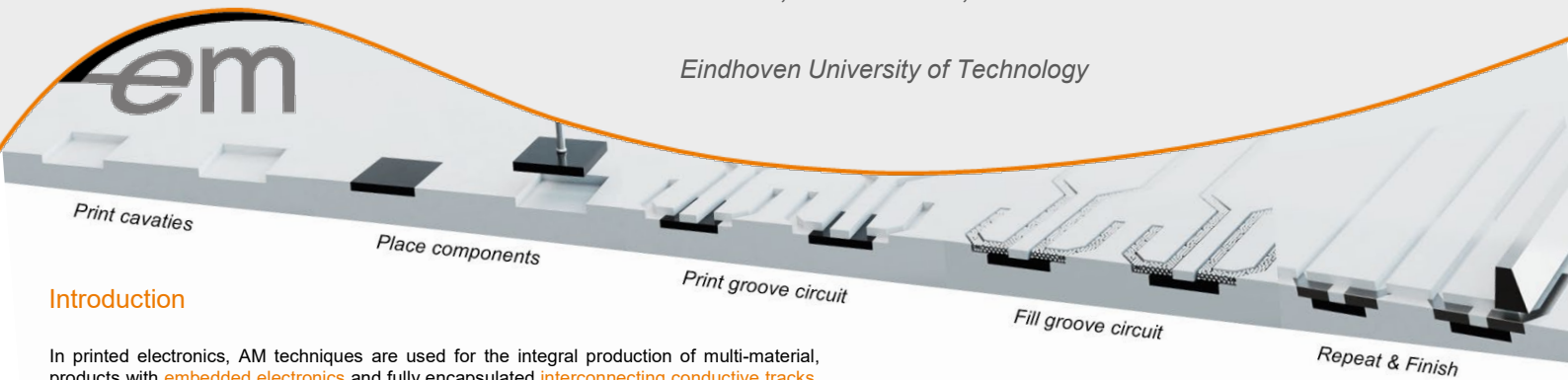
Introduction

In printed electronics, AM techniques are used for the integral production of multi-material, products with embedded electronics and fully encapsulated interconnecting conductive tracks. The electro-mechanical performance of the printed conductive tracks is strongly depending on the composition of the conductive inks and the microstructure obtained after processing of the inks. To analyze this performance in terms of the resistivity, a multi-physics model is created that allows for the analysis of the effects of strains imposed on the microstructure of a track and the prediction of the electro-mechanical performance of given ink compositions.

Aim

| Prediction of track performance for a given ink compositions
| Analyze & predict malfunctioning/failure tracks
| Improved strategies for printing of conductive tracks

Input
- Process Conditions
- Ink Characteristics

Microstructure generation
- Experimental data
- Statistic generation

FE Meshing
- Conformal meshing
- Immersed boundary

Multiphysical analysis
- Mechanics
- Electrostatics
- Damage

Results
- Ω Resistivity
- Mechanical properties

Design evenlop
- Process Conditions

Microstructure generation

Why |

An adequate geometrical representation of the microstructure is required as an input for the multi-physics model. Microstructure of sintered track depends on process conditions and Ink characteristics and governs the Electro-mechanical performance.

How |

✓ Experimental Data
- 2D → FIB SEM images
- 3D → CT scans

⬚ Statistic generation
- Particle size distribution
- Sintering
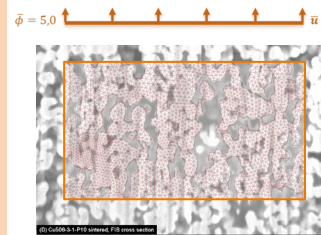
FE Meshing

Why |

Generation of suitable representations is challenging due to their computationally demanding nature as a result of the complexity of the porous printed microstructure
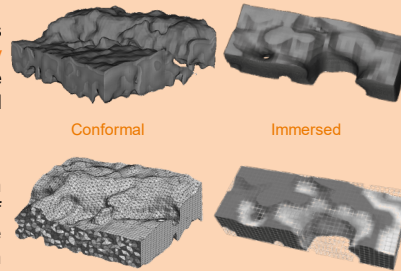
Result |

IB meshes show similar behavior, but in this format, do not approximate onset of fracture and exponential resistance increase, despite further mesh refinement.

Conformal | Immersed

$\bar{\phi} = 5,0$ $\bar{u}$

$\bar{\phi} = 0,0$ $\bar{u}$

What |

Modelling electro-mechanical fracture with two successive mechanisms:
I. Mechanical fracture of the solid
II. Decrease of conductivity as a direct result

How |

Multi-field approach:
- u Displacement
- ϕ Electric potential
- d Crack phase-field

The system is implemented in a finite element framework and solved using a staggered incremental procedure.

Displacement field u — Phase field d

Electric potential field ϕ

$d(x) = e^{-|x|/l}$

Solver II / Solver I

$u = \bar{u}$, $\phi = \bar{\phi}$, ε

Result |

The effective resistivity of simplified representations of conductive tracks under mechanical loading is analyzed. The contour plots show the development of damage and its consequence on the potential field distribution.

✓ An increase in resistivity is observed, which is caused by crack formation in the conductive material, that resembles the trends observed in experimental research.

⬚ Model will be validated with conductive tensile tests performed on printed tracks. A CT scan of the track is used to generate a representative FE mesh.

TU/e EINDHOVEN UNIVERSITY OF TECHNOLOGY

PhD progress
| 1 | 2 | 3 | 4 |

LEE·BED
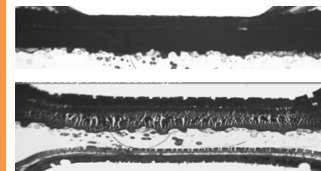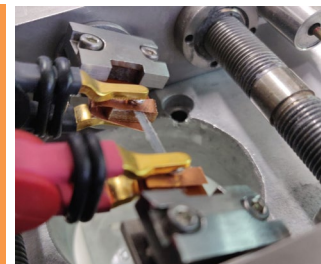
Extreme high aspect ratio mechanical resonators with low mechanical dissipation

A. Cupertino[1], D. Shin[2], P. G. Steeneken[1,3], M. A. Bessa[2], R. A. Norte[1,3]

[1]Department of Precision and Microsystems Engineering, Delft University of Technology, The Netherlands

[2]Department of Materials Science and Engineering, Delft University of Technology, The Netherlands

[3]Kavli Institute of Nanoscience, Department of Quantum Nanoscience, Delft University of Technology, The Netherlands

a.cupertino@tudelft.nl

Objective

Extreme aspect ratio mechanical resonators with high quality (Q) factor at room temperature

Challenge - Lack of design strategies and fabrication capability

- Reduce large simulation time
- Avoid collapse and mechanical failure of the fabricated structures

- Multi Fidelity Bayesian Optimization
- Dry release and larger gap size

Discovery of design with Q factor over 10 billion by Multi fidelity Bayesian optimization

- If only high-fidelity simulations are used, not enough data to find high Q
- If only low-fidelity, then accuracy is not enough an optimum is not real

- Combining fidelities strikes a balance to find the optimum

MF: Q maximize
MF: log(Q) maximize
SF: Q maximize
SF: log(Q) maximize

Training phase — Bayesian optimization

3 cm design simulation
3 mm design simulation
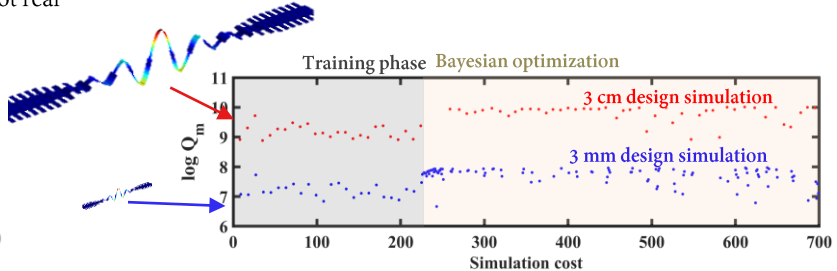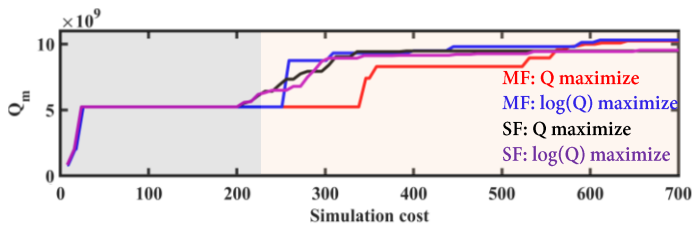
Fabrication of extreme high aspect ratio resonators with high yield by dry release

- Surface tension in wet processes can cause mechanical failure
- Small gap under high aspect ratio suspended resonator causes collapse

- Undercut with SF_6 dry release avoids wet process
- Deep silicon etching increases gap size

SiN
Si
resist
photoresist
LPCVD SiN deposited
100 um
50 um
50 um
1 mm
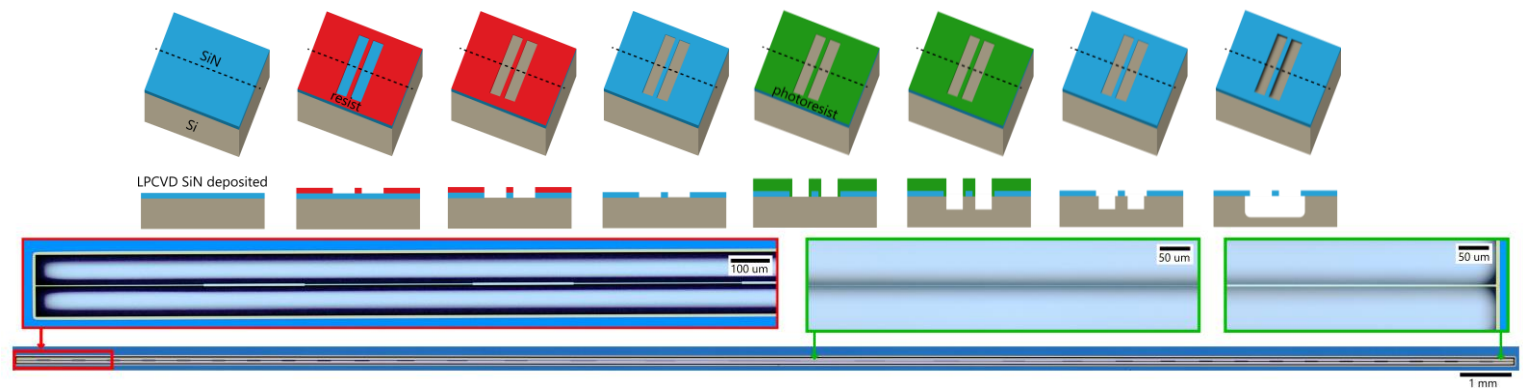
Experimental validation at room temperature

- Measured spectrum in good agreement with simulation
- Measured Q factor 3 times lower than simulation result

Discrepancy most likely due to fabrication imperfections and larger thickness, under further investigation

VOA   90%   FPC ϕ PID
10%
FPC
50%
CAM
50%
lensed fiber
$P < 10^{-8}$ hPa
piezoelectric actuator
3-axis nanopositioner
UHV chamber
Spectrum Analyzer

$Q = (3116.0 \pm 14.0) \cdot 10^6$
$f = 228.3$ kHz

White noise 10V
Thermal noise
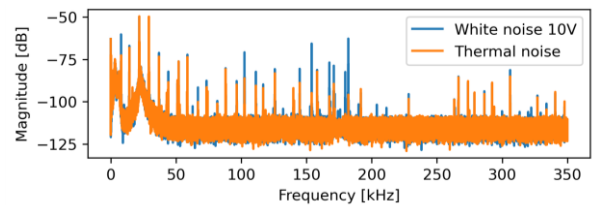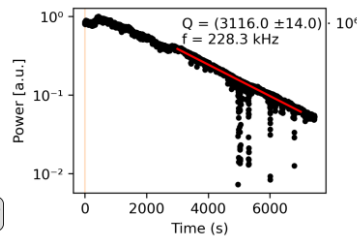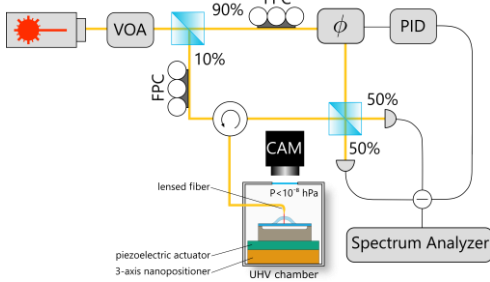
Conclusion - New platform towards new science and technology yet unexplored

Development of design strategy and fabrication process to allow extreme high aspect ratio resonators with $Q > 10^{10}$ at room temperature

- Detect fundamental small forces
- Explore quantum effects at room temperature
- Develop resonators with unprecedented sensitivity

PhD progress
1   2   3   4

TU Delft
Precision and Microsystems Engineering
KN Kavli Nanolab Delft — Enabling nanodevice fabrication

GPU-accelerated matrix-free topology optimization

A Delissen, J Wu, M Möller, AM Aragón, M Langelaar

Delft University of Technology

Motivation

Topology optimization of TU Delft's Flying-V airplane is a great computational challenge. For a fine-scale design resolution of a few millimeters, the large aircraft (65m span) requires billions of finite elements (13000×11000×2600). We propose a matrix-free approach in which the matrix-vector product is assembled on the fly on the GPU, avoiding explicit storage of the system matrix, which would otherwise exceed the memory capacity of even large supercomputers.
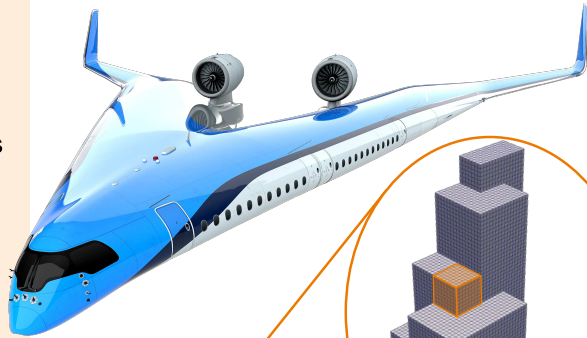
Finite element domain

Cube-shaped trilinear elements (voxels) enable the use of a singleton finite element matrix. The domain is built up using sectors of 8×8×8 elements, omitting sectors that are completely void. This allows for contiguous memory access and leads to highly efficient GPU utilization.
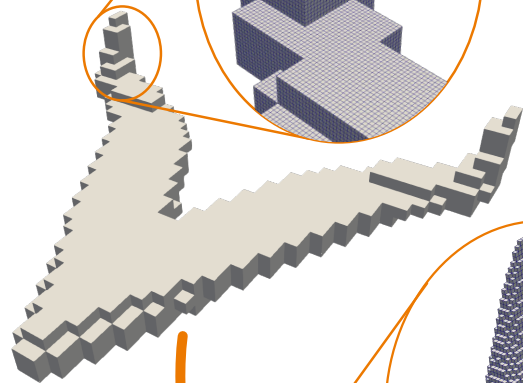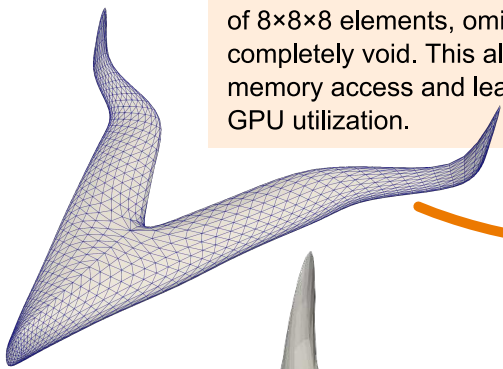
Topology optimization

The densities of voxels within the airplane surface are optimized. An optimal distribution of material for one or more given loadcase(s) is generated using an iterative process. In this case, 1.4 million voxels are meshed, requiring about 20 seconds per design iteration on a single V100s GPU.
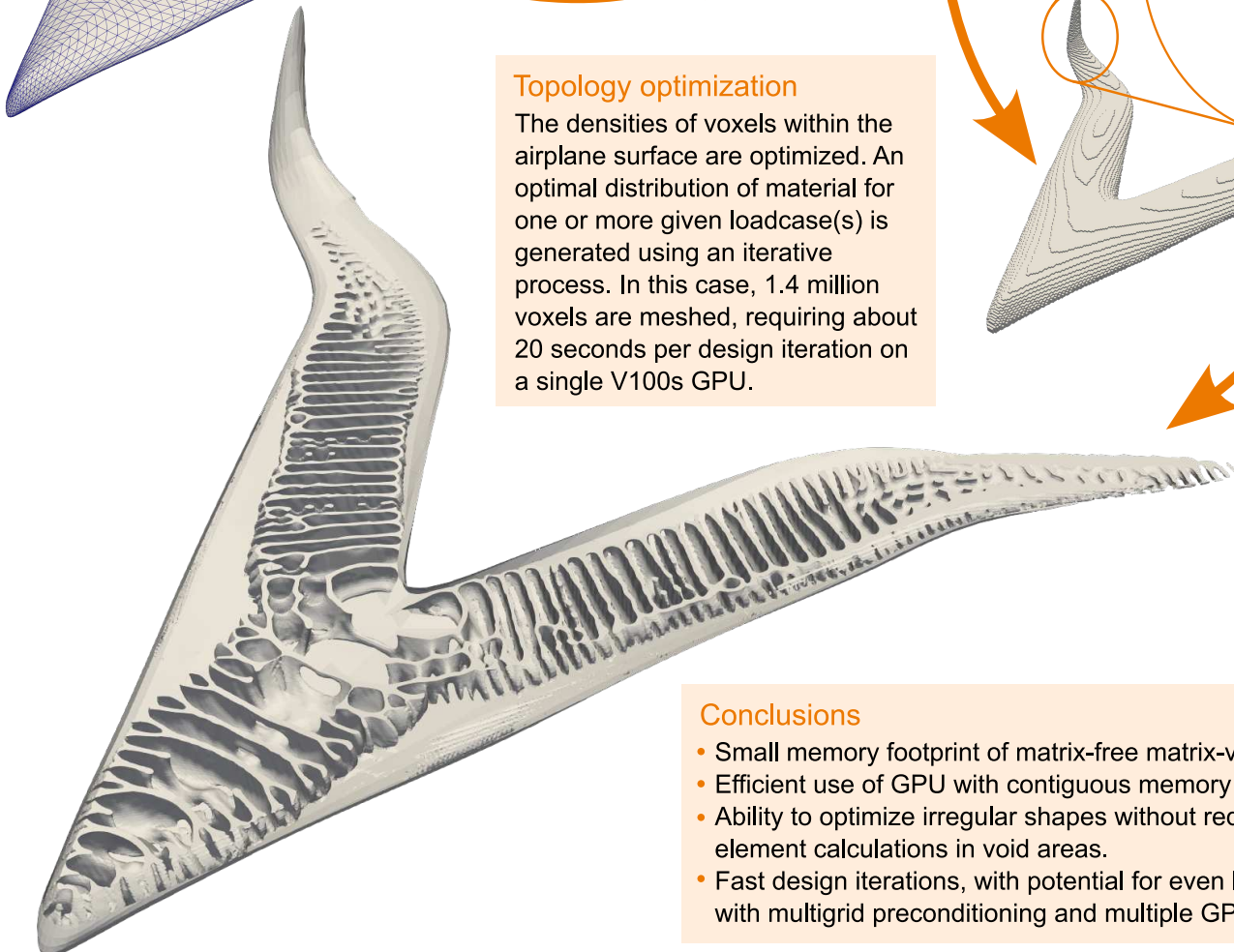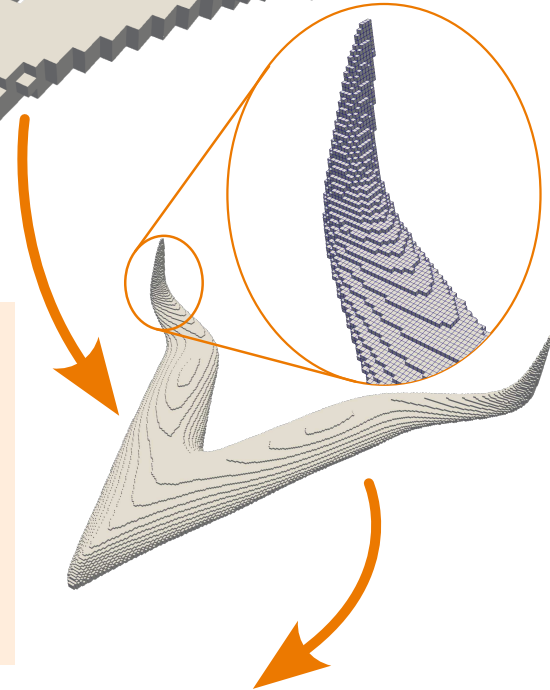
Conclusions

- Small memory footprint of matrix-free matrix-vector product.
- Efficient use of GPU with contiguous memory access.
- Ability to optimize irregular shapes without redundant finite-element calculations in void areas.
- Fast design iterations, with potential for even larger problems with multigrid preconditioning and multiple GPUs.

T U Delft

DCSE
Enabling Technology for Industry

Generalized Kalman Filtering for Nonlinear Dynamic Problems using Machine Learning

W. van Dijk, W.B.J. Hakvoort, B.V. Rosić

University of Twente,
Department of Mechanics of Solids, Surfaces &
Systems (MS3)

Introduction

Predictive models are used for high performance control of mechanical systems. Knowledge on the model uncertainties enables a proper trade-off between performance and robustness. Reducing these uncertainties by state and parameter estimation methods therefore allows for less conservative robust control. In this study, a **generalized Kalman filter** formulation is combined with a **neural network** (NN) for the task of **state and parameter estimation** under **non-linear dynamics**.

Problem

Assume a continuous nonlinear dynamical system,
$$\dot{\boldsymbol{x}} = f(\boldsymbol{x}, t),$$
which is observed at discrete time moments t_k with an observation function $h(\cdot)$
$$\boldsymbol{z}^k = h(\boldsymbol{x}^k) + \boldsymbol{v}^k, \qquad \boldsymbol{v}^k \sim \mathcal{N}(0, C_{\boldsymbol{v}}).$$

Methods

In the Bayesian framework, the unknown states are modelled a priori as random variables, $\boldsymbol{x}_f^k(\omega)$. Therefore, the measurement forecast also becomes a random variable,
$$\boldsymbol{y}_f^k(\omega) = h(\boldsymbol{x}_f^k(\omega)) + \boldsymbol{v}^k(\omega).$$

The **generalized Kalman filter** [1] is given by:
$$\boldsymbol{x}_a^k(\omega) = \boldsymbol{x}_f^k(\omega) + \mathbb{E}[\boldsymbol{x}_f^k(\omega)|\boldsymbol{z}^k] - \mathbb{E}[\boldsymbol{x}_f^k(\omega)|\boldsymbol{y}_f^k(\omega)],$$

where the conditional expectations can be approximated by a map, $\phi_{\boldsymbol{x}_f^k}(\cdot)$, parametrized on $\boldsymbol{\beta}$,
$$\mathbb{E}[\boldsymbol{x}_f^k(\omega)|\cdot] = \phi_{\boldsymbol{x}_f^k}(\cdot, \boldsymbol{\beta}),$$

found by minimizing the optimality condition,
$$\arg\min_{\boldsymbol{\beta}} \mathbb{E}[\left\| \boldsymbol{x}_f^k(\omega) - \phi_{\boldsymbol{x}_f^k}(\boldsymbol{y}_f^k(\omega), \boldsymbol{\beta}) \right\|^2].$$

Neural network

A **simple NN model structure** is used for the map $\phi_{\boldsymbol{x}_f^k}(\cdot)$:
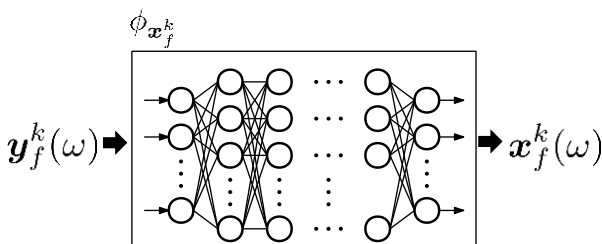
Figure 1: Simple feedforward neural network

Results

The nonlinear filter using the NN is applied on the Lorenz-63 system [2] for state and parameter estimation (**Figure 2** & **3**)
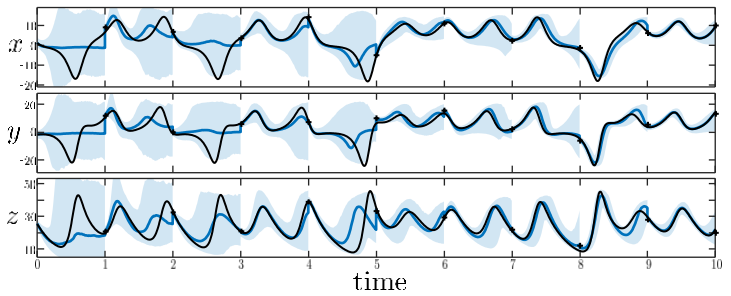
Figure 2: State estimates from NN based filter. Truth (—); Measurements (+); Est. mean (—); 95% conf. interval (▮).
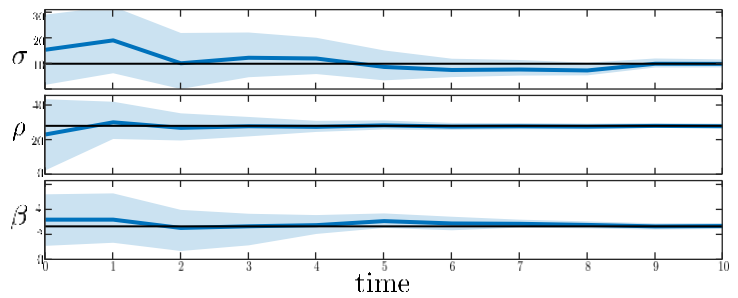
Figure 3: Parameter estimates from NN based filter.

Conclusion

A **nonlinear Kalman filter** using a simple **NN** was derived from a generalized Kalman filter formulation. It showed promising results when applied to the Lorenz-63 system for the task of state and parameter estimation. Compared to its linear counterpart, the Ensemble Kalman filter, it shows improved performance.

Future work

*   **Speed-up training of neural network**
*   **Tailor training of network to random inputs**
*   **Remove sampling from current implementation**

References

[1] B. V. Rosic, A. Kucerova, J. Sykora, O. Pajonk, A. Litvinenko, and H. G. Matthies, "Parameter identification in a probabilistic setting," Engineering Structures, vol. 50, pp. 179–196, 2013.

[2] E. N. Lorenz, "Deterministic nonperiodic flow," Journal of atmospheric sciences, vol. 20, no. 2, pp. 130–141, 1963.

A hybrid ray tracing and Discrete Element Method framework for the simulation of particle based Additive Manufacturing processes

B.J.A. Dorussen, M.G.D. Geers, J.J.C. Remmers

Eindhoven University of Technology
Mechanical Engineering – Mechanics of Materials
Graduate School Engineering Mechanics

Flowchart of the DEM framework

Increment time with Δt
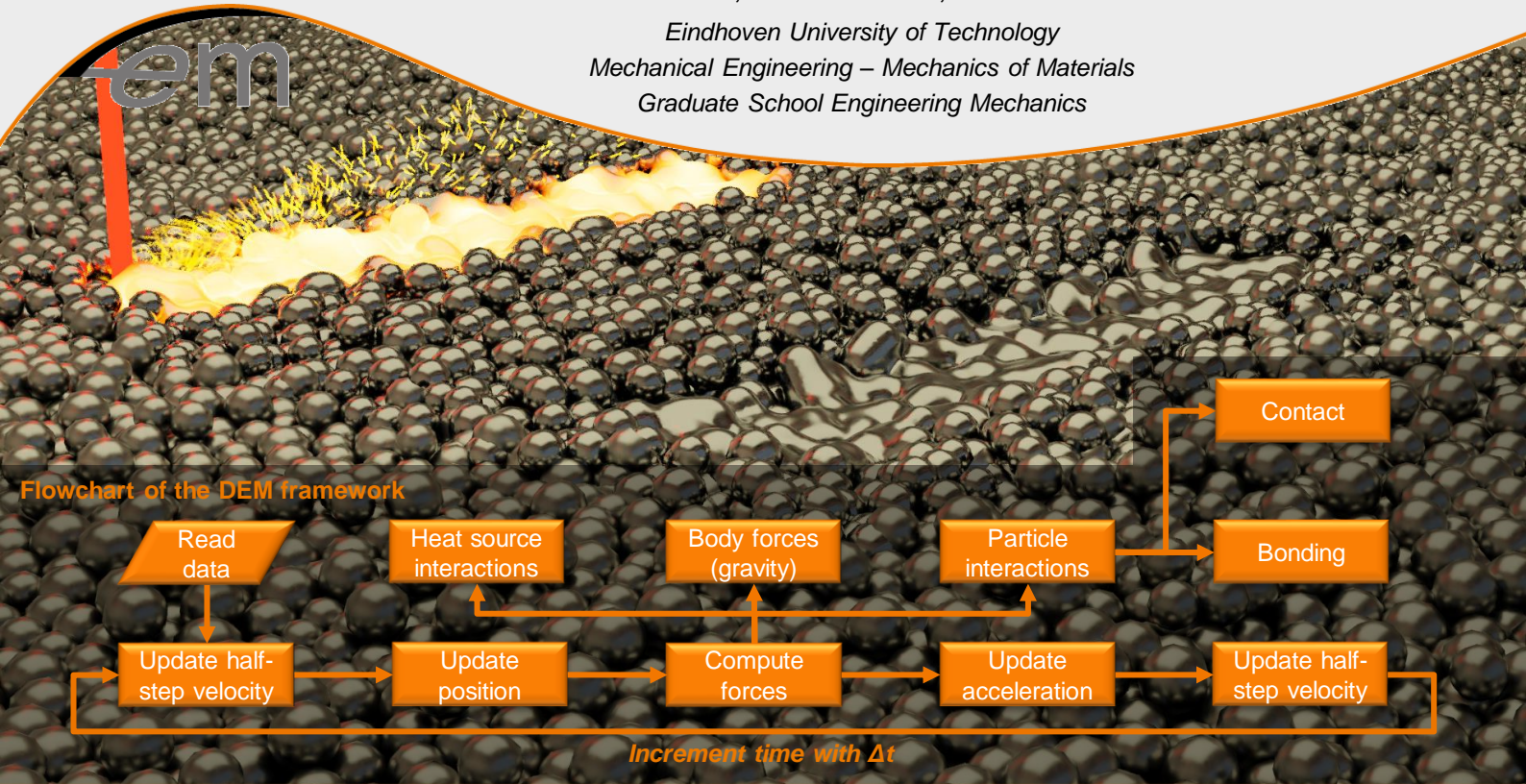
Introduction

Additive Manufacturing (AM) methods contain various, simultaneously active, complex multi-physical processes, which make prediction of printing product dimensions and properties difficult. Numerical simulations can help improve the fundamental understanding of AM processes.

Discrete Element Method (DEM) framework

A DEM framework is developed to simulate particle based AM processes [1]. The model includes distinct powder and solid particle interactions, both mechanical and thermal.
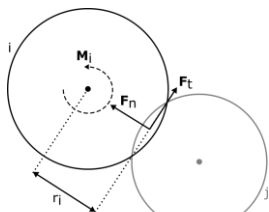
Fig 1: Schematic of particle contact, where forces and moments are generated depending on the amount of overlap.
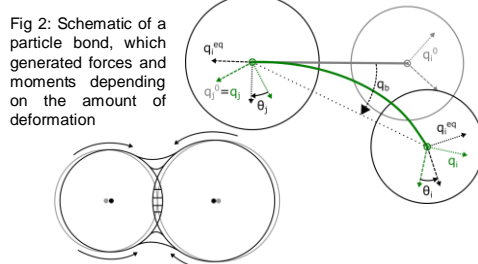
Fig 2: Schematic of a particle bond, which generated forces and moments depending on the amount of deformation
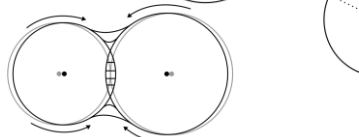
Fig 3: Schematic of particle bonding, where mass moves from the particles to the neck, effectively moving the mass points closer together.

Ray tracing

The heat source can be simulated with ray tracing, in which the laser is discretised with numerous rays which have an energy [2]. The exact traversal of the rays (and their energy) through the powder bed is calculated by reflection, refraction and absorption.
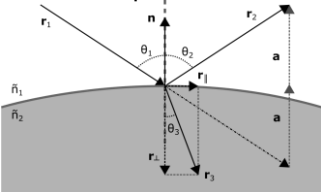
Fig 4: Schematic of ray interaction, where the incident ray r_1 splits up in a reflected r_2 and refracted ray r_3.
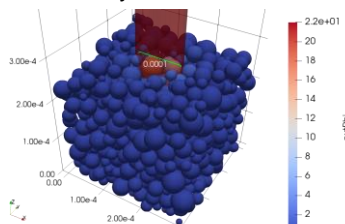
Fig 5: Example of a ray tracing simulation with a laser spot size of 100 μm.

Results

The developed DEM-ray tracing framework can be used to simulate various cases: powder or solid conduction, powder or solid mechanical performance, laser-powder bed interaction, the full AM process, influence of process parameters on a single track.
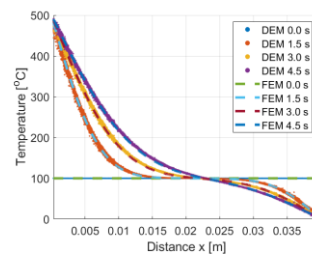
Fig 6: Transient heat conduction of a solid rod, simulated with DEM and compared to a Finite Element Method.

Fig 7: Mechanical response of a compression test performed on a DEM sample for an increasing amount of particles.
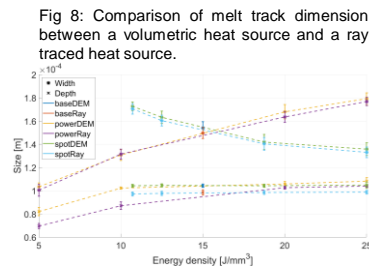
Fig 8: Comparison of melt track dimension between a volumetric heat source and a ray traced heat source.
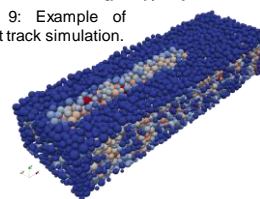
Fig 9: Example of melt track simulation.

Fig 10: Simulation of an H-shaped sample (intended shape in green), where various AM phenomena are observed: warpage of the side walls, delamination/insufficient bonding in the lower section of the walls, excessive addition on the bottom of the overhang.
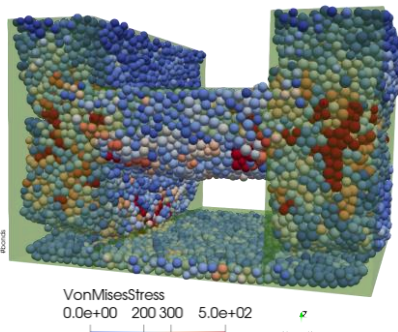
References

[1] Dorussen, B.J.A., Geers, M.G.D. & Remmers, J.J.C. A discrete element framework for the numerical analysis of particle bed-based additive manufacturing processes. Engineering with Computers (2022). https://doi.org/10.1007/s00366-021-01590-6
[2] Dorussen, B.J.A., Geers, M.G.D. & Remmers, J.J.C. Efficient ray tracing simulations for the numerical analysis of powder bed additive manufacturing processes. Manuscript in preparation (2022).

PhD progress 1 2 3 4

Drivability of piles under vibratory driving: small scale experiments

A.B. Fărăgău[1], M. Martinelli[1,3], A. Tsetas[1], A. Tsouvalas[1,2]

[1]Delft University of Technology, Department of Engineering
Structures, Section of Dynamics of Solids and Structures

[2]Delft University of Technology, Department of Hydraulic
Engineering, Section of Offshore Engineering

[3]Geo-Engineering Unit, Deltares

Introduction

In the current global climate, offshore wind is among the top green energy sources on which many countries rely on to make the energy transition. Its rapid expansion together with strict regulation poses challenges for the field. Vibratory driving is a promising installation technique for monopiles of offshore wind turbines which has advantages over a more standard impact driving technique (e.g., less noise pollution). Although, an established technique in other fields, the soil-structure interaction using this technique for monopiles is not completely understood.

To this end, a laboratory experimental campaign has been carried out. With the insight gained through these scaled experiments and an upcoming larger scale campaign, we hope to bridge the knowledge gap and lead to better drivability predictions for the vibratory driving technique.

Test setup

The test setup is presented in the figure below. Two types of soil have been used: dense and medium dense sand. The scale of the test is around 1/20-1/30. On top of the measured quantities specified below, the soil has been also instrumented with total pressure and pore-water pressure sensors at several locations. The **goal** of this experimental campaign is two-fold:
-   Infer soil-structure interaction characteristics using vibratory driving
-   Effect of driving technique on lateral bearing capacity (not discussed in this poster)

Crane — Load cell — Vibro-hammer — Accelerations — Penetration — Accelerations & Strains — Monopile — Strains — Sand container — Strains & Pressure
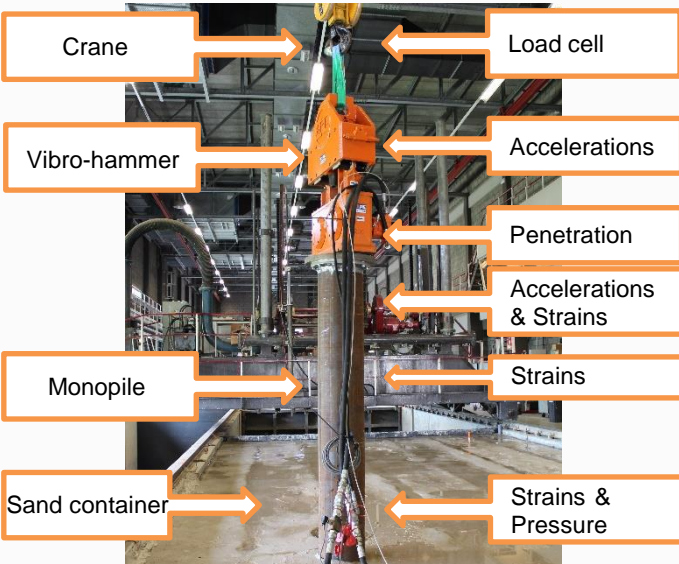
Preliminary results

Since the experimental campaign is ongoing, the final results and analysis are not yet available. Nonetheless, preliminary results for one of the pile drivings is presented hereafter.
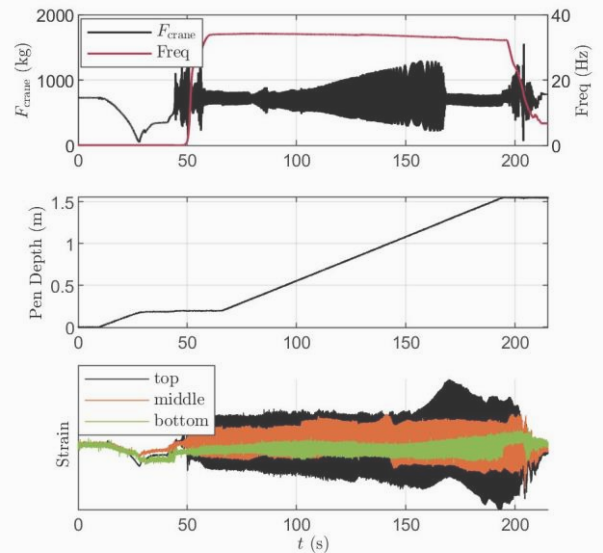
Figure 1: The force in the crane, frequency of driving, penetration depth, and strains at three locations on the pile versus time.

Using the load in the crane, the frequency of driving, and the imposed penetration rate as input, characteristics about the soil-structure interaction can be inferred from the strains observed at different locations along the pile (Figure 1). More specifically, the friction coefficient at the soil-pile interface for different friction models will be approximated. Furthermore, the influence of the higher harmonics (Figure 2) on the soil-structure interaction will also be analysed.
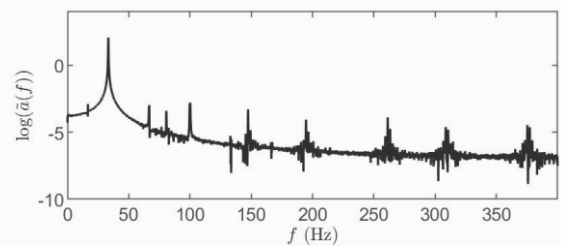
Figure 2: Frequency content of the accelerations measured on the pile.

Conclusions

The characteristics of the soil-structure interaction using vibratory driving are investigated through a scaled experimental campaign. Given the difficulty in scaling up these results, they will be mainly used in drawing qualitative conclusions.

Acknowledgements

Post-doc
1

TUDelft   Deltares   Enabling Delta Life   CAPE   grow

Multiscale modelling of plasticity in HCP metals

D. Fioravanti[1], J. Hoefnagels[2], E. van der Giessen[1], F. Maresca[1]

[1]University of Groningen
[2]Eindhoven University of Technology

Introduction

Hexagonal closed-packed (HCP) metals have several possible glide planes for **dislocations** (Fig.1). Macroscale plasticity and ductility depends on the hierarchy of activation of these slip systems. We adopt a **multiscale strategy** to connect the physics of single defects at the atomic scale to polycrystalline plastic behaviour of HCP metals.
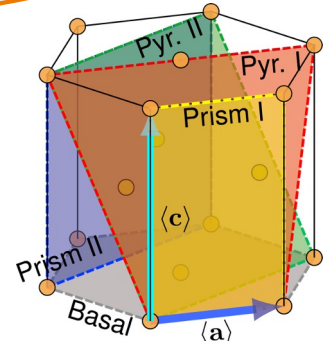
Fig. 1: HCP unit cell and glide planes. Image from [1].

Multiscale model

Density Functional Theory

$$\hat{H}\Psi = E\Psi$$
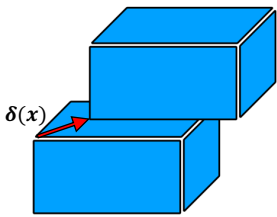
Fig. 2: Schematic of the system used to compute the Stacking Fault Energy function of the disregistry $\delta(x)$.
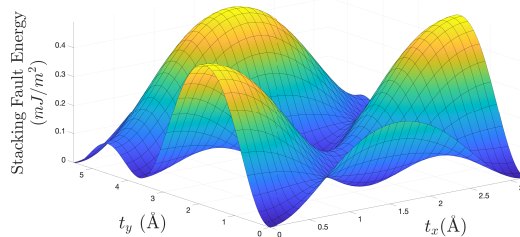
Fig. 3: Stacking Fault Energy of basal plane in Mg. t_x, t_y are the disregistry components

Output:
Stacking Fault Energy surface $\gamma(u)$

Peierls-Nabarro model

Minimization of the energy with respect to $\bar{\delta}(x)$ [2]

$$E[\delta(x)] = E_{elastic} + E_{misfit} = \int \int \frac{d\delta(x')}{dx'} \frac{H_s}{x - x'} \delta(x)dxdx' + \int \gamma[\delta(x)]dx$$

H_s = Anisotropic Energy Factors tensor
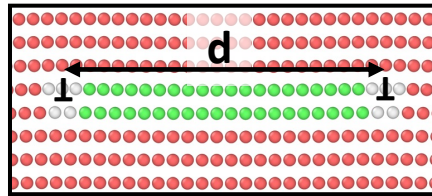
Fig. 4: Separation of a basal edge dislocation in Mg in two partials. Stacking fault region in green.

Element	d predicted (Angstrom)	d simulation (Angstrom)	τ_y predicted (MPa)
Mg	39.07	39.0	7.23
Co	21.90	20.6	74.68
Ti	8.21	11.1	11.48

Tab. 1: Predictions of the PN model for basal edge dislocations and comparison with simulations using interatomic potentials [3].

Output:
critical resolved shear stress τ_y

Crystal Plasticity

$$\frac{\dot{\gamma_\alpha}}{\dot{\gamma_0}} = \left(\frac{\tau^\alpha}{\tau_y}\right)^{1/m}$$

Plastic velocity gradient
$$L_p = \sum_{\alpha=1}^{N_s} \dot{\gamma_\alpha} \ (s_0^\alpha \otimes n_0^\alpha)$$

$\dot{\gamma_\alpha}$: plastic slip rate
$\dot{\gamma_0}, m$: rate sensitivity parameters
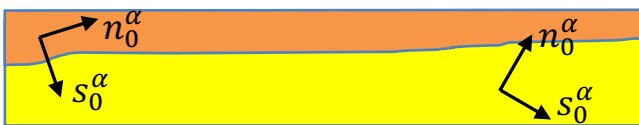
Fig. 5: Bi-crystal system with slip directions s_0^α and slip normals n_0^α

Comparison with experiments
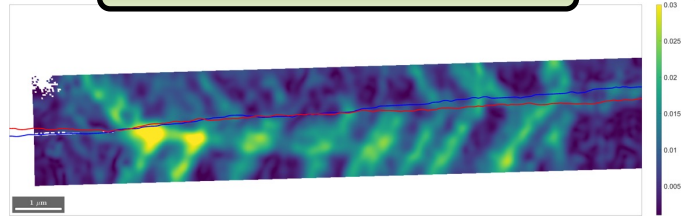
Fig. 6: Strain plots of a bi-crystal Zn sample obtained with nanotensile tests. Blue and red lines indicate the GB in both sides of the sample. Courtesy of Dennis König (TU/e).

Conclusions and future works

The ability of this multiscale framework to describe plastic deformation in HCP metals will be verified through comparison with experiments. Once validated, the model will be used to **design** new ductile alloys with HCP crystal structure.

References

[1] Yin et al. (2017) Acta Mater 123,223
[2] Shoeck (1994) Philos Mag A 69.6
[3] Chen et al. (2022) Adv. Theory Simul. 5.1

PhD progress
1 2 3 4

Comparison of the Nonlinear Elastic Behavior of Auxetic Lattice Architectures

T. Gärtner[1,2], S. van den Boom[2], J. Weerheijm[1], L.J. Sluys[1]

[1] *Delft University of Technology*
[2] *Netherlands Institute for Applied Scientific Research (TNO)*

Introduction

Mechanical metamaterials are man-made materials which derive their unusual properties from the geometry of their microstructure rather than their constituents. Auxetic metamaterials (materials with a negative Poisson's ratio) exhibit mechanical properties in the (quasi) static regime that are potentially promising for impact protection, given these properties are preserved in the highly dynamic regime. In this regime it is an open question to which extent the mechanical properties are retained and can possibly be maintained by adjustments in the microstructure, since the highly dynamic impact regime is typically accompanied by rate and inertia effects with geometrical nonlinearities as well as large plastic deformations and material nonlinearities.

Study

In a first step the geometrically nonlinear, elastic behavior of different auxetic architectures is investigated. The architectures shown in Figure 1 are all designed to posses the same Young's modulus of 20000 Pa and the same density of 1570 $kg\ m^{-3}$ and are subsequently compared for impact velocities ranging from quasi static (0 s^{-1}) up to strain rates of 10000 s^{-1} and for compression up to 30%. In Figure 2 the quasi-static responses of the different architectures with the given linear properties for large compression can be seen. The same architectures undergoing different strain rates are displayed in Figure 3.

re-entrant honeycomb · double arrowhead · chiral structure · anti-chiral structure · re-entrant honeycomb (rotated 90°) · double arrowhead (rotated 90°)
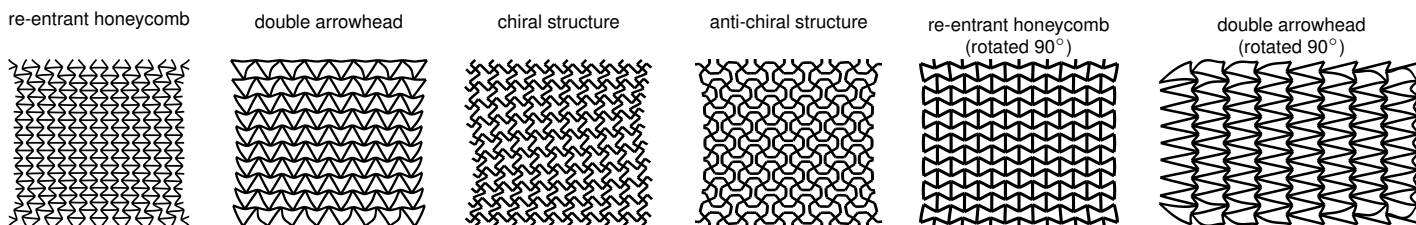
Figure 1: different architectures considered at 10% compression

Results

With the increase in strain, re-entrant honeycomb (rotated 90°) and double arrowhead architectures show an increased stiffness (see Figure 2), since here vertical beams are carrying the load. At higher strain levels, these structures are buckling and thus rapidly losing stiffness. Other structures exhibit a reduced stiffness from the start, due to a more horizontal orientation of the beams leading to longer leverage effects.

When looking at high strain rate cases a plateau stress is reached (compare Figure 3), which shows the maximum amount of resistance for the architecture. Whilst this plateau stress is independent of the velocity in most structures, it shows dependency on the velocity in re-entrant honeycomb (rotated 90°) and reduced resistance in the chiral structures architecture.
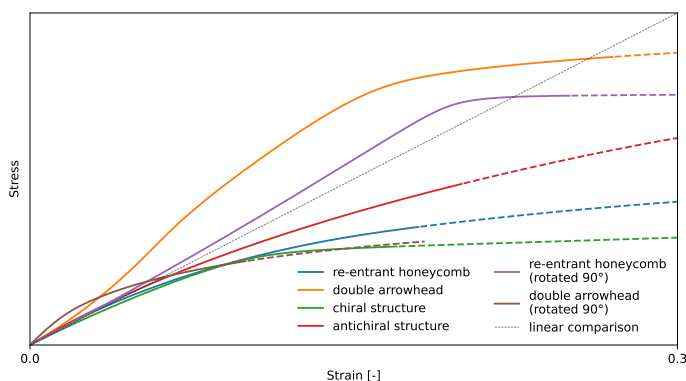
Figure 2: finite strain applied to the different architectures (dashes indicate not modeled self-contact in the structures)
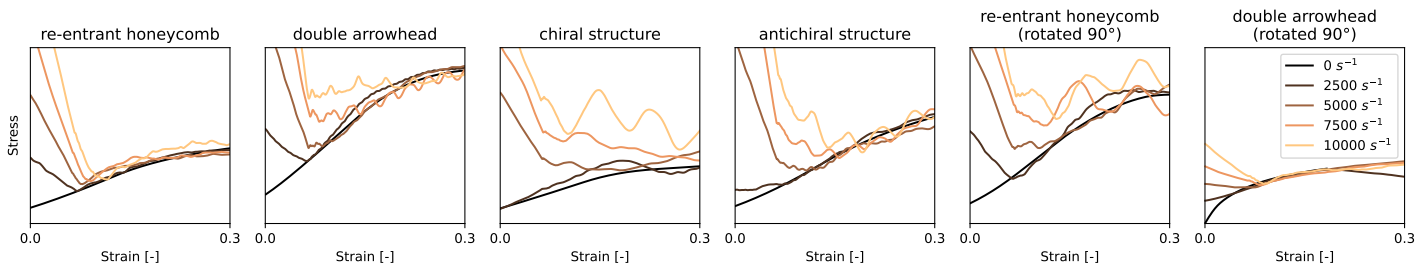
Figure 3: comparison of the effects of high strain rates on different architectures

PhD progress

1 | 2 | 3 | 4

TUDelft

TNO

Topology optimization with cleanability requirements

Reinier Giele, Can Ayas, Matthijs Langelaar

Delft University of Technology

Introduction

- Topology-optimized designs are typically geometrically complex and inaccessible.
- C*leanability* of structural components with jets is essential for many applications and requires accessible surfaces.
- The aim of this study is to take *jet accessibility* into account in topology optimization.
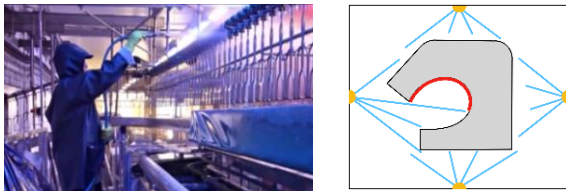
Figure 1: (left) sanitation of equipment by water jetting; (right) not all surfaces are accessible for jets.

Access measure method: Front propagation

In this method, front A propagates from the jet source which results in an arrival time field. Front B also propagates from the jet source but has a lower speed in solids. The delay caused by the density is a measure for accessibility.
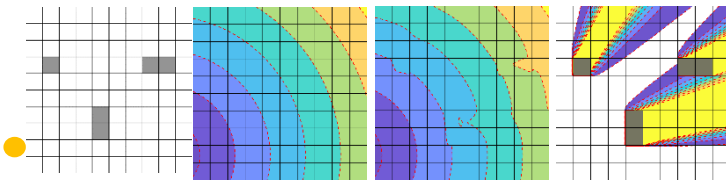
Figure 4: (from left to right) ; (1) blueprint design and jet position; (2) arrival time field A; (3) arrival time field B; (4) delay time field

Jetting method

Idea: All void, which is where dirt can reside, should be accessible by at least one jets.
Method: A filter converts any blueprint design into a jet accessible design, by converting inaccessible voids into solid: 1) for each jet an accessibility field is found ; 2) all accessibility fields are combined ; 3) the combined accessibility field is converted to a density field. This bans the void regions which are not reachable by a jet.
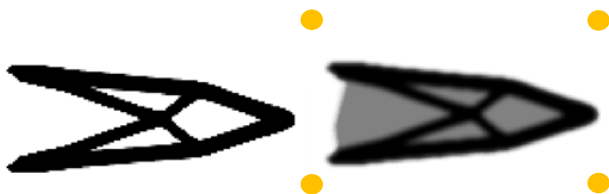
Figure 2: (left) exemplary blueprint design; (right) filtered design, where the inaccessible void regions are made solid.

2D tests

The method is tested with simple boundary conditions that create non-jettable designs if no filter is used. The structure is optimized for compliance/conduction with a fixed volume constraint.
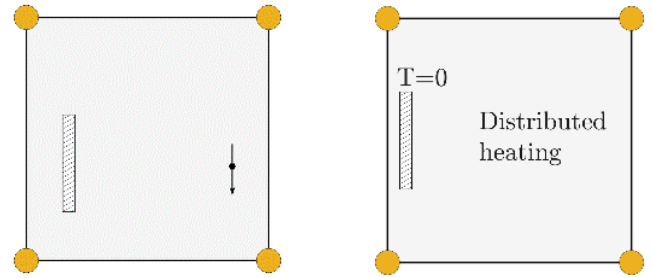
Figure 4: (left) the boundary conditions for the beam compliance problem; (right) the boundary conditions for the heat conduction problem

The filter succeeds in creating jettable designs, as all surfaces can be reached by at least one jet.
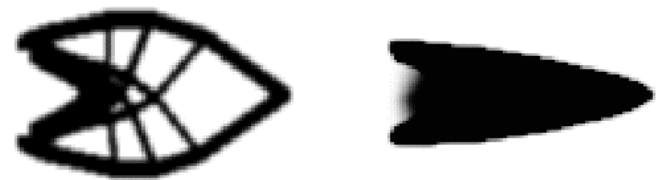
Figure 5: beam problem: (left) non jettable structure; (right) jettable structure
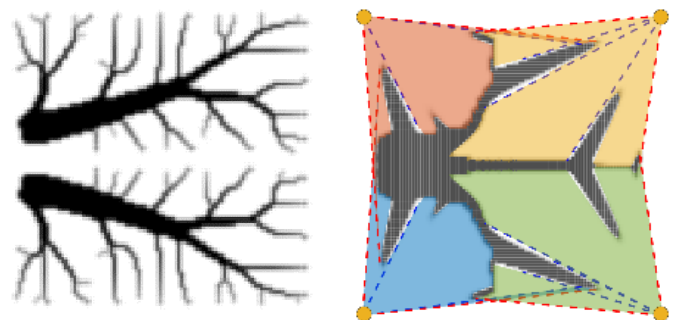
Figure 6: heat problem: (left) non jettable structure; (right) jettable structure and an analysis of the accessibility of each jet.

Conclusion and outlook

- The first successful method to ensure water jet access has been created for topology optimization.
- Front propagation allows for differentiable jettability identification.
- Future work: extension to 3D

Physically constrained machine learning: Simulating battery deformation

T. Gödde, Prof. Dr. ing. B. Rosić

Chair of Applied Mechanics & Data Analysis, University of Twente
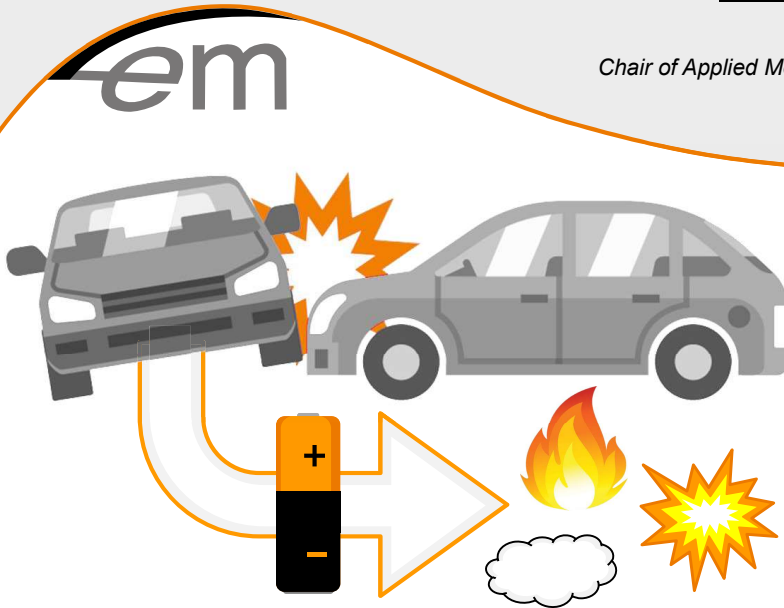
Challenges and Proposition

In this work the prediction of cylindrical battery mechanical response during crash is considered. Batteries are commonly modelled in a multiscale finite element framework [1] due to their multi-component structure, anisotropy and heterogeneity. In addition to the anisotropic behavior, battery mechanical behavior is dependent on state-of-charge and strain-rate. Such a simulation is, however, computationally demanding and must be substituted by a corresponding surrogate model.

The focus of this project is to replace the usually fully FEM-based solution by a neural network model. This model is called a physics constrained neural network (PCNN). Here, the PCNN is presented as a simple 2D battery model for axial compression.

A physical neural network

The governing equation of the mechanical response of cylindrical battery occupying the domain V in $\mathbb{R}^2$ under axial compression is [2]:

$$\nabla \boldsymbol{\sigma} + \boldsymbol{f} = \boldsymbol{0}, \qquad (1)$$

with displacement (Dirichlet) boundary conditions of the form:

$$\mathbf{u}(x_{BC}) = u_{BC}(x_{BC}), \qquad x_{BC} \in V_D. \qquad (2)$$

Here, $\nabla \boldsymbol{\sigma}$ is the gradient of the stress tensor, whereas $\boldsymbol{f}$ are the internal forces. In addition to that, stresses and Cauchy strains are related by:

$$\boldsymbol{\sigma} = \boldsymbol{C} : \boldsymbol{\varepsilon}, \qquad (3)$$

in which $\boldsymbol{C}$ is the fourth order elasticity tensor, which for an isotropic material depends on two parameters: Young's modulus E and Poisson ratio ν. These three equations can be rewritten into a sum weighted residual of the problem:

$$L(\boldsymbol{x}, \boldsymbol{x_b}, \boldsymbol{x_t}) = L_e(\boldsymbol{x}) + L_c(\boldsymbol{x}) + L_{u_b}(\boldsymbol{x_b}) + L_{\theta_b}(\boldsymbol{x_b}) + L_{u_t}(\boldsymbol{x_t}), \quad (4)$$

in which L_e and L_c are squared errors describing the component sum of squared residuals obtained from Eq. 1 and 3. Similarly, L_{u_b} and L_{θ_b} describe the fixed boundary at the bottom points x_b and L_{u_t} the influence of the external force (compression at the top of the battery). In Eq. 4,

$$L_{\theta_b}(\boldsymbol{x_b}) = ||\tfrac{\partial u_1}{\partial x}(\boldsymbol{x_b})||_2 + ||\tfrac{\partial u_2}{\partial y}(\boldsymbol{x_b})||_2, \qquad (5)$$

represents the loss term defining the displacement gradient (angle) boundary condition at the bottom. Here it is assumed that the angles are of small magnitude, i.e., $\theta_1 = \frac{\partial u_1}{\partial x}(\boldsymbol{x_b})$.

The loss function is utilized to train the feedforward neural network that maps spatial positions to displacements and stresses. The convergence of the algorithm is shown in Figure 1, whereas a comparison of the battery response for one displacement component is shown in Figure 2.
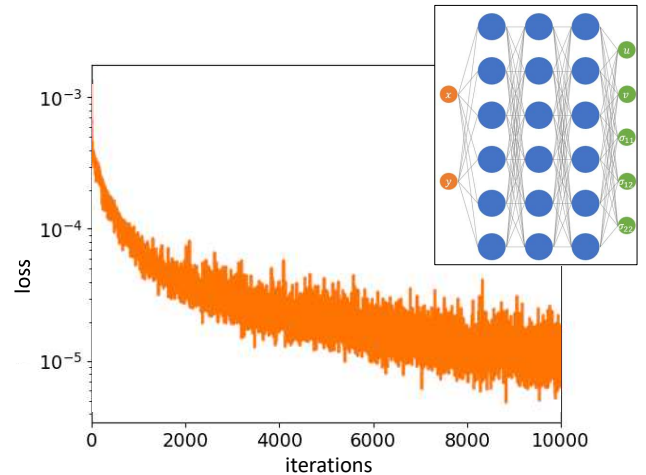
Figure 1: Loss plot 2D battery PCNN in logarithmic scale.
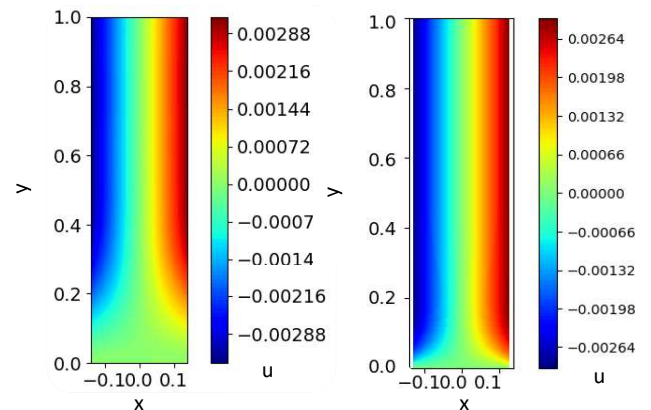
Figure 2: Horizontal displacement component PCNN (left) and FEM approximation (right) with normalized spatial coordinates.

Conclusion

The PCNN battery model can predict battery displacements accurately. However, stresses are not predicted well due to large local gradients in the stress fields. The main cause of this is the global definition of the formulation. Using physics-constrained models improves extrapolation properties when compared to data-driven fits.

References

[1] Gilaki M, Avdeev I. 2016. Impact modeling of cylindrical lithium-ion battery cells: a heterogeneous approach. *Journal of Power Sources*. 328:443–51.

[2] K. Bathe. Finite Element Procedures in Engineering Analysis. Prentice-Hall, Inc., Englewood Cliffs, New Jersey 07632, USA,1982.

[3] G. E. Karniadakis M. Raissi P. Perdikaris. "Physics Informed Deep Learning (Part I): Data-driven Solutions of Nonlinear Partial Differential Equations" (Nov. 2017). arXiv.1711.10651.

Contact details

t.godde@utwente.nl

UNIVERSITY OF TWENTE.

PhD progress
1 2 3 4

materials innovation institute

TATA STEEL

Computational Modelling of Discontinuous Tape Thermoplastic Composites

D.E. Gülmez, S. Turteltaub, J. Sinke, C. Dransfeld

Delft University of Technology
Faculty of Aerospace Engineering
Department of Aerospace Structures and Materials

Discontinuous Tape (DT) Thermoplastic Composites have have many advantages in terms of environmental (recyclability), manufacturing (complex-shaped components) and mechanical (tailorable) aspects. However, their high sensitivity to orientation and size causes difficulties in estimating mechanical properties due to spatial variability and complexity in the structure. This spatial variability is also related to the geometrical boundaries.

Scope of the project is to improve a modelling technique to understand the mechanical properties and failure behaviors of DTs considering the effects of geometrical boundaries such as the frame of the mould cavity and moulded-in pin holes.

Challenges are:
1. Limitations of the commercial software to generate Representative Volume Element (RVE)
2. Implementation of direction-dependent damage onset and propagation

Goals are:
1. To improve an RVE according to geometrical boundaries
2. To formulate anisotropic cohesive laws for a microstructural damage model

Generation of DT Structure:
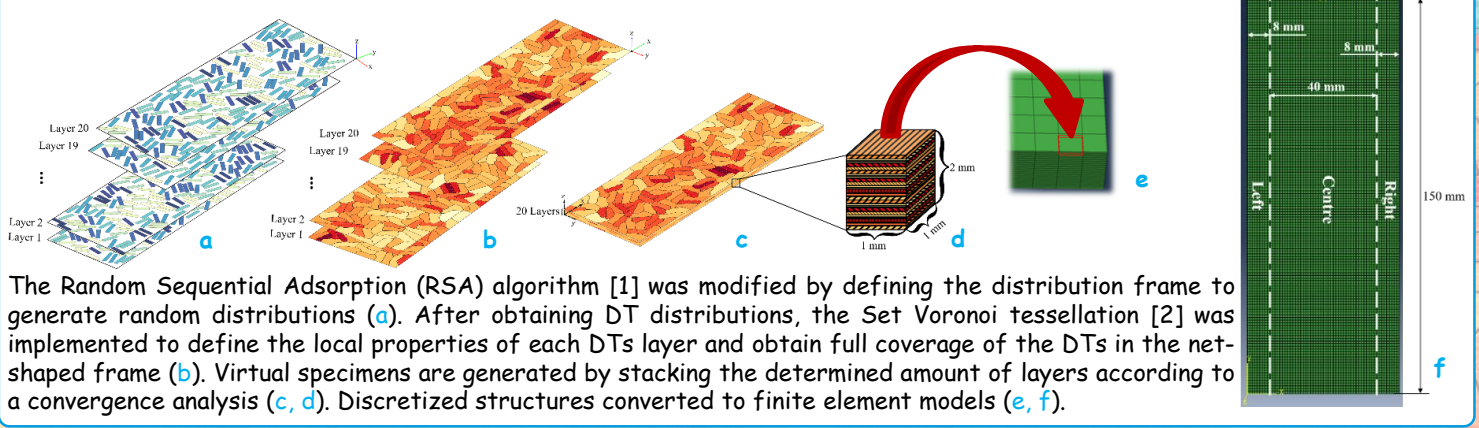
The Random Sequential Adsorption (RSA) algorithm [1] was modified by defining the distribution frame to generate random distributions (a). After obtaining DT distributions, the Set Voronoi tessellation [2] was implemented to define the local properties of each DTs layer and obtain full coverage of the DTs in the net-shaped frame (b). Virtual specimens are generated by stacking the determined amount of layers according to a convergence analysis (c, d). Discretized structures converted to finite element models (e, f).

Results (1):

(a) Orientation tensor and elastic modulus through the width of one virtual specimen (b) Stress-Strain curve of one virtual specimen

(c) Longitudinal stiffness and (d) Matrix failure distribution in one virtual specimen (e) Comparison of normalized stiffness according to CLT and FEM according to specimen regions
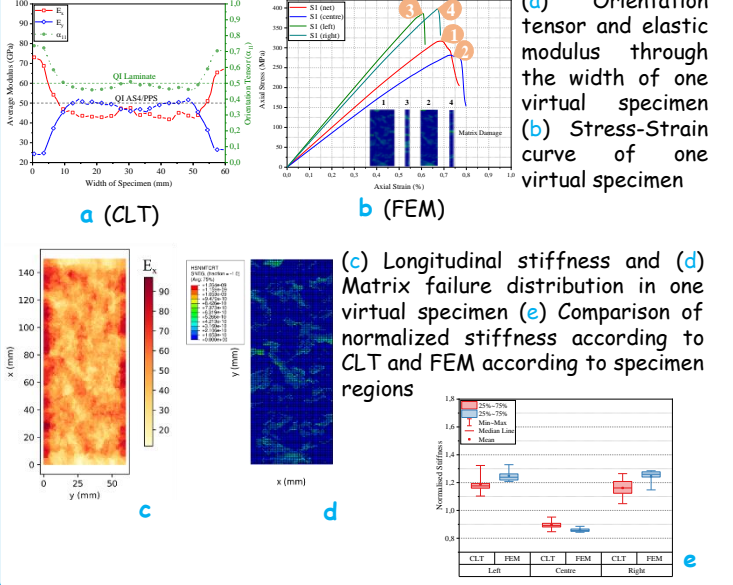
Results (2):

Anisotropic Cohesive Modelling:

The Cartesian discretization of the randomly orientated DTs for numerical calculations leads to limits on anisotropy in cohesive laws.

Due to the structural limitations, an orientation-dependent function was defined for the interpolation by considering the longitudinal and transverse mechanical response of DTs. A linear softening relation was implemented between the tractions and displacement jumps evolution under mixed-mode loading conditions.

Conclusion and Future Work: The results showed that stiffness at the edges of specimens is higher than in the centre of the specimens due to the high alignment of DTs. The modelling technique enables the analysis of hybridization of discontinuous-continuous tapes and open hole test with drilled and moulded-in pin holes.

References:
[1] Feder J. Random sequential adsorption. J Theor Biol. 1980;87(2):237–54.
[2] Schallerab F.M., et.al., Set Voronoi diagrams of 3D assemblies of aspherical particles. Philos Mag. 2013;93(31-33):3993-4017.

TUDelft

PhD progress
1 2 3 4

Fraunhofer
IBP

Residual stresses in fusion-bonded thermoplastic composites

M. Gurian[1], L. Warnet[1], E.T.J. Klompen[2]

[1]University of Twente

[2]Thermoplastic Composites Research Center

Introduction

The manufacturing of thermoplastic composite parts in high volumes is made possible by various production technologies, such as induction- and ultrasonic-welding or overmolding processes. However, a lack in detailed and physics-based understanding of the processes leads to uncertainties in the short- and long-term performance of the manufactured parts. Developing techniques that make the detailed stress-state of the parts more accessible enables a more predictable performance and, hence, an overall environmentally friendlier manufacturing. Not only because the amount of used material can be minimized but also because primary load carrying structures can be designed with composites instead of metals leading to lighter systems, and therefore reduced CO_2 emissions.

Background

(1) Induction welding — Coil, Magnetic field, Cooling, Blanks, Pressure

(2) Ultrasonic welding — Sonotrode, Clamps, Blanks, Base

(3) Overmolding — Form, Insert, Blank, Base, Oven

All three can fusion-bond two seperate parts.

How is this thermo-mechanically modelled?

Research

INPUT → MATERIAL STATE → TEMPERATURE HISTORY / RESIDUAL STRESSES
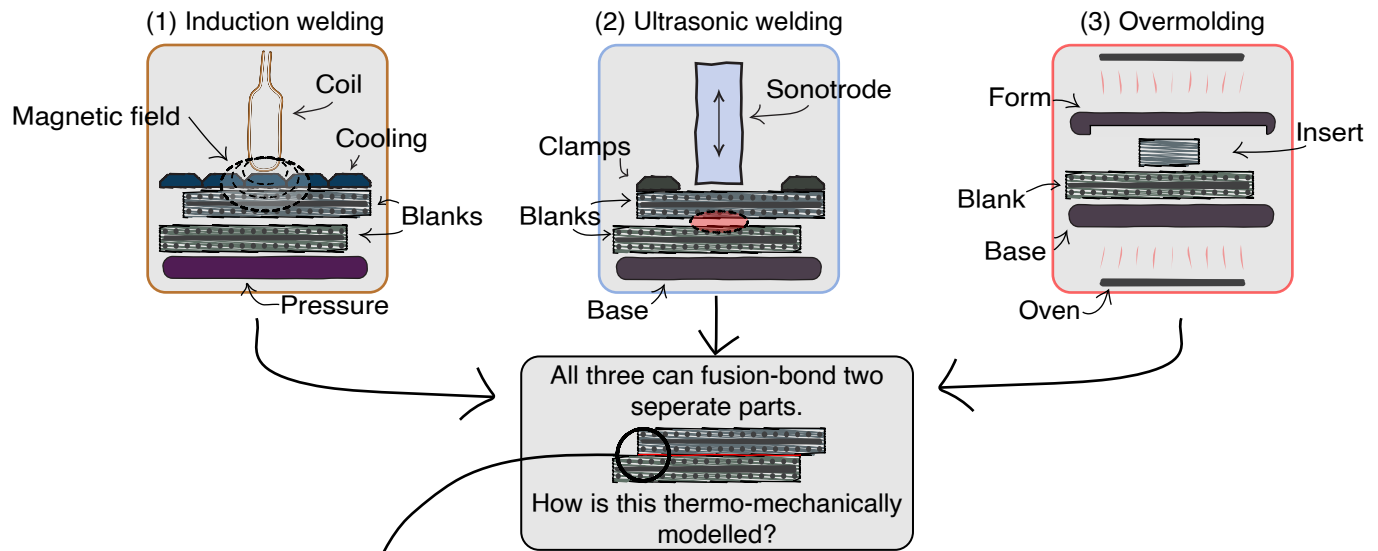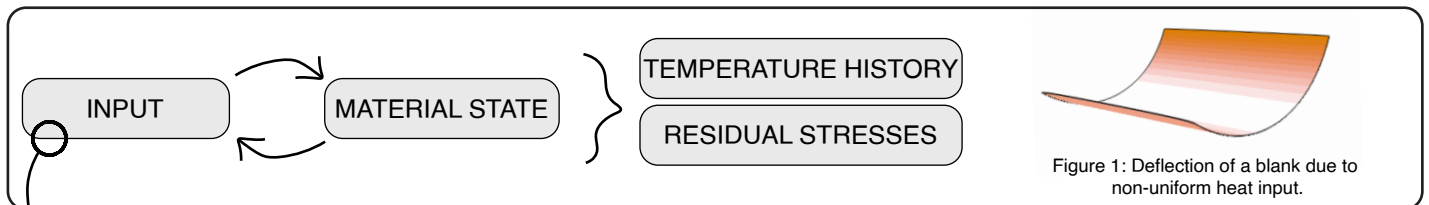
Figure 1: Deflection of a blank due to non-uniform heat input.

Input defined by process

They differ in...

	(1) Induction welding	(2) Ultrasonic welding	(3) Overmolding
Heating-rate	> 5 °C/s	> 500 °C/s	10 - 20 °C/s
Processing time	Seconds-Minutes	Seconds	Minutes
Heating-mechanism	Joule heating	Friction	Oven
Heat generation	In carbon fibres	Energy director	Uniformly
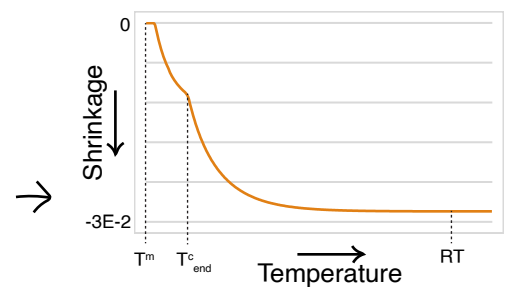
Figure 2: Shrinkage of a blank during uniform cooldown and input-dependent material state.

Progress

• Numerical input prediction for induction welding possible.
• Adaptable thermo-mechanical model available and validated against works in literature.
• Material characterization for material state started.

Aniticipated outcome

• Workflow of predicting residual stresses after manufacturing cycles.
• Validation of stresses over continuous deflection measurements or, if necessary, more advanced methods.
• Extended material characterization of different materials, focussing on widely used materials.
• Relating stress-states to experimentally determined parameters, for example fracture toughness measured by DCB.

Active noise control in anechoic chambers using an efficient scheme incorporating frequency-domain derived filters

R. Haasjes[1], A.P. Berkhoff[1,2]

[1]University of Twente ET-AMDA, Drienerlolaan 5, 7522 NB Eneschede (NL)
[2]TNO Acoustics and Sonar, Oude Waalsdorperweg 63, 2597 AK Den Haag (NL)

1. Introduction

Acoustic anechoic chambers:
• Conduct measurements and experiments under free-field conditions;
• **Low-frequency reflections** due to limitations of the passive absorption measures [1];

Active noise control:
• **Effective at lower frequencies**;
• Requires a large number of sensors and actuators in geometries with large dimensions.
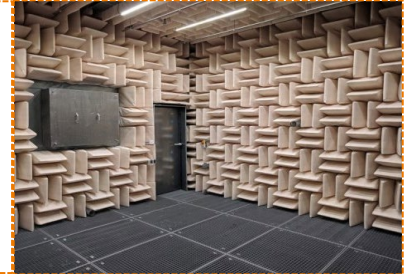
2. Objective

The goal is to obtain a controller with a **low computational effort** having the following requirements:
• The controller is fixed;
• The controller is computed with **measured transfer functions**, which:
  • Enables the use of **ordinary sensors and actuators**;
  • Eliminates a **calibration stage**.

3. Approach

• **Time-domain** algorithm, iteratively minimizing the mean squared error signal;
• **Prewhitening** via the **frequency-domain** to decorrelate and prewhiten the reference signals;
• **Preconditioning** via the **frequency-domain** to diagonalize the plant;
• **Causality** by appropriate **delay** and **truncation** techniques.

4. Signal decorrelation

Coherence between reference signals
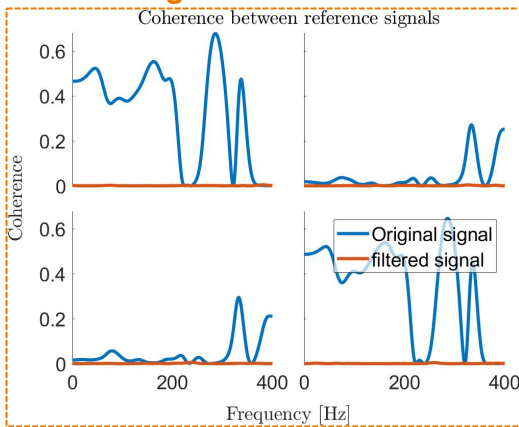
5. Plant diagonalization

Plant diagonalization

6. Convergence
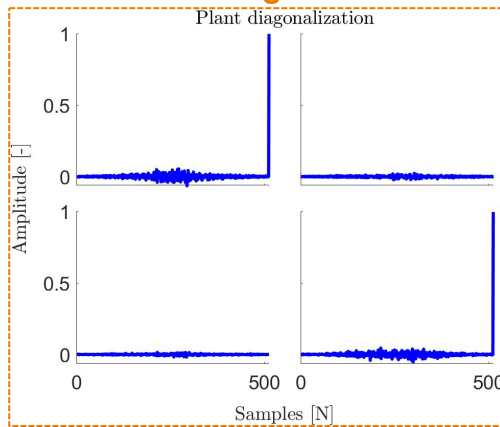
Training filter coefficients C(z): performance
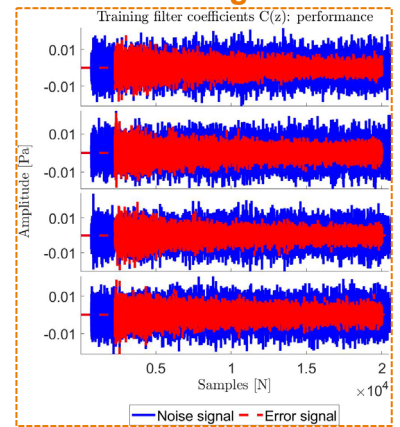
7. Fixed filter coefficients

$W(z)[1,1]$ filter coefficients
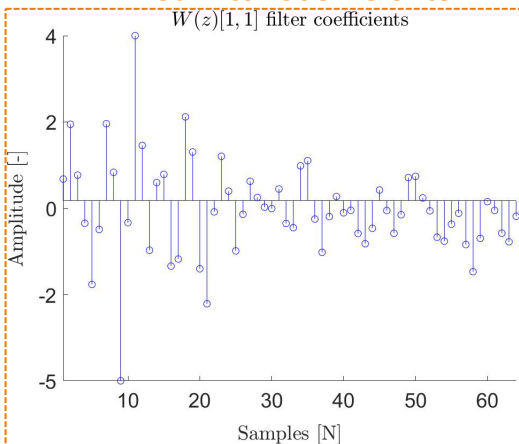
8. Fixed filter performance

$W(z)$ performance
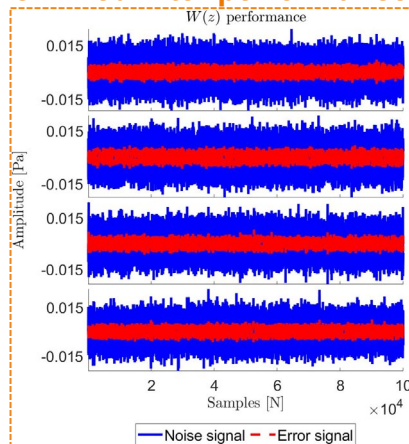
9. Conclusion

• Efficient because of the **frequency-domain computations**;
• Effective **signal decorrelation** using the prewhitening filter;
• Effective **decoupling of the plant** using the preconditioning filters;
• **Causality** ensured by delay and truncation techniques;
• **10.7 dB reduction** averaged over all sensor locations.

References [1] S. Schneider and C. Kern. "Acoustical Behavior of the Large Anechoic Chamber at the Laboratoire de Mécanique et d'Acoustique in the Low Frequency Range". In: Acta Acustica united with Acustica 94 (Jan. 2008), pp. 141-147.

UNIVERSITY OF TWENTE.

PhD progress
1 2 3 4

TNO innovation for life

Computational Micromechanics Modeling of Failure in Composites

Zhe Han[1,2], Frans van der Meer[1],
Boyang Chen[2]
[1] *Civil Engineering and Geosciences, Delft University of Technology*
[2] *Aerospace Engineering, Delft University of Technology*

Introduction

Composites are an attractive material for lightweight and high strength structures. However, damage behaviour of laminates leads over-safe design factors limiting utilization of the load carrying capacity. To make full use of the bearing ability, it is necessary to study failure behaviour in composite materials. Damage behavior of composite laminates is quite complex because of their multi-scale structures and anisotropic properties. The strength of composite materials mainly stem from fiber tension capacity along the axial direction. On this condition, tensile failure with fiber pull-out should be given more attention in details. Describing the process from individual fiber breaks to global failure of the composite material requires a micromechanical approach. Moreover, to capture fiber pull-out behaviour, the numerical model needs to be in 3D space, which would be computational costly. Therefore, building a finite element model at the micro-scale with damage details and good performances on computational efficiency is needed.

Research Approach

Researchers focused on the topic of fiber pull-out simulation have proposed a series of practical methods. Povirk and Needleman [1] put forward a friction constitutive relation for sliding incorporated with the fiber pull-out failure and implemented simulations by a 2D finite element code, while it might lost part of details due to the 3D nature of the problem. A 3D finite element model was employed by Singh [2] et al to investigate damage behaviour of a single fiber embedded in the matrix during fiber pull-out. However, capturing the interaction between multiple fibers would cost a lot computational resources considering the number of degree of freedoms in 3D solid elements.
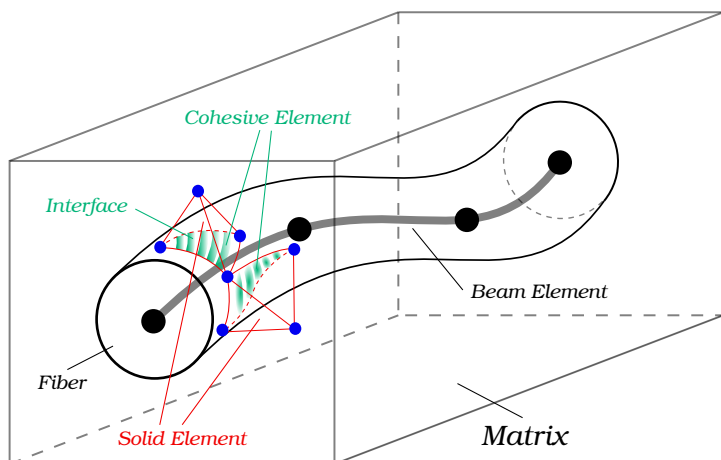
Figure 1: Schematic figure of the 3D beam-solid cohesive element

In this project, as depicted in the Figure 1, inspired by the method of structural-structural cohesive element proposed by Russo and Chen [3], instead of using solid elements in the whole domain, we propose a dedicated finite element model to simulate damage behaviour at the micro-level using higher order structural elements in combination with a cohesive zone model in 3D space. In this model, fiber failure, matrix cracks and debonding are expected to be captured by beam elements, solid elements and cohesive elements respectively.
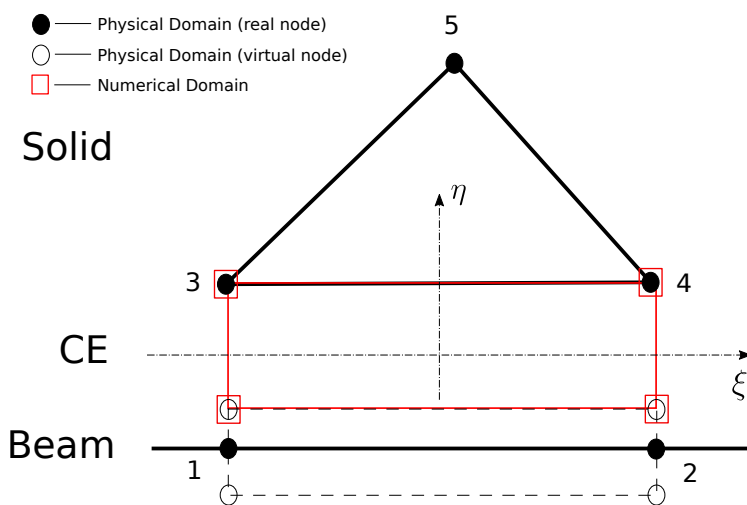
Figure 2: Schematic figure of the 2D beam-solid cohesive element (current stage of the project work)

Future Plans

In light of the above descriptions of the project, a few future research plans are hereby proposed:

(1) Extend the existing 2D beam-solid cohesive element to its counterpart in 3D space.

(2) Use the 3D beam-solid cohesive element to model failure in composite materials at the micro-level.

(3) Use the microscale computational damage model in a multiscale framework.

References

[1] G. L. Povirk, A. Needleman. Finite Element Simulations of Fiber Pull-Out. *J. Eng. Mater. Technol.*, 1993, 115(3): 286-291

[2] Daljeet K. Singh et al. Finite Element Modeling of the Fiber-Matrix Interface in Polymer Composites. *J. Compos. Sci.*, 2020, 4(2):58-70.

[3] Raffaele Russo, Boyang Chen. Overcoming the cohesive zone limit in composites delamination: modeling with slender structural elements and higher-order adaptive integration. *Int J Numer Methods Eng.*, 2020, 121:5511-5545.

PhD progress
1 2 3 4

A dynamic homogenization framework towards analysis of acoustic-structure coupling for metamaterials

Z.H. He[1,2], L. Liu[1], V.G. Kouznetsova[1]

[1]Eindhoven University of Technology
[2]Beijing Jiaotong University

I. Introduction

Background: Noise pollution is recognized as one of major environment pollutions in the world.

Different noise sources.
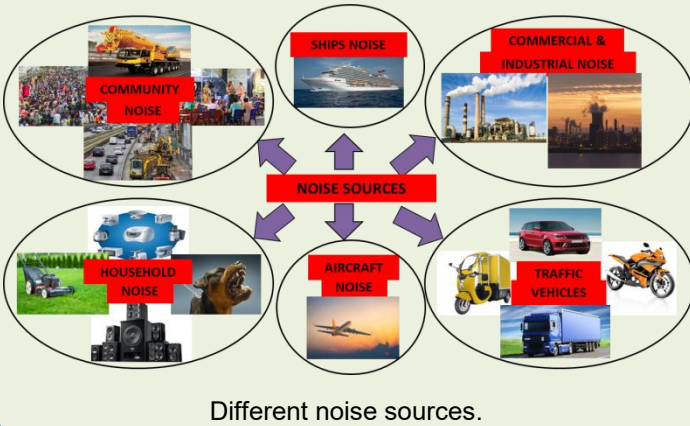
Motivation-1: Metamaterials/phononic crystals can realize sound insulation and noise reduction due to their excellent physical characteristics, such as negative mass density and negative stiffness.
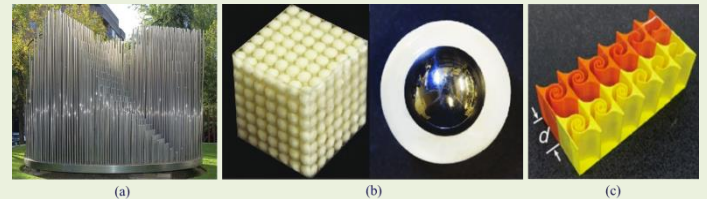
(a) Sculpture in Madrid [1]; (b) Locally resonant metamaterial [2]; (c) Thin planar metasurface with tapered labyrinthine unit cells for the wavefront modulation [3].

Motivation-2: The properties of the **acoustic-structure coupling** (sound radiation and sound transmission) can be studied to achieve vibration isolation and noise insulation in practical engineering.

Goal: Develop a framework for analyzing the **acoustic-structure coupling** problem for the locally resonant acoustic metamaterials using **homogenization approach**.

II. Homogenization framework

Hypothesis-1: Transverse shear is neglected;
Hypothesis-2: Small deflection;
Hypothesis-3: The acoustic fluid domain is **inviscid**.

Metamaterial plate

Unit cell

Linear Superposition

macro-to-micro scale transition

Acoustic-structure coupling

Sound radiation **Sound transmission**

Effective properties:
1. Local resonance;
2. Dynamic effective bending stiffness;
3. Dynamic effective density.

Quasi-static response + **Internal dynamics**

micro-to-macro scale transition

The main steps involved in computing the effective properties of the metamaterial

III. Numerical results and analysis

Metamaterial Models: Design different metamaterials for sound radiation and sound transmission.
Surrounding media: Analyse acoustic-structure coupling of metamaterials considering different media, such as in the air, immersed in the external mean flow and underwater.

Dynamic effective mass density: (a-2) in-phase and (a-3) anti-phase modes for the double plates metamaterial model.

Dynamic effective mass density

Sound pressure level (SPL)

Sound transmission loss (STL)

(a) Metamaterial model-- Sound radiation

(b) Metamaterial model— Sound transmission
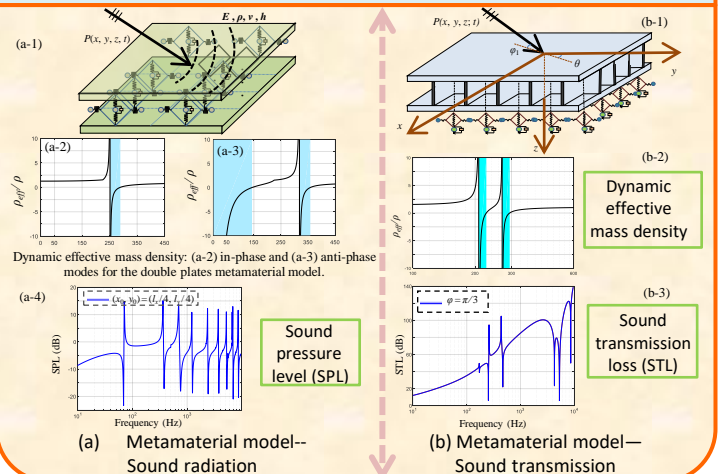
References

[1] R. Martinez-Sala et al. (1995). Nature.
[2] Z. Liu et al. (2000). Science.
[3] Y. Xie et al. (2014). Nat. Commun.
[4] L. Liu et al. (2021). Comput. Methods Appl. Mech. Engrg.
[5] A. Sridhar et al. (2016). Comput. Mech.
[6] B. Mace. (1981). J. Sound. Vib.

Technische Universiteit Eindhoven University of Technology

Email address: z.h.he@tue.nl

Predictive Maintenance Models for Military Aircraft Systems

N.A. Heerink, R. Loendersloot , T. Tinga
University of Twente
Department Mechanics of Solids, Surfaces and Systems
Dynamics Based Maintenance group

Introduction

Military aircraft maintenance follows the Aircraft Maintenance Program (AMP) or is triggered by defects. To benefit from flying in milder conditions, slower degradation rates and to utilize actual knowledge about the system's condition, the Operator is in need of a tool that enables him to maintain his aircraft more efficiently – a Predictive Maintenance (PdM) Tool.

Opportunities that emerge:
Newer generations military aircraft are increasingly more capable to support PdM through acquiring enormous amounts of data on usage, health/condition and degradation

Proposed **Solution**:
By using a physics-based approach, progressing of failure mechanisms is simulated, Remaining Useful Life (RUL) is determined, and optimal maintenance moments are found which may deviate from the original maintenance program, as depicted in figure 1.
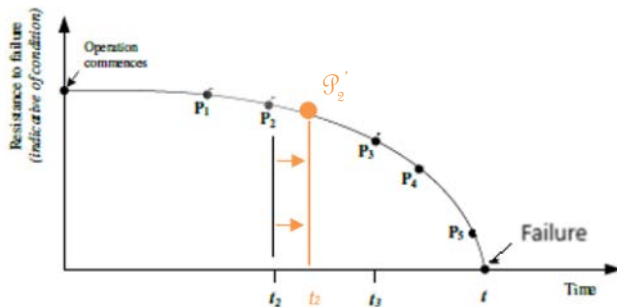
Figure 1. Adapted P-F chart. P_x represents an maintenance opportunity. The orange line presents a better suitable maintenance opportunity moment (P_2').

Approach
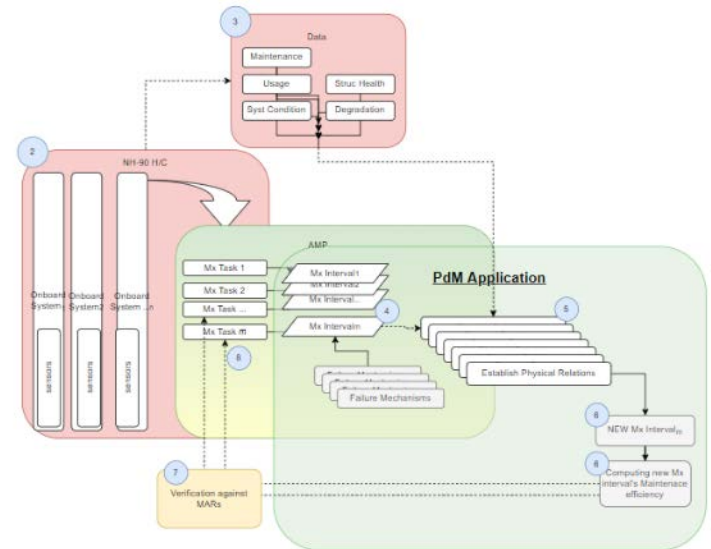
Figure 2. Schematic representation of the PdM Tool

The approach is a preliminary frame-work that combines acquired usage and loading data with identified failure modes, providing RUL predictions through a PdM application (Figure 2).
The PdM Tool combines the calculated RULs with the original maintenance program and proposes new maintenance moments in order to find an optimal maintenance efficiency

Results

Figure 3. Results of predictive calculations for leaking helicopter Main Landing Gear struts

Ref to figure 3. Through physical modelling, the degradation of helicopter components is simulated and a RUL estimate is calculated, enabling the Operator to choose its ideal maintenance moment.

The calculated result also satisfies the requirements for maintenance interval escalation according aviation regulations

Remaining Useful Landing Cycles for the NH-90 MLG-struts

Average weight category T/O- & landing weight cycle	RH MLG SA	LH MLG SA
8750	377	369
9000	375	369
9250	373	368
9500	371	366
9750	368	364
10000	366	363
10250	364	363

References

[1] Ochella, Sunday. Adopting machine learning and condition monitoring P-F curves in determining and prioritizing high-value assets for life extension. Expert Systems with Applications, Volume 176, 15 August 2021, Article number 114897 DOI:10.1016/j.eswa.2021.114897
[2] Heerink, Nick & Curran, Richard & Tinga, Tiedo & Ghobbar, Adel. (2013). Prognostic Enhancements on Health and Usage Monitoring Systems. 10.1007/978-1-4471-4426-7_61.

UNIVERSITY OF TWENTE.

Postdoc progress

Koninklijke Luchtmacht

Graph Neural Networks for computational homogenization

Fleur Hendriks[1], Ondřej Rokoš[1], Vlado Menkovski[1], Martin Doškář[2],
Marc G. D. Geers[1]

[1]*Eindhoven University of Technology*
[2]*Czech Technical University in Prague*

Introduction

With multiscale modeling, we try to predict the material behavior at the macroscale from its microstructure using a representative volume element (RVE). This involves determining the response of the material at every material point. Unfortunately, finite element (FE) simulations are often too slow. For this reason, we want to create a surrogate model of the material behavior, using graph neural networks (GNNs).

Microscale simulation gives homogenized stress and stiffness to macroscale

Macroscale gives a deformation to microscale simulation

$\mathbf{P}, \mathbf{A}$

$\mathbf{F}$

Microscale RVE problem (PDE)
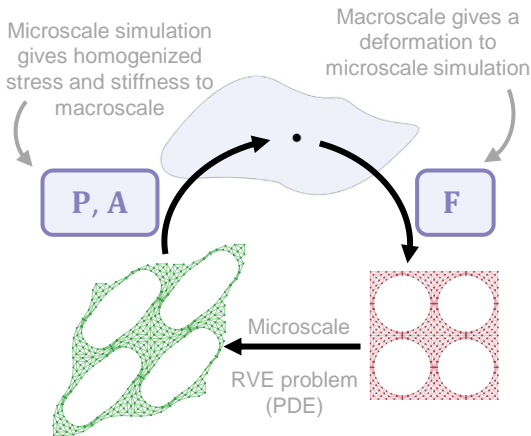
Graph neural network

A GNN is a neural network that takes a graph as input. It then updates the graph by, for example, updating the node positions, or updating the element and/or node attributes [1].

Why GNNs?

- Use geometry as input, which makes generalization to different microstructures possible
- Can easily represent FE mesh
- Allow for large deformations
- Can respect all relevant symmetries

References

[1] Satorras, Víctor Garcia, Emiel Hoogeboom, and Max Welling. "$E(n)$ equivariant graph neural networks." International conference on machine learning. PMLR, 2021.

RVE mesh before deformation

$\mathbf{F}$

Preprocessing

Mesh after affine deformation and preprocessing

GNN

Graph part

Dense part

$\mathfrak{W}$

Strain energy density of entire system

$\dfrac{\partial \mathfrak{W}}{\partial \mathbf{F}}$

1st Piola-Kirchhoff stress tensor $\mathbf{P}$

$\dfrac{\partial^2 \mathfrak{W}}{\partial \mathbf{F}^2}$

Stiffness tensor $\mathbf{D}$

Predicting

To predict how the material will deform, we simply train the network to move the vertices to the right positions. To predict the strain energy density of the material, we train a graph-level output. To obtain the stress and stiffness, we differentiate the energy once and twice, respectively, which machine learning libraries can do via automatic differentiation.

Results

Stiffness $\mathbf{D}$

Prediction

Deformation

FEM result

Strain energy density $\mathfrak{W}$

Stress $\mathbf{P}$

TU/e Technische Universiteit Eindhoven University of Technology

TU/e EAISI
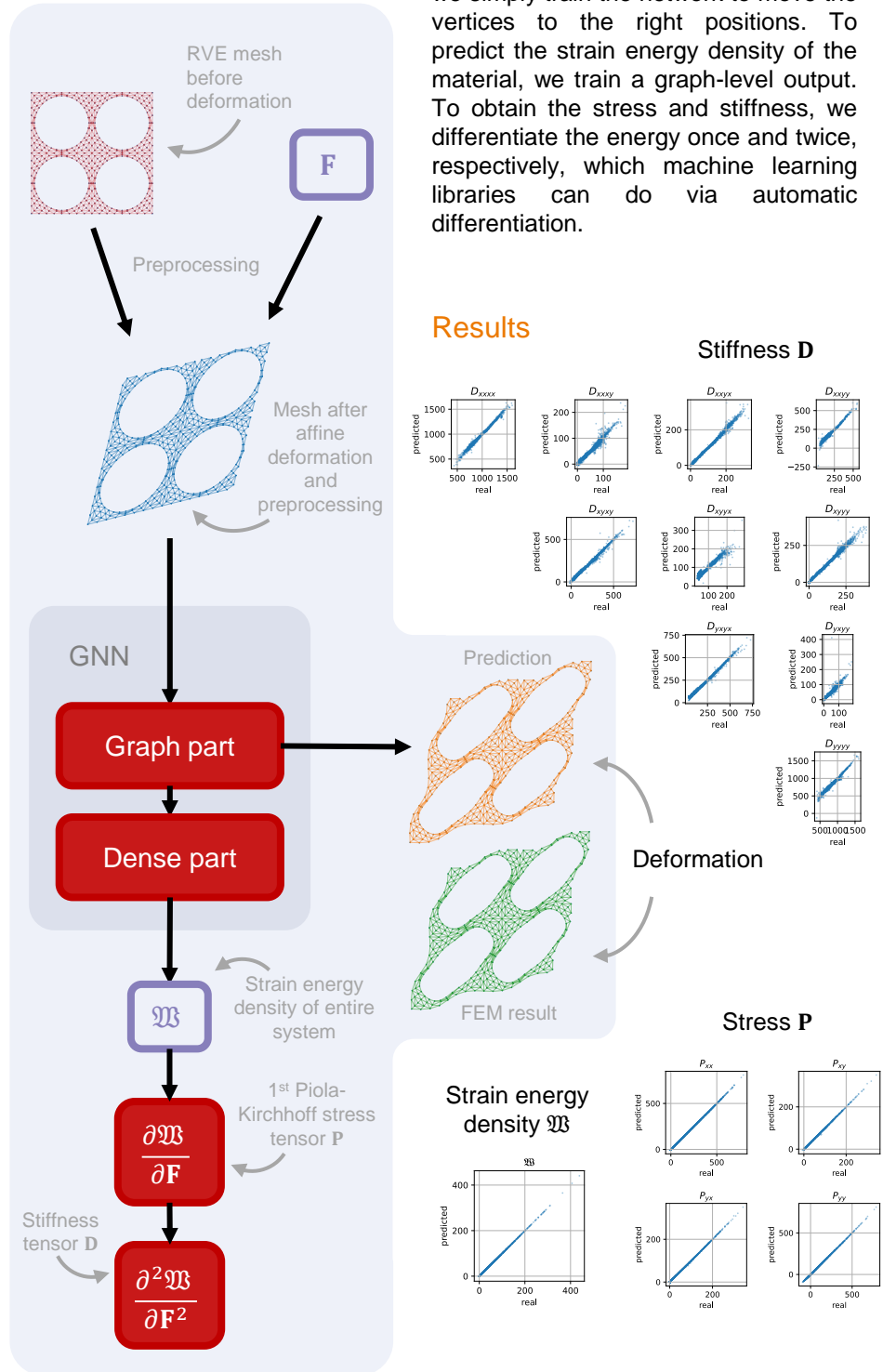
A level set eXtended IsoGeometric Analysis approach for finite strains

N. Hermann

Department of Precision and Microsystems Engineering, Delft University of Technology

Introduction

Motivation

- In biomedical and protective applications, structures are exposed to a wide variety of operational conditions
- Structural deformation, as well as material behavior go beyond linear approximation models
- Structures are constituted of combinations of different materials with complex geometries and physical responses

Aim of this work

- Development of a finite strain framework based on a XFEM level-set approach
- Application of higher-order B-spline functions for geometry representation and analysis
- Investigation of multi-material nonlinear elasticity problems

An eXtended IsoGeometric Analysis (XIGA) approach

Immersed boundary method that enables the prediction of discontinuous behavior within an element by enriching the classical finite element approximation via [1]:

$$\mathbf{u}^h(\mathbf{x}) = \sum_{k=1}^{K} \sum_{l=1}^{L_k} \phi_k(\mathbf{x}) B_k(\mathbf{x}) u_k^l \qquad (1)$$

with the indicator function $\phi_k(\mathbf{x})$ and the B-spline basis function $B_k(\mathbf{x})$. Boundary conditions are imposed at the boundary and interfaces using a weak formulation via Nitsche's method [2].

- Enriched nodes
- FEM
- XFEM
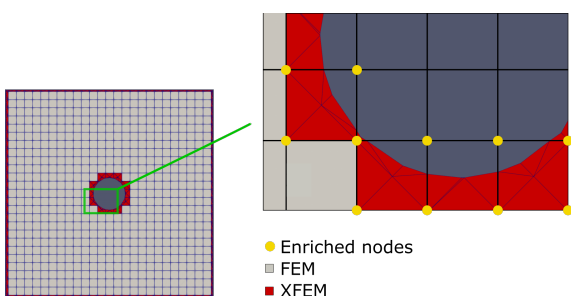
Finite strain theory

The finite strain theory deals with large strain, displacement, and rotations. As a result, the strain and stress definitions need to be modified, whereby the relation becomes nonlinear as the deformation increases. To solve these nonlinear equations, iterative solvers are needed. The nonlinear relation of the stress and strain, caused by material nonlinearities and large deformations inherently complicates the formulation of the governing equations.

Numerical results

To verify the framework, the approximation of the model is compared with analytical solutions of multi-material problems. Focused attention has been paid to the effect of higher-order approximation functions and mesh sizes.

Mesh refinement study of a for a pseudo 1D bar with planar interface geometries:
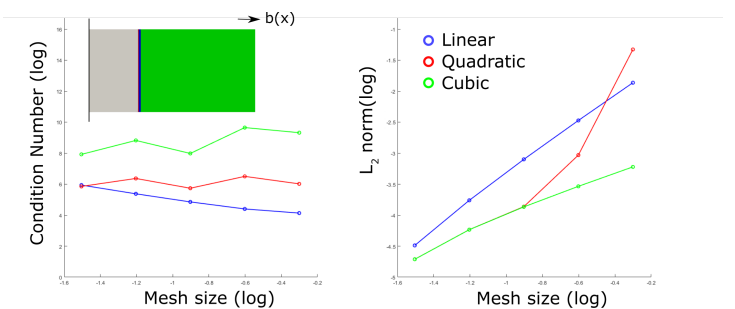
Deformation of a bi-layer cantilevered beam using linear, quadratic and cubic XFEM elements of different mesh sizes:
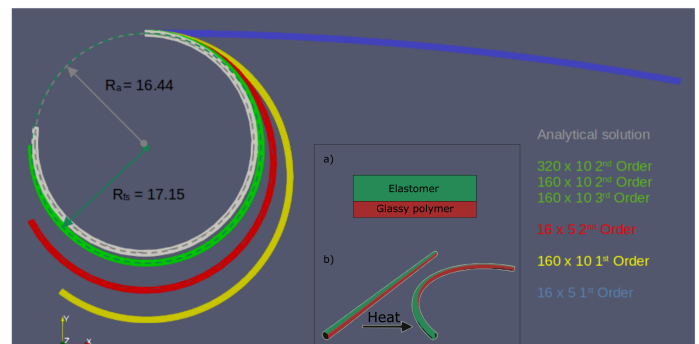
Conclusion

A finite strain framework based on an XIGA level set approach is developed and tested. Numerical examples show the importance of using higher-order approximation functions. The final aim of the research project is to exploit the developed framework to design protective structures that are able to exhibit enhanced protection properties, based on the latest biomechanical objectives while being physically sound and manufacturable.

References

[1] L. Noël et al. - XIGA: An eXtended IsoGeometric Analysis approach for multi-material problems, 2022.

[2] J. Nitsche. - Über ein Variationsprinzip zur Lösung von Dirichlet-Problemen bei Verwendung von Teilräumen, die keinen Randbedingungen unterworfen sind, 1971.

PhD progress

| 1 | 2 | 3 | 4 |

Computational Modeling of Fatigue Failure in Composite Laminates

P. Hofman, F.P. van der Meer, L.J. Sluys

Delft University of Technology

Introduction

The European Commission has announced to strive for a completely **green-house emission free economy** in the European Union by 2050. **Lighter structures** used for transportation will assist in achieving these goals. **Thermoplastic composites** are very well suited for reducing weight in structural components because of their high strength-to-weight ratio and their ability to be recycled.

As part of the **ENLIGHTEN** (Enabling Integrated Lightweight Structures in High Volumes) program, it is the objective of this PhD project to develop an **efficient, accurate** and **robust** numerical framework for predicting the progressive failure of **bonded composite parts** due to **short- and long-term** (cyclic) loading.

Numerical framework

To model **initiation** and **propagation** of matrix cracks and delamination, the cyclic cohesive zone model by Dávila [1] is used. The model is based on the quasi-static mixed-mode cohesive model by Turon et al. [2] and the load-envelope approach is used to simulate **high-cycle fatigue.** In this approach**,** the maximum load is applied to the specimen and the load cycling is taken into account in the constitutive relation (see Figure 1), by introducing a damage variable which evolves with load cycles N:

$$\frac{d\mathcal{D}}{dN} = f(\mathcal{D}, \Delta)$$

where Δ is the displacement jump and $\mathcal{D}$ is the damage variable, which is defined as the ratio of the dissipated energy and the fracture energy:

$$\mathcal{D} \equiv \frac{G}{G_c}$$

In our work, the current damage is obtained with an implicit scheme which is solved with Netwon's method on (local) integration point level:

$$\mathcal{D}^N \longleftarrow \mathcal{D}^{N-1} + \Delta N f(\mathcal{D}^N, \Delta^N)$$

This allows for the use of larger time steps compared to the explicit damage update presented in Ref. [1], which is crucial in full laminate analyses.

Initial results

The cyclic cohesive zone model is used to simulate fatigue crack growth in a double cantilever beam (DCB) specimen. First, the maximum load is applied quasi-statically. At the end of this phase, the fracture process zone has not fully developed. The fracture process zone develops to a complete zone (the onset phase) when the first load cycles are applied. When the process zone has fully developed, propagation of the crack takes place. The deformed DCB specimen and the three phases are depicted in Figure 2.
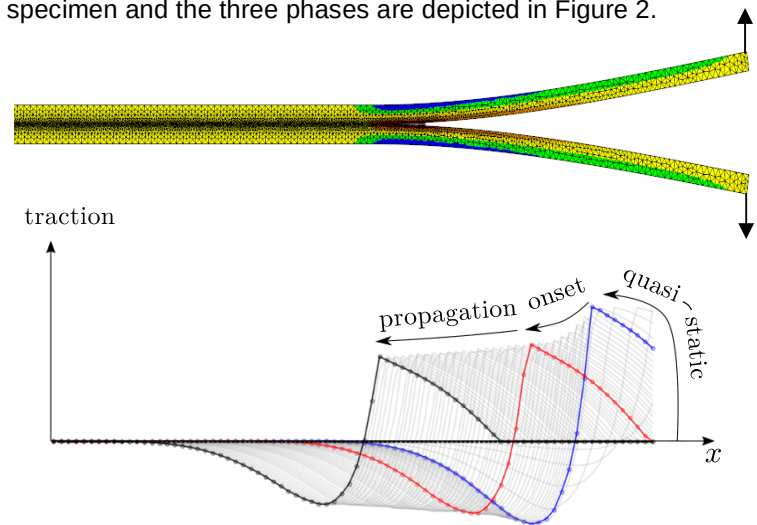
Figure 2: Loaded DCB specimen (top) with traction profile along the interface (bottom). The different colors refer to the traction profile at different timesteps.

Future goals

- ⌐ↄ Combine the cyclic cohesive zone model with **XFEM** to simulate mesh-independent matrix cracking.
- ⌐ↄ Develop a proper **fatigue initiation criterion** for inserting cohesive cracks.
- ⌐ↄ Include **process-induced multiscale effects** in the numerical framework.

References

[1] Dávila, C. G. From S-N to the Paris law with a new mixed-mode cohesive fatigue model for delamination in composites. *Theoretical and Applied Fracture Mechanics,* 2020.
[2] A. Turon, P.P. Camanho b, J. Costa, C.G. Dávila. A damage model for the simulation of delamination in advanced composites under variable-mode loading. *Mechanics of Materials,* 2006.

Figure 1: Fatigue damage in an integration point as a result of constant applied maximum load on the numerical model.

Modeling of rain erosion damage and lifetime of wind turbine blades

T.H. Hoksbergen (Nick)[1], R. Akkerman[1], I. Baran[1]

[1]University of Twente, Production Technology

Introduction

Global climate accords are stating lower CO_2 emissions and renewable energy is a popular method to achieve this. Offshore wind energy shows high potential for clean electricity production and technological development is made rapidly. Currently, the largest blades exceed 100m in length and have a tip speed of above 100ms^{-1}. These turbines provide electricity for up to 16.000 households. Unfortunately, these high tip speed blades interact with rain droplets that cause damage over time as shown in figure 1. This is called rain erosion and causes high maintenance cost.
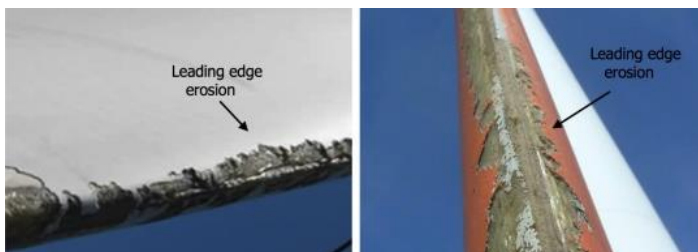
Figure 1: Rain erosion damage on wind turbine blades.

The current project aims to:
1. Understand the rain erosion damage mechanisms
2. Model liquid droplet impact stress of coated substrates
3. Predict lifetimes of coated substrates

Proposed modelling framework

In order to accurately model rain erosion damage of wind turbine blades. A three-step model was developed. 1 – Liquid droplet impact pressure model, 2 – Coating stress model, 3 – Lifetime prediction model. This approach utilizes a two-phase flow, fluid-structure interaction model in COMSOL and a fatigue lifetime prediction model based on the rainflow counting algorithm and the Palmgren-Miner rule. The problem to be solved, the resulting contact pressure and coating stress as well as the predicted lifetime for different impact velocities are shown in figure 2.
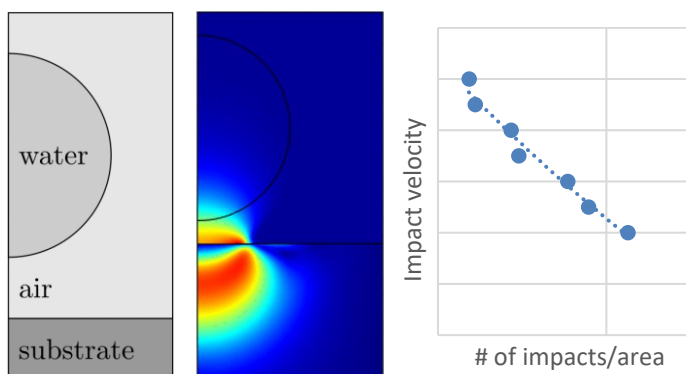
Figure 2: Schematic overview of the problem, pressure and stress field in the coating and the predicted lifetime as a function of impact velocity

Effect of layer thickness

The developed model allows to investigate the effect of impact, material and geometric parameters such as: Impact velocity, droplet diameter, Young's modulus, Poisson ratio, coating thickness, multilayer coating systems etc. For this poster, the effect of coating layer thickness is further investigated. Figure 3 shows timeframe with the highest coating-substrate stress for two different materials and three different coating layer thicknesses.

Figure 3: Coating stress for TPUD60 and PAI materials for different coating thicknesses.

It is seen from figure 3 that thin coatings lead to higher stresses then thicker coatings. It is also seen that depending on the material parameters, the highest stress is occurring at the interface at some distance from the center of impact or directly at the center of impact. It is also seen that when the coating thickness is relatively large, the highest stress no longer occurs at the interface but internally in the coating. This indicates that a limit for applied coating thickness exists beyond which further increasing the coating thickness is no longer leading to reduced stresses. Coating thickness is therefore an important design parameter for leading edge erosion protection systems. Next to coating thickness, it as found that droplet diameter, interphase parameters and coating material parameters play an important role in the lifetime of the coating-substrate system.

Conclusions

- A sophisticated numerical model for prediction of liquid droplet impact erosion of coated substrates was developed
- The model was used to study the effect of impact, material and geometric parameters on the stress state and predicted lifetime of the system.
- Coating thickness, droplet diameter and coating material have a significant effect on the magnitude and type of stress and therefore on the predicted lifetime.
- The developed model is a useful design tool for leading edge erosion protection systems for wind turbine blades.

Monitoring of dynamic strain and acoustic emissions of composite marine propellers using embedded piezoelectric sensors

A. Huijer[1], W. de Bles[1], C. Kassapoglou[2], L. Pahlavan[1]

[1] *Delft University of Technology, Maritime and Transport Technology*
[2] *Delft University of Technology, Aerospace Engineering*
A.J.Huijer@tudelft.nl

Introduction

The implementation of an embedded piezoelectric sensor network inside a composite marine propeller can allow for [2]:

- Measurement of dynamic strains related to hydrodynamic loads;

- Measurement of damage-induced acoustic emissions that can give an indication of the nature, location and growth of damages inside the blades.

These measurements can enable predictive maintenance of composite propellers and also allow for more detailed assessment of the models and assumptions that are used in the design process. An impression of the concept is given in Figure 1.
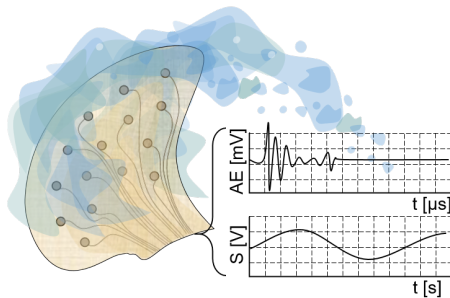
Figure 1: Impression of an fibre-reinforced plastic marine propeller blade with embedded piezoelectric sensors under hydrodynamic load. The sensors record contributions of acoustic emissions (AE) and dynamic strains (S).

Objective

Measurement of the dynamic response and structural integrity of marine composite propeller blades using embedded piezoelectric sensors.

Manufacturing of instrumented propeller blade

A propeller blade was made using vacuum-infusion. Twenty-four sensors were embedded during lay-up of the fibres. Details are shown in Figure 2.

Figure 2: Left: piezoelectric sensors placed in between glass fibre laminae. Right: Laminae placed in the propeller mould [1].

Measuring acoustic emissions

To test the ability to record acoustic emissions (AE) using embedded piezoelectric sensors, standardised pencil lead breaks (PLB) were performed on locations on the blade. Responses were successfully measured throughout the blade. Both can be seen in Figure 3.
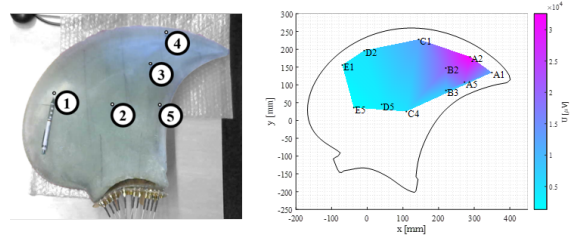
Figure 3: Left: A prototype blade with embedded sensors and five locations for PLB excitation. Right: Voltage amplitudes from an excitation at location 4.

Measuring dynamic strains

To assess the ability of the embedded sensors to measure dynamic strains, the blade was suspended and excited with an instrumented hammer. Preliminary results (Figure 4) of the frequency response function (FRF) show that the piezoelectric sensor can record a vibration response efficiently.
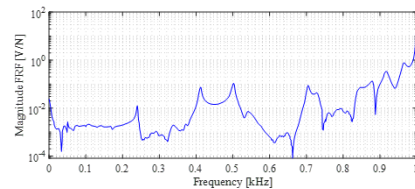
Figure 4: FRF of the suspended propeller blade measured by a single embedded sensor [1].

Conclusions

- Embedded piezoelectric sensors can measure AE throughout the dry propeller blade;

- Embedded piezoelectric sensors can be used in the measurement of dynamic strains.

Further development of the methodologies for damage and load monitoring using embedded sensors is carried out in the ECoProp project.

References

[1] W. DE BLES, *Dynamic response reconstruction of an FRC blade with embedded piezoelectric sensors*, Master's thesis, (2022).

[2] A. HUIJER, X. ZHANG, C. KASSAPOGLOU, AND L. PAHLAVAN, *Feasibility evaluation for development of composite propellers with embedded piezoelectric sensors*, Marine Structures, (2022).

PhD progress

| 1 | 2 | 3 | 4 |

Multi-scale friction model for Aluminum sheet metal forming

F. Jalalimoghadas[1], J. Hazrati[1], A.H. van den Boogaard[1], M.B. de Rooij[1]

[1]University of Twente, Faculty of Engineering Technology

Introduction

- Friction coefficient in sheet metal forming depends on contact condition and varies during the forming process in different locations.
- Recently, a physics-based friction model for steel sheet forming at different pressures and bulk strains has been developed, to be used in FE simulations[1-2].

Objective

The aim of this research is to modify the friction model for aluminum sheet forming and extend it to account for aging and temperature effects.

Friction model

Multi-scale friction model.

$$\frac{\Sigma_{i=1}^{n}(F_{friction})_i}{F_N}$$
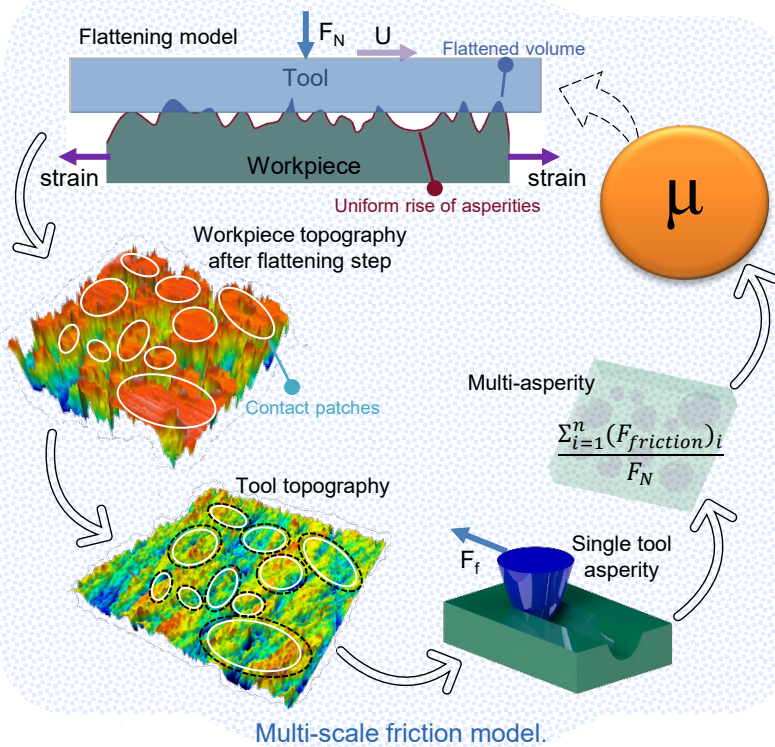
Preliminary results
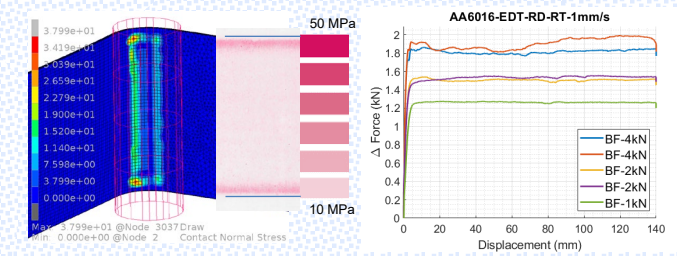
FE simulation and pressure film contact pressure results.

Experimental force displacement results.
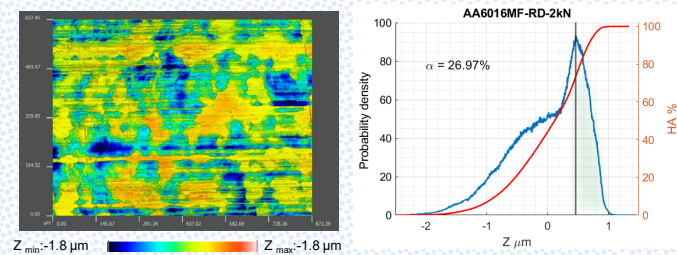
AA6016 mill finish sheet surface topography and height distribution after the test.

Validation experiment

- Sheet bends and unbends over a fixed roll under tension.
- Hot melt lubricant is applied on the sheet surface.
- Strain is measured using DIC technique.

Draw force   Back force

Draw-bend schematic.

Draw-bend test and DIC setup.
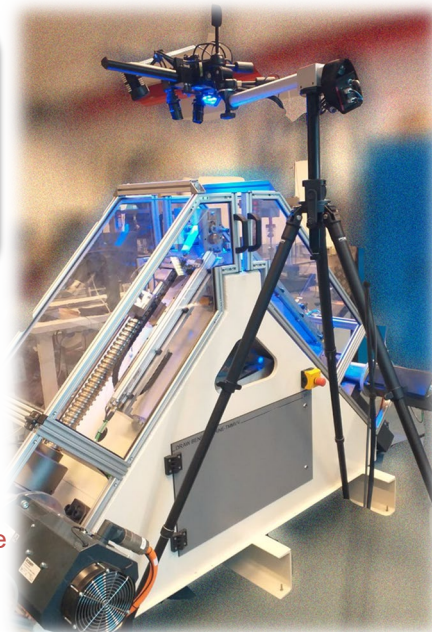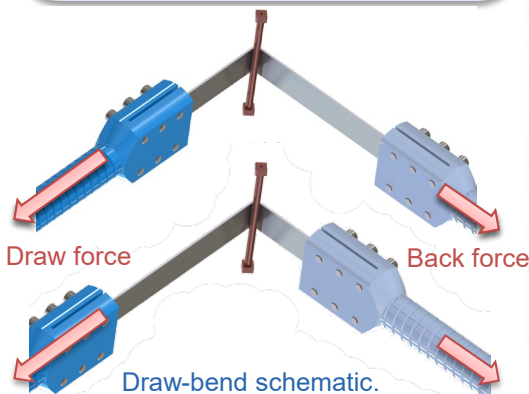
Conclusion

- Beside formation of plateaus due to flattening, valleys also form due to roughening, which should be included in the model.
- Force-displacement curve, strain, contact pressure and real area of contact from experiments can be compared with model results.
- Draw-bend is a good validation test, since different contact conditions are present and still it's possible to see the effects of different parameters separately.

References

[1] Shisode, M., 2021, Tribol. Int.,
https://doi.org/10.1016/j.triboint.2020.106554
[2] Mishra, T.et al., 2019, Tribol. Int.,
https://doi.org/10.1016/j.triboint.2019.05.015

UNIVERSITY OF TWENTE.

PhD progress
1 2 3 4

FORMALUB

Error Bounds in Model Reduction of Interconnected Systems: A Robust Performance Approach

L.A.L. Janssen[1] , R.H.B. Fey[1] , B. Besselink[2] , N. van de Wouw[1]

[1] *Eindhoven University of Technology, Mechanical Engineering, Dynamics & Control*

[2] *University of Groningen, Computer Science and Artificial Intelligence, Bernoulli Institute for Mathematics*

Introduction

Complex models of dynamic (multi-)physical systems are often based on an interconnection of subsystems with a high number of states. For such systems, model order reduction (MOR) is required to make controller synthesis, simulation and analysis computationally feasible.

In *modular model reduction,* each of the subsystems models is reduced individually. This preserves the interconnection structure of the model and dividing the problem into multiple smaller problems avoids the computationally challenging reduction of one high-dimensional model. However, although modular reduction leads to accurate subsystem models, it does not guarantee the accuracy of the reduced-order interconnected model. The question arises:

> "How can we relate subsystem reduction errors to the resulting error in the reduced interconnected model?"

A method is introduced which provides *a priori error bounds* on the frequency response of the reduced interconnected model given error bounds on reduced subsystem models [1].

Preliminaries

We combine k linear time-invariant subsystems $G_j, j = 1, \dots, k$ in the transfer function $G_b = \mathrm{diag}(G_1, \dots, G_k)$. Inputs u_b and outputs y_b of the subsystems are interconnected via matrix K. All subsystems are reduced to reduced-order subsystems given by $\hat{G}_b = \mathrm{diag}(\hat{G}_1, \dots, \hat{G}_k)$.

The high-order interconnected model G_c and reduced-order interconnected model $\hat{G}_c$ are then both given by a feedback of K with G_b and $\hat{G}_b$, respectively, external input u_c and output y_c, as shown in Fig. 1.
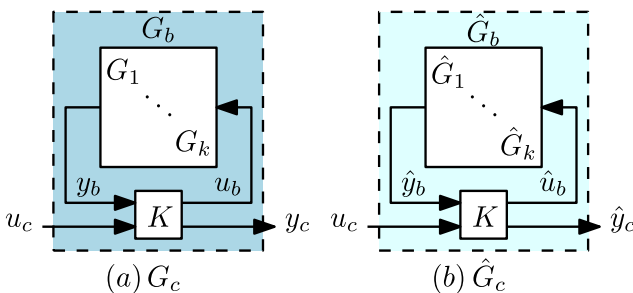
Fig. 1: Block diagram of a) high-order interconnected model G_c and b) reduced-order interconnected model $\hat{G}_c$

Methodology

In this work, we relate $E_j = G_j - \hat{G}_j$ to $E_c = G_c - \hat{G}_c$ by reformulating the problem such that the structured singular value μ, a tool from robust control [2], can be used.

We define a weighted uncertain subsystem for which $\mathrm{E}_j \in W_j \Delta_j V_j$ such that $\hat{G}_j \in G_j + W_j \Delta_j V_j$. Then, we model E_c as a feedback of VNW and Δ as shown in Fig. 2. Nominal system N is a function of G_b and K [1]. $V = \mathrm{diag}(V_1, \dots, V_k, V_c), W = \mathrm{diag}(W_1, \dots, W_k, W_c)$ and $\Delta = \mathrm{diag}(\Delta_1, \dots, \Delta_k, \Delta_c)$.
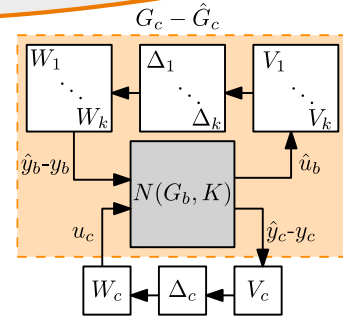
Fig. 2: MOR in a robust performance perspective

Results

From robust performance [2],

$$\sup_{\omega \in \mathbb{R}} \mu_\Delta(VNW) < 1,$$

if and only if the system in Fig. 2 is *internally stable* and

$$\|W_c E_c V_c\|_\infty < 1, \text{for all } E_j \text{ s.t.}$$
$$\left\|W_j^{-1} E_j V_j^{-1}\right\|_\infty \leq 1.$$

Given that $\mu_\Delta(VNW) < 1$ can be verified computationally, this relation can be used to find a *global* error bound on the interconnected model based on subsystem errors. Similarly, a *frequency-dependent* bound can be computed (see [1]).

Example and conclusion

To illustrate the proposed framework, we apply it to the system illustrated in Fig. 3. In this example, G_1 has order 500 and is reduced using balanced truncation to $\hat{G}_1$ with order 80 (G_2 and G_3 are left unreduced).
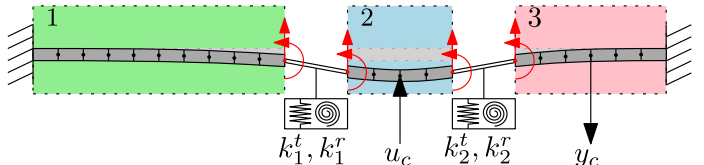
Fig. 3: Example system: Three interconnected beams

Using the proposed approach, an a priori global ε_c and frequency-dependent $\varepsilon_c(\omega)$ error bound is computed (see Fig. 4). For validation, the actual error $|E_c|$ is computed a posteriori. The example shows that the proposed method can be used to compute tight a priori error bounds for modular model reduction of interconnected systems.
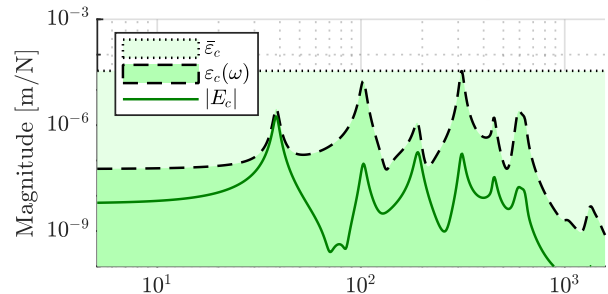
Fig. 4: Actual error $|E_c|$ and a priori global ε_c and frequency-dependent $\varepsilon_c(\omega)$ error bounds on $\hat{y}_c - y_c = E_c u_c$

References

[1] Janssen, L.A.L et al. A Priori Error Bounds for Model Reduction of Interconnected Linear Systems using Robust Performance Analysis. In *2022 American Control Conference (ACC)* (pp. 1867-1872). IEEE.
[2] Packard, A., & Doyle, J. (1993). The complex structured singular value. *Automatica*, *29*(1), 71-109.

TU/e EINDHOVEN UNIVERSITY OF TECHNOLOGY

PhD progress
1 2 3 4

Mechanical overtone frequency combs

M. H. J. de Jong[1,2], A. Ganesan[3,4], A. Cupertino[1], R. A. Norte[1,2]

[1]Department of Precision and Microsystems Engineering, Delft University of Technology
[2]Kavli Institute of Nanoscience, Delft University of Technology
[3]Ahmedabad University, Ahmedabad, India
[4]National Institute of Standards and Technology, Gaithersburg, Maryland, USA

Introduction [1]

Mechanical frequency combs are poised to bring the applications of optical frequency combs into the mechanical domain. So far, their use has been limited by strict conditions on drive frequencies and power, and complicated modes of operation. We demonstrate a new mechanism to create a frequency comb consisting of mechanical overtones (integer multiples) of a single eigenfrequency, by integrating a suspended dielectric membrane with a counter-propagating optical trap generated via its own substrate. This combination results in a versatile, easy-to-use mechanical frequency comb that requires no precise alignment, no feedback or control electronics, and only uses a continuous wave laser beam. This highlights the mechanical frequency comb as an alternative to optical frequency combs for sensing, timing and metrology applications.

Recipe for overtones

1. Suspend a Si_3N_4 trampoline membrane [2] above a Si substrate.
2. The Si substrate partially reflects a laser beam
3. The standing optical field exerts a force on the membrane
4. This creates a periodic modulation of the potential
5. The modulation generates overtones of the original motion

Figure from [1]
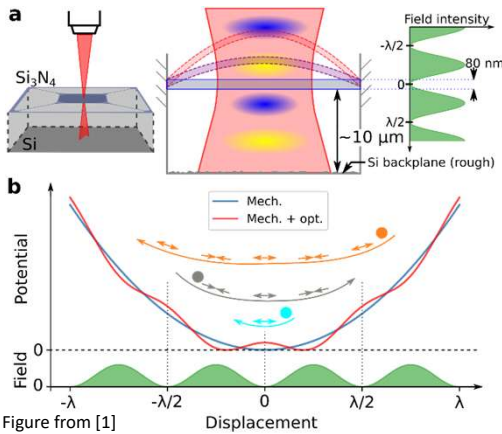
The optical component of the restoring force flips sign (always) an integer times per oscillation. The larger the displacement, the more overtones. This can be modelled by including the dielectrophoretic term F_o into the equation of motion.

$$\ddot{x} + \gamma\dot{x} + \omega_0^2 x = F_o \sin\left(\frac{4\pi}{\lambda}(x - x_{off})\right) \quad (1)$$

x resonator displacement	$F_o \simeq 60$ pN optical force
$\omega_0 = 118$ kHz resonance frequency	$\lambda = 633$ nm wavelength
$\gamma = 0.07$ Hz decay rate	x_{off} potential offset

Frequency comb

Experiments show 35 perfectly-spaced overtones in a 4 MHz bandwidth. By numerically integrating Eq. (1), we can simulate the frequency comb spectrum and find a good agreement.

We can **distinguish** the overtones from other eigenmodes by simultaneously observing them as separate spectral peaks.

We can **select** which mechanical mode to use for the comb by laser position. Shown are 257 kHz and 359 kHz, of the second and third modes.

Figure from [1]

Drive mechanism: The observed frequency combs are obtained without any external drive. Instead, a thermal parametric driving mechanism occurs due to the absorption from the laser. This leads to self oscillation: transforming the continuous wave laser (no modulation) into an effective drive at $2\omega_0$.

Dynamics

The displacement envelope shows the resonator driven from the thermal regime to 1 µm displacement maximum, 1000x the common operating amplitude. The overtone amplitudes grow in ascending order, but show dynamical behaviour that motivates further study.

Figure from [1]

Performance

Comparison of the linewidths in the thermal and comb regimes gives identical fits. The overtone mechanism does not introduce additional noise, which can be derived [1].

	This work	Literature
Frequency uniformity	$2.1 \cdot 10^{-7}$	10^{-9} [3]
Frequency stability	$7.5 \cdot 10^{-10}$s^{-1} (6 h)	N.A.
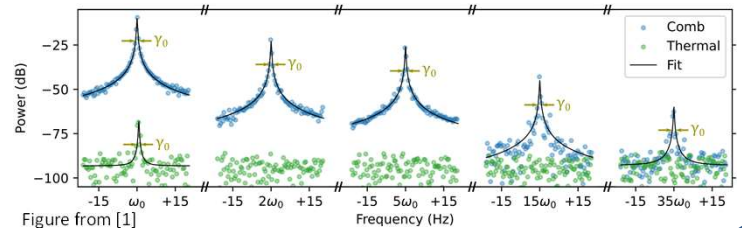
Figure from [1]

Conclusion

We have discovered a new optomechanical mechanism that creates mechanical frequency combs through the dielectrophoretic force. The resonator moves through a modulated potential, which creates overtones of the original motional frequency. These form a mechanical frequency comb, which we demonstrate for 35 overtones of a trampoline membranes in a 4 MHz bandwidth. This mechanism does not require any additional control or feedback electronics, and is thus significantly simpler than alternative methods.

References:
[1] M.H.J. de Jong et al., submitted, 2207.06401
[2] R.A. Norte et al., Phys. Rev. Lett. **116** (2016)
[3] A. Ashkin., Phys. Rev. Lett. **24** (1970)
[4] I. Mahboob et al., Appl. Phys Lett **100** (2012)

PhD progress
1 2 3 4

Noise and Vibration in Wet Soil: Micromechanical modelling for smart mitigation strategies

S.Joseph[1], Prof. S.Luding[1], Prof. V.Magnanimo[1], Dr.H.Cheng[1], Prof. J.Harting[2]

[1]University of Twente
[2]Helmholtz Institute Erlangen-Nürnberg

Introduction

Noise and vibration due to trains, traffic, blasting, piling, and earthquakes may cause excessive soil settlement and structural damage. When a wave propagates through soil, the wave characteristics change, and depending on how the soil reacts to the wave loads, the propagating wave can be dampened or amplified. Soil characteristics, including the microstructure, determine the nature of wave propagation. Major complexities arise when the soil is partially saturated due to the interplay between three phases: water, air and solid. The focus of the study is on granular soils at different degrees of saturation, subjected to vibration loads, with the goal to understand the interlink between the micromechanics of the solid skeleton, the hydraulic phase, and wave propagation. The lessons learnt will be back-engineered to design the most effective and economical mitigation measure against vibrations.
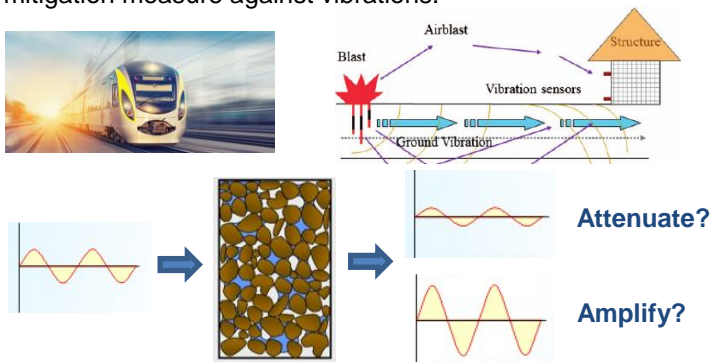
Figure 1: Noise and Vibration

Theory

The nature of wave propagation in soil depends on the configuration of soil at microscale, which differs along the SWRC (Figure 2). An acoustic excitation travelling through soil either gets attenuated or amplified. Attenuation is dependent on wave frequency, fluid properties and distribution, solid microstructure, as well as external factors like confining pressure [1, 2]. Attenuation can be different along the drying and wetting curve, shown in the SWRC [3]. Amplification could occur at resonance of fluid clusters and in transient state of fluids in soil.
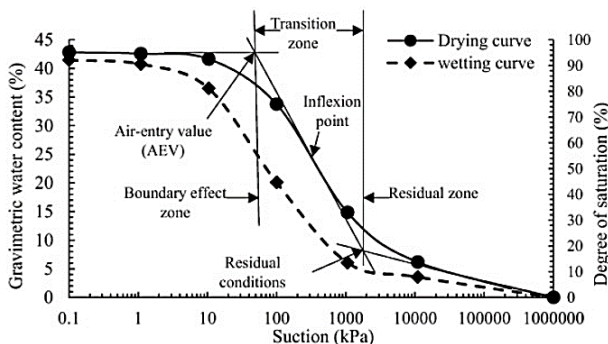
Figure 2:Soil water retention curve (SWRC)

Research Objectives

- Development of digital twin of unsaturated soil subjected to acoustic external loads.
- Study of acoustics in unsaturated soil.
- Design of sustainable mitigation measures against vibrations.

Research Methodology

A numerical microscale approach by coupling Lattice Boltzmann method and Discrete Element Method will be adopted to gain insights at the pore scale.
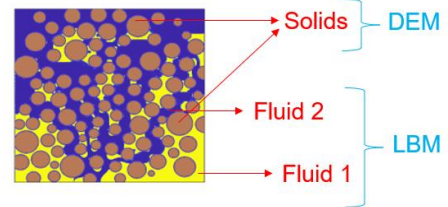
Figure 3: DEM for solids and LBM for fluids in the microstructure of soil

One LBM cycle
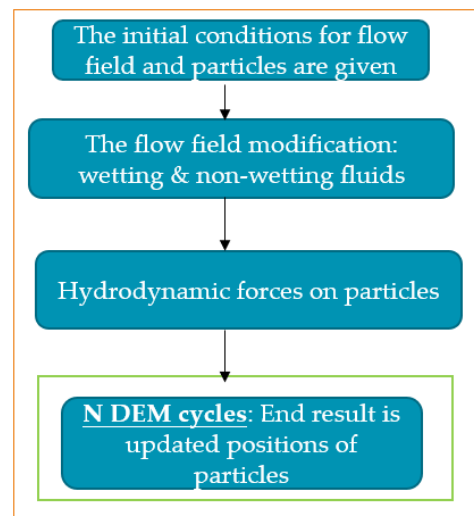
Figure 4: Coupling of LBM and DEM

References

[1]Berryman, J. G. (1988). Seismic wave attenuation in fluid-saturated porous media. In Scattering and Attenuations of Seismic Waves, Part I (pp. 423-432). Birkhäuser, Basel.
[2]Cheng, H., Luding, S., Rivas, N., Harting, J., & Magnanimo, V. (2019). Hydro-micromechanical modeling of wave propagation in saturated granular crystals. International journal for numerical and analytical methods in geomechanics, 43(5), 1115-1139.
[3] Lo, W. C., & Sposito, G. (2013). Acoustic waves in unsaturated soils. Water Resources Research, 49(9), 5674-5684.

UNIVERSITY OF TWENTE.

PhD progress
| 1 | 2 | 3 | 4 |

HI ERN
Helmholtz Institute
Erlangen-Nürnberg

Multiscale analysis of polymer composite materials filled with nanofiller using multigrid method

E. Karaseva[1], I. Gitman[2], T. Bor[3], A. Blume[4]

University of Twente, [1,3] Production Technology, [2] Computational Design of Structural Materials, [4] Elastomer Technology and Engineering

Introduction

Polymer composites reinforced with nanofillers are effective materials that traditionally have been used primarily in transport industry [1]. The polymer composites modeling in can be done by the homogenization approach, the principle of which is to replace a heterogeneous medium with homogeneous one with effective properties [2].
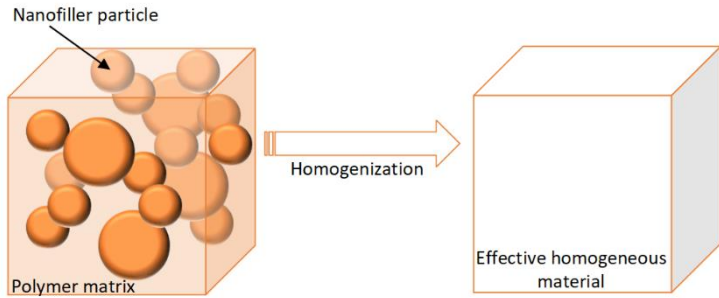
Figure 1: Homogenization schematics

Methods and means

The main aim of this study is to predict the mechanical behaviour of polymer (S-SBR) composite material reinforced with nanofiller (CB) through multiscale approach.
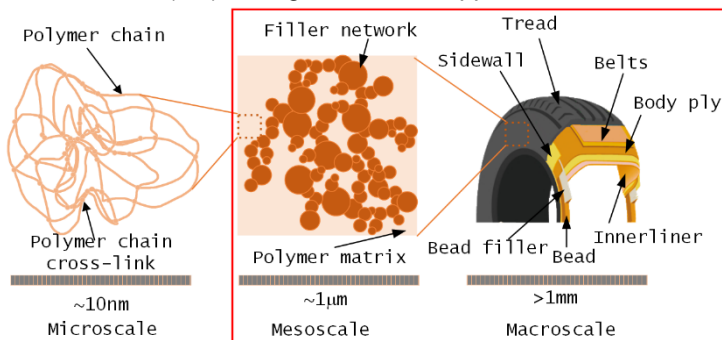
Figure 2: Observation scales of multiscale approach

Multigrid method (MG) is the practical method for solving systems of equations to accelerate the convergence of a basic method. In case of MG the iterative process requires significantly fewer computational power to bring the accuracy to the required limits. The MG basic steps:

- Define the problem in numerical form.

- Create a coarse grid and restrict the problem to this grid and solve.

- Create a finer grid and interpolate the coarse grid solution to the finer grid [3].
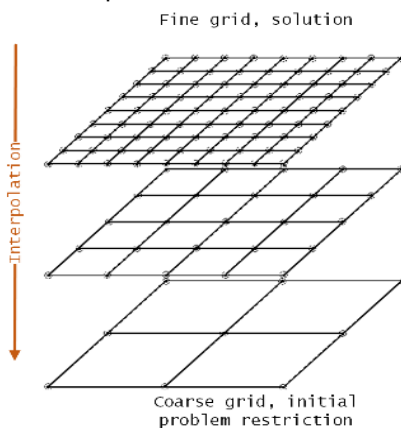
Figure 3: Multigrid method principle

Constitutive relations

A nanofiller such as Carbon Black is assumed to be a linear elastic material, while elastomer matrix can be described with the strain energy potential of the Ogden model:

$$W = \sum_{i=1}^{N} \frac{\mu_i}{\alpha_i}\left(\lambda_1^{-\alpha_i} + \lambda_2^{-\alpha_i} + \lambda_3^{-\alpha_i} - 3\right) + \sum_{k=1}^{N} \frac{1}{D_k}(J-1)^{2k}$$

Geometry generation

Since, the underlying geometry determines the mechanical behaviour of the composite, geometry-driven model is proposed. The nanofiller forms a network inside the polymer mass made from aggregations and agglomerations. Such a structure can be generated fractally.
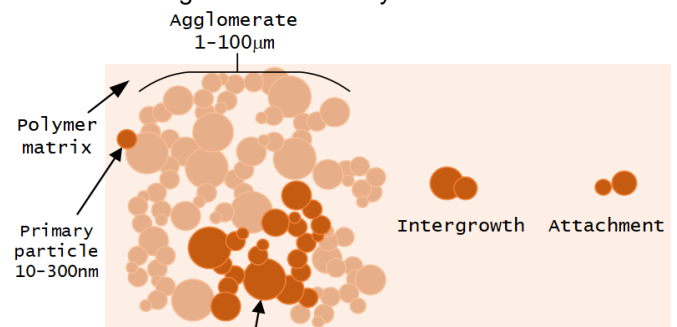
Figure 5: Nanofiller network
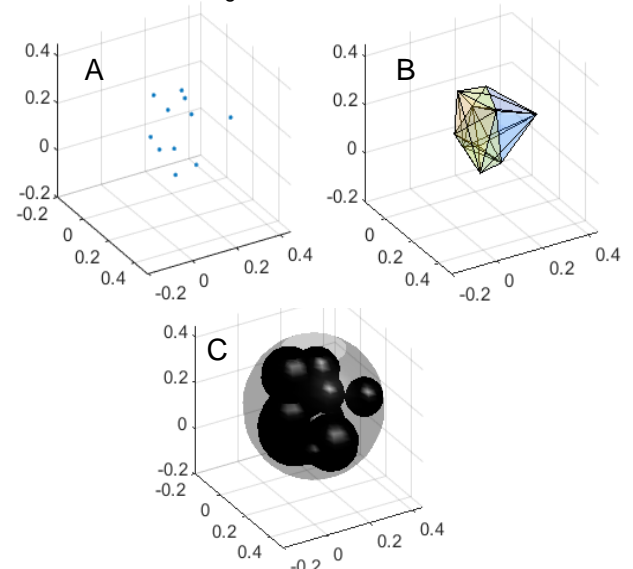
Figure 6: Aggregate generation. A) A cloud of aggregate particle centres, that has a centroid and a gyroid radius. B) The triangulation of these points, C) The aggregate model inscribed in a sphere

This generation of a filler network inside a homogeneous elastomer matrix material allows to model the material at the mesoscale. The transition to the macroscale can be done using the multigrid method for homogenization.

References

[1] Zaimova *et al.*, Composites Part B: Engineering, 2016, 11, 203
[2] Wang *et al.*, Mechanics of Materials, 2019, 12, 139
[3] Fadiji *et al.*, Acta Horticulturae, 2018, 4, 245

Atmospheric Corrosion Prognostics: Predicting the Unpredictable?

L.S. Keizers[1,2], R. Loendersloot[1], T. Tinga[1,2]

[1]University of Twente
[2]Netherlands Defence Academy

Motivation

- Corrosion prognostics increase **availability** and **reliability**

- **Complex physics** make prognostics challenging

- Solution: Combine **monitoring** & **modelling**

Method

- **Particle Filter** for Bayesian model update
- **Environmental effect** modelled by **accelerating factor**
- **Predict** and **update**
$$C_t = C_{t-1} + f(T_t, T_{nom})$$
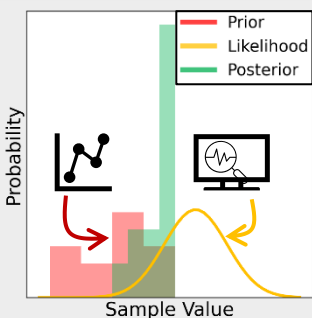
Visual representation of the Bayesian update

Data Set

Mass loss from monthly exposure tests [1]

Mass loss from monthly exposure tests

Cumulative sum of mass loss

Results

Prediction at t = 5 months

Prediction at t = 15 months
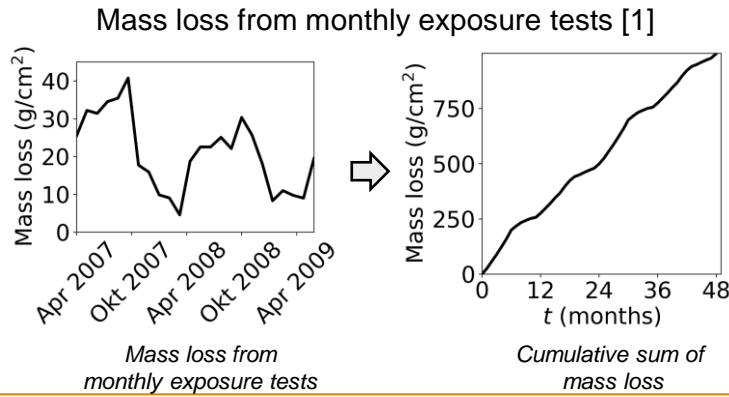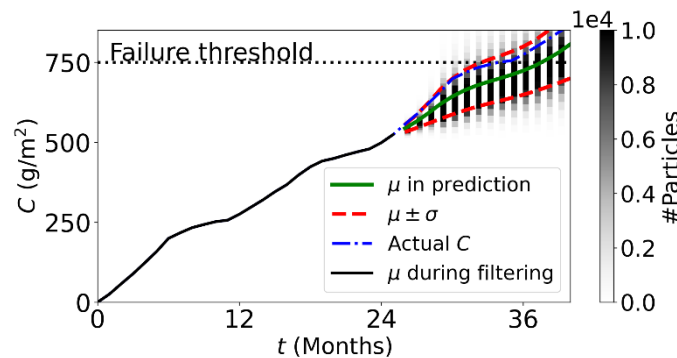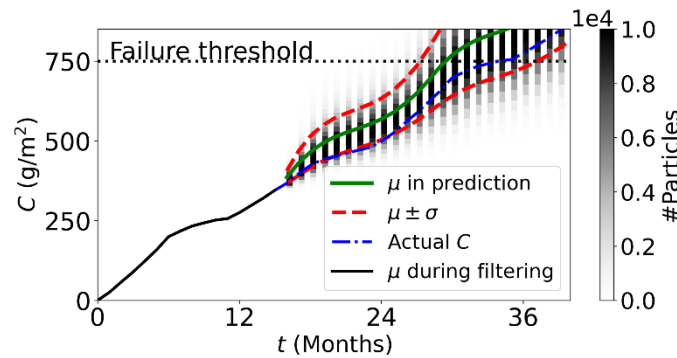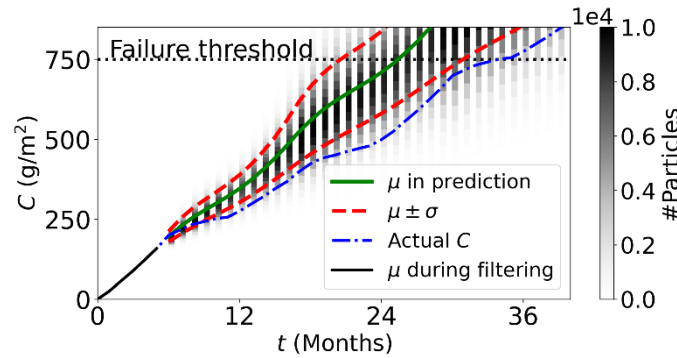
Prediction at t = 25 months
Corrosion predictions at three time steps

Conclusion

- **Good predictions** with **limited knowledge**
- Corrosion model **remains adaptive** to environment

Future work

- **Parameter** selection and **tuning**
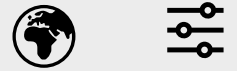
- **Long-term corrosion** prognostics

- **Validation** on more data sets

Acknowledgements

References

[1] NIMS (2011). Data sheet on atmospheric corrosion properties of carbon steels obtained by short term exposure tests, *https://mits.nims.go.jp/en/*, retrieved on 25-07-2022.
[2] L. S. Keizers, R. Loendersloot, T. Tinga (2022). Atmospheric corrosion prognostics using a particle filter. In *proceedings of the 32nd European Conference on Safety and Reliability*, 1259-1266.

Contact

l.s.keizers@utwente.nl

linkedin.com/in/luckeizers/

UNIVERSITY OF TWENTE.

PhD progress

1 2 3 4

Ministerie van Defensie

PrimaVera

NWO

Model Parameter Updating for Digital Twins using Gaussian Process Regression as Inverse Mapping Model

B.M. Kessels, R.H.B. Fey, N. van de Wouw

Eindhoven University of Technology,
Department of Mechanical Engineering, Dynamics and Control

Introduction

To ensure that a high-tech system digital twin is and remains an accurate representation of the physical system, model parameter updating can be applied. However, conventional methods for model updating, generally, do not simultaneously enable:

- (near) real-time updating,
- updating of physically interpretable parameters,
- updating of nonlinear models, and
- Uncertainty Quantification (UQ) of updated parameter values.

To meet these requirements, in this research, the Inverse Mapping Parameter Updating (IMPU) method is developed [1]. In engineering systems, such as the wire bonders designed and built by ASM-PT, see Figure 1, the IMPU method has several advantages:

- updated models resemble reality more closely, enabling improvement of the system's performance,
- machine-to-machine variations caused by manufacturing tolerances can be accounted for, and
- real-time condition monitoring is enabled.
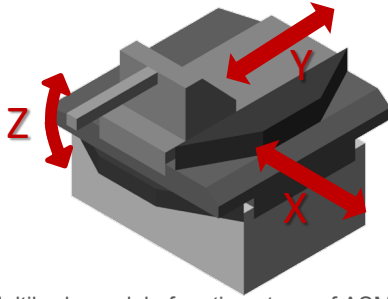
Figure 1: Multibody model of motion stage of ASM-PT wire bonder.

Methodology

The IMPU method employs an Inverse Mapping Model (IMM) to infer updating parameter values from a set of features of output responses. Here, the IMM is trained, offline, using simulated data, see Figure 2. Afterwards, in the online phase, measured features are used as input to the IMM yielding, with little computational cost, parameter value estimates. To enable UQ, Gaussian Processes (GPs) are used to constitute the IMM.
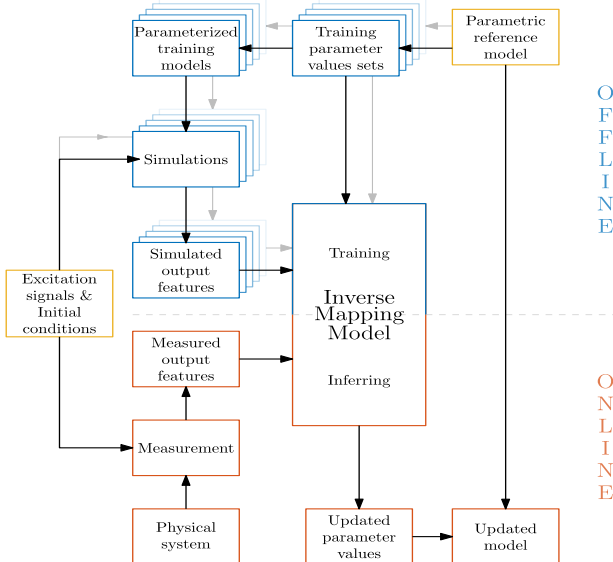
Figure 2: Block diagram for IMPU method with offline phase (top) and online phase (bottom).

Results

The IMPU method is illustrated by updating a nonlinear multibody model, see Figure 3. Here, $y(t)$ and $\theta(t)$ are available through (simulated) measurements. For the excitations $F(t)$ and $M(t)$, impulse-like signals are used.
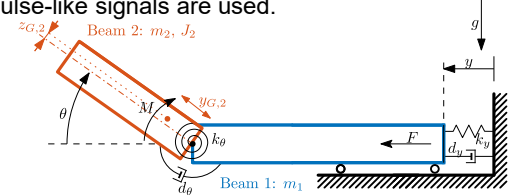
Figure 3: Schematic representation of the multibody model.

In this example, the updating parameters are the damping constants d_y and d_θ, and the spring constants k_y and k_θ. For each updating parameter, a separate GP is trained using 1000 training samples (of which the parameter values are sampled from a bounded parameter space $\mathbb{P}$ using a latin hypercube). As features, 100 temporally equidistant time samples of the response are used for each DoF. Using the trained GPs, parameter values are inferred for 500 simulated test measurements, where inferring one set of parameter values only takes 22 ms. The mean absolute relative errors of these parameter estimates are shown in Table 1.

Table 1: Mean (over all 500 test samples) relative absolute error of inferred parameter value estimates for all updating parameters.

Updating parameter	d_y	d_θ	k_y	k_θ
Mean relative absolute error [%]	0.72	0.97	0.21	0.20

In Figure 4, estimated standard deviations for k_y and k_θ, obtained using the GPs, are plotted in the k_y-k_θ subspace of $\mathbb{P}$. For reference, the values for k_y and k_θ in the center of $\mathbb{P}$ are 10 N/m and 0.039 Nm/rad, respectively.
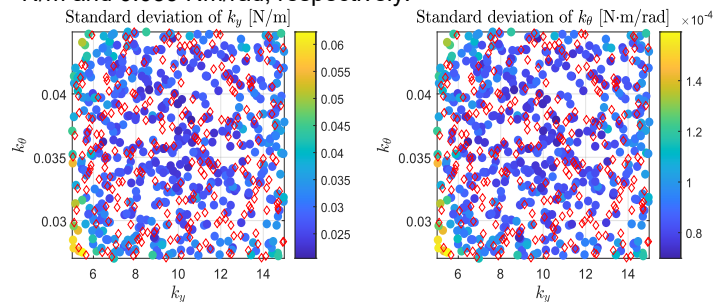
Figure 4: Estimated standard deviations of k_y and k_θ in subspace of $\mathbb{P}$. The values for d_y and d_θ are within a fixed range. The red diamonds represent the locations of the training samples.

Conclusions and future work

The NNUM enables (near) real-time interpretable updating of nonlinear models. It is shown that parameter estimates are accurate and that, additionally, the uncertainty in the parameter estimates is quantified and small. For future work, among others, we will apply this methodology to the physical wire bonder.

Acknowledgements

References

[1] Kessels, B.M., Fey, R.H.B., and van de Wouw, N. "Real-time parameter updating for nonlinear digital twins using inverse mapping models and transient-based features". In: *Nonlinear Dynamics (submitted)*.

Micromechanical characterization of Zinc coatings and high entropy alloys (Next-Coat)

D. König[1], T. Vermeij[1], J. Hoefnagels[1], F. Maresca[2]

[1]Eindhoven University of Technology
[2]University of Groningen

Problem

Zinc is commercially used to protect steel from a corrosive environment, as it prevents the oxidizing molecules to reach the substrate and acts as a sacrificial anode. The major problem about these coatings is the inherently brittle and soft nature of zinc. Even though many deformation mechanisms are available for zinc, strains of only 0.05-0.12 [2],[3] are usually achieved before fracture, thus during deformation processes of steel, the zinc layer breaks and reveals the substrate, making the substrate prone to corrosion.
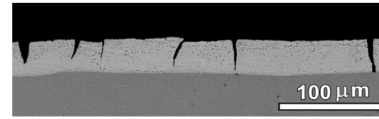
Zinc coating after 4% tensile strain [1]
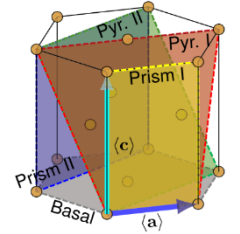
HCP slip planes [4]

Goal: **Understanding** the influence of **grain boundaries** on the **mechanics** of Zinc

Methodology

Electron Backscatter diffraction for determination of crystal orientation
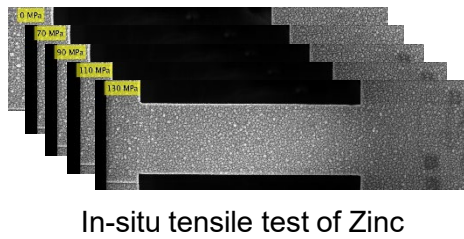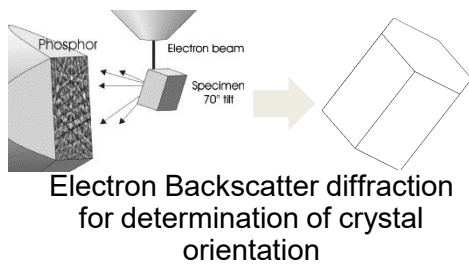
In-situ tensile test of Zinc

Strain computed locally

Reference Image   Deformed Image

Digital Image Correlation for local strain field
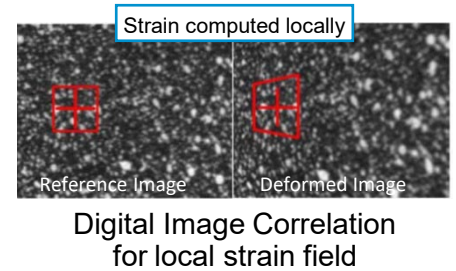
Results

Basal plane parallel to tensile direction

Orientation map of single crystal gauge
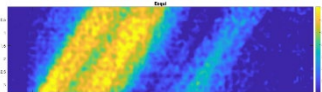
Strain map with diffuse Pyramidal slip

- Fails at 255 MPa
- Diffuse Pyramidal Slip
- Underlying Basal Slip

Bicrystal with grain boundary running through centre of gauge
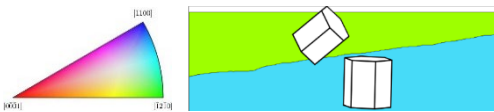
Orientation map of Bicrystal gauge
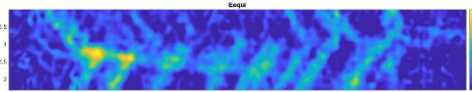
Strain map with discrete slip systems

- Fails at 380 MPa
- Basal + PyrI Slip in bottom crystal
- Bottom Crystal high strain values

Single crystal with high Schmid factor for basal slip

Orientation map of single crystal gauge
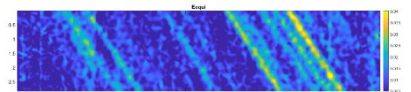
Strain map with discrete Basal slip

- Fails 130 MPa
- Discrete Basal Slip only

Conclusions

- Pyramidal slip diffuse in single crystal but discrete in bicrystal
- Stronger crystal dominates overall strain in bi-crystal
- Bicrystal shows basal slip in unfavourable oriented crystal

References

[1] G.M. Song et al. (2012) Acta Materialia 60 2973–2981
[2] Bell, R. L., & Cahn, R. W. (1957) *Mathematical and Physical Sciences*
[3] Price, P. B. (1960) *Philosophical Magazine*, *5*(57), 873-886..
[4] Yin, B., Wu, Z., & Curtin, W. A. (2017) *Acta Materialia*, *123*, 223-234

TU/e EINDHOVEN UNIVERSITY OF TECHNOLOGY

PhD progress
1 2 3 4

TATA

NWO

Topology optimization of multi-DOF compliant structures

S. Koppen, M. Langelaar & F. van Keulen

Delft University of Technology
Structural Optimization and Mechanics

Optimization problem formulation

$$\max_{\mathbf{x}} \quad \sum_i \mathcal{K}_i[\mathbf{x}]$$
$$\text{s.t.} \quad \mathcal{K}_j[\mathbf{x}] \leq \overline{\mathcal{K}}_j$$

Decoupled precision stages
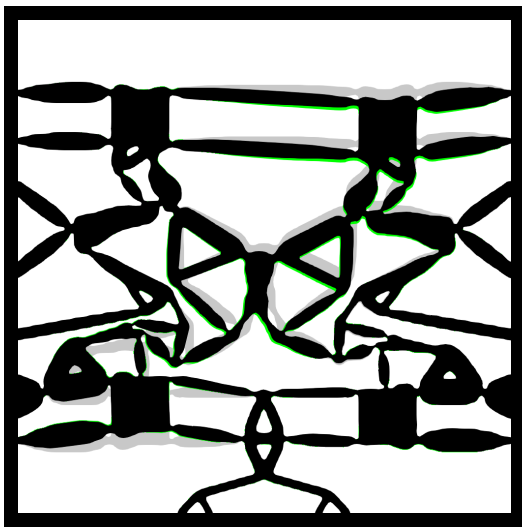
Figure 1: Two decoupled actuation-modes of a planar topology optimized micro-fluidic pump.

Micro-fluidic pump
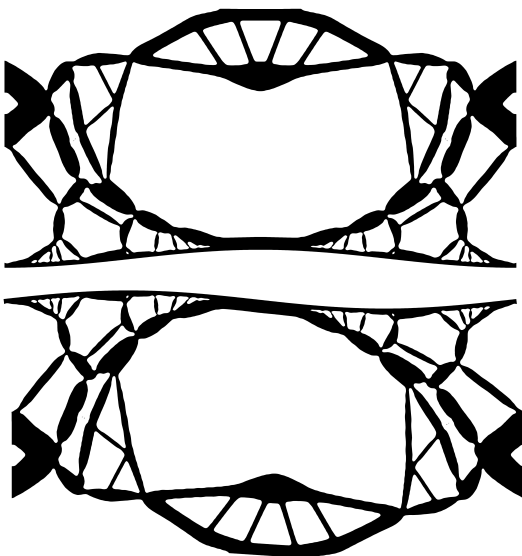
Figure 2: Two decoupled actuation-modes making a planar topology optimized micro-fluidic pump.

Non-fusion spinal implant
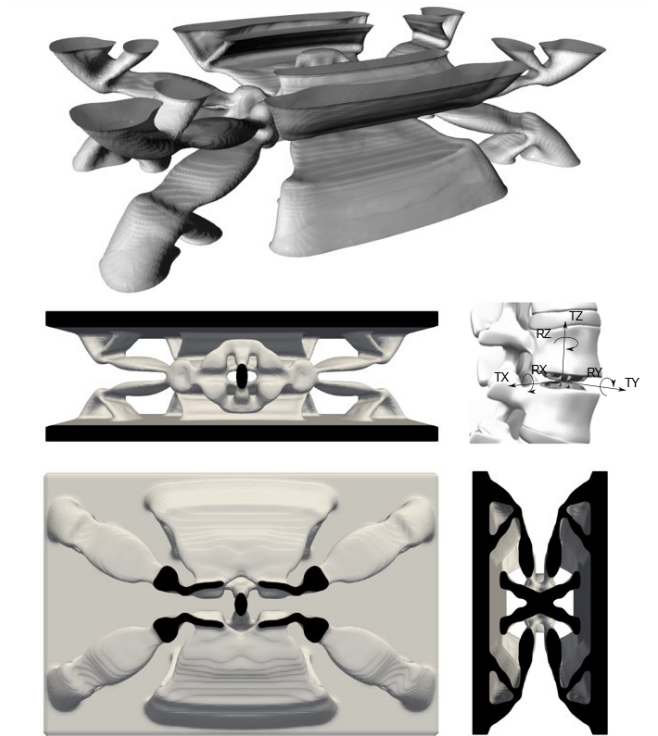
Figure 3: Cross-sections and schematic of a topology optimized monolithic compliant non-fusion multi-DOF spinal implant (patent pending).

Flexures
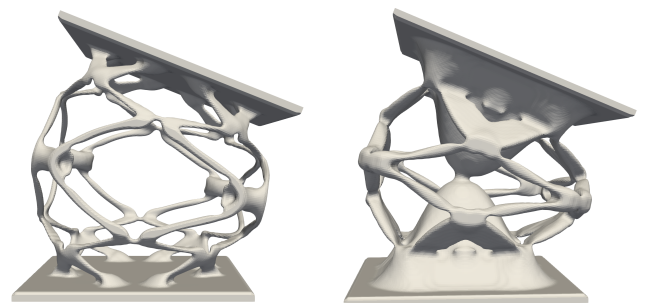
Figure 4: High-resolution three-dimensional topology optimized multi-DOF flexures for precision applications [1].

References

[1] Koppen, S., Langelaar, M. and van Keulen, A. (2022) *"A simple and versatile topology optimization formulation for flexure synthesis"* Mechanism and Machine Theory

$\tilde{T}U$Delft

PhD progress

| 1 | 2 | 3 | 4 |

NWO

Numerical Investigation of Supercritical CO$_2$ Extrusion Using the Level Set Method

T.M. Kousemaker[1], dr.ir. P.D. Druetta[2], prof.dr.ir. A.I. Vakis[3], prof.dr. F. Picchioni[2]

[1]University of Groningen – FSE – ENTEG (CMME and PT)
[2]University of Groningen – FSE – ENTEG – PT
[3]University of Groningen – FSE – ENTEG – CMME

Introduction

Extrusion is widely considered to be the workhorse in the the plastics industry. Advantages of the processing method include being able to combine multiple unit operations in one device (e.g. mixing and reaction)[1.] Supercritical CO$_2$ (sCO$_2$) is an environmentally agent that can be used to create foams. This study models the evolution of the multiphase system using CFD, tracking the interface between the polymer and sCO$_2$ phase.
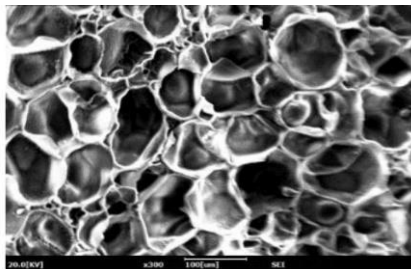
Figure 1: Porous structure of a polymer matrix after foaming with sCO$_2$ [1].

Model
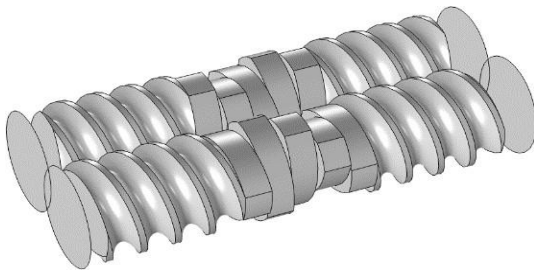
Figure 2: Twin screw extruder simulation domain

$$\frac{\partial \boldsymbol{u}}{\partial t} + \rho(\nabla \cdot \boldsymbol{u})\boldsymbol{u} = \nabla \cdot (-p\boldsymbol{I} + \tau) + \boldsymbol{F}$$

With a conservative level-set method to track the interface:

$$\frac{\partial \phi}{\partial t} + \nabla \cdot (\boldsymbol{u}\phi) = \gamma \nabla \cdot \left(\epsilon_{ls} \nabla \phi - \phi(1-\phi)\frac{\nabla \phi}{\nabla \phi|} \right)$$

And non-Newtonian flow described by Carreau-Yasuda:

$$\mu = \mu_\infty + (\mu_0 - \mu_\infty)[1 + (\lambda\gamma\dot{\phi})^2]^{\frac{n-1}{2}}$$

References

[1] Zhang, T.; Jang, Y.; Lee, E.; Shin, S.; Kang, H.-J. Supercritical CO2 Foaming of Poly(3-hydroxybutyrateco-4-hydroxybutyrate). Polymers 2022, 14, 2018. https://doi.org/10.3390/ polym14102018

Results

t = 5s   t = 20s
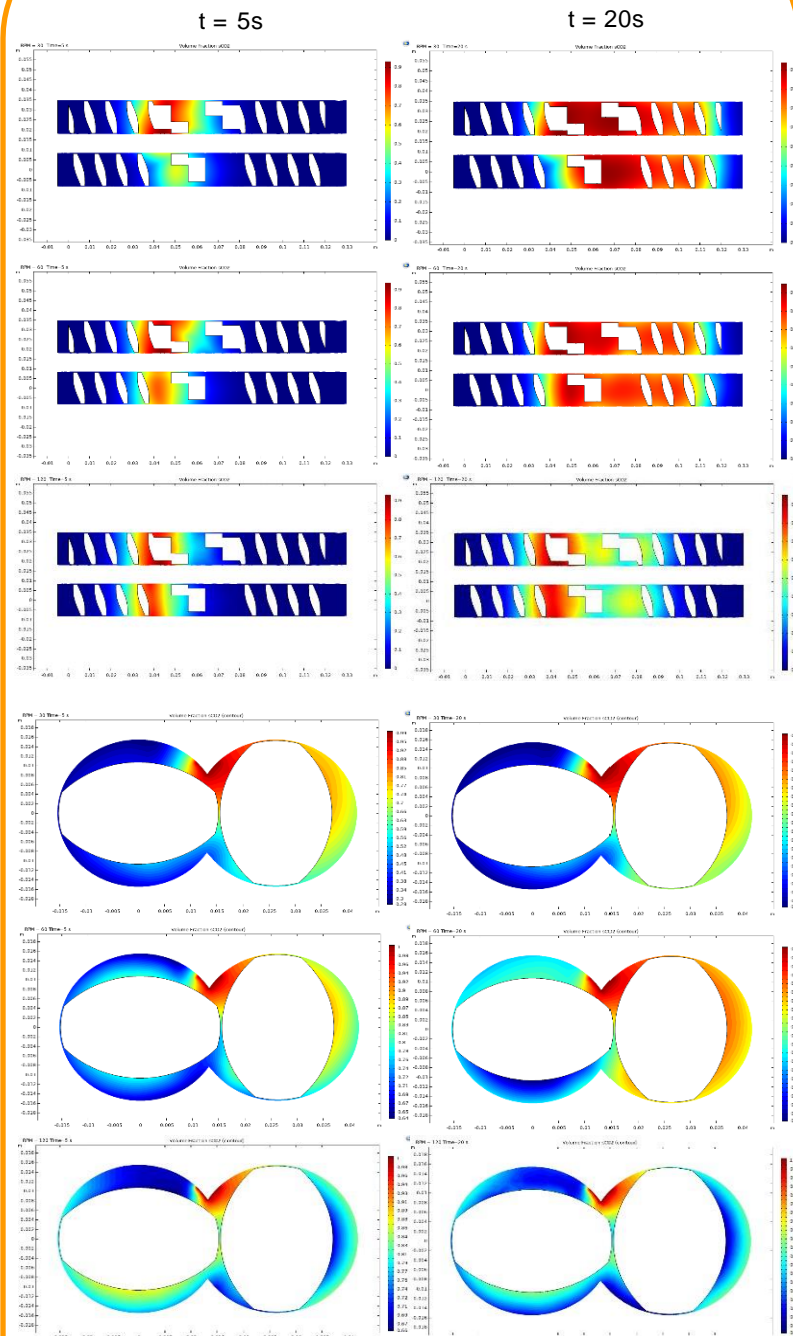
Higher rotational speeds at a given configuration produces considerably more backflow, a higher residence time and less throughput, but disperses the sCO$_2$ more effectively.

PhD progress

1   2   3   4

university of groningen

faculty of science and engineering

CmME

M 2i Materials innovation institute

STW Enabling new technology

Microscale model for off-axis creep rupture in unidirectional composites undergoing finite strains

D. Kovačević[1,2], F.P. van der Meer[1]

[1] TU Delft, P.O. Box 5048, 2600 GA Delft, The Netherlands
[2] DPI, P.O. Box 902, 5600 AX Eindhoven, The Netherlands

Problem statement

Unidirectional composite material is exposed to a constant stress σ_{yy}, i.e., to creep loading conditions, see Fig. 1(left). Beside the extensional deformation, this uniaxial loading will deform the orthotropic material also in shear, see Fig. 1(middle). Due to the viscous nature of the polymer matrix, deformation in the material will keep increasing. Accounting for finite strains in the material, local coordinate frame aligned with the reinforcement may change orientation from the angle θ_0 to a new angle θ_1. Given the angle θ_1 the stress state can be transformed to the local coordinate frame, resulting in the Cauchy stress components shown in Fig. 1(right).
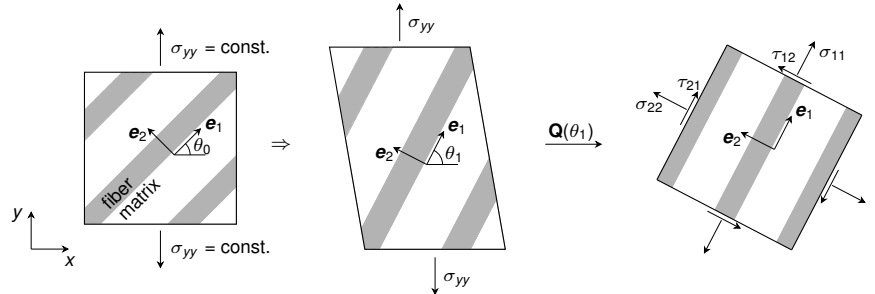
Figure 1: Constant stress applied on unidirectional composite material (left); deformed material due to uniaxial loading (middle); Cauchy stresses in local coordinate system (right)

We aim to simulate this deformation process on the microscale, by means of a Representative Volume Element (RVE) model, which is defined in the local coordinate frame aligned with the reinforcement, see Fig. 2.

Formulation
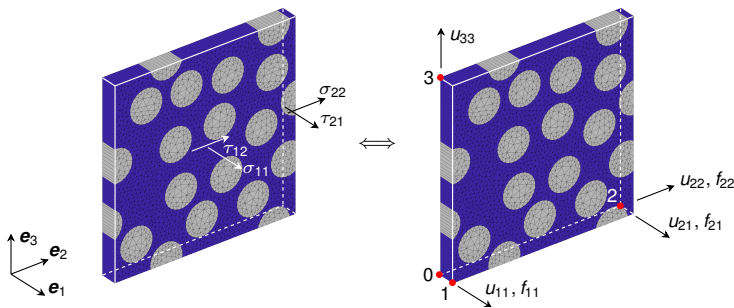
Figure 2: Homogenized stress components acting on RVE (left) as a result of the force vector applied on the RVE master nodes (right)

To impose an off-axis creep stress on the composite microstructure, an RVE with periodic boundary conditions [1] is considered. Non-zero master node displacements are indicated in Fig. 2(right), together with non-zero force vector components. The force vector components are derived as:

$$f_{11}=\sigma_{yy}A_1^0 J\left(\frac{s_1^2}{\bar{F}_{11}}-c_1 s_1\frac{\bar{F}_{12}}{\bar{F}_{11}\bar{F}_{22}}\right),\quad f_{21}=\sigma_{yy}A_2^0 J\frac{c_1 s_1}{\bar{F}_{22}},\quad f_{22}=\sigma_{yy}A_2^0 J\frac{c_1^2}{\bar{F}_{22}}$$

where A_i^0 is the initial surface on which a stress component is acting, c_1 and s_1 stand for $\cos\theta_1$ and $\sin\theta_1$, J is the determinant of the RVE homogenized deformation gradient, while $\bar{F}_{ij}$ represent components of the same deformation gradient. To trigger creep rupture, cohesive segments are inserted between finite element edges when the Helmholtz free energy in the polymer matrix reaches a critical value.

Results

The RVE composed of PEEK polymer matrix and carbon fibers is subjected to different stress levels, under two different off-axis angles: $\chi = 90°$ and $\chi = 45°$, where $\chi = 90° - \theta_0$. Model predictions are compared with experimental results in Fig. 3. The creep rupture time is taken as the minimum point in the strain-rate as a function of time [2].
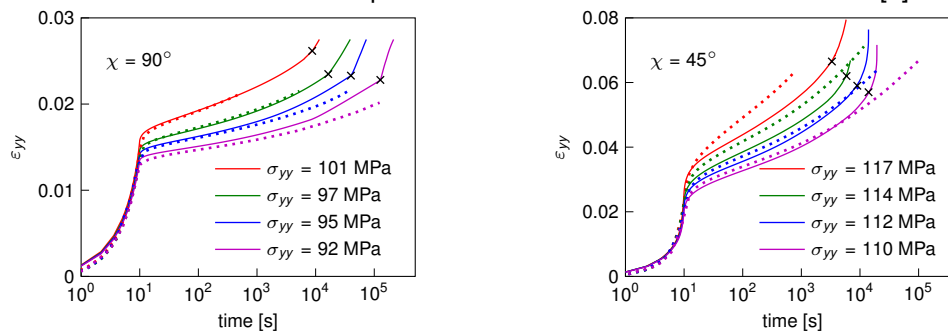
Figure 3: Creep response obtained by the model (solid lines) compared with experimental results (dotted lines), for temperature $T = 25°C$; $\times$ represents creep rupture point predicted by the model

References

[1] Van der Meer, *Eur J Mech A Solids*, 2016

[2] Spathis and Kontou, *Compos Sci Technol*, 2012

Acknowledgment

PhD progress
1 2 3 4

TUDelft Delft University of Technology

DPI Shaping polymer innovation

Acoustic metasurface for Enhanced reflectivity and Redirection of ultrasound waves

X. Kuci, M.G.D. Geers, V.G. Kouznetsova

Eindhoven University of Technology

Introduction

Needle visualization is essential to accurately identify the location of the device to avoid unintentional injury for the patient. Therefore, new visualization solutions are needed to improve needle procedure accuracy.

Ultrasound guided needle placement
(www.embedded-computing.com)
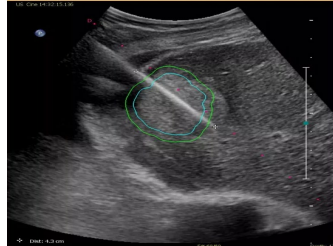
Needle visualization
(www.philips.nl)

Locally resonant acoustic metamaterials (LRAM) are proposed to develop new generation coatings for these medical devices:

- operate in subwavelength regime
- band gap formation (waves cannot propagate)
- waves reflect back to the source

LRAM unit cell:

- Polyethylene (stiff)
- Rubber (soft)
- Tungsten (heavy)
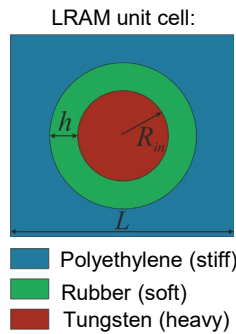
Enhanced reflection by LRAM

Numerical model:

$10\text{-}30\mu m$

ultrasound — PML | human tissue | metamaterial | needle | PML
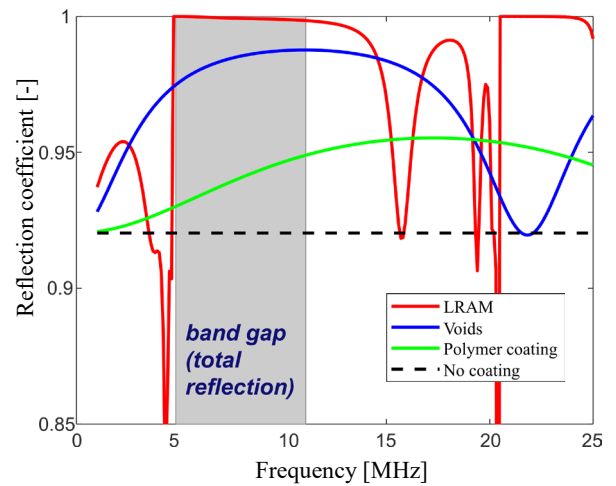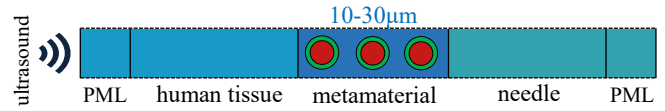
- LRAM coating improves reflection, and thus, the visibility of needle compared to alternatives, for frequencies inside the band gap

Redirection of waves by gradient metasurface

I. Methodology

- Manipulation of reflected angle: Generalized law of reflection

$$\sin\theta_r = \sin\theta_i + m\frac{\lambda_1}{2\pi}\boxed{\frac{d\phi(x)}{dx}}$$

reflected   incident   diffraction order   variation of phase along the surface

take k subdivisions: $\Delta\phi = \frac{2\pi}{k}$

$$\Rightarrow \Delta x = \frac{m\lambda_1}{k(\sin\theta_r - \sin\theta_i)}$$

$$\Rightarrow n = \frac{\Delta x}{L} \quad \text{nr. of unit cells per subdivision } k$$
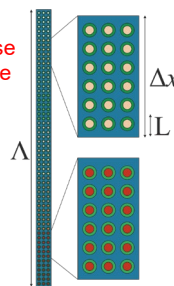
Grading of R_{in} to produce the required 2π phase shift:
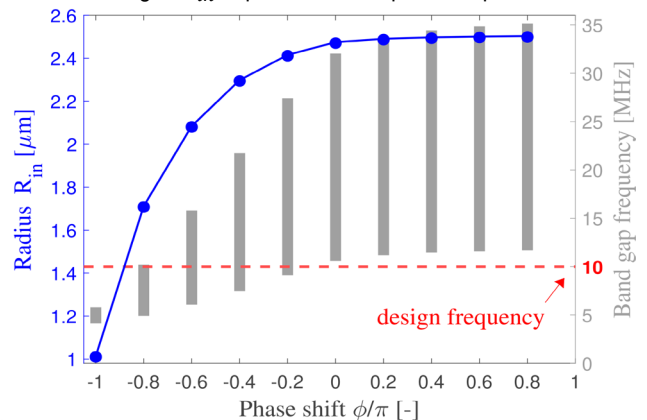
II. Negative reflection
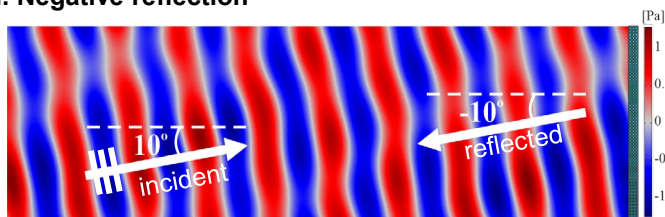
- Negative reflected angle -10° (not plane wavefront)
- Robust design w.r.t variations in angle of incidence
- Good performance for a frequency band of 17% from the design frequency

III. Reflected energy distribution over diffracted order m

- Gradient metasurface diffracts energy into different directions
- Highest energy is reflected in the designed negative direction ($m = -1$)
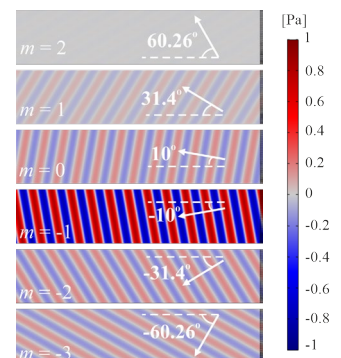
Atomistic simulations of twin boundaries in Ni-Ti Shape-Memory Alloys

L. La Rosa[1], F. Maresca[1]

[1] *Computational Mechanical and Materials Engineering, Engineering and Technology Institute, University of Groningen*

Introduction

Shape-Memory Alloys (SMAs) recover large strains under stress/temperature cycles. The **high twin interface mobility plays** a key role in SMAs (Fig.1a).

A **twin boundary** is a planar crystal defect whereby one side of the lattice can be obtained from the other by a **simple shear deformation** (Fig.1b).
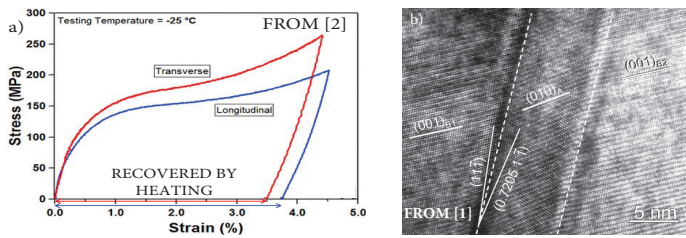
Figure 1: Under isothermal stress, twin interfaces in martensite [1] move and cause large macroscale deformation [2]. SMAs can recover the deformation if they are heated.

Research goal

Atomistic modelling has not yet addressed the **mechanics** of martensitic twin interfaces under shear stresses (**detwinning**). Our work aims to construct a reliable **atomistic model** for analysing twin interfaces.

Methodology

We used LAMMPS [3] to perform Molecular Statics (MS) simulations on Ni-Ti SMA. We performed **energy minimization** and **shear stress** simulations with a **reliable** [4] 2NN MEAM [5] Interatomic Potential.

Atomistic model

We constructed the twin atomic structure by **enforcing a simple shear deformation**. The system can then relax by a **coupled minimization scheme**. We applied this procedure to construct **rational compounds & Type I** and **irrational Type II** (Fig.2) twin boundaries observed in experiments.
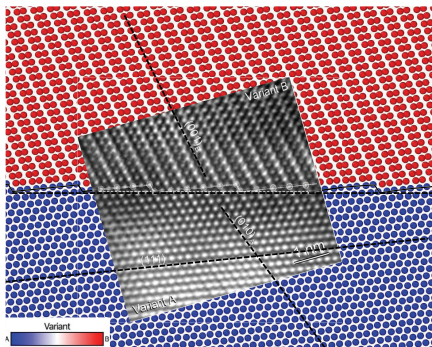
Figure 2: Our atomistic model for the Type II twin agrees with HRTEM experiments [1]. None authors had shown this result before.

Analysis

Fig.3 shows the **twin surface energy** and the required stress level to move the twin boundaries (**twinning stress**) along with the frequency of twin experimental observations.
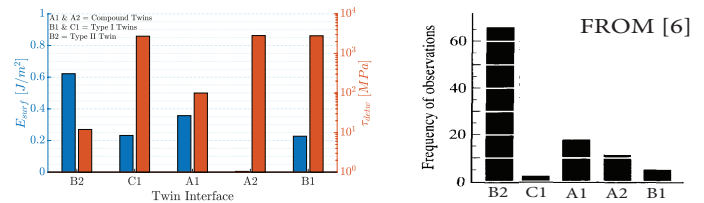
Figure 3: The most observed interface is the one with the lowest twinning stress.

Fig.4 shows the MS simulation of the **Type II interface detwinning**.
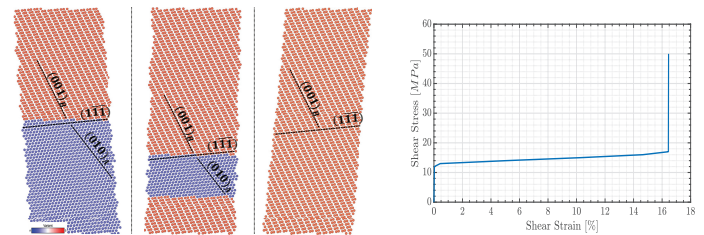
Figure 4: During detwinning, one lattice side grows until the complete transformation of the other.

Conclusions

The prevalence of Type II interfaces in Ni-Ti led to the belief that **these structures are more energetically favourable** than other twin boundaries. Instead, our work shows that **Type II twins are the most mobile**, despite having a **more significant twin surface energy** than rational interfaces.

Future research

Irrational atomic interfaces propagate at low stresses due to the **natural presence of internal defects** in the structure of the twin interface. A thorough atomistic analysis of the **defects' nature and structure** can give fascinating insights into the mechanics of such interfaces and help to design **better and more efficient** SMAs.

References

[1] Xie, Z. L., and Yong L., *Philos Mag* (2004)

[2] Tabesh, M., *et al.*, *J Intell Mater Syst Struct* (2018)

[3] Plimpton, S., *J Comput Phys* (1995)

[4] La Rosa, L., and Maresca F., *Modelling Simul Mater Sci Eng* (2021)

[5] Ko, W.S., *et al.*, *Phys Rev B* (2015)

[6] Nishida, M., *et al.*, *Acta Metall Mater* (1995)

university of groningen

faculty of science and engineering

PhD progress
| 1 | 2 | 3 | 4 |

CmME

Predicting the rate-dependent behaviour of polyvinylidene fluoride (PVDF) using an elasto-viscoplastic constitutive model

T. Lenders[1], J.J.C. Remmers[1], T. Pini[1], P. Veenstra[2], L.E. Govaert[1], M.G.D. Geers[1]

[1]Eindhoven University of Technology
[2]Shell Global Solutions International B.V.

Introduction

Polyvinylidene fluoride (PVDF) is a semi-crystalline polymer used in offshore oil- and gas applications because of its excellent mechanical and thermal properties and its chemical resistance. The intrinsic response of PVDF is obtained from uniaxial compression experiments performed at different temperatures and strain rates, see Fig. 1. To ensure a safe and sustainable operational lifetime, the short- and long-term behaviour of PVDF must be described. To this end, a 3D elasto-viscoplastic constitutive model described by Van Breemen et al. [2] is extended and used in finite element (FE) simulations to describe the intrinsic response. The extended model is then used to predict the long-term response of PVDF at three different temperatures. Here, this general approach is shown for 23°C.
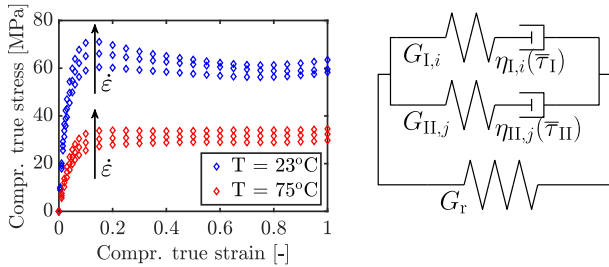
Figure 1: (left) True stress-strain curves of uniaxial compression experiments, data obtained from Pini et al. [1]. (right) The mechanical analogue of the multi-process multi-mode EGP-model described by Van Breemen et al. [2].

3D constitutive model

The elasto-viscoplastic Eindhoven Glassy Polymer (EGP) constitutive model described by Van Breemen et al. [2] is used in its multi-mode multi-process format of which the mechanical analogue is shown in Fig. 1. The stress is calculated according to Eq. 1.

$$\boldsymbol{\sigma} = \kappa(J-1)\mathbf{I} + G_r \widetilde{\boldsymbol{B}}^d + \sum_{i=1}^{n} G_{\text{I},i} \widetilde{\boldsymbol{B}}_{e_{\text{I},i}}^d + \sum_{j=1}^{m} G_{\text{II},j} \widetilde{\boldsymbol{B}}_{e_{\text{II},j}}^d \qquad (1)$$

The Eyring flow viscosity η is used to describe the rate- and temperature-dependence of the material. The viscosity related to mode k of process $\pi = \text{I}, \text{II}$ is defined in Eq. 2.

$$\eta_{\pi,k} = \eta_{0_{\pi,k},\text{ref}} \frac{\frac{\bar{\tau}_\pi V_\pi^*}{k_B T}}{\sinh\left(\frac{\bar{\tau}_\pi V_\pi^*}{k_B T}\right)} \exp\left(\frac{\mu_\pi p V_\pi^*}{k_B T} + S_\pi(\bar{\gamma}_{\text{pl},\pi})\right) \qquad (2)$$

Extension to the model

The parameters in Eqs. 1 and 2 are characterized using uniaxial compression tests performed at strain rates between $\dot{\varepsilon} = 10^{-2}$ s^{-1} and $\dot{\varepsilon} = 10^{-4}$ s^{-1} and a uniaxial tensile test performed at constant strain rate $\dot{\varepsilon} = 10^{-3}$ s^{-1}.

Using the constitutive model described in [2], the behaviour of PVDF can only be described accurately up to the yield point. To enable the large-strain description, a deformation-dependent evolution of the reference viscosity $\eta_{0_{\text{I},k},\text{ref}}$ and activation volume V_I^* of process $\pi = \text{I}$ is proposed in [3]. The parameters are dependent on the equivalent plastic strain $\bar{\gamma}_{\text{pl}}$. The evolution of these parameters is determined by fitting a modified Eyring equation (Eq. 3) to the experimental driving stress.

This equation is fit at different levels of plastic strain $\bar{\gamma}_{\text{pl}}$ and describes the solid lines in Fig. 2. In this figure, the markers represent experimental data.

$$\sigma_{\text{s},\text{I}} = \frac{k_B T}{V_\text{I}^*(\bar{\gamma}_{\text{pl}})} \sinh^{-1}\left[\frac{\dot{\bar{\varepsilon}}_{\text{pl}}}{\dot{\varepsilon}_{0,\text{I}}(\bar{\gamma}_{\text{pl}})}\right] \qquad (3)$$

The rate-factor $\dot{\varepsilon}_{0,\text{I}}$ is then converted to the reference viscosity according to $\eta_{0,\text{I}}(\bar{\gamma}_{\text{p}}) = \frac{k_B T}{V_\text{I}^*(\bar{\gamma}_{\text{pl}})\dot{\varepsilon}_{0,\text{I}}(\bar{\gamma}_{\text{pl}})}$. Finally, an expression is obtained for the evolution of the reference viscosity and activation volume as function of $\bar{\gamma}_{\text{pl}}$ which is implemented in the constitutive model.

Results and discussion

The extended constitutive model is used to describe the intrinsic behaviour of PVDF by performing FE simulations of uniaxial compression tests at different strain rates. The stress-strain curves are compared to experimental data in Fig. 2 and show a good description using the extended model.
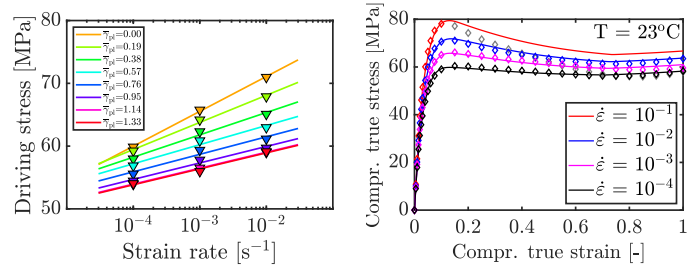
Figure 2: (left) Least-squares fit of experimental driving stress using Eq. 3. (right) Uniaxial compression tests at different strain rates obtained from FE simulations (solid lines) compared to experiments (markers).

Finally, the constitutive model is validated by performing simulations of uniaxial tensile tests at different constant strain rates and tensile creep tests at different constant applied stresses. The results are compared to experimental data in Fig. 3 and show the predictive capability of the extended model.
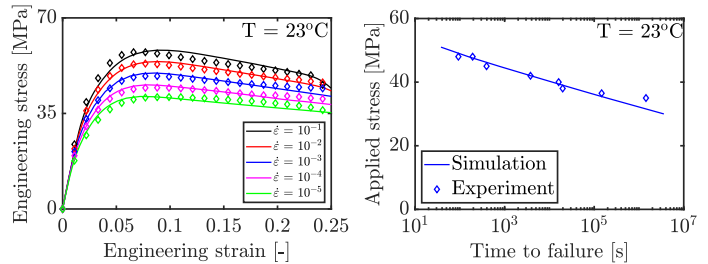
Figure 3: (left) Stress-strain curves of uniaxial tensile tests obtained from FE simulations (solid lines) compared to experiments (markers). (right) Time-to-failure vs. applied stress for tensile creep simulations compared to experiments.

Conclusion

The constitutive model is successfully extended and used to describe and predict the short- and long-term response of PVDF at different strain rates, only requiring a limited set of experimental data.

References

[1] Pini, T. et al. *J Polym Sci*, **59**, 1209 (2021)
[2] Van Breemen, L.C.A. et al., *J Polym Sci: B*, **50**, 1757 (2012)
[3] Lenders, T. et al. *In preparation*, (2022)

Continuous fiber reinforced woven composites : geometry, meshing and homogenization

Anqi Li[1,2], Joris J. C. Remmers[2], Marc G. D. Geers[2], Thierry J. Massart[1]

[1]Université libre de Bruxelles
[2] Eindhoven University of Technology

Geometry generation
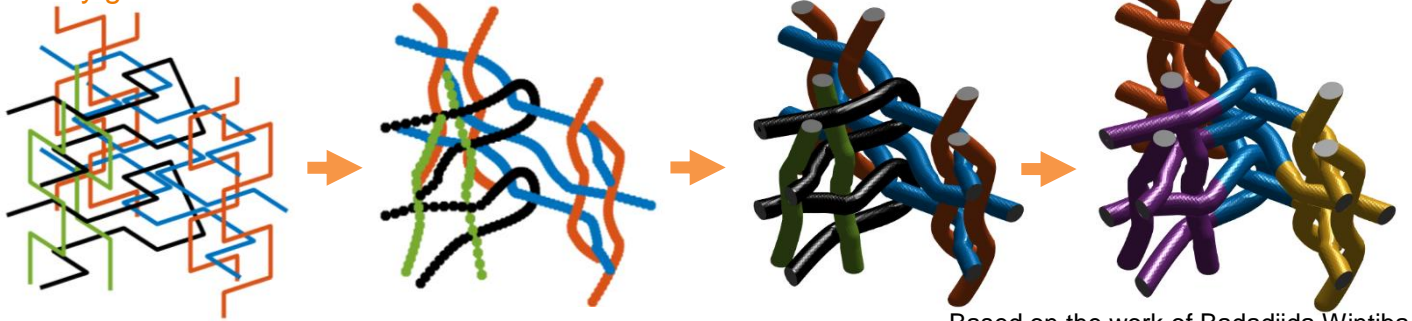
Based on the work of Badadjida Wintiba.

Numerical simulation
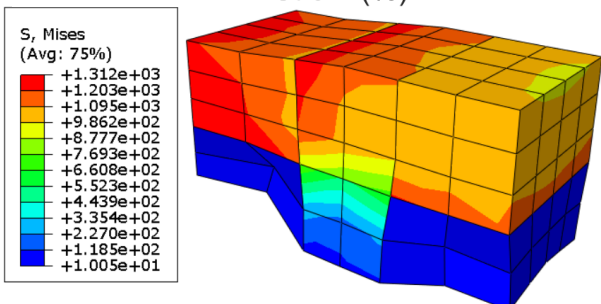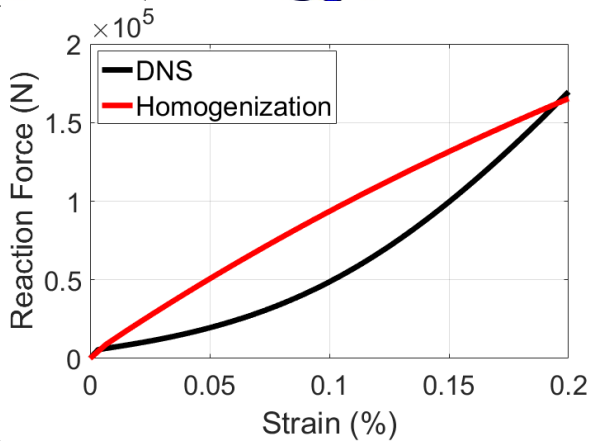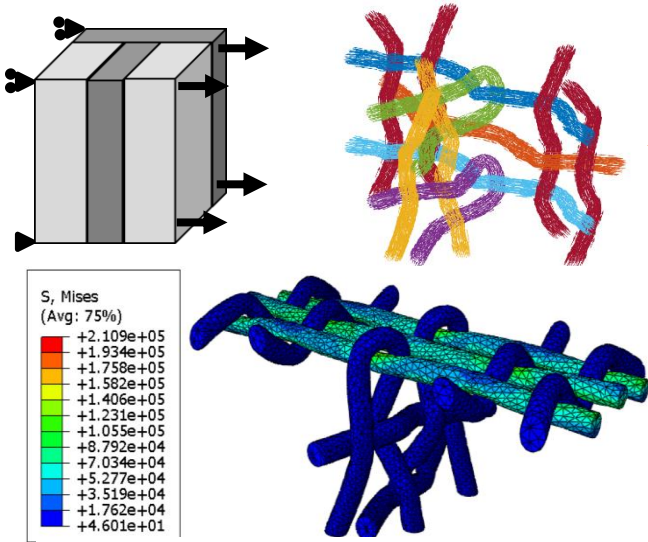
A better homogenization technique is requied.

Mesh generation
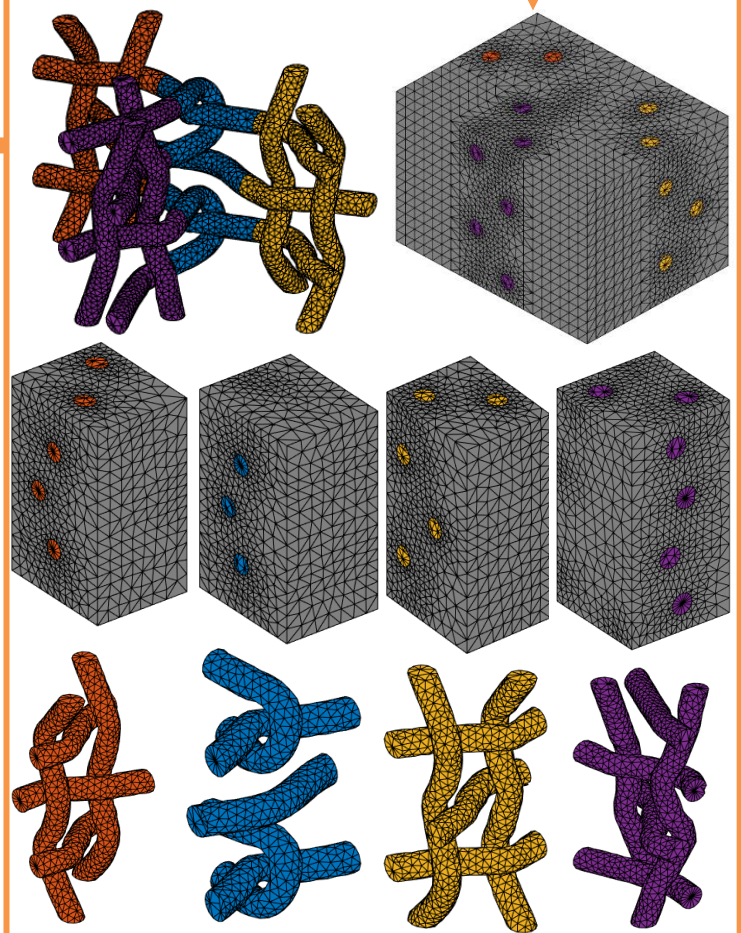
Homogenization

1. Grey elements represents matrix pocket.
2. Linear perturbation step is used to determine the property of the coloured elements (combined material property of matrix and yarns).
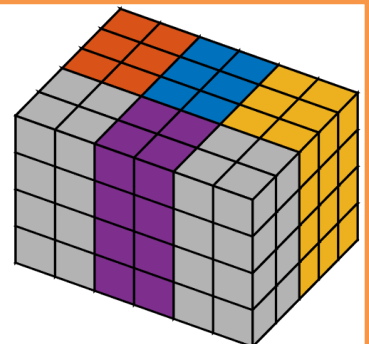
PhD progress
1   2   3   4

Computational homogenization of martensite/ferrite interface microstructures towards enhanced cohesive interfaces

L. Liu[1,2], F. Maresca[3], J.P.M. Hoefnagels[1], M.G.D. Geers[1], V.G. Kouznetsova[1]

[1]Eindhoven University of Technology
[2]Materials Innovation Institute
[3]University of Groningen

I. Introduction

Background: Martensite/ferrite (M/F) interface damage largely governs the failure of dual-phase (DP) steels, which are among the most widely used advanced high strength steels (AHSS) for automotive applications.

DP 500, DP600 (11.8%)
DP 800 (9.5%)
DP 1000 (10.0%)

A battery electric vehicle (BEV) frame with >30 wt% made of DP steels[1]

M/A: martensite island consisting of martensite laths and retained austenite (RA) films
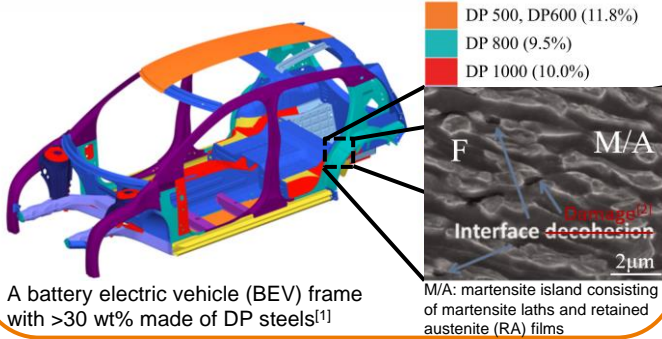
Goal: Computational homogenization towards effective meso M/F interface model described by an **enhanced cohesive law** based on the interface microstructure.

Motivation-1: Direct numerical simulations of DP steel microstructures are **computationally prohibitive**.

M/F interface in general:
• Multi-phase
• Small features
• Highly variable

Interfacial morphology[3]
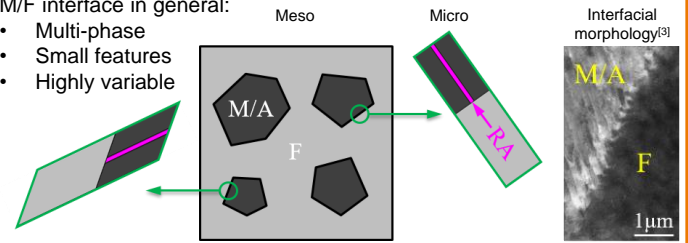
Motivation-2: Existing approaches for meso M/F interface modelling do not incorporate the underlying **microphysics**.

Cohesive interface with ad-hoc assumptions[4]

Martensite substructure boundary sliding and its interaction with the near-interface ferrite[5]

Microphysics:
• Sliding-induced damage mode
• Cannot be described with a classical cohesive law
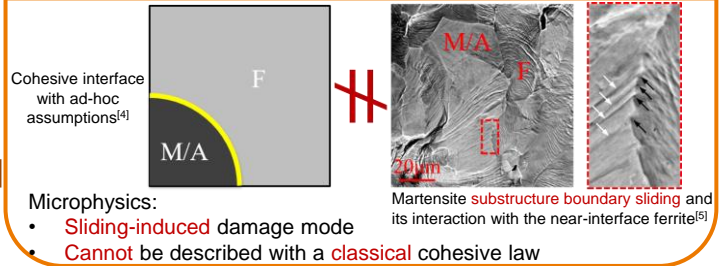
II. Multi-scale framework

Hypothesis-1: Two distinctive M/F interface damage modes can lead to interface separation at the mesoscale.
Hypothesis-2: Additive superposition of the contribution by two damage modes.

Interface damage analysis:

Micro damage pattern

Meso interface separation

Habit plane active mode (HP, enhanced)

Sliding is active

Habit plane inactive mode (NHP, classical)

Sliding is inactive
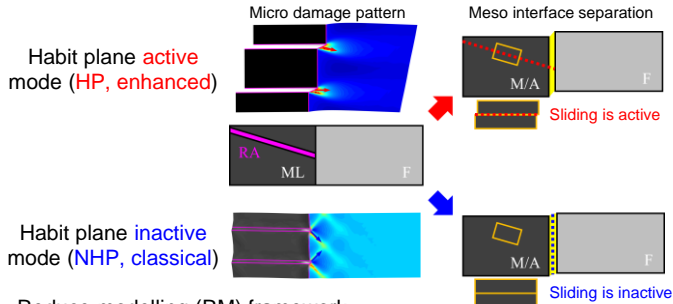
Reduce modelling (RM) framework:

Microscale

Effective interface kinematics

Micro BVP solution

Loading set HP+NHP

Effective generalized tractions

Effective model identification

Off-line

Mesoscale

Enhanced interface cohesive law

$$\vec{\Delta}_{M/F} = \mathfrak{D}_{M/F}\left(\vec{\gamma}^{hp}, \vec{\Delta}^{nhp}\right), \vec{\gamma}^{hp} = \mathfrak{G}^{hp}\left(\mathbf{F}_{M/A}\right)$$
$$\vec{\tau}^{hp} = \mathfrak{T}^{hp}\left(\vec{\gamma}^{hp}\right), \vec{T}^{nhp} = \mathfrak{T}^{nhp}\left(\vec{\Delta}^{nhp}\right)$$
$$\vec{T}_{M/F} = \mathfrak{T}_{M/F}\left(\vec{\tau}^{hp}, \vec{T}^{nhp}\right)$$

On-line
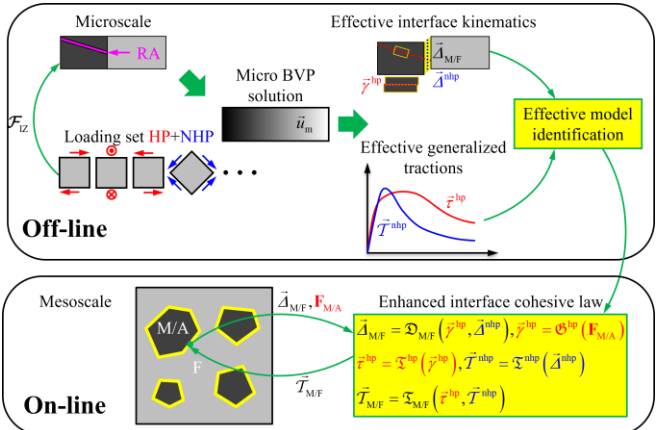
Enhanced cohesive law for M/F interfaces:
• Identified using a multi-scale framework
• Incorporating the underlying microphysics

III. Results

Validation: Reduced modelling (RM) with the effective interface model (W/ IF) closely reproduces full modelling (FM) on a M/F interface microstructure.

Effective stress-strain response

M/F strain partitioning
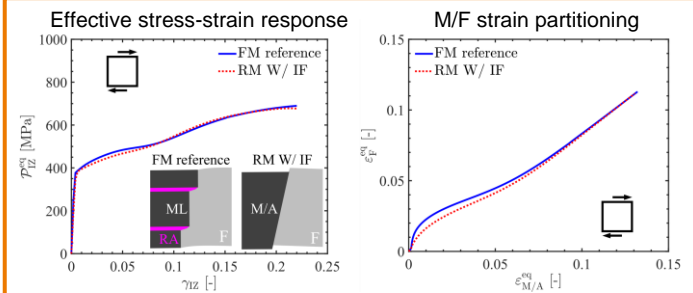
FM reference
RM W/ IF

Application: Reduced modelling on a DP steel mesostructure with a single M/A island embedded in a ferrite matrix.

RM W/ IF

RM W/O IF

M/A island plastic strain   F matrix inelastic strain
0 — 13 [%]   0 — 13 [%]

Plastic strain localization in ferrite matrix is underestimated without taking the M/F interface behaviour into account.
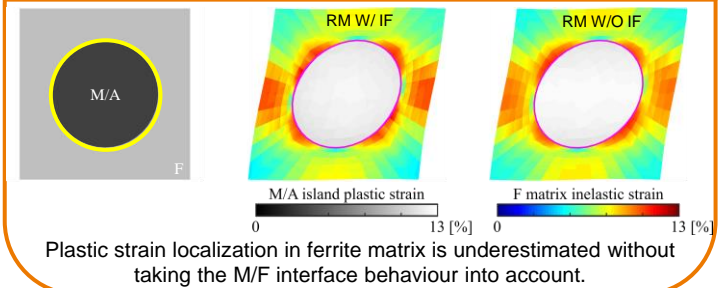
References

[1] AHSSs application guidelines 6.0 (2017).
[2] Q. Lai et al. (2015). Mater. Sci. Eng. A.
[3] L. Liu et al. (2021). Acta Mater.
[4] H. Hosseini-Toudeshky et al. (2015). Mater. Des.
[5] T. Vermeij, et al. (2022). In preparation.

Email address: l.liu@tue.nl

Computational Homogenisation of Locally-Resonant Poroelastic Medium

R. Liupekevicius [1], J. A. W. van Dommelen [1], M. G. D. Geers [1], V. G. Kouznetsova [1]

[1]Eindhoven University of Technology

Introduction

Discovering innovative noise control strategies can considerably upgrade comfort in urban areas and reduce the incidence of noise-related health problems. The purpose of an acoustic treatment by means of a material is twofold: preventing acoustic waves from crossing the material and mitigating reflected acoustic waves. Three acoustic indicators are depicted in Figure 1(B).

(A)   **(B)**
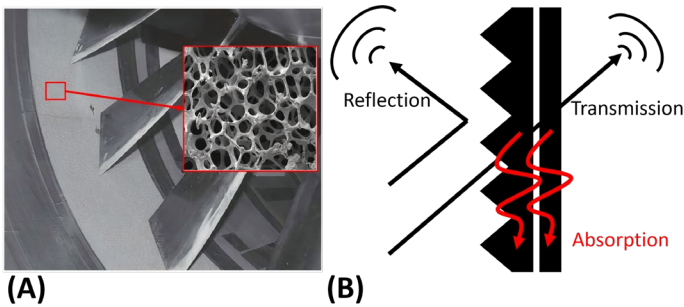
Figure 1: (A) Foam liner placed over the rotor inside a turbofan engine [1]. (B) Foam interacting with impinging wave.

Acoustic Metafoam

A new generation of acoustic foam is designed by combining standard acoustic foams with the Locally Resonant Acoustic Metamaterial (LRAM) features.
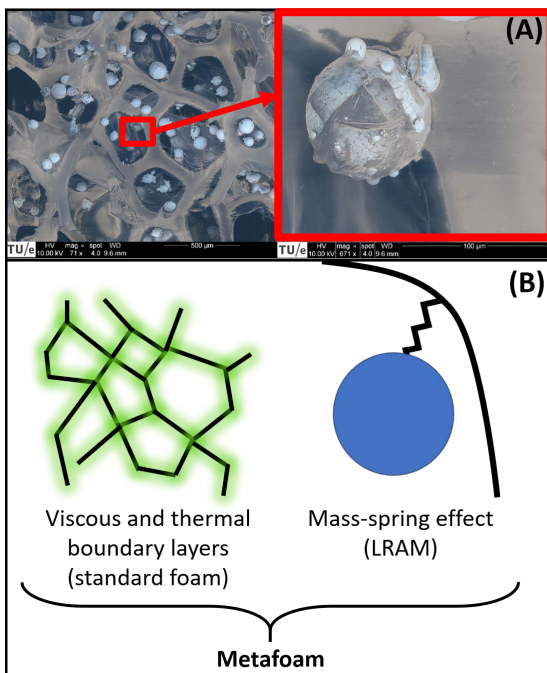
Figure 2: (A) Metafoam prototype manufactured within METAFOAM project (ERC-PoC, PI M. Geers) (B) Two depicted phenomena are combined.

In regular foams, acoustic waves are dissipated within the boundary layers. In LRAMs, local resonance gives birth to enhanced reflection at tunable frequencies. The low-audible frequency range is the target for the envisaged application.

Multi-scale Framework

Acoustic propagation activates fine-scale mechanisms at the pore level, such as the local resonance and thermal-viscous dissipation. The multi-scale approach developed in this work can handle the macroscopic finite-size problem (governed by Biot-like equations) while accounting for the exotic LRAM behaviour that emerges from the microscopic scale through a computational homogenisation procedure.
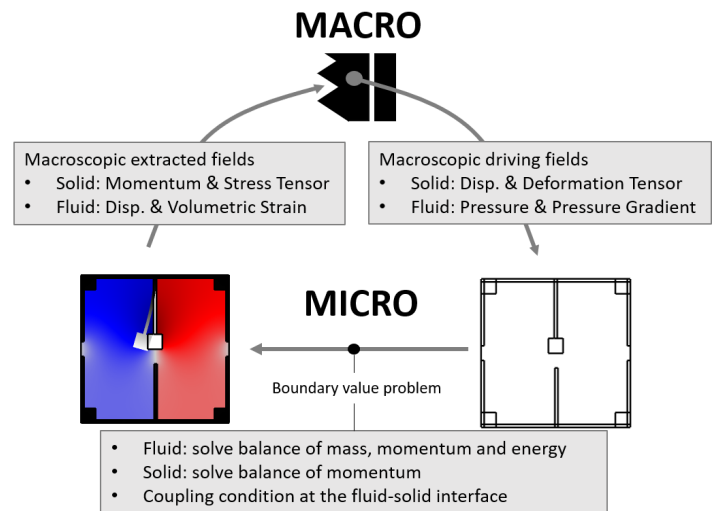
Figure 4: Simplified summary of the computational homogenisation framework inspired by [3] and [4]. Microscopic computation part is called offline procedure because it is computed once for a given microstructure.
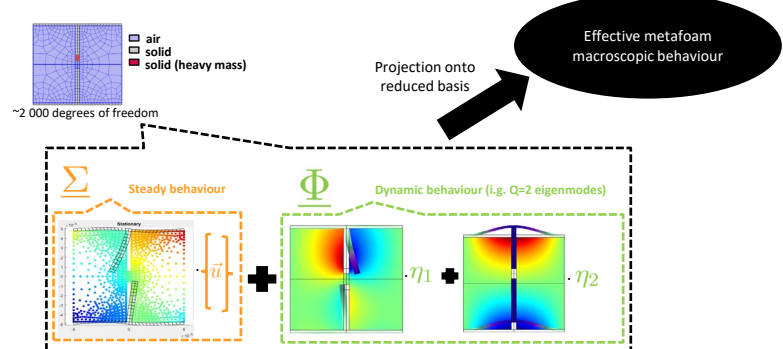
Figure 5: The full microscopic finite element model is projected onto a reduced basis composed of a steady part and a dynamic part. The steady-dynamic split gives rise to constitutive relations with a clear separation between terms corresponding to conventional foams and terms corresponding to the local resonance contribution.

References

[1] D. L. Sutliff and M. G. Jones. Journal of Aircraft, 46(4):1381–1394, 2009.

[2] M. A. Lewinska. PhD Thesis, 2019.

[3] A. Sridhar. PhD thesis, 2019.

[4] K. Gao. PhD Thesis, 2016.

PhD progress

1 2 3 4

Homogenization of hygro-mechanical response of oak wood based on 3D micro-CT images and finite cell method

M.A. Livani, E. Bosco, A.S.J. Suiker

Department of the Built Environment
Eindhoven University of Technology

This research aims at developing a relation between the ultra-structural features and the effective hygro-mechanical properties of oak wood, in order to gain advanced insight on the response of historical oak art objects subjected to indoor climate variations [1]. Representative volume elements (RVEs) of the wood micro-structure are generated based on 3D images of oak growth rings obtained by computational tomography. The geometry of the growth ring is extracted from the images by using the finite cell method. Individual fibrils are modeled at the nano-scale level by considering the moisture-dependent elastic properties and the adsorption isotherm, resulting in their effective hygro-elastic properties. Together with the microfibril angle of the cell wall layer, the homogenized fibril properties are subsequently used as input for computing the effective hygro-elastic properties of cell walls at the meso-scale level.

3D image processing

Level-set based segmentation of the 3D micro-CT volume of oak

Fiber

Connection between rays and axial cells

Rays

Vessel

3D binary volume of part of the wood cells
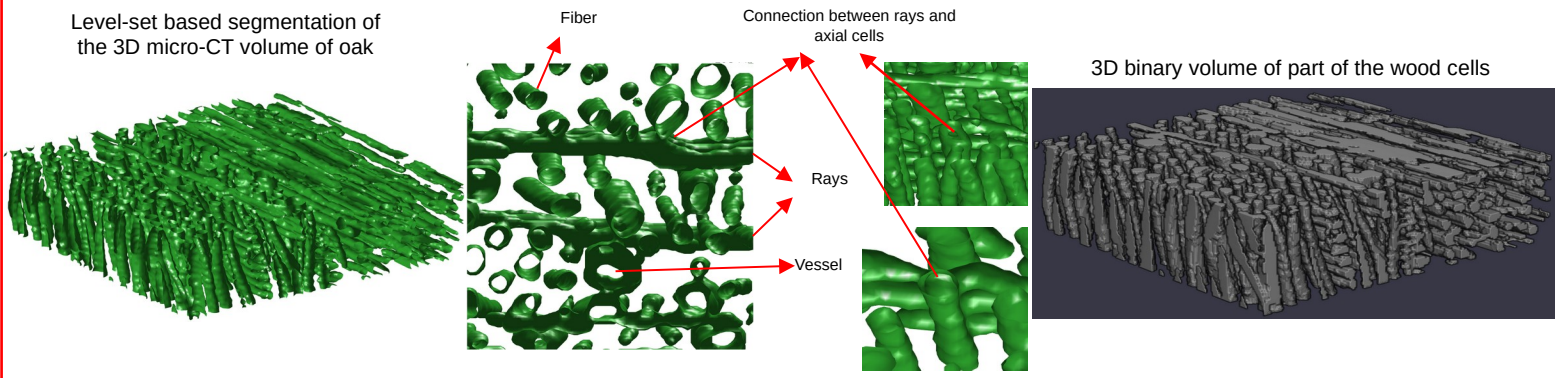
Homogenization of the cell walls as the input of the growth ring model

Cellulose nano-fibril model

Dislocated cellulose

Non-crystalline cellulose

Crystalline cellulose

Hemicellulose

Lignin

Laminate model of the cell walls

2D view of the level-set function for gradient-based definition of the material orientation

Material orientation of the orthotropic cell walls

Moisture dependent elastic modulus of the wood polymers

E [GPa] vs RH [%]

Hemicellulose
Amorphous cellulose
Lignin

Meso-scale model

Part of structured finite element mesh cut by the isosurface

Moisture dependent effective radial elastic modulus of wood

$\bar{E}_R$ [GPa] vs Moisture content [%]

CI=73%
CI=50%
Ozyhar et al. [2]
Guntekin et al. [3]
Luimes et al. [4]
Guntekin et al. [5]
ρ=582 kg/m^3
ρ=685 kg/m^3
ρ=798 kg/m^3

References:

[1] M.A. Livani, E. Bosco, and A.S.J. Suiker, vol. 91, no. 10, pp. 4141–4162, 2021.
[2] T. Ozyhar, L. Mohl, S. Hering, P. Hass, L. Zeindler, R. Ackermann, and P. Niemz, Wood Material Science & Engineering, vol. 11, no. 1, pp. 36–45, 2016.
[3] E. Güntekin, T. Yılmaz Aydın, and M. Aydın, in International Forestry Symposium, pp. 645–649, 2016.
[4] R.A. Luimes, A.S.J. Suiker, C.V. Verhoosel, A.J.M. Jorissen, and H.L. Schellen, Wood Science and Technology, vol. 52, no. 5, pp. 1243–1269, 2018.
[5] E. Güntekin, T.Y. AYDIN, and P. NİEMZ, Eurasian Journal of Forest Science, vol. 4, no. 1, pp. 40–47, 2016.

TU/e EINDHOVEN UNIVERSITY OF TECHNOLOGY

PhD progress
1 2 3 4

NWO Netherlands Organisation for Scientific Research

RIJKS MUSEUM amsterdam

Continuum-DEM modelling of fluid-solid transition in weakly compacted systems of polydisperse particles of varying shapes

R. Lubbe[1], V. Magnanimo[1], S. Luding[1], H. Cheng[1], P. Gupta[2]

[1]University of Twente
[2]Procter & Gamble, UK

Introduction

Figure 1: Household sugar [1]

Fluid-solid transition of granular materials is common in our everyday lives (e.g, sugar)

Challenge in industry handling the regime change (e.g hopper flows)

Solution is to develop a tool to virtually prototype designs to reduce wasteful resources

Methodology

Fluid-solid transition

MPM Simulate regime change

DEM Micro to macro

Virtual Prototyping Industrial application
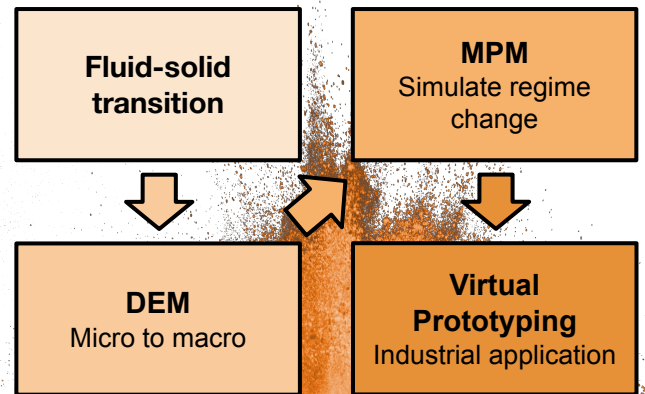
Objectives

1. Develop an **continuum-discrete** solver to capture the **fluid-solid transition** of granular materials

2. Study the influence of **polydisperse** and **multi-component** systems on the **flowability**

3. **Prototype** various **powders and geometries** to aid designs

Key Techniques

Solvers: Material Point Method (**MPM**), Discrete Element Method (**DEM**)

Constitutive models: μ-I rheology models [2], plasticity models (soil mechanics)

Statistics: Probabilistic inference, coarse graining fields

Applications

Aid in the design of products or processes to ensure **uniform flowability** to prevent **clogging** and **over/under dosage** of granular materials.

Figure 2: Hopper lays out raw ingredients

Preliminary Results

(a)   (b)

Figure 3: Studying DEM systems: (a) column collapse and (b) chute flow

(a)   (b)
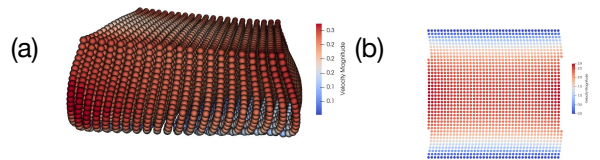
Figure 4: Developing and verifying MPM solver: (a) column collapse and (b) simple channel flow

Outlook

1. **Develop** MPM solver further by adding rheological and plasticity constitutive models.

2. **Study** fluid-solid transition in DEM (especially at the jamming/unjamming point)

4. **Quantify** uncertainty using GrainLearning [4]

3. **Validate** numerics with **experiments** (e.g, chute flow, angle of repose)

References

[1] Stock photo taken from Freepik.com
[2] Shi, H, et al. (2020). Steady state rheology of homogeneous and inhomogeneous cohesive granular materials. Granular matter, 22(1), 1-20.
[3] Turner, B (2015). *Mosa porcelain tiles production tour*. Retrieved September 20, 2022, https://www.materialscouncil.com/mosa-porcelain-tiles-production-tour/
[4] Cheng, H., et. al (2019). An iterative Bayesian filtering framework for fast and automated calibration of DEM models. Computer methods in applied mechanics and engineering, 350, 268-294.

Optimization of Laminated Composites

Swapan Madabhushi V , Boyang Chen

*Aerospace Structures and Computational Mechanics,
Delft University of Technology*

Composite Parameterization

The tailoring powers of composite materials have been clearly demonstrated through structural optimization. However, the plethora of design D.O.Fs that give composite structures their high tailorability also produces a complex search space with both continuous and discrete design variables.

A common preliminary design process of composite structures is shown in Fig. 1, stiffness characteristics of a laminate are parametrized using 12 lamination parameters and a thickness variable. This implies that large number of N variables required by CLT can be replaced by just 13 parameters. More crucially, using lamination parameters as design variables reformulates composite optimization that may be solved by computationally efficient gradient-based optimizers.
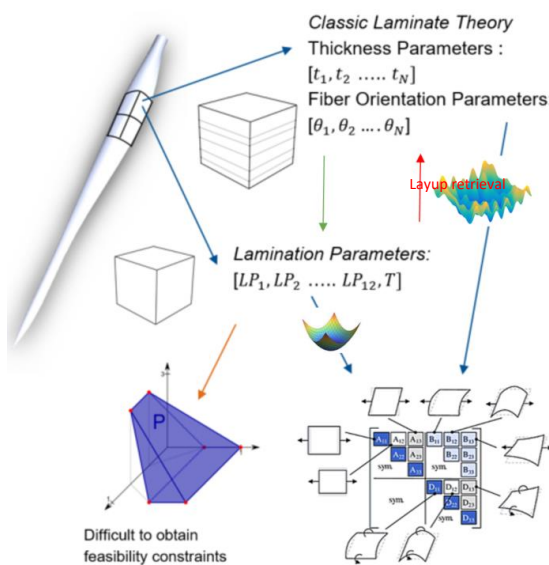
Figure 1: Composite structure parameterizations

Layup Optimization Problem

The optimized composite structures are subject to another optimization process to accommodate manufacturability. The manufacture of composite structure depends on detailed layup sequence of all discrete panels. Despite many approaches in literature, there is no computationally efficient approach able to cover a larger design space of thick Unconventional laminates [2] (shown in Fig. 2). During an ideal Layup retrieval process complete enumeration is impractical due to the exponential relationship between the number of stacking sequence combinations and the number of plies.

However, recent advances in Machine learning and Quantum computing could be leveraged to find (blending constraints) linkage between Lamination parameter space and manufacturability especially for unconventional laminates.

Quantum Computing and Machine Learning Methods
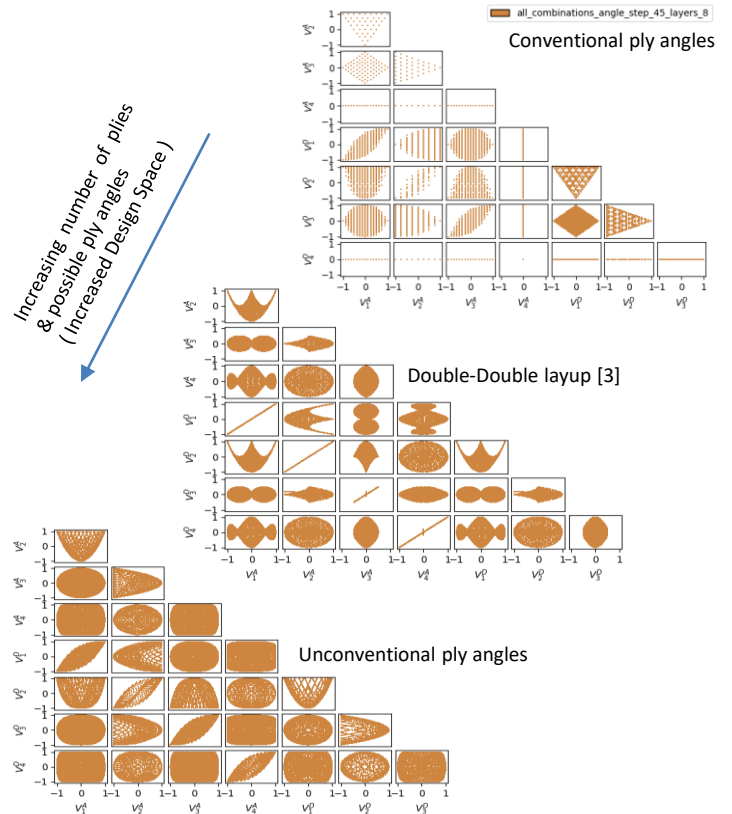
Figure 2: Design Spaces comparison shown by scatter plot of physical LPs

The non-linear and non-bijective nature of LP design space and stacking sequences forms a combinatorial optimization problem. Various approaches in quantum computing for structural optimization [4] such as quantum kernel methods [3] could be employed to search the design space to find a true global optimum stacking sequence.

However, the challenge lies in formulating a suitable objective function to account for blending constraints.

References

[1] S.W.Tsai, H.T.Hahn, Introduction to composite materials, Technomic Pub. (1980)

[2] Mazen A. Albazzan et al, " Efficient design optimization of nonconventional laminated composites using lamination parameters: A state of the art", Composite Struct. Volume 209, 2019, Pages 362-374, ISSN 0263-8223

[3] Stephen W.Tsai, "Double-Double: New family of Composite Laminates," AIAA Journal 2021 59:11, 4293-4305

[3] Mengoni, R., Di Pierro, A., " Kernel methods in Quantum Machine Learning ", *Quantum Mach. Intell.* **1**, 65–71 (2019)

[4] Sato, Yuki, et al. " Quantum topology optimization of ground structures using noisy intermediate-scale quantum devices" *arXiv:2207.09181* (2022)

PhD progress

| 1 | 2 | 3 | 4 |

Building a Multi-Layer Stress Depth Profiler

R.F.M Martens[1], J.P.M Hoefnagels[1], O. van der Sluis[1,2], M. Geers[1]

[1]Eindhoven University of Technology
[2]Philips Electronics Netherlands

Residual stresses

Thin films are used to obtain high performance and reliability in a large number of technologies including optical communications, microelectronics and wear-resistant coatings[1]. Knowledge about the **residual stress** is crucial because it can limit the performance and lifetime. Residual stresses already start developing during deposition and growth of the thin films and will further change due to short and long term relaxation effects.

Numerical models have been developed to calculate these residual stress as a function of the thickness for single layers. Due to the complex origin of the residual stress the models in literature depend on many parameters making accurate determination of these parameters challenging. When a multi-layer stack is deposited, the layers start to interact with each other significantly affecting the residual stress. There are **no models available** to accurately describe these changes in residual stress due to this interaction.

What can not be modelled; must be measured

A **new experimental setup** is needed to measure the through thickness relaxed stress profile of a multi-layered stack with a resolution in thickness of 1 nm and resolution of stress in a layer of 10 nm of 10 MPa, also in case of a multilayer stack.

In the new setup, the stress will be measured with an inhouse developed **high accuracy stress sensor** that will measure the average stress in the multilayer stack. To obtain the stress as function of thickness, the multilayer stack will slowly **be etched** and from the change in average residual stress, the residual stress in the removed layer can be assessed. At the same time, the change in thickness must be monitored.
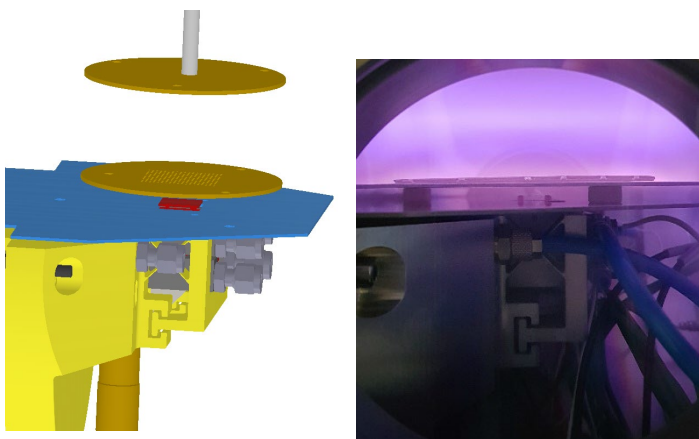
Figure 1: *(Left) Plasma setup to slowly remove material uniformly without introducing damage in layers underneath. (Right) Plasma setup incorporated in stress measurement setup.*

Figure 2: *Vacuum compatible, monolithic, high-precision, high-capacity microbalance to measure how much material has been removed.*

The setup

The through thickness stress measurement setup consists of three components; a stress sensor *(Figure 3)* to measure in-situ the average residual stress, a setup able to uniformly remove the material *(Figure 1)*, and a device capable of measuring how much material has been removed *(Figure 2)*.
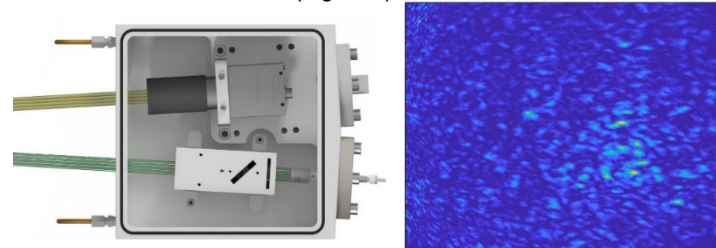
Figure 3: *(Left) Ultra-high accurate speckle stress sensor, insensitive to vibrations, measuring the residual stress in ultra-thin layers. (Right) Speckle pattern from which the residual stress is determined with integrated digital image correlation (IDIC).*
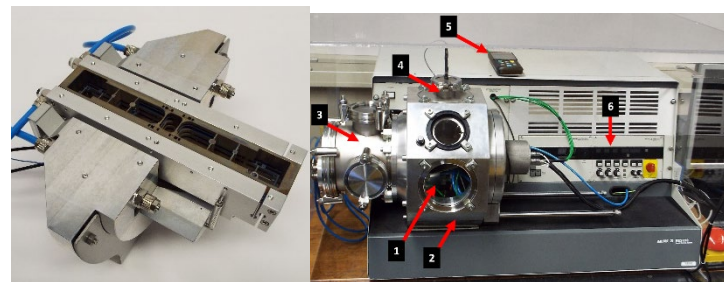
Figure 4: *(Left) Mount to install microbalance into vacuum chamber and simultaneously align the balance with stress sensor, minimize vibrations and cool the setup. (Right) The thickness stress measurement setup without the control system of the microbalance.*

Unlocking the full potential of ultra-thin films.

In the same PhD-project, the mechanical properties are measured. To achieve this**, a new bulge-setup** has been developed that can measure the properties of ultra thin films without zero state stress reference and with a higher accuracy than other setups. Besides, a new methodology has been developed to measure buckled membranes.

The experimental data from both the stress measurement setup and bulge setup are used in a **numerical model** to optimize the design of nanodevices. With this model, the manufacturability and performance of nanodevices is greatly improved.
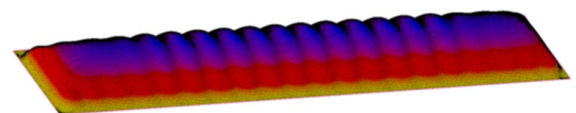
Figure 5: *Even the mechanical properties of ultra thin buckled membranes can easily be accurately determined with the new bulge setup[2].*

References

[1] Chason, et al. 2018. Tutorial: Understanding residual stress in polycrystalline thin films through real-time measurements and physical models
[2] A bulge test based methodology for characterizing ultra-thin buckled membranes S. Shafqat et al. (2018)

TU/e Technische Universiteit Eindhoven University of Technology

PhD progress

| 25% | 50% | 75% | 100% |

POSITION innovation in smart medical instruments

PHILIPS

Controlling the motion of a pendulum with magnetic actuation

P.C. Meijers[1], P. Atzampou[1], A.V. Metrikine[1]

[1] Delft University of Technology

Introduction

In the coming years, the number of newly-build offshore wind farms in Europe will increase significantly [2]. In the future, floating crane vessels will be used more often for turbine assembly, see Figure 1a. Wave-induced vessel motions are transferred to the load that is suspended in the crane, creating undesired swinging motions. This project investigates a non-contact method to suppress these motions.

(a)   (b)

Figure 1: (a) Floating installation of a wind turbine. (b) Scaled lab set-up.

Mathematical model

The new non-contact method uses an electromagnet to control the motions of the suspended load. Figure 1b shows the scaled lab set-up, which can be schematised as shown in Figure 2.
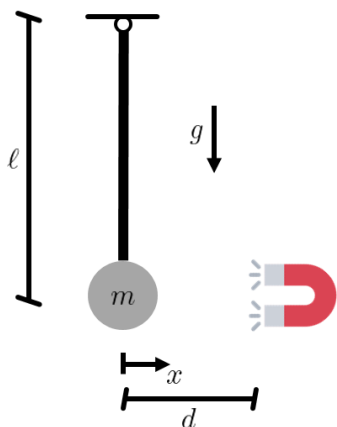
Figure 2: Schematic of a pendulum and magnetic actuator.

The small angle approximation of the equation of motion of a pendulum with mass m and length ℓ subject to Coulomb friction T is

$$m\ddot{x} + \text{sign}\left(\dot{x}\right) T + \frac{mg}{\ell}x = \frac{\alpha u}{(x-d)^3}, \quad (1)$$

in which the right hand side represents the non-linear distance-depended force of the electromagnet. The initial

distance between the mass and the magnet is d, and α is a system parameter to quantify the strength of the magnetic interaction. In the above, derivatives with respect to time are denoted by dots above the variables. To control the system, the voltage u of the magnet is determined by a PD control law [1]:

$$u = \left[\frac{(x-d)^3}{\alpha}\left(K_p e + K_d \dot{e}\right)\right]_{u_-}^{u_+}, \quad (2)$$

where the error $e = \delta - x$, in which δ is the desired motion. K_p and K_d are the controller gains. Note that output of the controller is physically bounded by the operational voltage of the electromagnet.

Results and conclusions

Figure 3 presents the simulated and measured motions of the controlled pendulum for a typical wave-induced signal. It is clear that the model can represent the measurements very well (top graph). Moreover, the controller is able to follow the desired motion (middle graph), using the control signals which remain within the bound for most of the time (bottom graph). These results show that the motion of a suspended load can be controlled using a non-linear actuator.
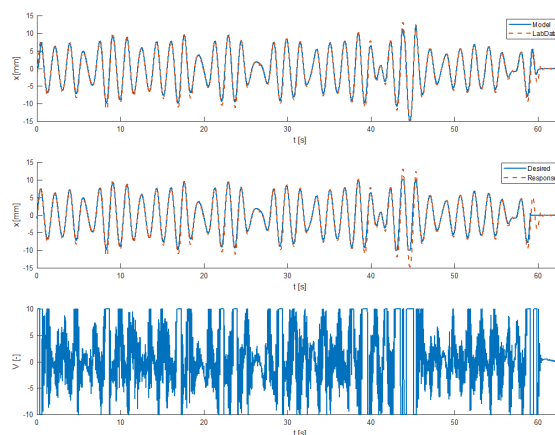
Figure 3: Simulation and measurement results for a controlled pendulum. (top) Simulation vs. measurement. (middle) Desired vs. measured motion. (bottom) Control signal.

References

[1] K. J. Åström and R. M. Murray. *Feedback Systems*. Princeton University Press, Princeton, 2008.

[2] WindEurope. Offshore Wind in Europe. Key trends and statistics 2019. Technical report, WindEurope, 2020.

Computational Design for Wire Arc Additive Manufacturing

V. Mishra[1], C. Ayas[1], M. Langelaar[1], F. van Keulen[1]

[1]Delft University of Technology

Introduction and Objectives

Wire Arc Additive Manufacturing (WAAM) used for manufacturing large scale structures such as ship propellers and bridges. Design and process optimization considering manufacturability and influence of the WAAM process on the material properties.
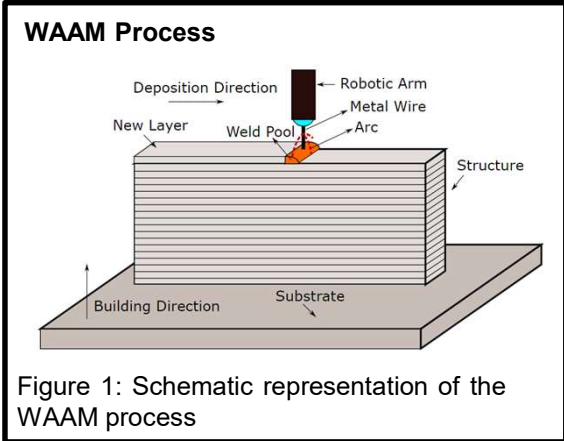
WAAM Process

Figure 1: Schematic representation of the WAAM process

Manufacturing Requirement : Avoid defect prone thin intersections
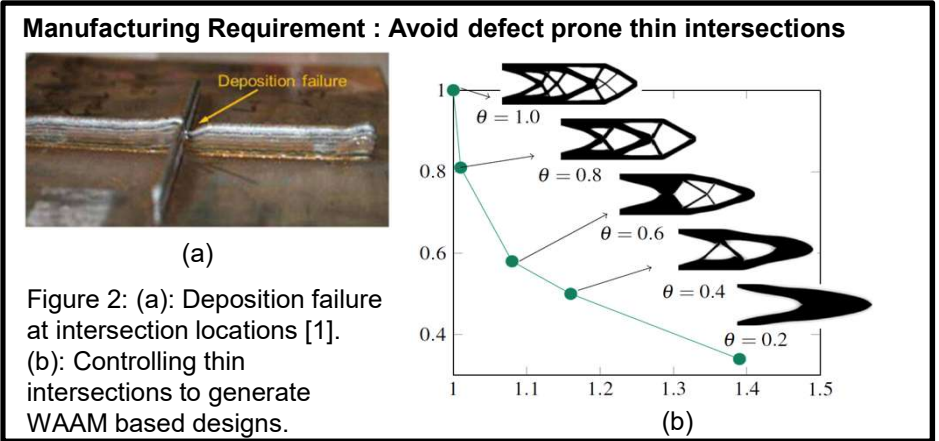
Figure 2: (a): Deposition failure at intersection locations [1]. (b): Controlling thin intersections to generate WAAM based designs.

Elastic anisotropy in stainless steels
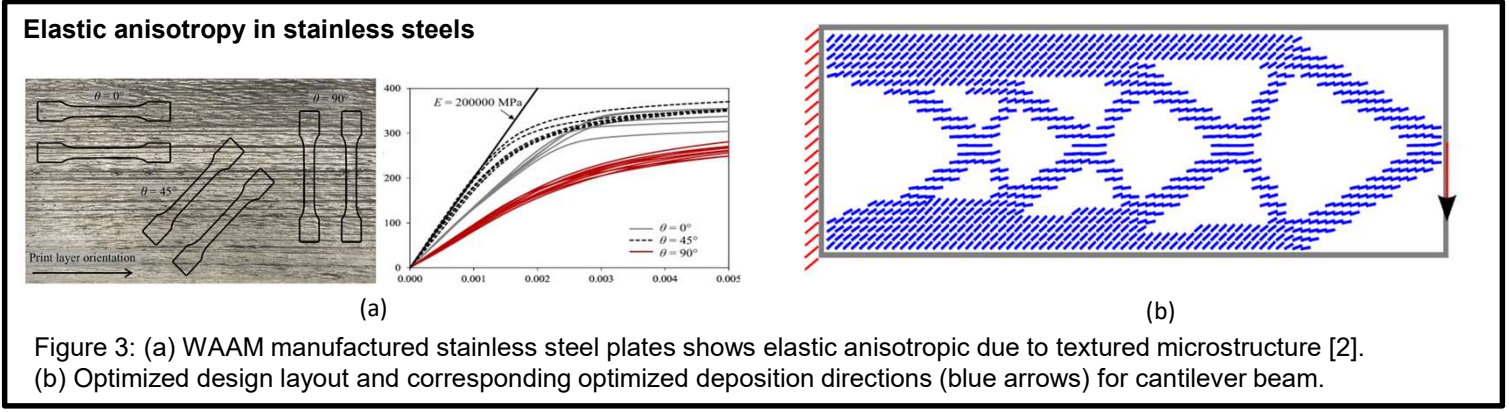
Figure 3: (a) WAAM manufactured stainless steel plates shows elastic anisotropic due to textured microstructure [2]. (b) Optimized design layout and corresponding optimized deposition directions (blue arrows) for cantilever beam.

Cooling rates effects the microstructure development of High strength low alloy steels
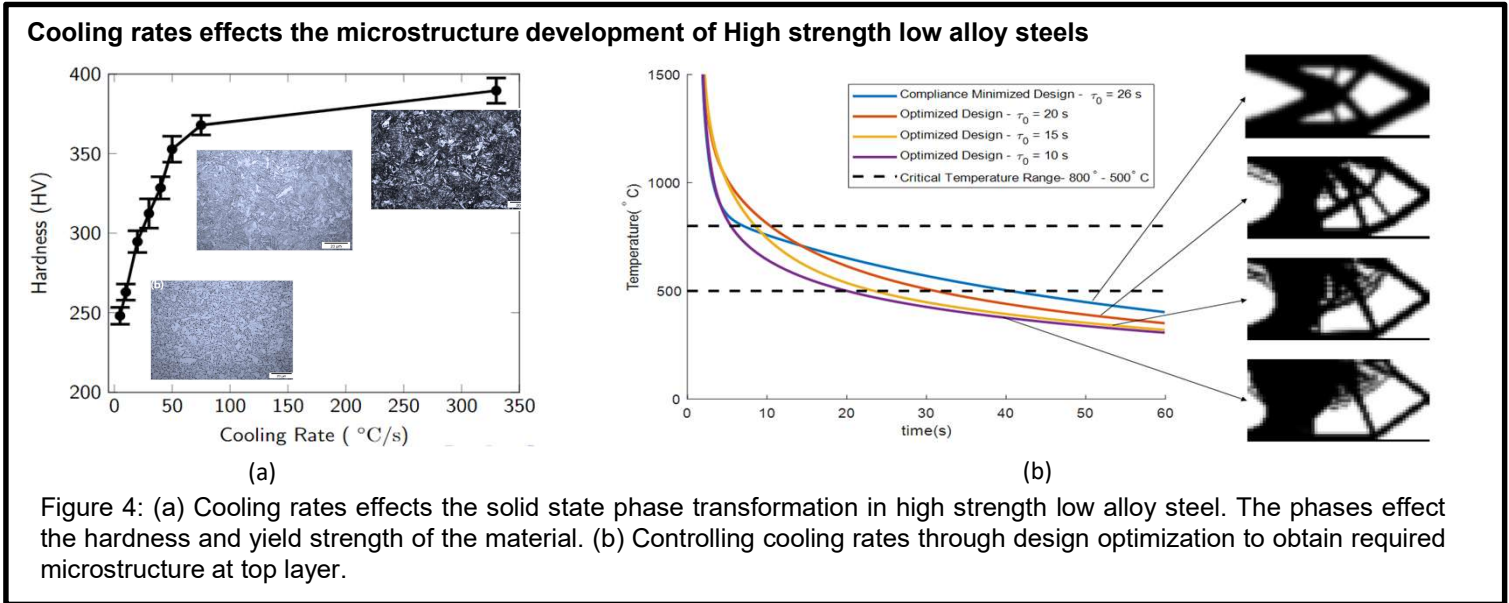
Figure 4: (a) Cooling rates effects the solid state phase transformation in high strength low alloy steel. The phases effect the hardness and yield strength of the material. (b) Controlling cooling rates through design optimization to obtain required microstructure at top layer.

Conclusions

WAAM requires design with low geometrical complexity. Design, WAAM process and mechanical properties are interdependent. Design and process can be optimized to improve or get required mechanical properties.

References

[1] Mehnen, J., Ding, J., Lockett, H., & Kazanas, P. (2014). Design study for wire and arc additive manufacture. International Journal of Product Development, 19(1/2/3), 2-20.

[2] P. Kyvelou, H. Slack, D. D. Mountanou, M. A. Wadee, T. B. Britton, C. Buchanan, L. Gardner, Mechanical and microstructural testing of wire and arc additively manufactured sheet material, Materials & Design 192 (2020) 108675

PhD progress

| 1 | 2 | 3 | 4 |

Time-dependent Anisotropic Behavior of Fibre Reinforced Thermoplastics.

S.N.R. Mudunuru[1], L.E. Govaert[1], J.A.W. van Dommelen[1]

[1] *Eindhoven University of Technology*

Introduction

The high performance and low weight of fibre reinforced plastics (FRP) promoted the use of these materials in aerospace, automotive, and other applications. While the current generation of FRP are made of thermosets, an exceptional growth in the use of thermoplastics is expected in the near future as they can be rapidly produced and easily recycled.
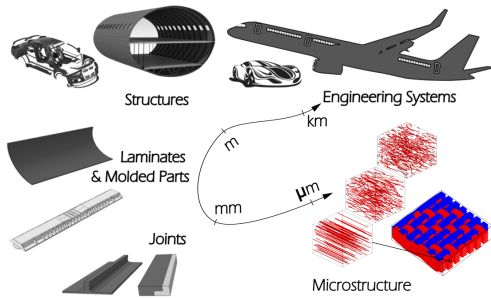
Figure 1: Hierarchy of scales in FRP structures

The consortium program **ENLIGHTEN** aims to develop production methods, control, and monitoring techniques for large integrated Thermoplastic Composite (TPC) structures and assemblies for air, and land transportation. **As part of the Enlighten program, this project aims to provide a methodology that links the microstructural information such as matrix morphology, and fibre distribution to macroscopic laminate performance.** The methodology will be validated by characterizing the mechanical behavior of two Fibre Reinforced Thermoplastic Composite (FR-TPC) systems: glass fibres in PA410 matrix, and carbon fibres in PEEK matrix.

Approach

The Eindhoven Glass Polymer (EGP) model [2] is a 3D constitutive model developed for glassy polymers based on the framework proposed by Haward and Thackray [1]. Over the years, this continuum-based EGP model was extended to deal with complexities from figure 3 associated with the mechanical behavior of solid polymers. Further, **an anisotropic viscoelastic-viscoplastic constitutive model was developed based on the extended EGP model for short fibre reinforced polymer (SFRP) composites [3].**

While the proposed continuum model can simulate the post-yield and long-term behavior, only the pre-yield response has been validated thus far. Additionally, large strains may lead to change in local fibre orientation distribution. Due to the strong anisotropy observed in FRP, this would result in complex post-yield behavior compared to unreinforced polymers. Therefore, large strain micromechanical response of Representative Volume Elements (RVE) will be studied as means to observe such orientation dependent complexities. The fibres in the RVE will be modeled as elastic materials, while the matrix will be modeled using a version of the EGP model that best fit the polymer systems under consideration.
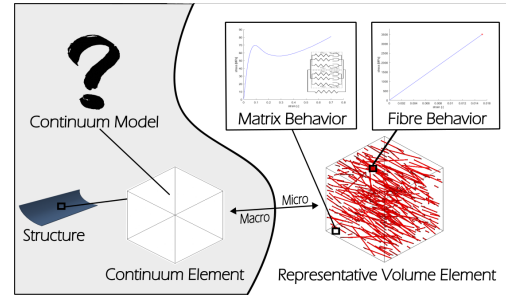
Figure 2: Two scale mechanical modeling concept

Research Objectives

- Characterization of the short- and long-term behavior of PEEK, and Nylon-PA.
- RVE generation and micromechanical simulation of large strain response of the FR-TPC systems.
- Extend or validate the anisotropic viscoelastic-viscoplastic continuum model to fit the response of the FR-TPC systems.

References

[1] Haward, R.; Thackray, G. Proc. R. Soc. London A 1968, 302, 453-472.
[2] Tervoort, T. A.; Smit, R. J. M.; Brekelmans, W. A. M.; Govaert, L. E. Mech. Time-Dep. Mater. 1998, 1, 269-291.
[3] Amiri-Rad, A.; Pastukhov, L. V.; Govaert, L. E.; Van Dommelen, J. A. Mechanics of Materials 137 (2019): 103141.
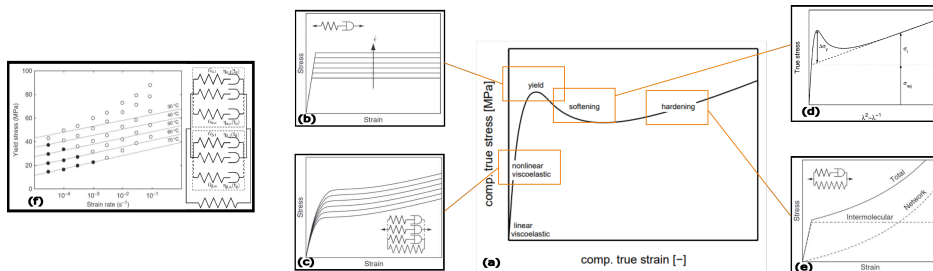
Figure 3: a) Representative stress-strain response of polymers. b) Single mode Maxwell model and strain rate dependant response. c) Multimode EGP model and strain rate dependant response. d) Post-yield strain softening response due to thermo-mechanical aging from the rejuvenated state. e) EGP model capturing the hardening response. f) Multiprocess model accounting for multiple deformation mechanisms.

PhD progress

| 1 | 2 | 3 | 4 |

A data-driven model updating approach for robust optimization of (multi-stage) production processes

F. Munzone[1], J. Hazrati[1], W.B.J. Hakvoort[2], T. van den Boogaard[1]

[1]University of Twente, Faculty of Engineering Technology, Nonlinear Solid Mechanics
[2]University of Twente, Faculty of Engineering Technology, Precision Engineering

Introduction

With higher demands on production of manufacturing products, the industries are moving towards real-time virtual simulation of physical processes, aiming to reduce waste, manpower and CO_2 production. Data-driven models have shown their potential in this field due to their capability to predict complex phenomena without manual calibration, as happens for physics-driven methods. However, they lack interpretability and are difficult to validate.

Research Goal

✓ Develop methods for automated updating of physics informed meta-models based on measurement data to account for the uncertainties and unphysical assumptions in the virtual models.

✓ Develop inverse metamodels to trace back the measured responses to the input parameters for root cause identifications of deviations in product.

✓ Implementing robust optimization methods for multi-stage manufacturing processes.

DATA-DRIVEN MODEL UPDATING PROCESS

$\sigma_y, \nu, E, (x, y, z),$

F_{tool}, u_{tool}

(x, y, z)

$F_{tool}, u_{tool},$

T_{tool}

BUILDING BASED ON

Physic based virtual model

$\bar{\sigma}, \bar{\varepsilon}, \bar{u}$

Physics Informed Meta-Model

T_{exp}
$\bar{u}_{exp}$

Production measurement data

$\bar{\sigma}^*, \bar{\varepsilon}^*, \bar{u}^*$

Redrawing process – Stage-2 [1]

Flange Diameter and Temperatures over time [1]

Future work

• Different meta-models will be studied (i.e., neural networks, RSM) to develop physically regularized model based on FE models of the demonstrator process.

• A meta-model updating approach will be developed based on sensitivity analyses and uncertainty quantification.

Fig.1: Schematic view of the envisioned value chain with feedback loops [2]

REFERENCES

[1] Mark Veldhuis, et al., Procedia Manufacturing, 2020, https://doi.org/10.1016/j.promfg.2020.04.176.
[2] Integration of Data-drIven and model-based enGIneering in fuTure industriAL Technology With value chaIn optimizatioN (DIGITAL TWIN) - proposal

UNIVERSITY OF TWENTE.

PhD progress
| 1 | 2 | 3 | 4 |

PHILIPS

Digital Twin

Modelling of Recycled Fibre-Reinforced Polymer Composites

N. Nazemzadeh[1,*], M. Van Drongelen[2], R. Akkerman[2], I. Gitman[1]

[1]University of Twente, Computational Design of Structural Materials
[2]University of Twente, Production Technology
*n.nazemzadeh@utwente.nl

Introduction and problem statement

Fibre-reinforced polymer (FRP) composites are engineered materials used in many industries, including aerospace, automobile, sports and healthcare, due to their excellent strength-to-weight and stiffness-to-weight ratios. Due to their wide usage, these materials unfortunately produce industrial scraps and end-of-life parts.

Recycling and reusing composites' scraps and end-of-life composites could potentially reduce disposal expenses, the demand for new materials and the negative effects on the environment.

This process starts with size reduction of composite and follows by compression molding process to remanufacture.

Size reduction

Random deposition

Compression molding
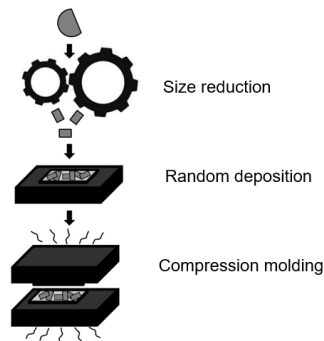
Figure 1: Recycling and remanufacturing processes

Project Aim

Develop understanding and predict the behaviour of recycled fibre-reinforced polymers via a comprehensive multi-scale modelling approach.

Modelling strategy

Multiscale modeling brings essential information from material's lower level of observation to a higher level in order to improve accuracy of material's behaviour predictions.

Macro-Scale

chip-Scale

Chip-Packing Scale

$[10^0 - 10^{-2}]$ $[10^{-2} - 10^{-3}]$ $[10^{-3} - 10^{-6}]$ Length [m]
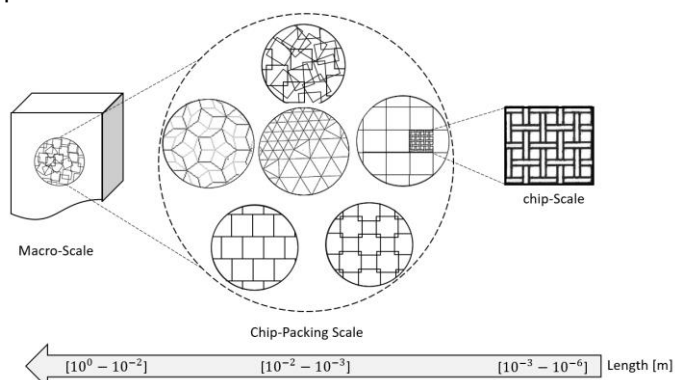
Figure 2: Multiscale modelling strategy

Mechanical and geometrical characteristics of fibres, together with properties of a polymer material are taken from the chip-scale to the chip-packing scale. Naturally, the arrangement of flakes on the chip-packing scale affects the overall macroscopic mechanical properties (stiffness and strength).

Modelling assumptions

	Macro-Scale	Chip-Packing scale	Chip-Scale
Assumption	Homogenous	Heterogenous Periodic and Non-periodic	Heterogenous Periodic
Outcome	Overall mechanical properties	Overall geometry properties	Overall flake properties
Specific Issues	Constitutive equations	1. Resin-rich area 2. High Volume fraction 3. Thickness variations	

Figure 3: Multiscale modelling assumptions and issues

Current objective

Random meso-scale morphology is the most common geometry structure in recycled fibre-reinforced composites due to the random deposition in the recycling process. The random geometric mesostructured models can be divided into different categories.

Figure 4: Random geometric mesostructured model; overlapped (A,D), non-overlapped in-plane (B,E), non-overlapped out-of-plane geometric models (C).

Since the overlapped geometric models share the same areas between chips (Fig. 3D) and the non-over-lapped in-plane geometric models do not provide the high-volume fraction (Fig. 3E) as observed in the experiment, non-overlapped out-of-plane geometric models have the potential to be most realistic.

Future Objective

Model different chip-packing morphologies and investigate the influence of different geometries on the overall mechanical characteristics of recycled fibre-reinforced composite for different applications and loading cases.

References

[1] M. I. A. Rasheed., "Compression molding of chopped woven thermoplastic composite flakes." (2016), PhD dissertation, University of Twente.
[2] S. Z. H. Shah, "A new approach for strength and stiffness prediction of discontinuous fibre reinforced composites (DFC)." Composites Part B: Engineering 183 (2020): 107676.

Quantifying the Round-trip Efficiency of a Novel Offshore Pumped Hydro Energy Storage System

R.M. Nienhuis[1], B. Jayawardhana[2], A.I. Vakis[1]

[1]CMME, ENTEG, FSE, University of Groningen
[2]DTPA, ENTEG, FSE, University of Groningen

Developing
Offshore
Storage &
Transport
Alternatives

PhD Project

The NWO-DOSTA research project is initiated by the Dutch Research Council (NWO) together with the TopSector Energy (TSE), which focusses on the feasibility of implementing offshore energy storage in the Dutch North Sea through [1]:

- Offshore pumped hydro storage
- Hybrid wind-storage systems
- Hydrogen as an alternative energy carrier

Research Aim

I. Predictive Models of System Behavior to Calculate Round-Trip Efficiency

II. Isolation and Degradation Mechanics from the Marine-Structure Interface

III. Embedded Mooring Stability and Survivability under Dynamic Loading

IV. Optimization with Alternative Energy Carriers in Hybrid Wind-Farm Systems

Ocean Battery

The Ocean Battery is an underwater Pumped-Hydro Storage (PHS) device that comprises of one rigid reservoir maintained at atmospheric pressure and one flexible reservoir that is pressurized by the surrounding seawater.

The two reservoirs are connected through the hydraulic system that moves the internal working fluid via pumps to the flexible bladder when the device stores energy, or uses the pressure difference to let the working fluid flow back through a hydro-turbine and into the rigid reservoir when electricity is

Efficiency 75 - 80%
Lifetime > 20 years
Storage volume 2 - 8 MWh/unit
Cycles charge and discharge
Scalable volume and capacity
Modular

Pressure Sensor
- Hydrostatic pressure
- Flexible Bladder
- Turbine Inlet
- Turbine Outlet
- Rigid Reservoir (pump)
- Rigid Reservoir (turbine)

Flexible Bladder
Umbilical
Rigid Reservoir
Turbine System
Pumping System
Adapted from [2]

Ocean Battery

Modelling Dynamic System Behaviour

The performance of the Ocean Battery is subjected to a range of dependencies such as dynamic changes in pressure, head and flowrate within the internal system. This dynamic behaviour needs to be accounted for when deriving the round trip efficiency of the energy storage system.

Analytical Results

Analytical Model
Compare Case | Depth = 3.42 [m]
Experimental Measurements

Legend:
- Hydrostatic pressure
- Flexible Bladder
- Turbine Inlet
- Turbine Outlet
- Rigid Reservoir 1
- Rigid Reservoir 2

Pressure Head [m] vs Time [s]
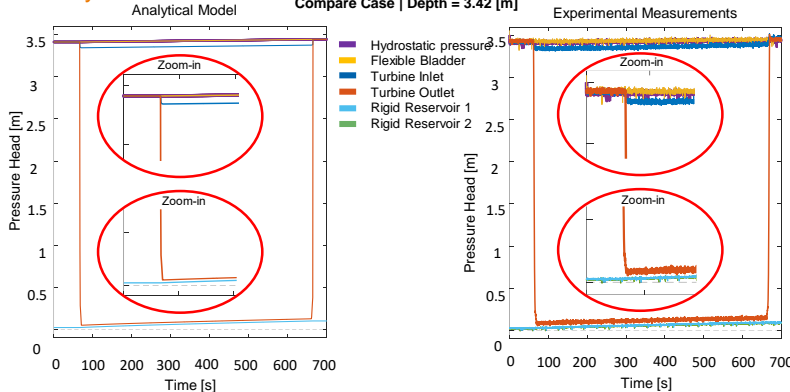
Pressure Head error calculation - Analytical Model vs Measurement

Hydrostatic Pressure | Flexible Bladder | Turbine Inlet Side | Turbine Outlet Side
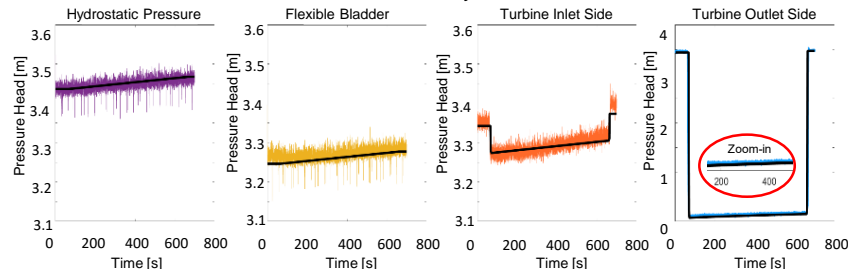
Empirical Results

A scaled down prototype of the Ocean Battery was developed by the Ocean Grazer B.V. company and installed at the Eemshaven to validate the initial round trip efficiency estimates and provide empirical data of the novel PHS technology. The initial data analysis of the prototype shows that the expected results are in line with the theoretical losses and the current round trip efficiency models.
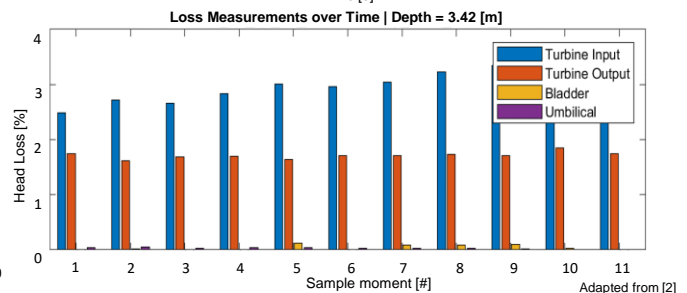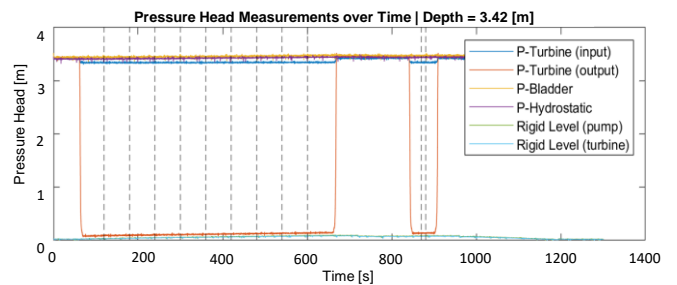
Pressure Head Measurements over Time | Depth = 3.42 [m]
- P-Turbine (input)
- P-Turbine (output)
- P-Bladder
- P-Hydrostatic
- Rigid Level (pump)
- Rigid Level (turbine)

Loss Measurements over Time | Depth = 3.42 [m]
- Turbine Input
- Turbine Output
- Bladder
- Umbilical

Sample moment [#]
Adapted from [2]

References

[1] NWO, 2019, "Research Proposal - DOSTA", pp. 1-19.
[2] van Rooij, M., 2021, Ocean Battery - Efficiency and Dynamics, Ocean Grazer BV, pp. 1-13.

SCAN ME

PhD progress
1 2 3 4 5

university of groningen
CmME
NWO
OCEAN GRAZER

Process-structure-properties of wire arc additively manufactured stainless steels

L. Palmeira Belotti[a], M.G.D. Geers[a], W.Ya[b], J.A.W. van Dommelen[a], J.P.M. Hoefnagels[a]

[a] Eindhoven University of Technology
[b] RAMLAB BV

Goal

Creating "tailored" microstructures and mechanical properties by varying the printing strategies during the manufacturing procedure

Layer-wise unidirectional | Bidirectional continuous | Layer-wise zig-zag
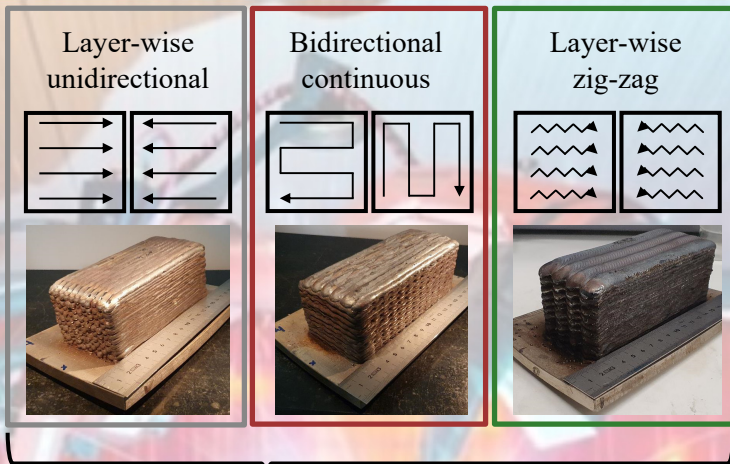
Scanning strategies

Basic information
Material: 1 mm Ø LNM 316LSi wire
Interlayer temperature: 150 ºC
Geometry: 140 (L) x 60 (W) x 60 (H) mm
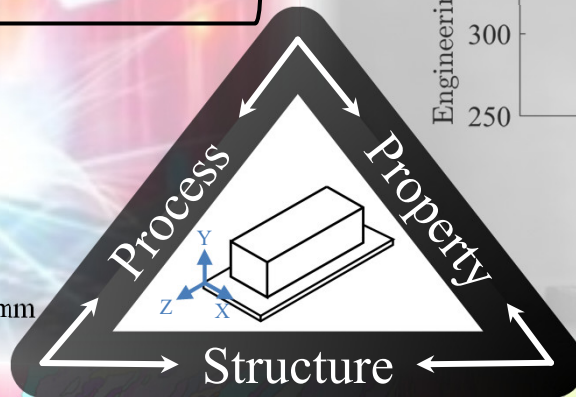
Orientation-dependent mechanical response

Loading directions
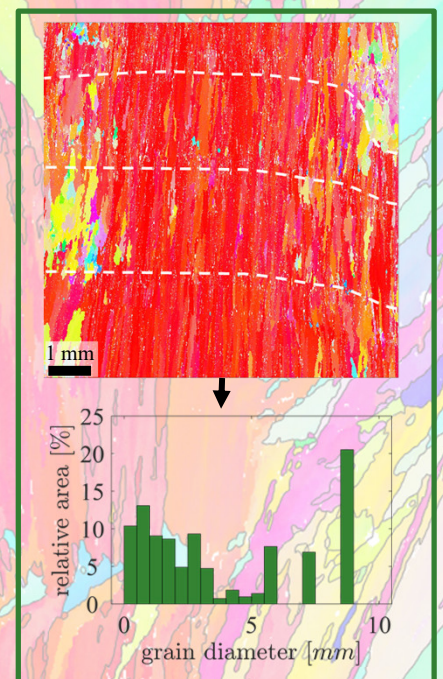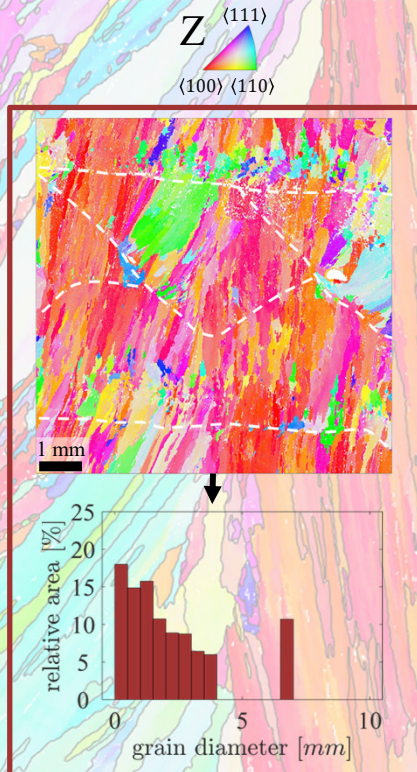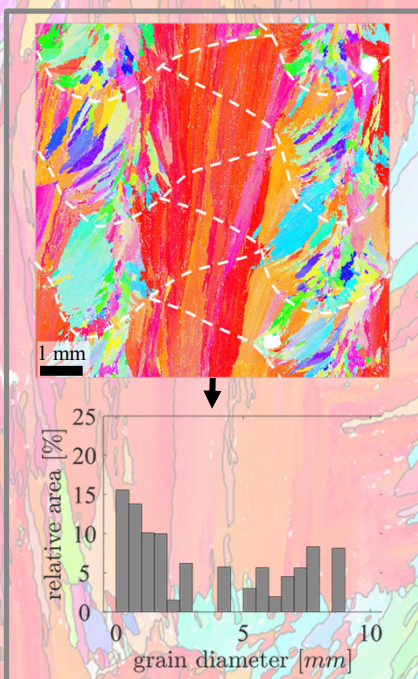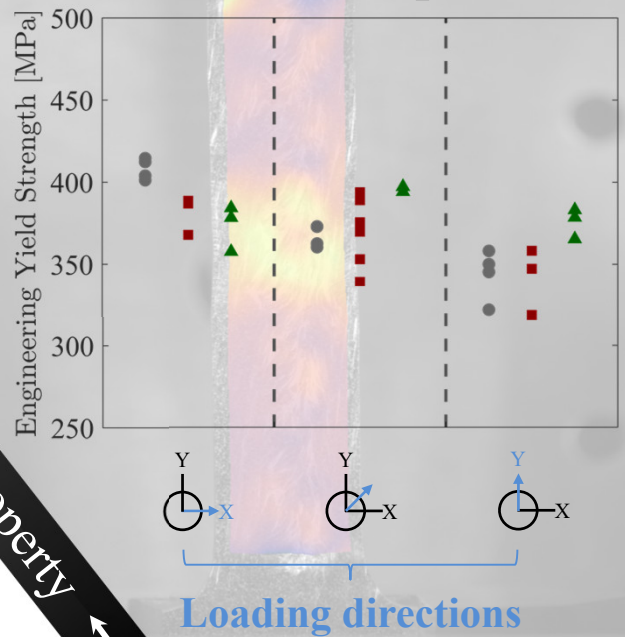
A multi-physics and multi-scale model for the degradation of historical paper

A. Parsa Sadr[1], E. Bosco[1], A.S.J. Suiker[1]

[1]*Eindhoven University of Technology*
Department of the Built Environment

Introduction

The degradation of paper is due to complex physical and chemical processes that occur as the paper ages. The chemical degradation of paper occurs over a large timescale and leading to a decrease of the mechanical properties of fibers. Moreover, the induced expansions of individual fibers by moisture content variations leads to internal stresses that may affect the integrity of paper. In this research, the influence of the distribution of fibres orientations, softening effect of water on cellulose fibres, and age-dependent acidity of paper is investigated using a multi-scale and multi-physics approach to provide a deep insight of the age-dependent behavior of historical paper-based documents.

Method:

The chemical process related to the weakening of the fiber's mechanical properties can be described in terms of the degree of polymerization (*DP*) of celluloses [1]. The rate of the chemical reaction depends on moisture content (*m*), temperature (*T*) and acidity of paper (*pH*) [2] (Fig. 1).

Furthermore, the mechanical properties of paper fibres depend on the moisture content. Here, the softening effect of water on paper has been modelled by Nissan's hydrogen-bond dissociation theory [3] (Fig. 2).
The different alignments of fibres at the inter-fibre areas leads to the interaction between hygroscopic and mechanical phenomena and arise internal stresses across paper.

Fig 1. pH variation as a function of degree of polymerization.

Fig 2. Influence of moisture content on the Young's modulus.

Results

To incorporate the effects of fibres orientations, softening effect of water on fibres, and age-dependent acidity on the degradation of paper, Asymptotic Homogenization (AH) is used. This method provides both the internal stresses within the fibrous network and the homogenized hygro-elastic properties of paper. Once the stress in a local material point within a fiber reaches the age-dependent fiber's tensile strength, brittle failure will occur. The homogenized mechanical properties will be evaluated with respect to the updated, degraded microstructure [1] (Fig. 3).

(1) t = 0 years   (2) t = 410 years   (3) t = 1075 years   (4) t = 1740 years
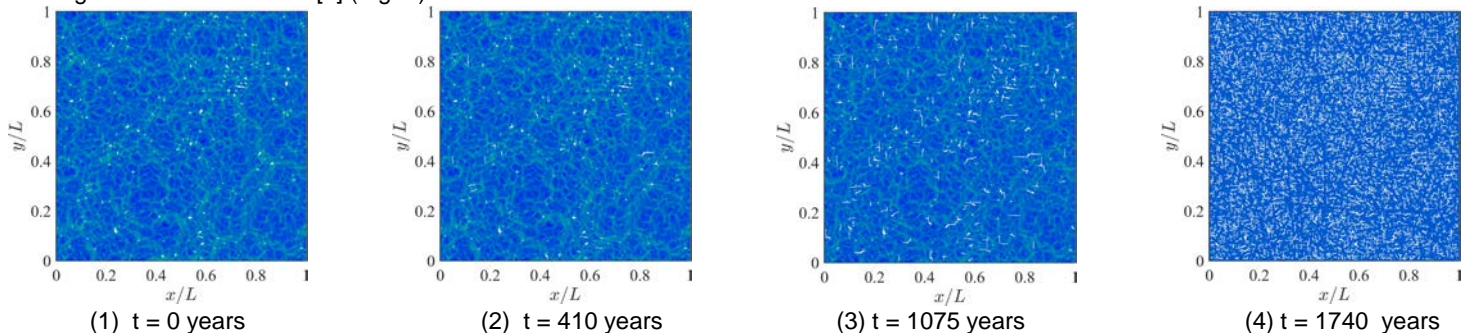
Fig 2. Time-dependent degradation of the micro-structure (*RH* = 50%; *T* = 20 °C; *pH* = 6)

Fig. 4 illustrate the effective stiffness component in the x−direction as a function of time for four networks with different measure of anisotropy (*q*). Fig. 5 shows the stiffness degradation at the three different *RH* by considering the softening effect of water on cellulose fibres. Fig. 6 presents the numerical results of the stiffness degradation of a paper with similar initial and storage conditions (*RH* = 50%, *T* = 20 °C, *pH* = 6.5), considering that acidity of the paper varies dependent on *DP* (according to Fig. 1) and acidity remains constant while paper ages (black dashed line).
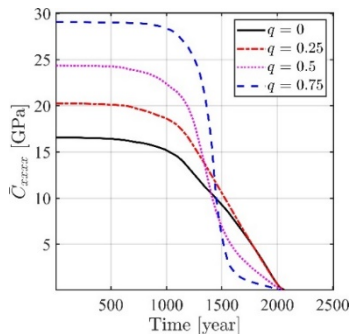
Fig 4. Stiffness degradation of papers with different anisotropy.
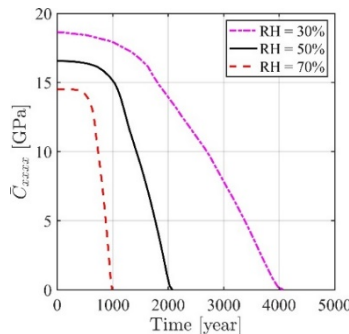
Fig 5. Influence on stiffness of softening effect of water on fibres
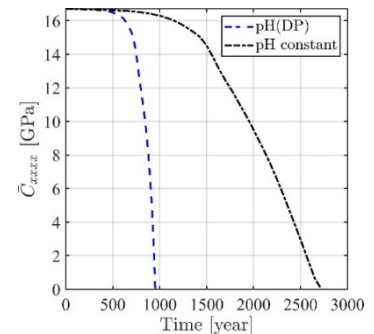
Fig 6. Influence on stiffness on age dependent acidity

References

[1] Parsa Sadr A, Bosco E, and Suiker ASJ. "Multi-scale model for time-dependent degradation of historic paper artifacts". In: International Journal of Solids and Structures (2022).
[2] Tétreault, J., Bégin, P., Paris-Lacombe, S. et al. Modelling considerations for the degradation of cellulosic paper. Cellulose 26, 2013–2033 (2019).
[3] Nissan AH. "H-bond dissociation in hydrogen bond dominated solids". In: Macromolecules 9.5 (1976).

PhD progress   4

From no-slip to full slip in the matrix-fiber interface: a state-rate approach

E.R. Pierik[1,2], W.J.B. Grouve[1], S. Wijskamp[2], R. Akkerman[1,2]

[1]University of Twente, Enschede, The Netherlands
[2]ThermoPlastic composite Research Center (TPRC)
Enschede, The Netherlands

Hot Press Forming & Process Simulations for First-Time-Right Manufacturing of TPC parts

Heat → Form → Shaped part   Process simulations ← Characterize formability

Accurate predictions require **accurate modeling** of the material behavior. Ply-ply slip is currently characterized by a single-point, steady-state friction. Hence, we developed **a transient model** to describe the **full start-up friction response**.

1 Conceptualization

The typical friction response exhibits a peak and a steady-state shear stress:
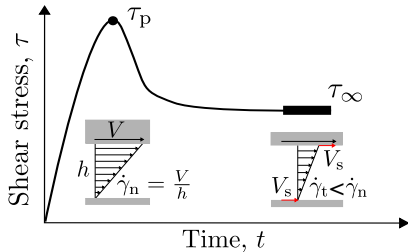
We proposed a (wall) slip relaxation effect as the underlying mechanism [1] and accurately modeled τ_p and τ_∞ [2] based on shear flow in the interface and a disentanglement process [3,4]:

Rest state; surface chains (orange) well entangled with bulk polymer chains

Surface chains retract from bulk due to shear flow

Surface chains settled to eq. state with less bulk interaction
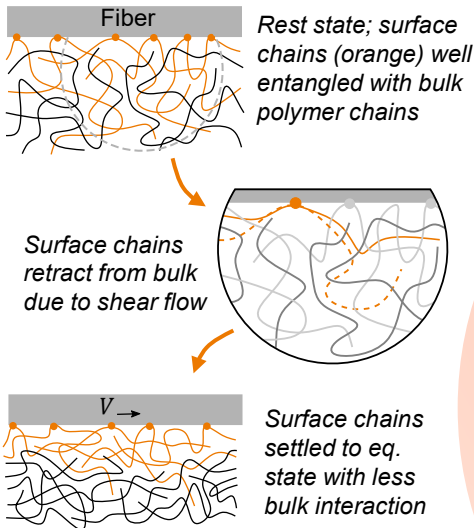
Now we just need to describe the transient disentanglement process to account for the changing BC in a VE model, such as White-Metzner [5].

2 Model changing BC

We propose a state-rate approach to describe the disentanglement process:
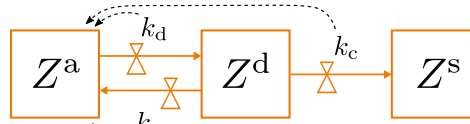
With active, disentangled and settled states, respectively. Evolution with t:
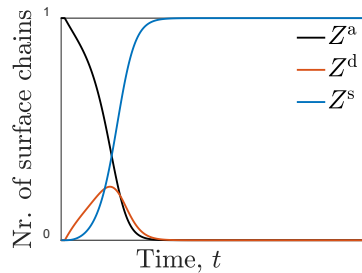
3 Implementation of slip evolution

The evolution of the settled state Z^s can be used for the slip velocity V_s:
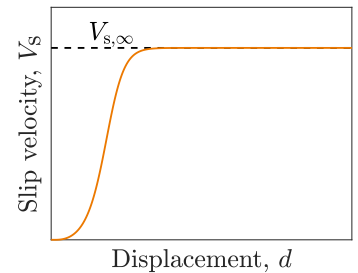
to adjust $\dot{\gamma}_n$ in the White-Metzner model.

Model & Measurement

C/PEEK

UD tape C/LM-PAEK

125 mm/min	Model
60 mm/min	Model
40 mm/min	Model
25 mm/min	Model
5 mm/min	Model
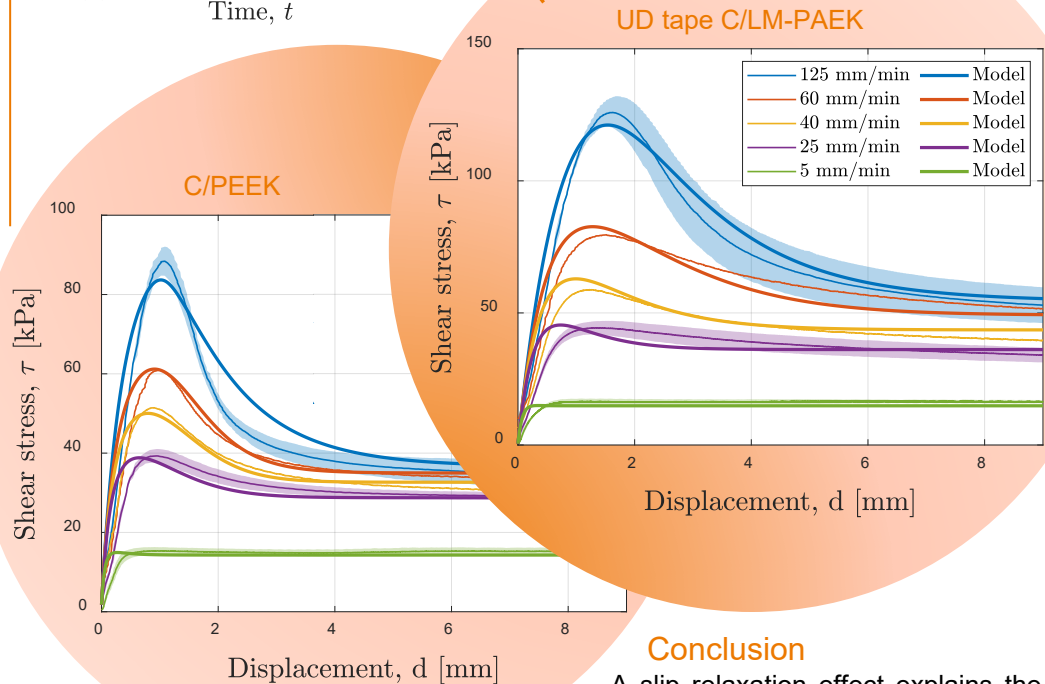
Conclusion

A slip relaxation effect explains the observed peak behavior in (start-up) friction of UD tapes, which can be described with a combined White-Metzner state-rate model.

References

1. Pierik et al. (2021). *On the origin of start-up effects in ply-ply friction for UD fiber-reinforced thermoplastics in melt.* 24th Inter. Conf. on Mater. Forming, Liège, Belgium: ESAFORM.
2. Pierik et al. (2022). *Prediction of the peak and steady-state ply-ply friction response for UD C/PAEK tapes.* Compos. Part A.
3. Hatzikiriakos, S.G. (2012). *Wall slip of molten polymers.* Prog. Polym. Sci., 37 (4), 624-643.
4. Brochard, de Gennes (1992). *Shear-dependent slippage at a polymer/solid surface.* Langmuir 8, 3033-3037.
5. White, Metzner (1963). *Development of constitutive equations for polymeric melts and solutions.* J. of App. Polym. Sci., 7, 1867-1889.

UNIVERSITY OF TWENTE.

PhD progress

1 2 3 4

TPRC
THERMOPLASTIC COMPOSITES
RESEARCH CENTER

NWO

Multi-Scale Modeling of Fiber-Reinforced Concrete using Granular Micromechanics Approach

P.Pirmoradi[1], P.Poorsolhjouy[1], A.S.J Suiker[1]

[1]Chair of Applied Mechanics, Department of the Built Environment,
Eindhoven University of Technology

Introduction

Plain concrete is a brittle material with a low tensile strength and deformation capacity. An appealing solution for enhancing the mechanical properties of concrete is through the inclusion of short, randomly orientated fibers.
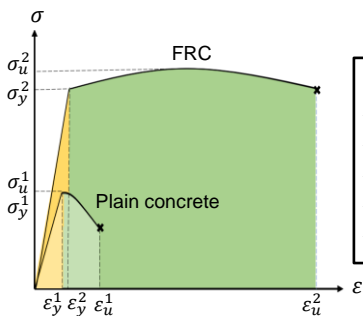
Advantages of FRCs
✓ Higher stiffness
✓ Higher yield strength
✓ Higher ultimate strength
✓ Higher deformation capacity
✓ Higher toughness

Anisotropic behavior of FRCs

Geometrical alignment of the fibers in a 3D-printed-FRC structure [1]

Mold cast FRC   3D-printed FRC

Probability distribution
········ 3DP
- - - Mold cast

Fibers' orientation angle [°]
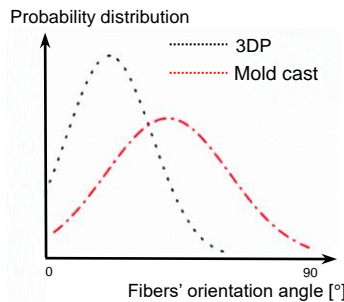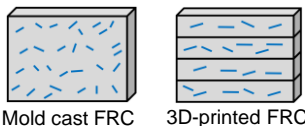
Model Description

A multi-scale model based on Granular Micromechanics Approach (GMA) [2] is developed for the analysis of FRCs.

$$\varepsilon_{kl} \xrightarrow{\text{Kinematic assumption}} \delta_k \xrightarrow{\text{Constitutive equations}} f_i \xrightarrow{\text{Principle of virtual work}} \sigma_{ij}$$

REV

(a)   (b)   (c)
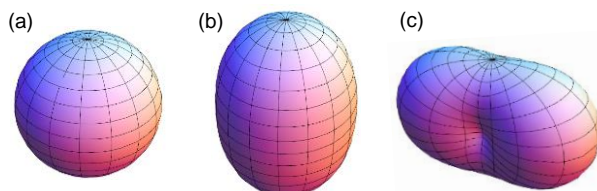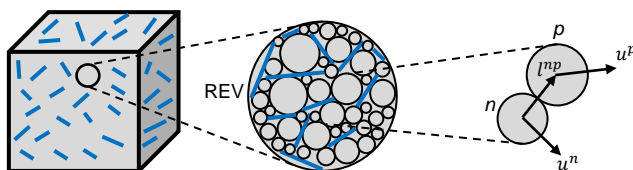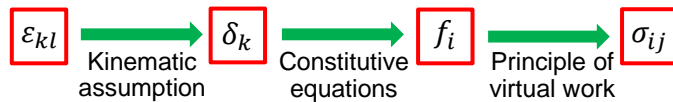
$$\xi(\theta,\phi) = \frac{1}{4\pi}\left[1 + \sum_{k=2}^{\infty}{}' \left[a_{k0}P_k(\cos\theta) + \sum_{m=2}^{\infty}{}' P_k^m(\cos\theta)\left[a_{km}\cos m\phi\right]\right]\right]$$

Distribution function facilitating incorporation of microstructure directionality for a) isotropic, b) transversely isotropic, and c) orthotropic materials

Numerical Results

Uniaxial tensile test

$\sigma_1(MPa)$ — $\nu_f = 6\%$, $\nu_f = 3\%$, $\nu_f = 2\%$, $\nu_f = 0\%$
— GMA results
◦◦◦ Experimental results [3]

$\sigma_1(MPa)$ — $\nu_f = 6\%$, $\nu_f = 3\%$, $\nu_f = 2\%$, $\nu_f = 0\%$
— GMA results
◦◦◦ Experimental results [3]

Uniaxial compressive test

$\sigma_1(MPa)$ — $\sigma_{conf} = 40\,MPa$, $\sigma_{conf} = 20\,MPa$, $\sigma_{conf} = 10\,MPa$
— GMA results
◦◦◦ Experimental results [4]
Plain concrete

$\sigma_1(MPa)$ — $\sigma_{conf} = 40\,MPa$, $\sigma_{conf} = 20\,MPa$, $\sigma_{conf} = 10\,MPa$
— GMA results
◦◦◦ Experimental results [4]
FRC with $\nu_f = 2\%$
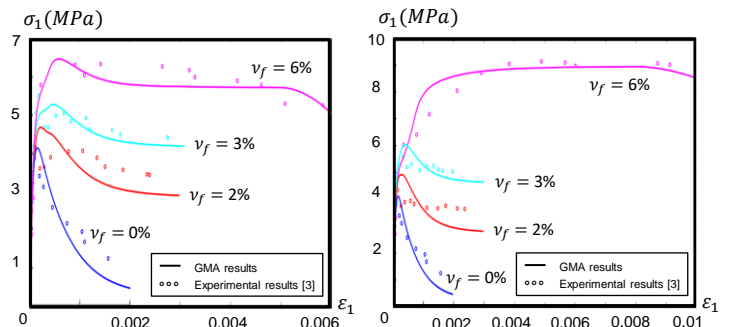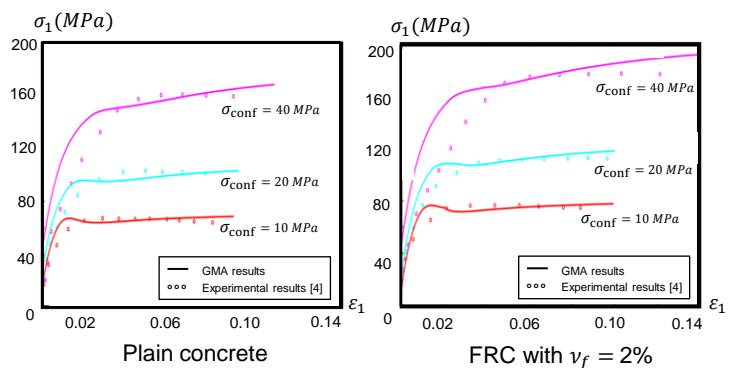
Biaxial compressive failure envelope

$\sigma_2(MPa)$
$\frac{\sigma_2}{\sigma_3} = \infty$
$\frac{\sigma_2}{\sigma_3} = 5$
$\frac{\sigma_2}{\sigma_3} = 2$
$\nu_f = 0\%$
$\nu_f = 2\%$
$\nu_f = 1\%$
$\frac{\sigma_2}{\sigma_3} = 1$
$\frac{\sigma_2}{\sigma_3} = 0.5$
$\frac{\sigma_2}{\sigma_3} = 0.2$
$\frac{\sigma_2}{\sigma_3} = 0$
$\sigma_3(MPa)$
— GMA results
◦◦◦ Experimental results [5]
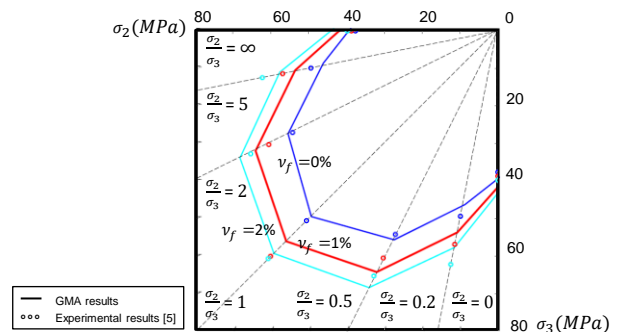
References

[1] Bos, Freek, et al. "Additive manufacturing of concrete in construction: potentials and challenges of 3D concrete printing." *Virtual and physical prototyping* 11.3 (2016): 209-225.

[2] Poorsolhjouy, Payam, and Anil Misra. "Effect of intermediate principal stress and loading-path on failure of cementitious materials using granular micromechanics." *International Journal of Solids and Structures* 108 (2017): 139-152.

[3] Li, Zongjin, et al. "Uniaxial tensile behavior of concrete reinforced with randomly distributed short fibers." *Materials Journal* 95.5 (1998): 564-574.

[4] Chern, Jenn-Chuan, et al. "Behavior of steel fiber reinforced concrete in multiaxial loading." *Materials Journal* 89.1 (1993): 32-40.

[5] Yin, W. S., et al. "Biaxial tests of plain and fiber concrete." *Materials Journal* 86.3 (1989): 236-243.

Passivity Preserving Reduction of Interconnected Linear Models of Dynamic Systems

L. Poort[1], R.H.B. Fey[1], B. Besselink[2], N. van de Wouw[1]

[1] *Eindhoven University of Technology, Dept. of Mechanical Engineering, D&C group*
[2] *University of Groningen, Bernoulli Institute*

Introduction

Complex systems Σ_c often consist several interconnected components Σ_j (Figure 1). Model reduction is required to achieve low-order, yet high-fidelity models for tasks such as simulation and model-based control. A new reduction method is introduced that

- reduces locally, i.e., on component level (Σ_j);
- accurately approximates dynamics of Σ_c;
- guarantees stability and passivity preservation.
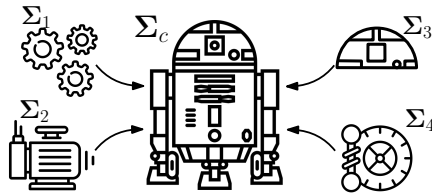
Figure 1: An example of an interconnected system.

System representation

All the k component models Σ_j have states $x_j \in \mathbb{R}^{n_j}$, inputs $v_j \in \mathbb{R}^{p_j}$ and outputs $z_j \in \mathbb{R}^{p_j}$, and are represented by a minimal system of state and output equations

$$\Sigma_j : \begin{cases} \dot{x}_j = A_j x_j + B_j v_j, \\ z_j = C_j x_j + D_j v_j, \end{cases} \quad \forall j \in \{1, \dots, k\}. \tag{1}$$

These component models Σ_j and the interconnected system Σ_c are assumed to be passive such that there exist *storage Gramians* Ξ_j and Ξ_c satisfying the LMI of Figure 3.

Balanced reduction

Balancing is a type of transformation, sorting the states of the system by relevance in descending order. This relevance is determined by the type of Gramians G that are selected, which depend on the input-output behaviour of the model. The procedure can be summarized in 4 steps [1]:

1) Pick input and output Gramians G_i, G_o from Figure 3.
2) Determine a regular transformation $\bar{x} = Tx$, such that the balanced Gramians $\bar{G}_i = \bar{G}_o$ descend diagonally, with $\bar{G}_i = TG_iT^\top$ and $\bar{G}_o = T^{-\top}G_oT^{-1}$.
3) The balanced form is $\bar{A} = TAT^{-1}$, $\bar{B} = TB$, $\bar{C} = CT^{-1}$, $\bar{D} = D$.
4) Reduce by retaining only the static contribution of the least relevant states of the balanced realization.

Based on the selected Gramians, different reduction methods are obtained, of which three are highlighted in Figure 2: Mixed-Gramian Balanced Reduction (MGBR) [1], Interconnected Systems BR (ISBR) [2], and our new method of Passive Interconnected BR (PIBR).

MGBR (P_j, Ξ_j)	PIBR (P_c, Ξ_j)	ISBR (P_c, Q_c)
- Stable & Passive - Accurate $\hat{\Sigma}_j$, does not imply accurate $\hat{\Sigma}_c$	- Stable & Passive - Accurate $\hat{\Sigma}_c$	- No stability or passivity guarantees - Accurate $\hat{\Sigma}_c$
Local	Local/Global	Global

Figure 2: Three balancing methods and their properties.

		Local, Σ_j	Global, Σ_c
Input	**Controllability** $AP + PA^\top + BB^\top = 0$	$P_j, \ \forall j \in \{1,\dots,k\}$	$P_c = \begin{bmatrix} P_{1,1} \cdots P_{1,k} \\ \vdots \ddots \vdots \\ P_{k,1} \cdots P_{k,k} \end{bmatrix}$
Output	**Observability** $A^\top Q + QA + C^\top C = 0$	$Q_j, \ \forall j \in \{1,\dots,k\}$	$Q_c = \begin{bmatrix} Q_{1,1} \cdots Q_{1,k} \\ \vdots \ddots \vdots \\ Q_{k,1} \cdots Q_{k,k} \end{bmatrix}$
	Storage $\begin{bmatrix} A^\top\Xi + \Xi A & \Xi B - C^\top \\ B^\top\Xi - C & -(D+D^\top) \end{bmatrix} \preceq 0$	$\Xi_j, \ \forall j \in \{1,\dots,k\}$	$\Xi_c = \begin{bmatrix} \Xi_{1,1} \cdots \Xi_{1,k} \\ \vdots \ddots \vdots \\ \Xi_{k,1} \cdots \Xi_{k,k} \end{bmatrix}$

Figure 3: Different Gramian types: P is an input Gramian, Q and Ξ are output Gramians. All can be either local or global.

Results

PIBR is compared to MGBR, ISBR and the state-of-the-art Hintz-Herting CMS method by a simple SISO system, representing two Euler beams interconnected with dampers, as shown in Figure 4. In all reduction methods, each beam model is reduced to 6 states. The resulting frequency responses are shown in Figure 5.
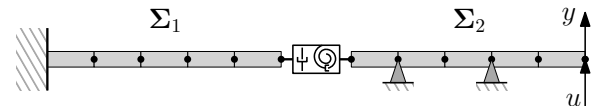
Figure 4: Two damping-wise coupled Euler beams forming Σ_c with external input force u and output velocity y.
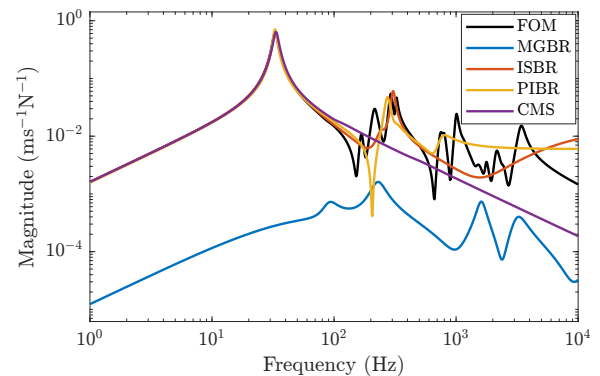
Figure 5: Frequency response magnitude of the Full Order Model (FOM) and differently reduced models.

PIBR outperforms CMS and MGBR in terms of frequency response accuracy. Its accuracy is similar to ISBR, but it also gives stability and passivity guarantees in constrast to ISBT.

Conclusion

The new method PIBT combines local and global Gramian information to guarantee passivity, while remaining accurate on an interconnected level.

References

[1] K. Unneland, P. Van Dooren, and O. Egeland, "New schemes for positive real truncation," *Modeling, Identification and Control*, vol. 28, no. 3, pp. 53–67, 2007.

[2] A. Vandendorpe and P. Van Dooren, "Model Reduction of Interconnected Systems," in *Model Order Reduction: Theory, Research Aspects and Applications*, 2008, pp. 305–321.

EINDHOVEN UNIVERSITY OF TECHNOLOGY

PhD progress

| 1 | 2 | 3 | 4 |

A Novel Bayesian Finite Element Method

A. Poot[1], I.B.C.M. Rocha[1], P. Kerfriden[2], F.P. van der Meer[1]

[1] 3MD, CiTG, Delft University of Technology
[2] SIMS, MAT, Mines Paris – PSL

Introduction

A major drawback of the finite element method is the fact that its spatial discretization step introduces a discretization error. In order to assess the reliability of the approximate solution, quantifying the magnitude of the discretization error is an important task, which is often neglected.

In this work, the discretization error is interpreted as a source of epistemic uncertainty. Following the Bayesian paradigm, a prior belief about the PDE solution is assumed (fig 1), which is then updated based on data from a discretized solution space. This provides an estimate of the true PDE solution, while including the uncertainty in this solution due to the finite element discretization.
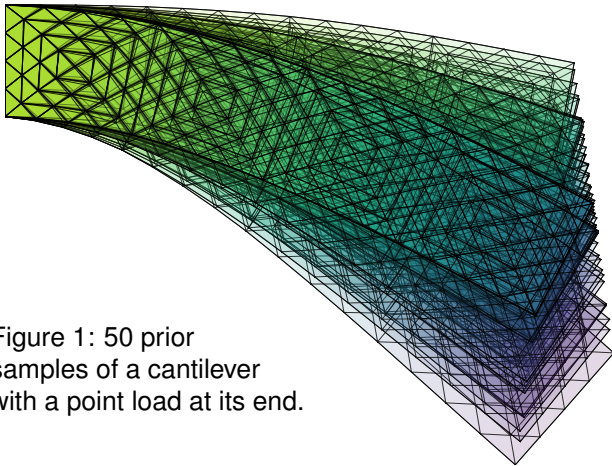
Figure 1: 50 prior samples of a cantilever with a point load at its end.

Methodology

The method works by comparing a coarse and a fine discretization of the same problem. The prior distribution is assumed on the solution space of the fine mesh, which is then conditioned on the right-hand side of the coarse discretization. Some variance remains in the posterior, which reflects the uncertainty in the solution due to conditioning on limited data.

Demonstration

To showcase the fundamental ideas behind the method, a 1D tapered beam is used as a toy example, shown in figure 2. The coarse and fine mesh consist of 4 and 64 elements, respectively.

The prior is shown to constrain the possible displacement fields to those that obey the boundary conditions of the problem. Despite conditioning only on data from the coarse discretization, the posterior mean is closer to the fine solution than the coarse solution. Lastly, note that the posterior variance is largest in the regions where the mismatch of the coarse and fine solution is largest.
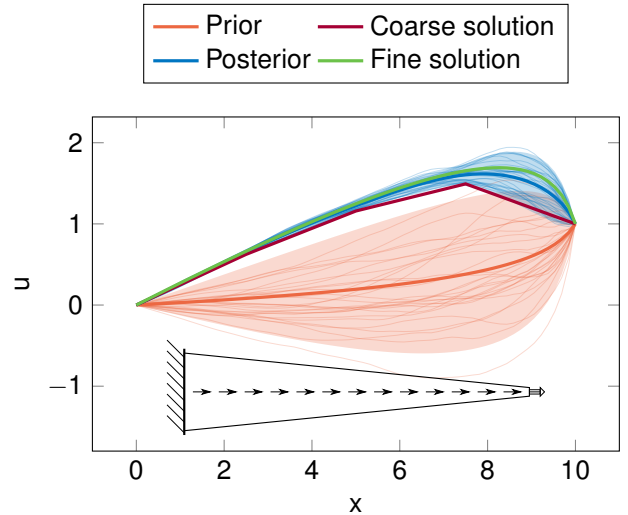
Figure 2: The prior and posterior distributions of the tapered bar problem

In figure 3, the discretization error and posterior variance of a simple beam are compared. Although their magnitude differs, a similarity in shape can be observed.

Challenges and Goals

The long term goal of this project is to develop a Bayesian finite element method with a built-in estimator of the discretization error. Some challenges posed by this goal include: making the method competitive by employing advanced MCMC sampling methods; ensuring that the method is robust enough to handle complex geometries and boundary conditions; and extending the method to also be applicable to non-linear PDEs. These challenges will be addressed in the coming years.
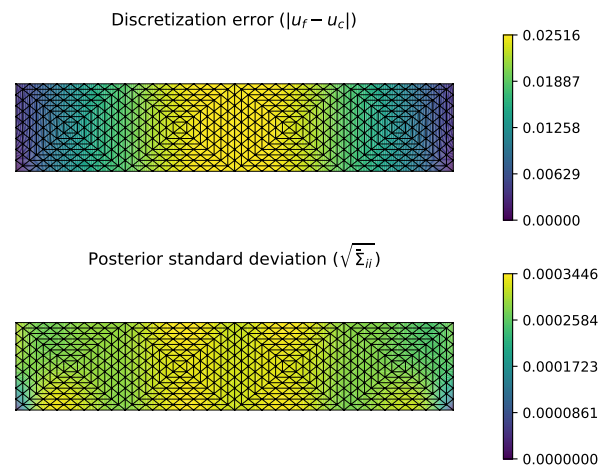
Figure 3: The discretization error and posterior standard deviation af a beam loaded by its self-weight

PhD progress

| 1 | 2 | 3 | 4 | 5 |

Modelling the Battery-can manufacturing process for cylindrical batteries

S. Rathore[1], E. Atzema[1,2], A.H. van den Boogaard[1]

1University of Twente, ET-NSM, P.O. Box 217, 7500 AE Enschede,

2Tata Steel, R&D, PTA-A&E-FRM, P.O. Box 10000, 1970 CA IJmuiden

Research Objective

The battery can produced by the deep drawing wall ironing (DWI) process undergoes drawing, redrawing and ironing stages. During this process, sometimes there occurs occasional failure. The cause of this failure is still unclear. This project aims to quantify the effects of different parameters on such failure and optimize the production process.
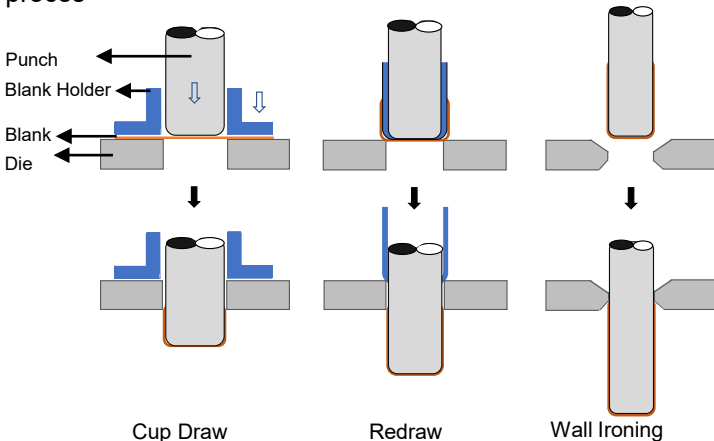
Stages of the DWI Process

- Anisotropy in sheet metal lead to the formation of the ears in the battery-can
- High plastic strain in the DWI results in strain hardening
- Friction force in different zones of the deformation is not same
- In the wall ironing stages the contact stresses are very high, which results in some expansion of the die
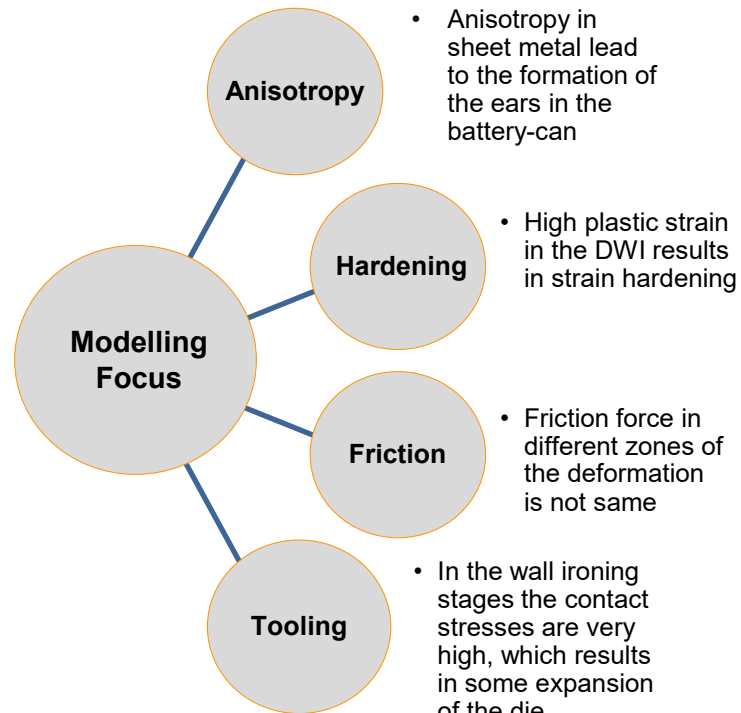
FE Modelling

For simplification purposes in this first iteration of the model:

- Anisotropy is modelled with Hill'48 yield locus with in-plane parameters calculated based on r-values and out-of-plane parameters (L&M) kept at a constant value 1,5 [1]
- Hardening was modelled with Bergström, van Liempt's theory [2] [3]
- Coulomb friction model was used.
- Tool were assumed to be rigid
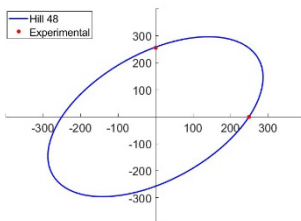
Yield locus with Hill'48 Anisotropy model
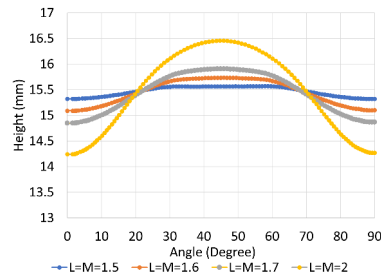
Sensitivity of the Cup height to L&M Hill parameter

Results
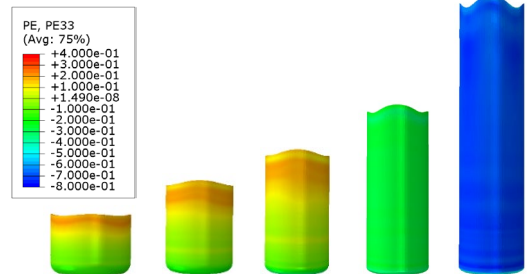
Thickness strain distribution at Cup-draw, Redraw-1, Redraw-2, Ironing-1 Ironing-2 stages respectively

Blank at Cup-draw, Redraw-1, Redraw-2, Ironing-1 Ironing-2 stages respectively

Conclusions and outlook

- The simplified FE model provides an approximate profile of the battery-can at each stage. However, it fails to capture the details such as material rupture at the top.
- The earing profile prediction is sensitive to the L&M parameters which in DWI applications is often approximated by a constant value of 1,5.

References

[1] R. Hill, 1948. Royal Society London vol. https://doi.org/10.1098/rspa.1948.0045

[2] Y. Bergström, H. Hallén. 1982. Mater. Sci. Eng.https://doi.org/10.1016/0025-5416(82)90083-0

[3] P. van Liempt. 1994. J. Mater. Process. Technol. https://doi.org/10.1016/0924-0136(94)90382-4

UNIVERSITY OF TWENTE.

PhD progress
1 2 3 4

materials innovation institute

TATA STEEL

Thermocouple Design for Cooling Purposes Through Non-Convex Topology Optimization with Power Allocation Constraints

G. Reales[1,2], F. van Keulen[1],
J.F.L, Goosen[1], A.M. Aragón[1]
[1]Faculty of Mechanical, Maritime and Materials Engineering,
Delft University of Technology, Mekelweg 2, 2628 CD
Delft, The Netherlands
[2]EP-CMX-DA,CERN, 1211 Geneve 23, Switzerland

Introduction

Thermoelectric cooling has numerous advantages to compressor- and refrigerant-based cooling systems including static operation, miniaturization and reverse operation capabilities. However, the high cost and low efficiency of thermoelectric-coolers (TECs, Fig. 1), limits their applications. Research on the last decade on the smallest unit of the TECs, or thermocouples, shows that changes to their design can improve their efficiency. TO applied to thermocouples can reduce material usage and cost while improving the overall efficiency of TECs.

Analysis

There are several considerations for this optimization problem:

- Thermoelectricity is a non-linear problem which can be solved through FEM and iterative procedures.
- The right initial points need to be used to facilitate FEM convergence
- The SIMP penalization coefficients have to be studied for the multi-physics problem.
- Higher power can lead to higher cooling but in practice there is a fixed power allocation for TECs

Results

As can be seen in Fig 2,
- The power dominates the problem
- The volume constraint modifies the final converged design.
- Lower volume constraints provide better electrical and thermal resistance ratios
- The material is removed close to the copper contacts.

Fig 1. Bulk-Flat Thermoelectric Cooler
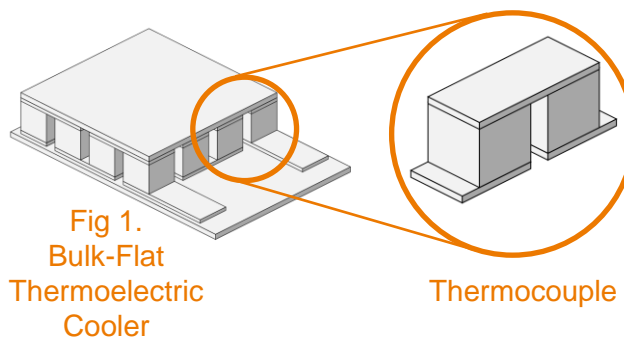
Thermocouple

Conclusions

- TECs performance can be drastically improved through thermocouple design and TO
- Volume constraints can lead to manufacturing issues but help finding other minima
- TO applied to thermoelectric devices can lead to future cooling technologies with lower carbon emissions and complexity

T_C [°C]

25.02

15.07

5.012

Lower Volume Constraint Objective
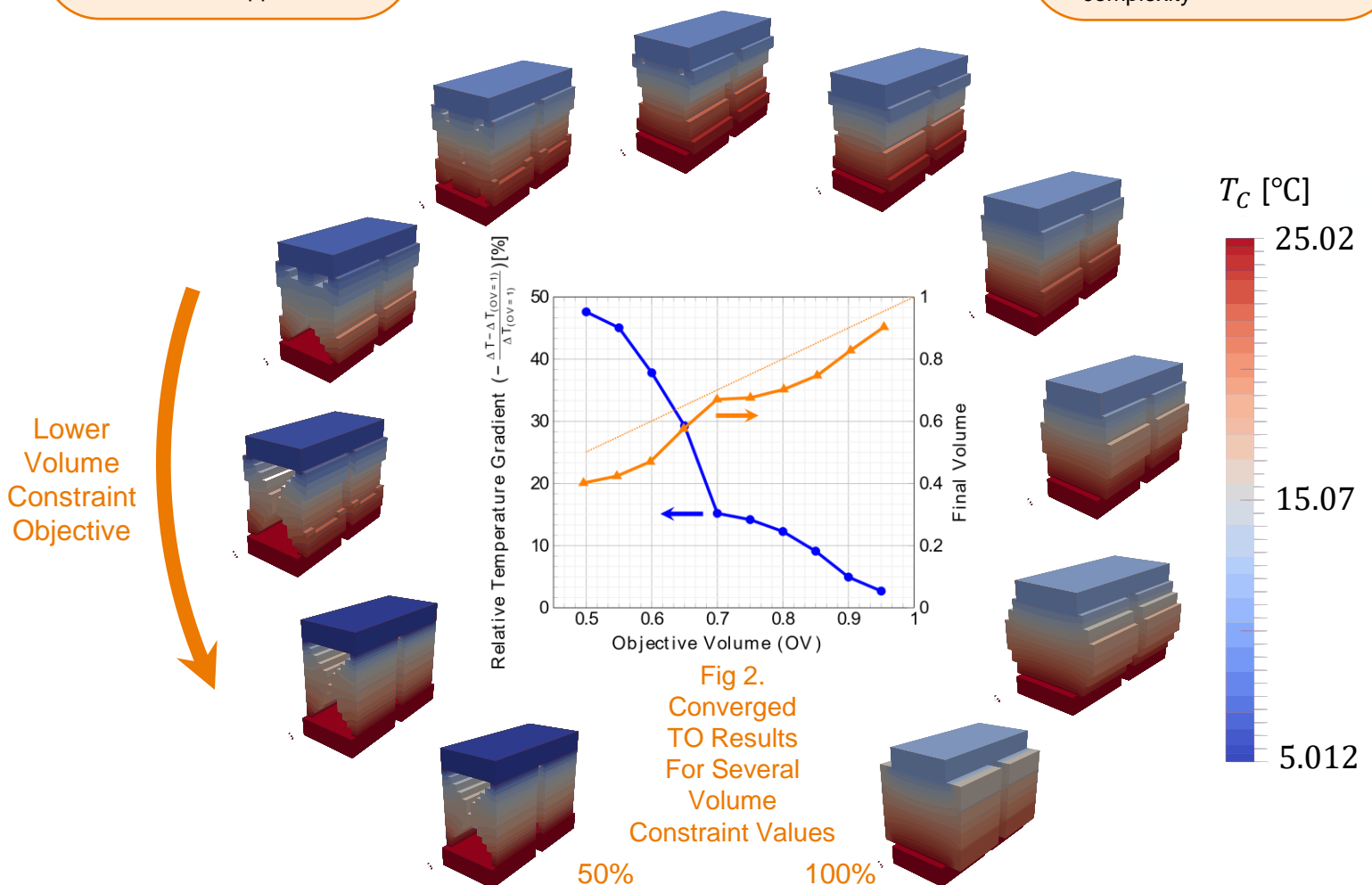
Fig 2. Converged TO Results For Several Volume Constraint Values

50%   100%

A feasibility study on friction screw extrusion additive manufacturing of AA6060

S.S. Rezaeinejad[1*], T.C. Bor[1], M. Luckabauer[1], R. Akkerman[1]

[1]University of Twente, Production Technology
* s.rezaei@utwente.nl

Introduction

High-strength lightweight materials such as aluminum alloys decrease the fuel usage and carbon dioxide emission, and increase the performance in the aerospace, marine, and automobile sectors because of their excellent strength-to-weight ratio and advantageous machinability. However, achieving a dimensionally complex component made up of an Al alloy with acceptable mechanical and metallurgical properties is challenging. This study focus on a fabrication method based on solid-state additive manufacturing to produce Al alloys with beneficial metallurgical and mechanical properties. The Friction Screw Extrusion Additive Manufacturing (FSEAM) approach is based on a screw-like rotating tool that generates heat through severe plastic deformation (SPD) of the feedstock material. Then, the screwed-shape tool transports the plasticized material towards the substrate and fabricates the final product layer by layer with high precision (Fig. 1).
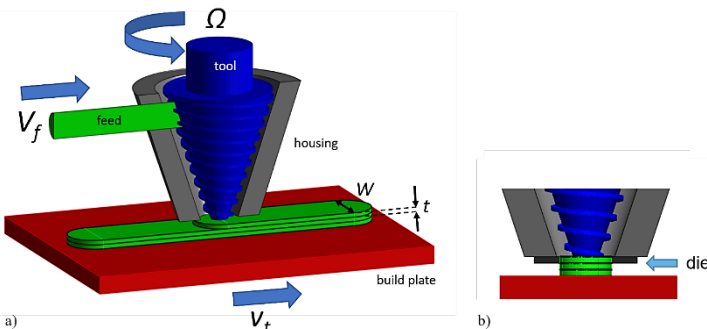
Figure 1: Schematic outline of the FSEAM setup

Process parameters

Some of the more important parameters which should be adjusted in the FSEAM process are as follows:

1- Rotational speed of the tool (Ω),
2- Transverse speed of the substrate/table (V_t),
3- Volumetric supply rate of the feedstock (V_f),
4- Vertical position of the exit opening (t),
5- Tool gap, i.e. tool-to-housing distance (t_{tool}),
6- Cooling rate of the system.

Printing experiment

The FSEAM experiment was performed successfully for AA6060 on top of an AA2024 substrate. Round 8 mm rod AA6060-T6 material was utilized as feedstock. The rotational speed and the table speed were 400 RPM and 250 mm/min, respectively. The build width W was about 30 % larger than the nozzle opening. The build appearance is shown at Fig. 2.
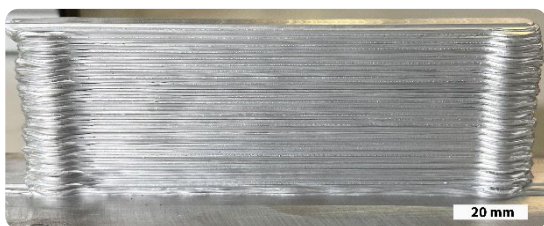
Figure 2: Macroscopic image of a build through FSEAM

Microstructural and Mechanical properties

The cross section of the wall through an optical microscopy, the microhardness values from the midplane of the build, as well as the tensile test results in the build direction are shown in Fig. 3. No macroscopic defects are visible from the cross-section of the build. The hardness remains almost constant through the height of the build; however, it is reduced with respect to the hardness of the feed material of 80 HV which is ascribed to the thermomechanical nature of the process leading to changes in the size and distribution of the strengthening precipitates. In all tensile tests, plastic deformation of the test specimens occurred showing ductile fracture. The values of the yield strength and tensile strength were approximately equal at values around 80 MPa and 145 MPa, respectively. The elongation-at-fracture showed some spread.
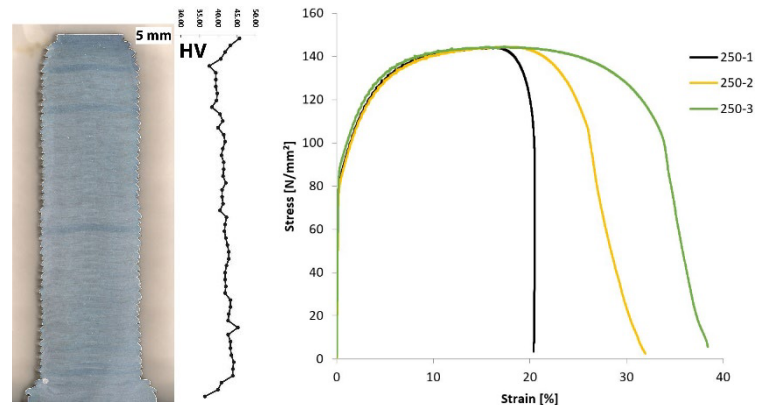
Figure 3: Cross-section of the build, microhardness measurement through the height, and the tensile test results

Microstructural analyses have been performed using SEM. Grain refinement and the distribution of the precipitates are visible in Fig. 4. The average grain size is less than 10 µm through the height of the build, and multimodal strengthening precipitates can be observed inside the grains and at grain boundaries which should be further investigated.
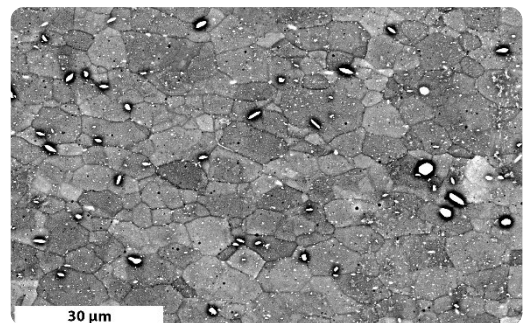
Figure 4: SEM image of the microstructure of the build

References

[1] Avery, D.Z., et al., Journal of Engineering Materials and Technology, 2022, 144 (3).
[2] Griffiths, R.J., et al., Applied Sciences, 2019, 9 (17).
[3] Mishra, R.S., et al., Science and Technology of Welding and Joining, 2022, 1(1).
[4] Khodabakhshi, F., and Gerlich, A.P., Journal of manufacturing processes, 2018, 36 (77).

IMPACT IDENTIFICATION METHOD FOR COMPOSITE STRUCTURES
A structured approach for a full-scale aircraft component

N.R. Marinho[1], R. Loendersloot[1], T. Tinga[1], and F. Grooteman[2]

[1] Dynamics Based Maintenance Group, University of Twente, P.O. Box 217, 7500AE Enschede, The Netherlands
[2] National Aerospace Laboratory (NLR), P.O. Box 153, 8300AD Emmeloord, The Netherlands

Project Overview

Develop a monitoring method by using combined sensing systems for structures with smart functionality to localize impact events and estimate the impact energy level.
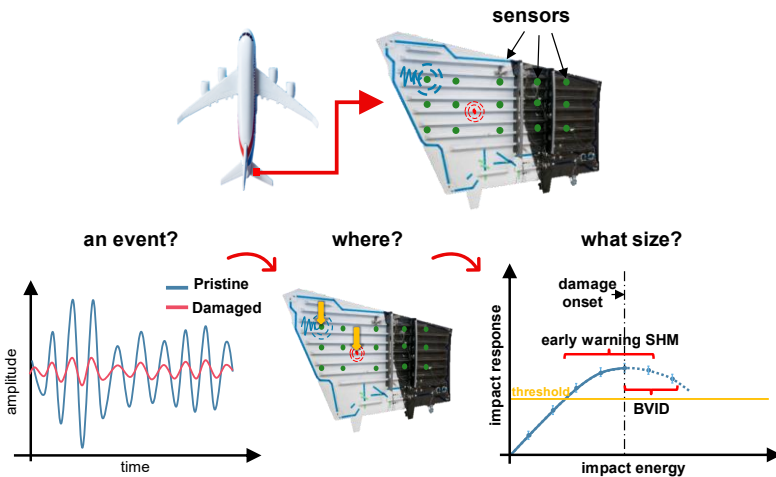
Figure 1: Impact identification and monitoring

Main challenges

Reconstruct the energy flow due to an impact event with the required accuracy in a realistic aerospace composite structure

Monitoring and data collection

- **Identify features sensitive to impact event** coupled with an adequate data acquisition rate to capture the impact event;
- **Understand how the heterogeneity and anisotropy of composite structures** affects the system;
- **Define sensor configuration** to overcome its limitation getting the most optimally information;

Data analysis

- **Discriminate changes in features** caused by impact event from those caused by environmental and operational conditions, structural complexity and material properties;
- **Know the influence of structural features** for impact monitoring;
- **Determine suitable signal processing technique** to extract relevant information from signal response.

Methods

Building Block Approach

Integration of SHM

Level 3
Sub-component
Full scale aircraft component

Level 2 - Element
Mono-stringer stiffened panel & Variable thickness plate

Level 1 - Coupon
Composite panel

Critical load cases & Quantity of tests and models
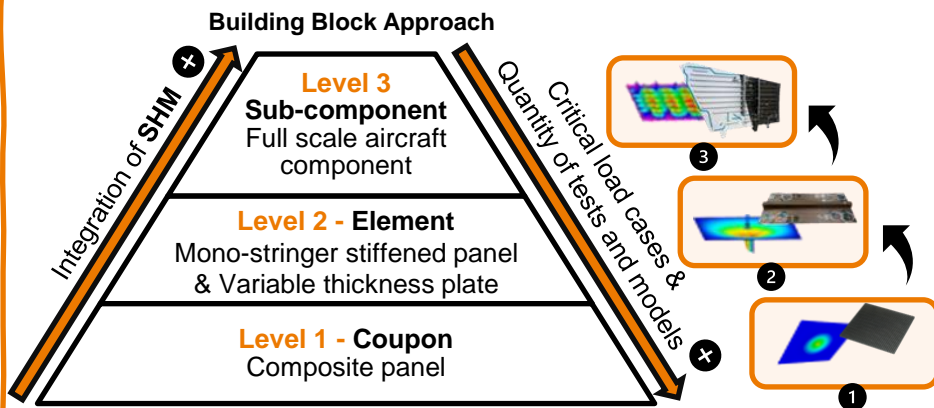
Figure 2: Building Block Approach (Adapted from [2])

Combine Numerical Simulation & Experimental Tests

+

Design of Experiments (DOE)

- Statement of the problem
- Response variable
- Factors, levels, and ranges
- Experimental design
- Performing the experiment
- Statistical analysis of the data
- Conclusions

Experimental Set-up

Current stage: Impact identification method using combined sensing technologies at *level 1*.

Response variables: a) effect of energy level on impact response; b) sensor technology performance, limitations and benefits; c) impact asses using active measurement.

Factors: a) multiple energy levels; b) increasing distance from sensors; c) directivity for FBG sensors.

Figure 3: Experimental design
(● Optics11 ━ FBG ● PZT)

Outlook

Future work will investigate guided wave behavior, define a pristine reference dataset and establish the optimal sensor configuration from *level 1* results. Higher-level structure test programs will use coupon-level data to address typical structural complexity, i.e., thickness variations and stiffeners. Lastly, the next step is to validate the identification method at the sub-component level.

References

[1] Janapati, V. et al. (2016).Structural Health Monitoring,15, 143-161.
[2] Yue, N., Khodaei, Z. S., & Aliabadi, M. H. (2021). Smart Materials and Structures, 30(4), 045004.
[3] Montgomery, D. C. (2017). Design and analysis of experiments. John Wiley & sons.

UNIVERSITY OF TWENTE.

Take a picture to contact me

PhD progress

| 1 | 2 | 3 | 4 |

Predictive digital twin for offshore structures

F. Riccioli*, L. Pahlavan

Maritime and Transport Technology
Delft University of Technology
*F.Riccioli@tudelft.nl

Introduction

Reliable assessment of the integrity of offshore structures is of substantial importance for offshore energy production systems, such as floating wind turbines (FOWT) and floating production and storage units (FPSOs). Structural integrity issues can create unacceptable risks to the entire asset threatening the environment and continuous production of energy. Within various co-existing damage mechanisms, corrosion, fatigue, and their combination (i.e. corrosion-fatigue) are widely considered as main degradation mechanisms. Moreover, the submerged support part of these structures is often covered by a thick layer of marine growth which constitutes a challenge for inspection and integrity assessment of these structures.

Figure 1: Mooring chain sample showing corrosion

Approach

This research aims at digital twinning of offshore support structures covered by marine growth enabling damage diagnosis and prognosis using combination of non-intrusive non-destructive assessment techniques and damage growth models without the need for surface cleaning.

The approach in this research comprises:
- Damage diagnosis system with non-contact passive ultrasound, i.e. Acoustic Emission (AE) monitoring, to detection, localization and characterization of damage in submerged steel structures covered by marine growth
- Damage prognosis by estimating the crack growth rate based on the AE monitoring data and fracture mechanics fatigue models

The results will be projected on a 3D model of the test structure for demonstration of the digital twin concept.

Scope of the research

The detectability of corrosion-fatigue damage using non-contact AE technique is investigated. Correlation of AE extracted features with corrosion-fatigue damage evolution and accurate localisation of corrosion-fatigue damage are addressed to characterize corrosion-fatigue damage. The influence of the presence of marine growth on damaged induced AE signatures is experimentally assessed. The relation between crack growth rate and AE measurements data is investigated.
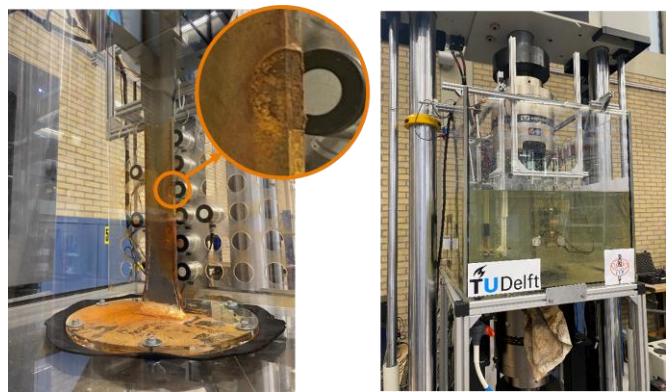
Figure 2: Dog-bone specimen showing the corroded exposed surface (left) and simultaneous corrosion-fatigue experimental setup (right)

Research progress

Corrosion-fatigue experiments have been executed using dog-bone shaped steel specimens to investigate the detectability of corrosion-fatigue damage using non-contact AE technique. Three samples have been tested in an immersion tank under simultaneous corrosion-fatigue (Figure 2).

A damage localization algorithm has been implemented based on the AE signals arrival time. Results from the application of the localization algorithm on the dog-bone shaped specimens subject to corrosion-fatigue showed good agreement with the observed damage (Figure 3).
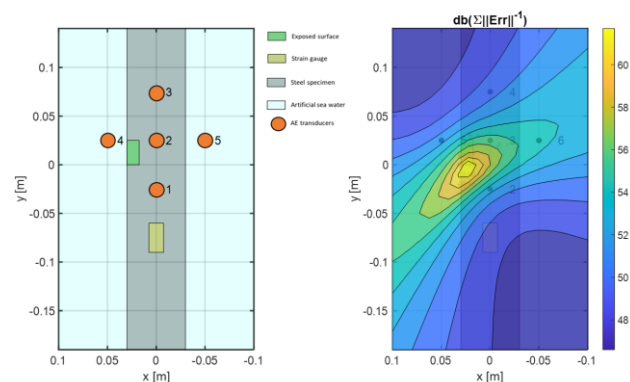
Figure 3: Sensors layout and specimen geometry (left) and sample results of damage localization (right)

PhD progress

| 1 | 2 | 3 | 4 |

Bayesian Machine Learning for Multiscale Modeling of 3D-printed Materials

L.F. Riccius, I.B.C.M. Rocha, F.P. van der Meer

Delft University of Technology, Faculty of Civil Engineering and Geosciences

Introduction

Complex computational models usually feature a large number of model parameters that require careful calibration for reliable predictions, leading to non-linear, non-convex, and ill-posed inverse identification problems with expensive forward models.

This project aims at enabling a Bayesian analysis for inferring material properties. A naive application of Bayesian statistics is infeasible, but breakthroughs in **Markov Chain Monte Carlo** sampling and **surrogate modeling** are opening up a Bayesian analysis to a broader set of problems.
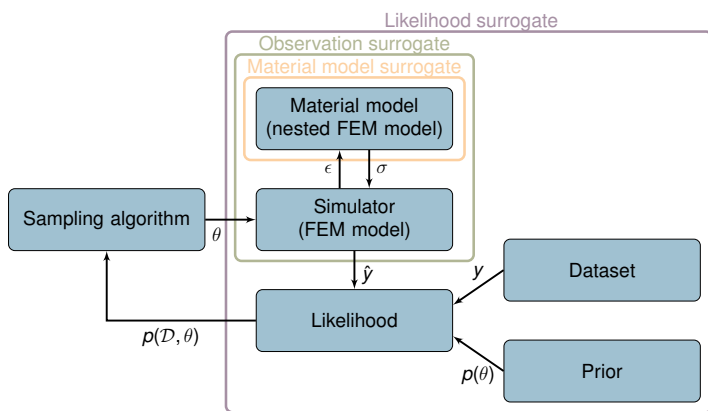
Figure 1: Components of an inference framework. The colored frames depict the three options to insert a surrogate.

Approach

First: expose the limits of standard Metropolis-Hastings (MH) sampling in terms of dimensionality of the latent space and investigate whether advanced samplers offer better convergence in practice.
Second: determine which computationally heavy tasks can be replaced, which types of surrogates are suitable, and how they can be trained efficiently.
Third: combine samplers and surrogates, investigate the interplay between them, and select the best performing components.
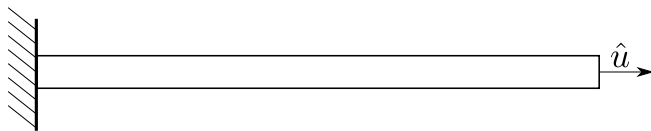
Figure 2: 1D-bar with Dirichlet boundary conditions and unknown yield stress field. Resulting force and displacements are observed.
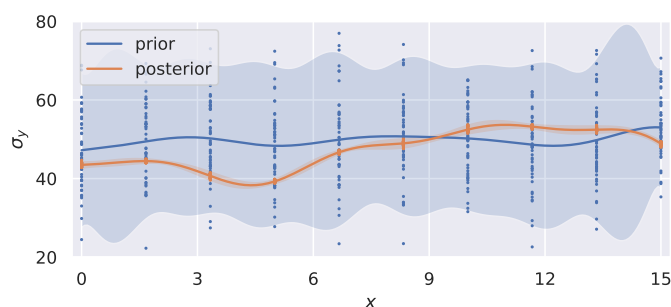
Figure 3: Prior and posterior fields for the yield stress.

Results

The inference framework, consisting of the basic building blocks depicted, acts as a wrapper for existing finite element models.
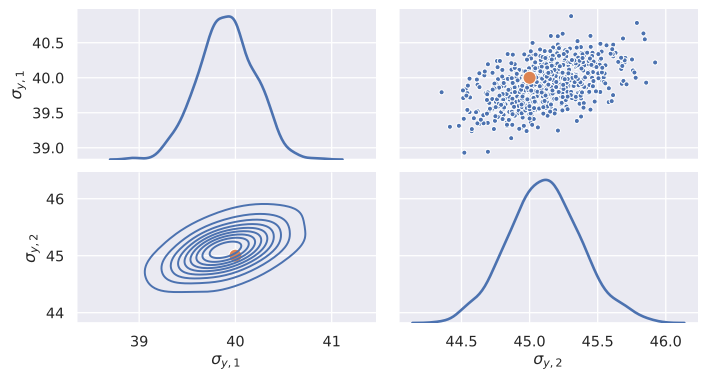
Figure 4: Joint and marginal posterior distributions of σ_y for a discretization of the random field with two anchor points.

The performance of the MH sampler is assessed on a simple 1D bar problem with an unknown spatial distribution of the yield stress. The random field is discretized as a Gaussian process, conditioned on a set of anchor points, at which the values are to be inferred. The dimensionality is controlled by increasing the number of said anchors.
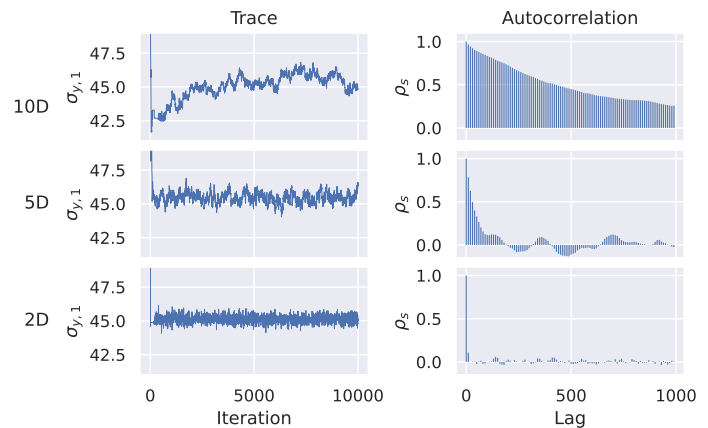
Figure 5: Trace and autocorrelation of posterior samples in one anchor location for varying resolution of the random field.

Conclusion & Outlook

The performance of the MH sampler deteriorates with an increased dimensionality of the latent space. The traces show increasingly poor mixing and a higher autocorrelation with growing dimensionality of the parameter space.

This numerical evidence motivates the use of advanced sampling algorithms to tackle the curse of dimensionality and surrogates to accelerate model evaluations, which will be at the center of future investigations.

TUDelft Delft University of Technology

PhD progress
1 2 3 4 5

SLIM MLAB LABS

Meso-scale description of wet powders for industrial-scale modelling

R. Saghafian Larijani[1], V. Vivacqua[2], S. Luding[1], V. Magnanimo[1]

[1]University of Twente
[2]Johnson Matthey (UK)

Motivation

- Importance of **wet granulation** process in various industries
- **High computational cost** of **industrial-scale** DEM simulations with millions of particles
- **Solid to liquid binder ratio** as one of the important operational parameters
- Focus of the previous studies on **pendular** state with **binary liquid bridges**

Discrete Element Modelling (DEM)

$$m_i \frac{dv_{p,i}}{dt} = \sum_j (F^n_{cont,ij} + F^t_{cont,ij} + \mathbf{F_{coh,ij}}) + m_i g$$

Linear visco-elastic contact model

$$F^n_{cont,ij} = k_n \delta_n n_{ij} + c_n \dot{\delta}_n n_{ij}$$

$$F^t_{cont,ij} = \min(\left| F^n_{cont,ij} \right| \mu \, t_{ij}, \, k_t \delta_t \, t_{ij} + c_t \dot{\delta}_t t_{ij})$$

$\mathbf{F_{coh,ij}}$ due to **liquid bridge capillary** and **viscous forces**

Objectives

1. Numerical upscaling of wet powder system using **coarse-grained particles [1]**

Original system   Coarse grain model
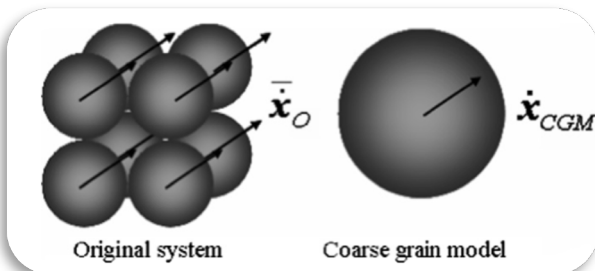
2. Modelling the **funicular** state **[2]**

(a) Model P   (b) Model F
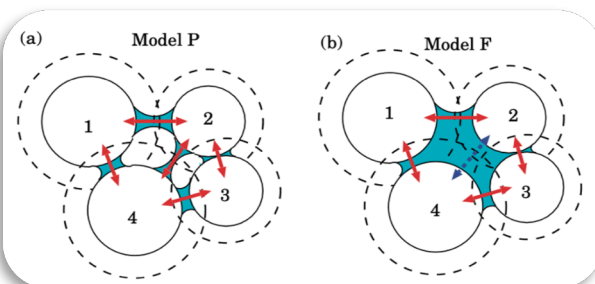
3. **Validation** by application of models to granulation at **Johnson Matthey** and **Nestlé.**

Preliminary simulations: Drum granulator
Demonstration of the binder distribution after 1 min

CG ratio=2

CG ratio=3

CG ratio=4

References

[1] M. Sakai and S. Koshizuka, 2009, *Chemical Engineering Science*, 64(3).
[2] N. Mitarai and H. Nakanishi, 2009, *EPL*, 88(6).

UNIVERSITY OF TWENTE.   JM Johnson Matthey — Inspiring science, enhancing life   Nestlé   tusail   HORIZON 2020

PhD progress
1 2 3 4

Efficient tools for the analysis of 4D printing processes

N.M. Sanchez Martinez[1], O.v.d. Sluis[1,2], J.J.C. Remmers[1]

[1]Eindhoven University of Technology
[2]Philips Research

The future of electronics

The demand for integrated electronic products is causing manufacturers to explore 4D printing to combine electrical and mechanical functionality in a tightly packed product.

Electronics today
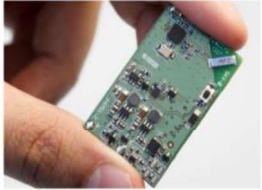
How?

4D printing

Electronics tomorrow
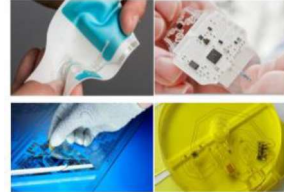
The AMPERE consortium plans to aid manufacturers to meet such demands by developing robust, scalable and reliable 4D technology.

VAT photopolymerization in 4D printing

VAT photopolymerization is a promising technology for printed electronics. However, it is complex, costly and slow, therefore fast simulation tools are needed to make quality products at affordable prices.

VAT printing — Heat source, Slurry, Printed part

Run simulation → Read attributes (~ 40% run time) → Assembly system matrix K → Create system of equations Ku = f → Solve system of equations for u (~ 46% run time) → Final layer? No/Yes → End simulation
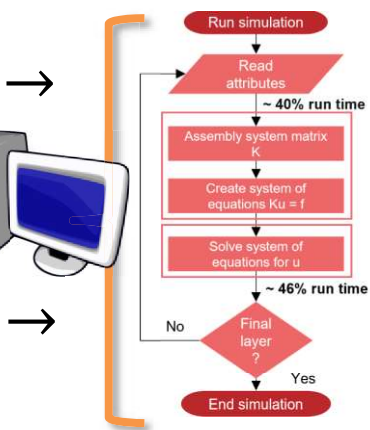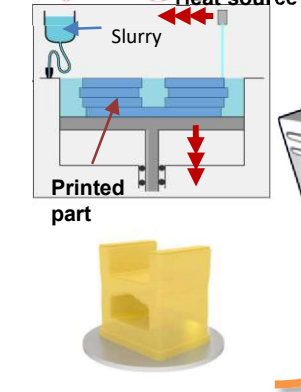
Speeding it up

The Laplace domain Finite Element Method [1] is proposed to simulate efficiently the heat transfer mechanism driving the VAT photopolymerization process.

Transient   Steady

$$\overline{k}\nabla^2 T + Q = \rho c \frac{\partial T}{\partial t} \;\rightarrow\; \mathcal{L}(T) \;\rightarrow\; \overline{k}\nabla^2 \tilde{T} + \tilde{Q} = \rho c(s\tilde{T} - T_0)$$

Time-stepping   Direct solution

References

1] Chen, C et al. (1991) International Journal for Numerical Methods in Engineering, vol. 32, pp. 45–61.
2] Sheen, at al. (2003) IMA Journal of Numerical Analysis, vol. 23, no. 2, pp. 269–99.
3] Westbeek (2020), Eindhoven University of Technology, Eindhoven University of Technology research portal.

In the Laplace domain, advancing solutions through time is not needed. Solutions can be recovered at any time, therefore a substantial decrease in computation time is expected.

Parallel: Parametrize Γ with N points → Solve N problems → Combine and evaluate time points

$$T = \frac{1}{2\pi i}\int_\Gamma e^{st}\tilde{T}\,dz = \mathcal{L}^{-1}(\tilde{T})$$

Numerical Laplace inversion [2]
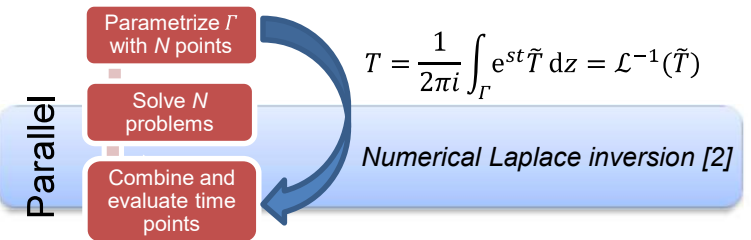
Moving heat source test case

The analytical solution of a heat source traversing a plate from side to side is compared to the solution obtained with our Laplace implementation.

Test case — Heat source path, Observation line, Fixed temperature (**0**°C)

Analytical   Laplace

Relative error comparison

Time integration vs Laplace method

7.1   23   50   78

Simulation time: 1.5s, 5.0s, 10.0s, 15.0s
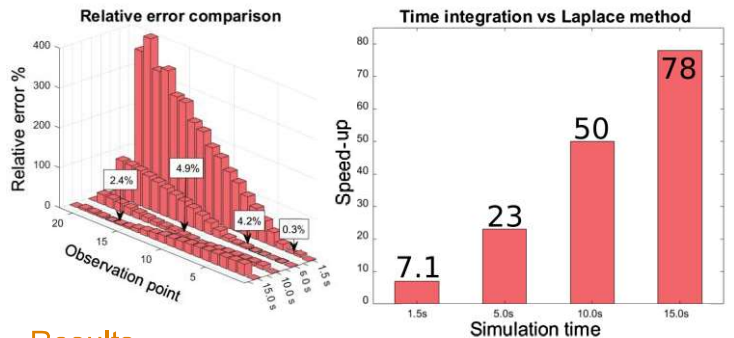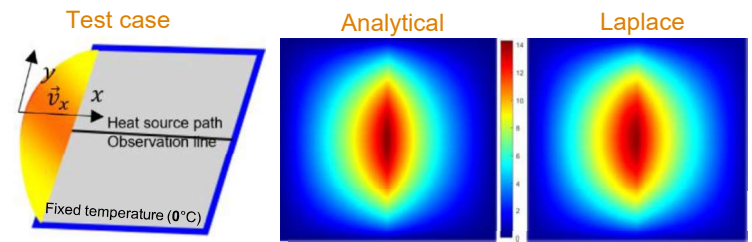
Results

Relative errors and speed-up at different times are recorded and shown above.
- Speed-up considers the time needed by a FEM solver to reach the simulation time given a fixed time increment
- The longer the simulation the larger the benefit
- Accurate results only at peak temperature (white boxes)

Conclusions and outlook

- A speed-up of over **78** times was achieved
- The accuracy of the framework needs improvement
- Effort will be directed towards quality improvement and the addition of arbitrary printing paths

PhD progress: 1 2 3 4

Assessment of Natural Degradation in a Low-speed Roller Bearing using Acoustic Emission Monitoring

B. Scheeren[1,2], L. Pahlavan[1]

[1] *Delft University of Technology, Department of Maritime & Transport Technology*
[2] *b.scheeren@tudelft.nl*

Introduction

The reliability of low-speed roller bearings is essential to the safe operation of several offshore installations, such as heavy-lifting cranes, single-point-mooring systems, and wind turbines. Condition monitoring of such systems is still an unresolved challenge. The present study aims to develop a monitoring methodology based on acoustic emissions (AE), which are transient elastic stress waves generated by the material as it degrades.

Methodology

The shape of an AE waveform at the location of a receiver is uniquely defined by the source mechanism and transfer path [1, 2]. Therefore similarity of the recorded waveform indicates consistency in the origin and type of an acoustic emission. This similarity (1) may be assessed using the cross-correlation (2).

$$\varsigma_{i,j} = \max\left(\left|\frac{(s_i \star s_j)(\tau)}{\sqrt{(s_i \star s_i)(0)(s_j \star s_j)(0)}}\right|\right) \quad (1)$$

$$(s_i \star s_j)(\tau) \equiv \int_{-\infty}^{\infty} s_j^*(t) s_j(s - \tau) dt \quad (2)$$

Utilising sensors arrays covering distinct frequency ranges in multiple locations, a single source event may be characterised by a structure of clusters. These multi-channel structures provide further information on the source location and strength.

Experiment

A purpose-built linear bearing (Figure 1) containing two rolling elements was subjected to vertical loading of 1215 kN, while a horizontal stroke of 70 mm was cycled through at 11.6 mm/s. In approximately 225,000 cycles natural wear was developed. Ultrasonic activity was monitored in the range of 40-580 kHz using passive AE transducers.
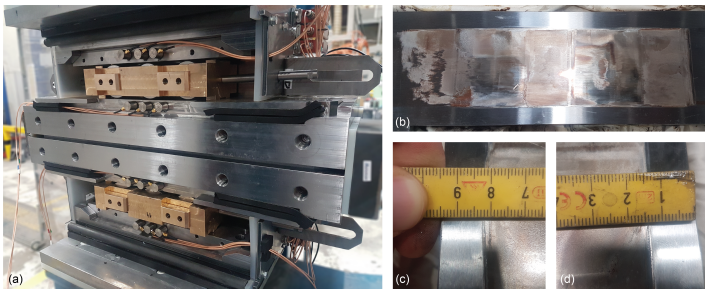
Figure 1: The set-up (a), and wear pattern on nose raceway at **I6** (b–d).

Visual Inspections

Six inspections were performed over the course of the experiment (also referenced in Figure 3), leading to the following observations:

I1 No excessive wear, slight contamination of lubrication.
I2 Excessive wear in contact area, contamination throughout grease
I3 Increased surface roughness
I4 Light pitting in rollers, further increased surface roughness
I5 Further wear development
I6 No significant change (end of test)

Results

Over the course of 225,000 cycles, an extensive sample of AE hits was recorded. These have been clustered to identify consistency in the source mechanism and transfer path. From the clustered hits multi-channel events have been composed. An example of this is depicted in Figure 2.
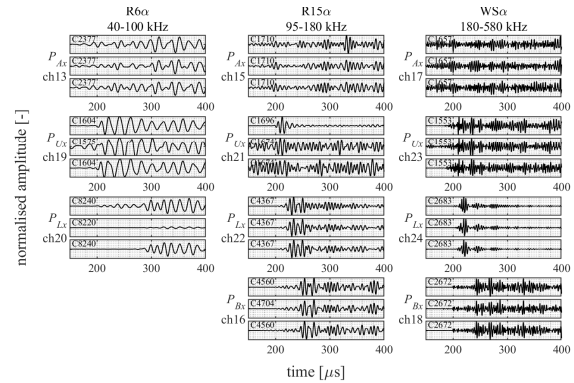
Figure 2: Example of clustered waveforms.

Combined clustering and event-building has been used to filter the total number of accumulated AE hits as depicted in Figure 3. The trend in this cumulative hit-count seems to coincide with the observed wear development.
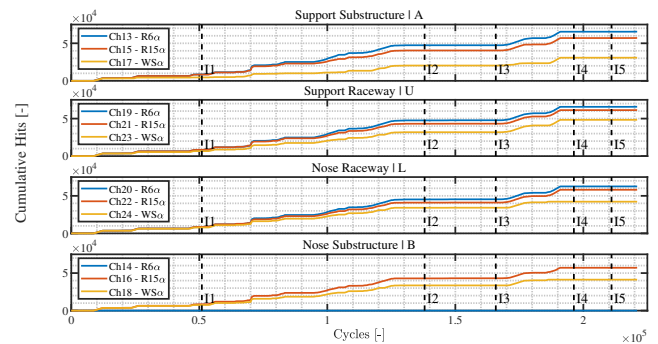
Figure 3: Filtered cumulative hit-count in top chamber.

Conclusions

- Over the course of 225,000 cycles, wear composed of pitting, grooving, and increased surface roughness was naturally developed.
- Recorded AE signals were successfully clustered.
- The resulting cumulative hit-count shows agreement with observations of significant wear change during visual inspections.
- Combined clustering and event-building is demonstrated to be effective at isolating significant AE activity.

References

[1] B. Scheeren, M.L. Kaminski, and L. Pahlavan. (2022). "Evaluation of Ultrasonic Stress Wave Transmission in Cylindrical Roller Bearings for Acoustic Emission Condition Monitoring," in *Sensors 22(4), 1500.*

[2] B. Scheeren, and L. Pahlavan. (2023). "Condition Assessment of Low-Speed Slew Bearings in Offshore Applications Using Acoustic Emission Monitoring," in *European Workshop on Structural Health Monitoring. EWSHM 2022. Lecture Notes in Civil Engineering, Vol 270, pp. 892–901.*

PhD progress
1 2 3 4 5

Photopolymerization Kinetics in Stereolithography Modeling and Simulation

Maged Shaban[1,2,3], Clemens Verhoosel[1], Herman Wijshoff[2], Ferdinando Auricchio[3], Alessandro Reali[3] and Harald van Brummelen[1]

[1] Eindhoven University of Technology, The Netherlands
[2] Canon Production Printing B.V.
[3] University of Pavia, Italy

Objective

The research goal is to develop a complete model for UV curing in photopolymerization process, with its applications in Stereolithography.

Introduction

Photopolymerization is a process of producing polymers in which the chemical reaction is initiated by exposing photosensitive, mono-functional, or multi-functional monomers to a high-intensity light source.
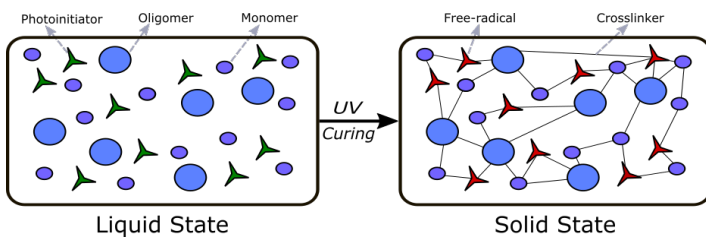
Stereolithography (SL) is a sophisticated additive manufacturing technique that creates three-dimensional polymer and ceramic objects from a CAD file using laser-initiated photopolymerization
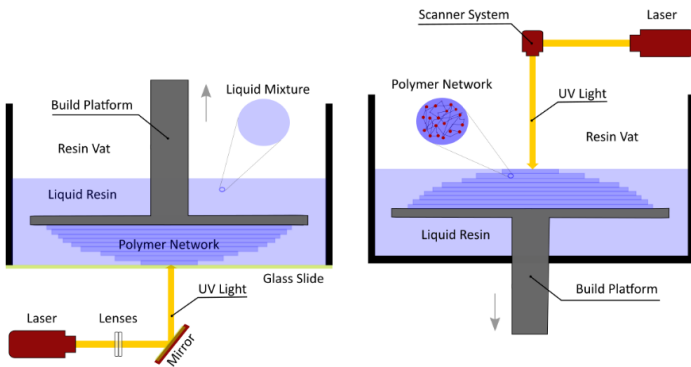
Multi-Physics Model for Photopolymerization

- Irradiation modeling: by using the generalized Beer-Lambert law for the light diffusion within the printed layer, coupled with the optical properties of resin and the photo-initiators concentrations.

- Kinetic model: reaction-diffusion equation for photopolymerization process with including reactants kinetics, concentrations and considering the oxygen inhibition. Coupled to irradiation process and temperature equation.

- Temperature modeling: by using the energy balance equation considering the polymerization rate.

Results

The model is solved numerically for a thick single layer with depth and width 20 mm for 40 seconds for the top-down SL:

- The free-radicals normalized concentration within the printed layer.
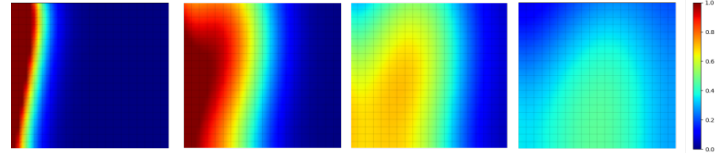
- The produced polymers (Monomer conversion to polymer) concentration.
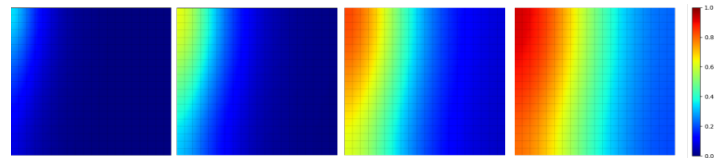
- The diffused oxygen concentration within the layer from the ambient forming an inhibition for the process.
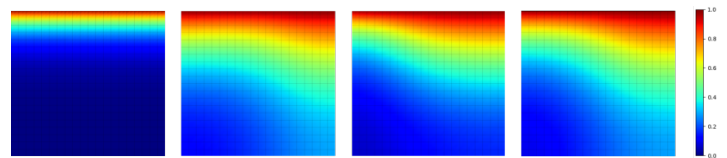
- The temperature distribution within the sample produced from the exothermic reaction.
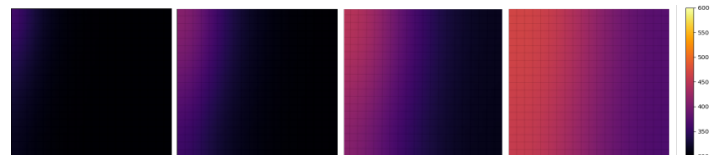
Next Steps

- To validate the model using the analytical solution and literature benchmarks.

- Study the influence of the cross-linking concentration.

- Further model development including mechanical and thermal properties, considering a heterogeneous resin.

References

[1] Anastasio, R., Peerbooms, W., Cardinaels, R., & Van Breemen, L. C. A. (2019). *Characterization of Ultraviolet-Cured Methacrylate Networks: From Photopolymerization to Ultimate Mechanical Properties.* Macromolecules, 52(23), 9220–9231.

[2] Goodner M., & Geers, M. G. D. (2002). *Development of a comprehensive free radical photopolymerization model incorporating heat and mass transfer effects in thick films.* Chemical Engineering Science.

Does H strengthen iron?: Insights from atomic-scale H-dislocation interaction

Varun Shah, Erik van der Giessen, Francesco Maresca

Email: v.d.shah@rug.nl
Computational Mechanical and Materials Engineering
University of Groningen

1. Introduction:

- Bottleneck for H economy → Transport of H via steel pipelines
- Challenge: Extending the **lifetime** of the pipelines
- H **diffuses** fast and **trapping** at **defects** → Loss of **ductility** (fig 1a)
- Several H embrittlement theories → defect based (fig 1b)

  HELP (H enhanced localized plasticity) → Increased dislocation mobility
  HEDE (H enhanced decohesion) → Weaking of atomic bonds
  HESIV (H enhanced strain induced vacancies) → Vacancy cluster stabilization

- No clear consensus on operating mechanism

- Goal: understand micro-mechanisms of H-defect interaction → physics based H-embrittlement theory
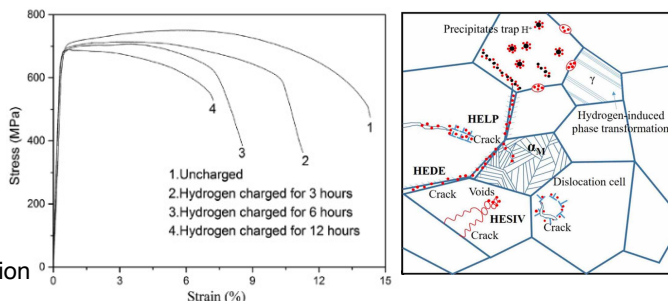
Figure 1: (a) Stress-strain plot depicting the loss of ductility with increasing H charging time in X100 steel grade [1] (b) Schematic showing the different proposed H embrittlement theories [2].

2. Approach: Insights on dislocation mechanics: H – edge/screw dislocation interaction in iron

$[12\bar{1}]||X, [\bar{1}11]||Y, [101]||Z$

Simulation details:

- Edge dislocation with **{110}<111>** slip system
- Screw dislocation with **{112}<111>** slip system
- Fe-H EAM potentials from Ramasubramaniam, A. et al.[3]
- H randomly distributed at tetrahedral interstitial sites (TIS)
- Influence of H conc. and distribution on Peierls stress
- Molecular statics and dynamic simulations
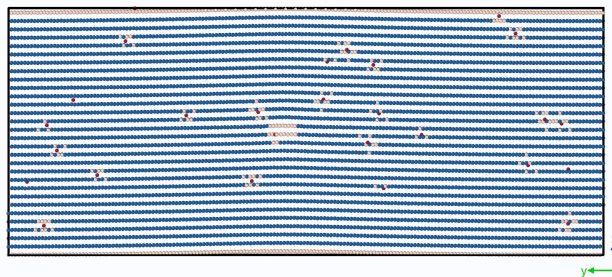
Figure 2: {110}<111> edge dislocation setup in iron. The blue atoms denote the bcc symmetry of the Fe atoms, while the red atoms between planes resemble the H atoms.

3. Results and discussion:

Edge dislocation

Random configuration (fig 3a):

- Deformation at 0 K
- H assisted pinning of dislocation
- Increasing trend with H conc.
- Pinning extent: local H atoms arrangement

Clustered configuration (fig 3b):
- Diffusion at 500 K followed by deformation at 0 K
- Identical increasing trend
- Magnitude significantly higher → 6-7 times than random
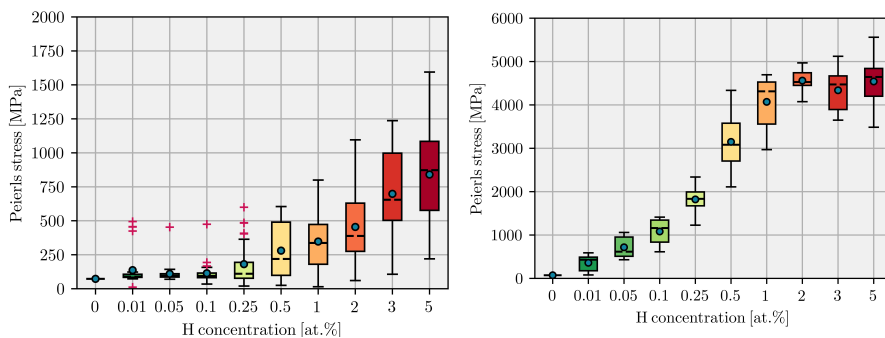
Figure 3: Effect of varying local H conc. on Peierls stress of edge dislocation for (a) randomly distributed H atom and (b) clustered H atom configuration.

Screw dislocation

Random configuration (fig 4):

- Deformation at 0 K
- H assisted softening
- Decreasing trend with H conc.
- Reliability of EAM for screw → questionable
- Need for an reliable Fe-H potential
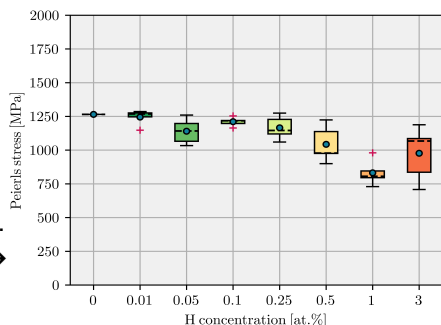
Figure 4: Effect of varying local H conc. on Peierls stress of screw dislocation for randomly distributed H atoms.

4. Conclusion and future work:

- Strengthening/softening in iron due to H → dislocation character governed
- Effect of finite temperature on strengthening/softening → ongoing
- Development of reliable Fe-H potential → ongoing

5. References:

[1] Han, Y.D. *et al. Int. J. Hydrog. Energy* (2019) 44:22380–22393.
[2] Gong, P. *et al. Sci. Adv.* (2020) 6.46: eabb6152.
[3] Ramasubramaniam, A. *et al. Phys. Rev. B* (2010) 79:174101.

PostDoc progress 1 2 3

university of groningen

CmME

materials innovation institute

NWO

Modelling the thermomechanical behaviour of functional ceramic membranes

H. Shi[1], D. Giuntini [1], J.A.W.V. Dommelen[1], J.J.C. Remmers[1], M.G.D. Geers[1]

[1]Mechanics of Materials, Department of Mechanical
Engineering, Eindhoven University of Technology
h.shi1@tue.nl

Introduction

Functional ceramic membranes made from LaWO are of great interest, for the process of H_2 extraction. We aim at building up a modelling framework that captures the thermo-mechanical behaviour of ceramic membranes during the sintering stage, thereby optimizing the manufacturing process with the help of a tailored virtual framework [1].
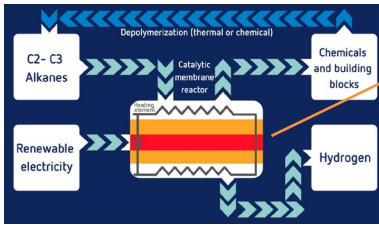
Catalytic membrane reactor for H2 extraction.
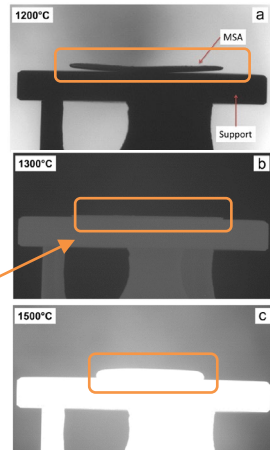
Bending of an asymmetric membrane during sintering [2].

Model

Skorohold-Olevsky Viscous Sintering (SOVS) model

The Skorohold-Olevsky Viscous Sintering (SOVS) model [3] is one of the most popular models for the sintering of ceramics. It is based on the concept of the generalized viscous flow of porous solids and derived on a thermodynamical basis within a continuum mechanics context.

Constitutive relation for linear-viscous porous material:

$$\sigma_{ij} = 2\eta \left[\varphi \dot{\varepsilon}_{ij} + \left(\psi - \frac{\varphi}{3} \right) \dot{e} \delta_{ij} \right] + P_L \delta_{ij}$$

Density evolution (continuity equation):

$$\frac{\dot{\rho}}{\rho} = -\dot{e}$$

σ_{ij} – stress tensor; η – material viscosity; φ – normalized shear viscosity; ψ – normalized bulk viscosity; $\dot{e}$ - trace of the strain rate tensor; P_L - sintering stress; ρ – bulk density.

Experiments
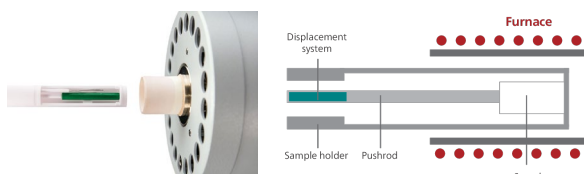
Figure 1: Dilatometry to measure shrinkage during the sintering process.

Determination of Model Parameters

With the help of dilatometry, the viscosity dependency on temperature and bulk density (not shown) of the sample material can be determined:
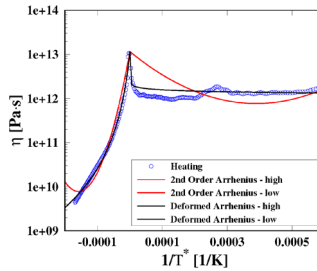
2nd Order Arrhenius [4]:

$$\eta(T) = A \exp\left(\frac{B}{RT} + \frac{C}{RT^2} \right)$$

Deformed Arrhenius [4]:

$$\eta(T) = A \exp_d\left(\frac{-\varepsilon}{RT} \right)$$

Results
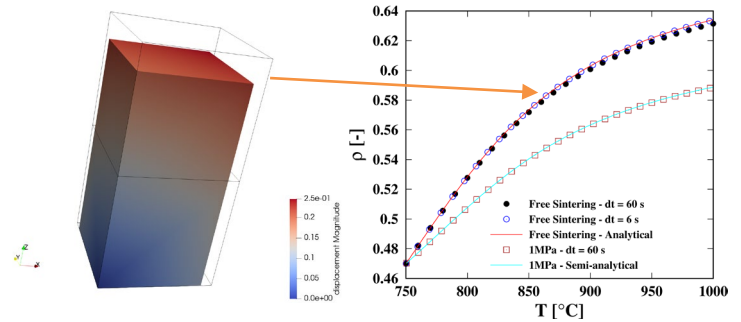
Figure 2: (left) free sintering of two elements, (right) bulk density evolutions and comparison with analytical solutions.
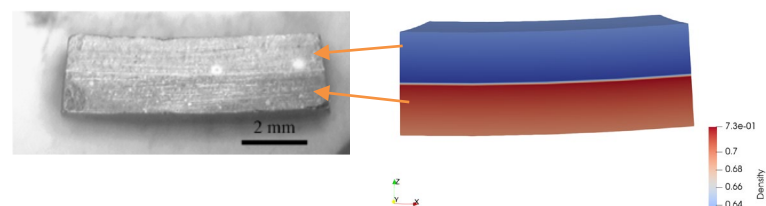
Figure 3: (left) bilayer bar sintered at 1000 ˚C [5], (right) simulation of the bilayer bar sintered at the same temperature.

Conclusions

• SOVS model is successfully applied to model the sintering of ceramics.
• A novel model parameters determination method is proposed.
• The density evolutions match very well with the analytical solutions.
• The bending observed in the experiment is well captured by our model.

References

[1] Giuntini, D., et al. (2016). Scripta Materialia, 124, 38-41.
[2] Deibert, W., et al. (2015). Journal of membrane science 492: 439-451.
[3] Olevsky, E. A. (1998). Materials Science and Engineering: R: Reports, 23(2), 41-100.
[4] Aquilanti, V., et al. (2010. Chemical Physics Letters, 498(1-3), 209-213.
[5] Olevsky, E. A., et al. (2006). Journal of the American Ceramic Society, 89(6), 1914-1922.

PostDoc progress

1   2

Mesh-based surrogate for FE² microstructure simulations

J. Storm, I.B.C.M. Rocha, F.P. van der Meer

Delft University of Technology

Introduction

Surrogate models are required to facilitate the demand for simulating increasingly complex phenomena using multiscale simulations. Where most surrogate models aim to directly relate macroscopic stresses to macroscopic strains, here a Graph Neural Network (GNN) is used which learns to predict the full microscale behavior. Additional information available at the microscale makes it possible to simulate local behavior.
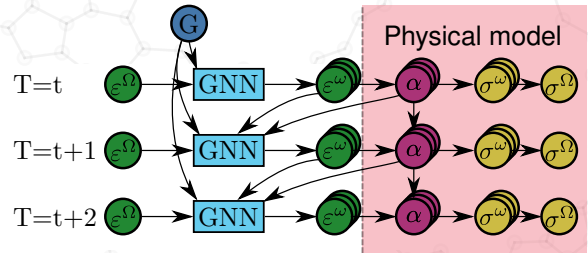
Train on small microstructures

Input
$\varepsilon^\Omega = [0.855, 0.438, -0.277]$

Target
ε_x

FEM

GNN

Prediction

Graph network close-up
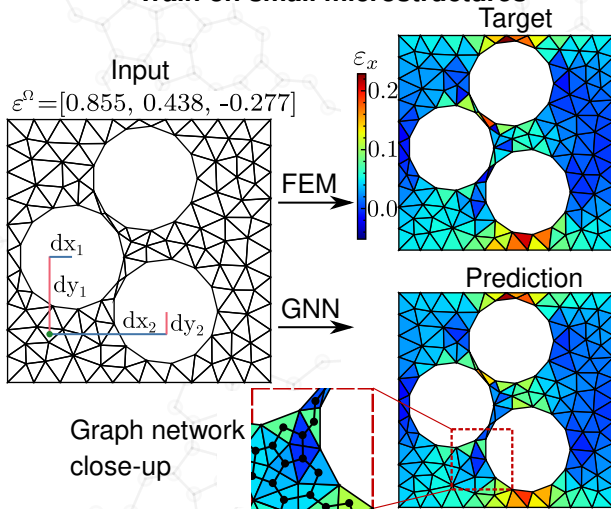
Neighborhood information

GNN layers: 1   2   3
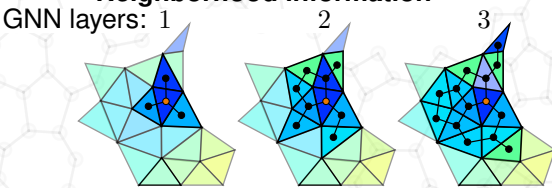
Motivation

Obtaining consistent FEM responses requires a large microstructure, i.e. a representative volume element (RVE). These are expensive to compute, making it burdensome to create data. A GNN can instead be trained on small RVEs, which are cheaper to simulate, and still predict for larger RVEs. Making predictings using a GNN is much faster and scales linearly with the number of elements.

Methodology

➤ Create a dual graph over the mesh.
➤ Learn a function to update a node state based on its neighborhood.
➤ This function is mesh-independent and can be applied to unseen load cases & meshes.

Predict larger microstructures

FEM   3-void input GNN   1-void input GNN
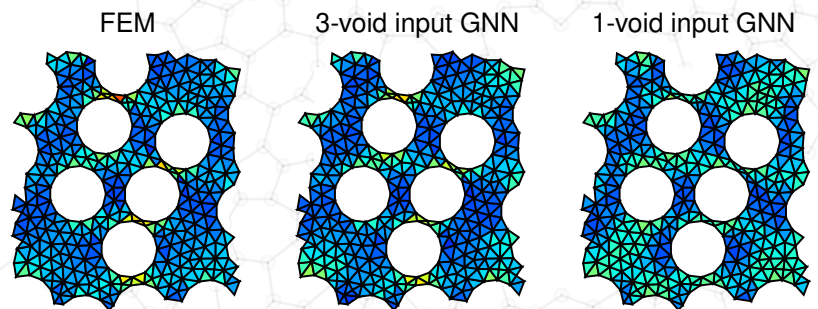
Findings

➤ For linear computations, a GNN accurately predicts strain distributions for the size it is trained on.
➤ The homogenized response transfers to large RVEs.
➤ Including nearby fiber positions increases accuracy.

Future work

Non-linear load cases with multiple timesteps will be implemented, for which it is expected that the neighborhood connections play an increasingly important role to model localization effects. Physical models will be included to model path-dependent behavior. In addition, fibers will be modeled instead of voids

Global stiffness transfers to large meshes
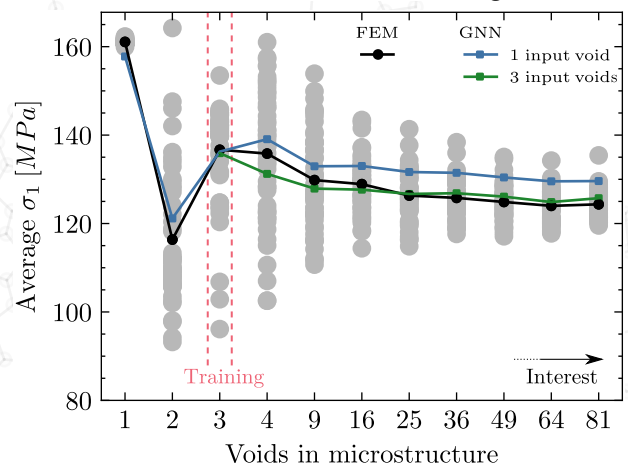
Vibration-Induced Friction Force Modulation

E. Sulollari[1], A. Cabboi[1]

[1]Fautly of Civil Engineering and Geosciences,
Delft University of Technology

Introduction

Some facts on friction

✖ Wear and tear

✖ Noise pollution

✖ Unwanted heat

✖ Machinery failure

✖ Unwanted vibrations
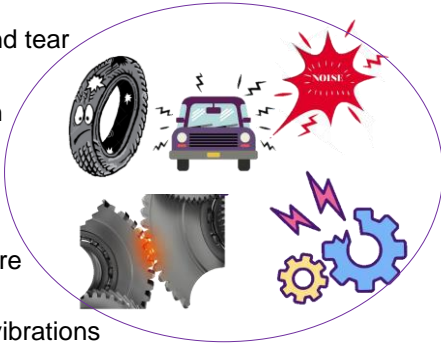
Figure 1: Disadvantages of friction

What can we do about this ❓

💡 **Alter friction forces**

1 By using lubricants

Figure 2: Lubricants to alter friction forces
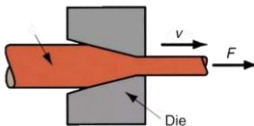
2 By using external vibrations

Figure 3: Ultrasonic vibration to alter friction forces

Research goal

What is lacking?

Friction alteration by vibration already observed experimentally **BUT…**

➡ Ultrasonic vibration only considered [1].

Effect of a single load only considered [2]. ⬅

➡ Microstructure effect only considered [3].
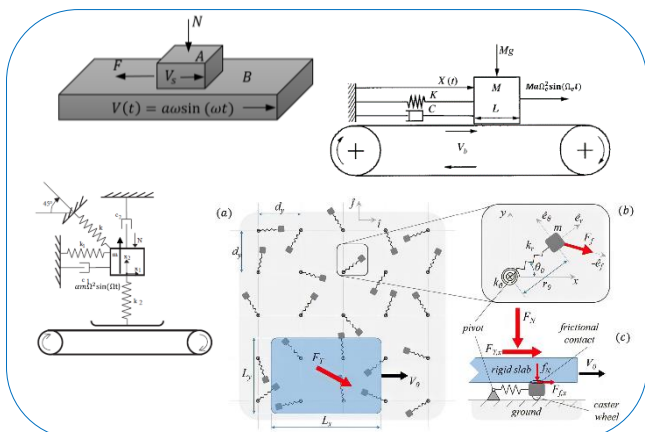
Figure 4: Existing models on frictional behaviour

What is next?

Quantify the effect of excitation on friction by increasing model complexity including:

✓ Micro- and macrostructure

✓ Local and global dynamics

✓ Contact temperature
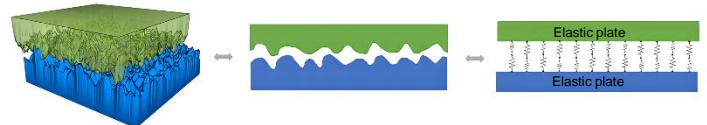
Figure 5: Example of interface representation

Preliminary results

o Method of Direct Separation of Motion used and extended

o Friction alteration for any frequency

o Results for sliding, stick-slip defined
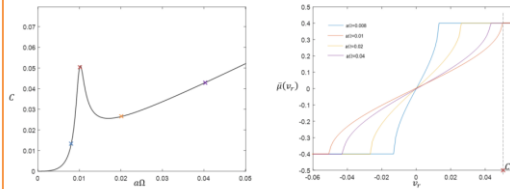
Figure 6: Friction alteration for any frequency

o Friction alteration for loads applied simultaneously
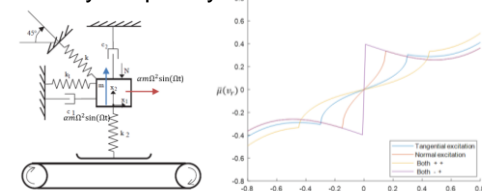
Figure 7: Friction alteration for load combinations

Relevant applications
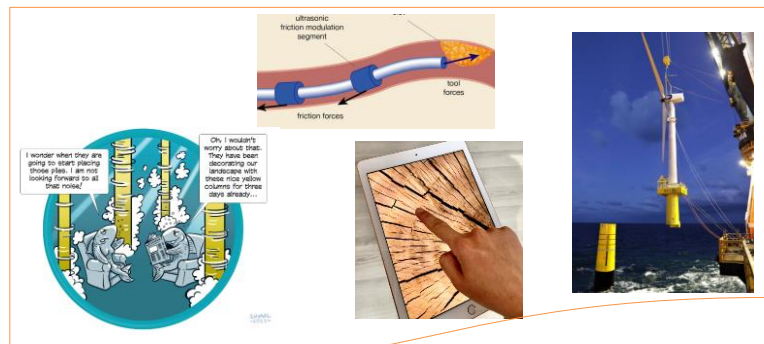
Figure 8: From left to right :gentle pile driving, catheter development, surface haptics, slip joint installation/decommission

References

[1] V.C Kumar and I.M Hutchings. Reduction of the sliding friction of metals by the application of longitudinal or transverse ultrasonic vibration. Tribology International, 37(10):833–840, 2004.

[2] J. J. Thomsen. Using fast vibrations to quench friction- induced oscillations. Journal of Sound and Vibration, 228(5):1079–1102, 1999.

[3] N. Menga, F. Bottiglione, and G. Carbone. Dynamically induced friction reduction in microstructured interfaces. Nature, 11(1):171–184, 2021.

TU Delft — Delft University of Technology

Searching for designs in a neural network's parameter space may be more rewarding!

Suryanarayanan M. S. [a]., Miguel Bessa [b], Alejandro M. Aragón [a]
Delft University of Technology, Netherlands [a]
Brown University, U.S.A [b]

1 Topology Optimization

❖ Automated designing tool
❖ Optimize material distribution (Design)
❖ Metric – objective (Compliance)
❖ Gradient-based optimizer (MMA)
❖ **Problem – suboptimal designs**

2 Neural networks

❖ Blackbox function approximators - tunable parameters
❖ Creates map from inputs to outputs
❖ Type of network is important

3 Neurally reparameterized TO

❖ Network → material distribution
❖ Use this design for TO
❖ Update network's parameters
❖ 3 main methods
❖ **Different conditions need different methods**
❖ Modified one method (F-tounn[1])
❖ **Modified method > Conventional (All tested conditions)**
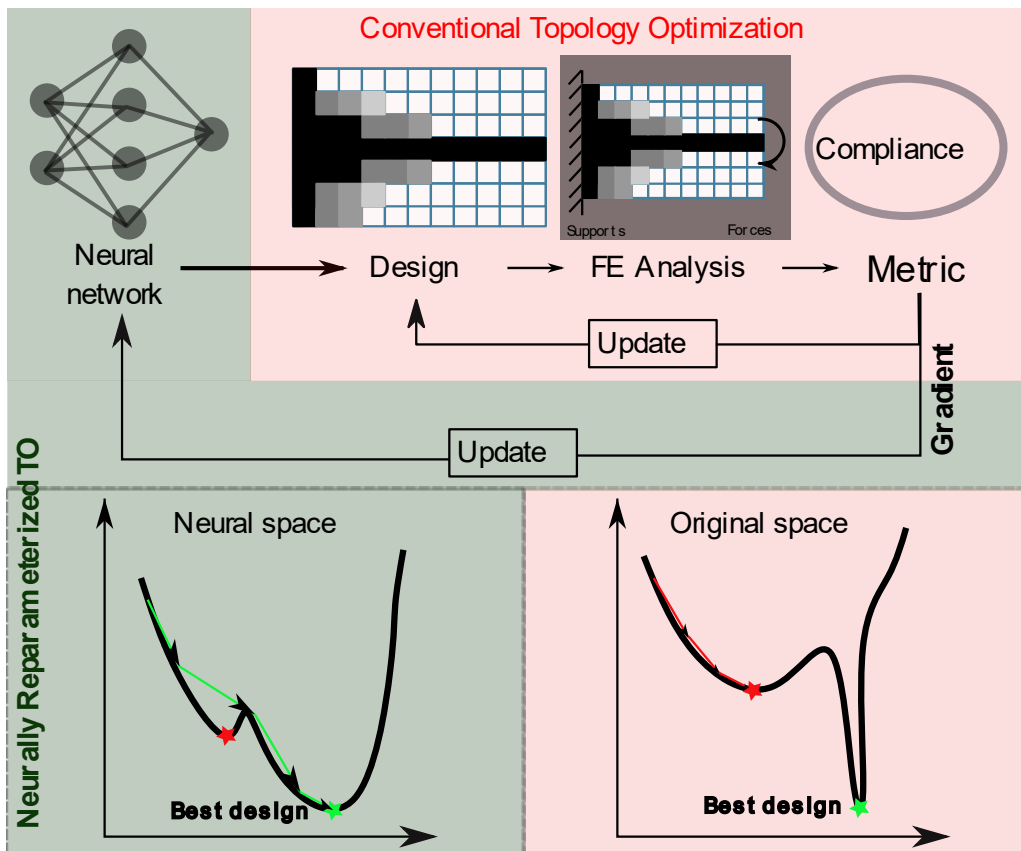
4 Preliminary results – median compliance over random initializations

Our method 247.6
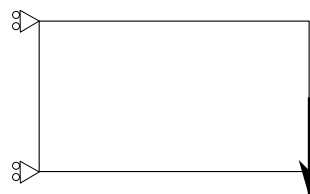
Conventional 545.2

5 References

[1]. Chandrasekhar, A., & Suresh, K. (2021), https://arxiv.org/abs/2109.01861

TUDelft

PhD progress
1 2 3 4

Learning hyperelasticity without stress data

P. Thakolkaran[1,a], A. Joshi[1], Y. Zheng[1], M. Flaschel[2], Laura De Lorenzis[2], S. Kumar[1]

[1]TU Delft, [2]ETH Zurich
[a]P.Thakolkaran@tudelft.nl, mech-mat.com
euclid-code.github.io
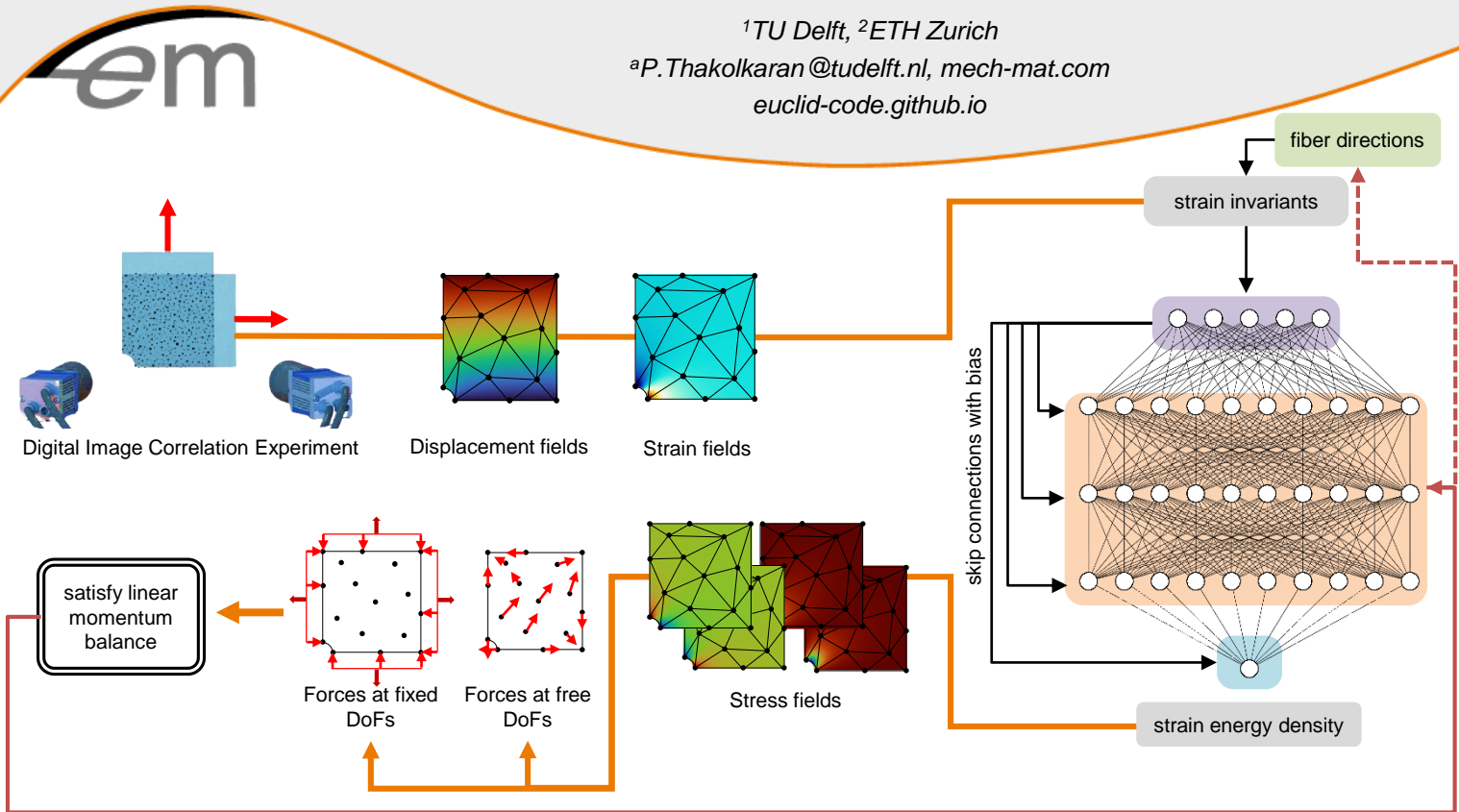
Unsupervised deep-learning of hyperelastic constitutive laws

Unsupervised learning

Existing work

- Finite Element Model Updating:
  - Iteratively updating an *a priori* assumed model for the unknown material to match simulation vs. experiments.
- Virtual Fields Method:
  - Tune *a priori* model until principle of virtual work is satisfied.
- Data-driven constitutive modeling:
  - Use of large dataset of stress-strain pairs from multiscale simulations / experiments via model-based (e.g., NNs) or model-free approach

Our approach

- <u>Unsupervised</u>: Requires no stress data. Only uses full-field displacement and global reaction force data from a single experiment.
- <u>Physically guided</u>: Model training is guided by satisfying linear momentum balance (as opposed to stress labels)
- <u>Physically consistent</u>: The deep learning framework automatically satisfies physical requirements.
- <u>No model assumptions</u>: Departure from parameter identification – Deep learning framework can take on any form.

Physics-guided input convex neural networks

- Hidden data-driven material model is based on input convex neural networks (ICNNs):
  - ICNNs are essentially a positive sum of strictly increasing convex transformations.
  - Automatically satisfies material stability.
  - Due to squared softplus activation function, the derivatives of the NN-based strain energy density is ensured to be smooth and continuous.

Arruda-Boyce solid
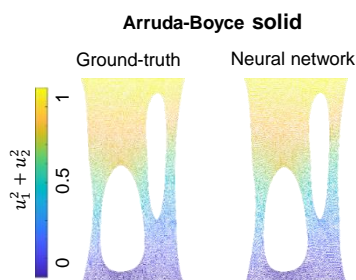
Learning anisotropic hyperelasticity

- Trainable angle parameter allows the framework to identify the hidden fiber arrangements in anisotropic hyperelastic solids.
- The angle is learned jointly with ICNN parameters.
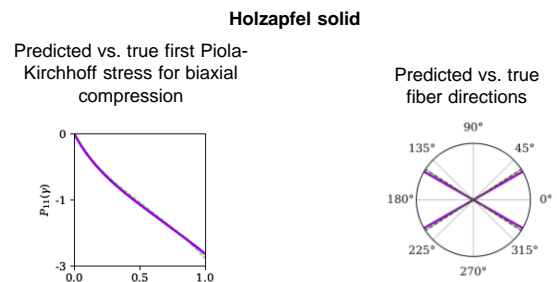
Holzapfel solid

Thakolkaran, P., Joshi, A., Zheng, Y., Flaschel, M., De Lorenzis, L., & Kumar, S. (2022). NN-EUCLID: deep-learning hyperelasticity without stress data. *arXiv preprint arXiv:2205.06664.*

PhD progress

1	2	3	4

MECHANICS MATERIALS COMPUTING

Towards improved porous models for solid/fluid topology optimization

M.J.B. Theulings[1,2], M. Langelaar[2],
F. van Keulen[2], R. Maas[1]
[1] *Netherlands Aerospace centre*
[2] *Delft University of Technology*

Motivation

Fluidic systems are relevant for a wide range of aerospace applications such as wing profiles, cooling systems and propulsion systems. To optimize such structures density-based topology optimization procedures can be used which find an optimal solid/fluid distribution within a design domain by representing the solid domain as a **highly impermeable porous material**.

Methods

We optimize a solid/fluid distribution using Figure 1 by representing the solid domain as a porous material coupled to the fluid volume fraction:

$$\alpha = \frac{V_f}{V} = \frac{\text{Fluid volume}}{\text{Averaging volume}}.$$
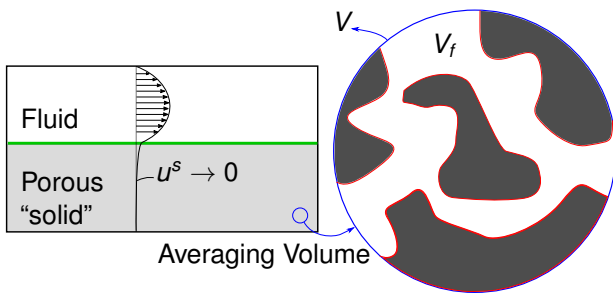
Figure 1: The representation of the solid domain as an impermeable porous domain.

The **volume average** is used to define and optimize using the superficial flow average ($\mathbf{v}^s$) and intrinsic pressure average (p^i):

	Fluid	Porous "solid"
α	$\overline{\alpha} = 1$	$\underline{\alpha} \rightarrow 0$
p^i	Finite value	Finite value
$\mathbf{v}^s$	Finite value	$\rightarrow \mathbf{0}$

Challenges

Common approaches use the **Navier-Stokes with Darcy Penalization (NSDP)** equations, with momentum equation:

$$\rho\dot{\mathbf{v}}^s + \rho\nabla\mathbf{v}^s \cdot \mathbf{v}^s = \mu\nabla^2\mathbf{v}^s - \nabla p^i \boxed{-\kappa(\alpha)\mathbf{v}^s}.$$

Flow in the porous "solid" domain is inhibited by introducing a large **Darcy penalization** $\left(\overline{\kappa}(\alpha \rightarrow 0) \gg 1\right)$:

$\boxed{-\kappa(\alpha)\mathbf{v}^s} \rightarrow$ Adds friction proportional to the flow.

Challenges in this approach lie with finding a balance between:

1. **Accuracy of the flow solution** (high $\overline{\kappa}$).

2. **Convergence of the optimization algorithm** (low $\overline{\kappa}$).

Volume Averaged Navier-Stokes

We extend the NSDP equations to the more general **Volume Averaged Navier-Stokes (VANS)** for modeling flow in the porous/fluid domain using the momentum equation:

$$\rho\frac{\partial\mathbf{v}^s}{\partial t} + \rho\nabla\frac{\mathbf{v}^s}{\alpha}\cdot\mathbf{v}^s = \mu\nabla^2\mathbf{v}^s \boxed{-\mu\nabla\alpha\cdot\nabla\frac{\mathbf{v}^s}{\alpha}} - \boxed{\alpha}\nabla p^i - \boxed{\kappa(\alpha)\mathbf{v}^s}.$$

The VANS equations add three new terms:

$$\rho\nabla\frac{\mathbf{v}^s}{\boxed{\alpha}}\cdot\mathbf{v}^s \rightarrow \text{Adds "mass" in the porous domain.}$$

$$\boxed{-\mu\nabla\alpha\cdot\nabla\frac{\mathbf{v}^s}{\alpha}} \rightarrow \text{Supports viscous forces.}$$

$$\boxed{\alpha}\nabla p^i \rightarrow \text{Reduces driving force in the "solid" domain.}$$

Results

Optimizing for minimal pressure drop results in the designs and objective values in Figure 2.
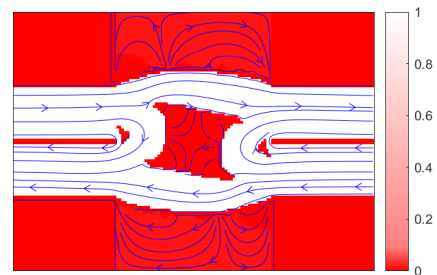
(a) NSDP based desgin, $f^r = 1.45$.
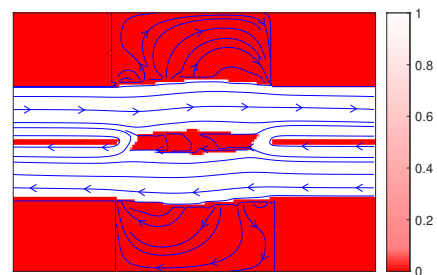
(b) VANS based desgin, $f^r = 1.03$.

Figure 2: Two optimized designs with post processed objective f^r. The NSDP based design performs worse for similar errors.

Conclusions

In conclusion, the VANS equations improve:

1. **Design convergence for similar accuracy.**

2. **Robustness of the optimization settings.**

TUDelft

PhD progress

| 1 | 2 | 3 | 4 |

Predicting composite structures failure with the help of quantum neural networks

G. Tosti Balducci[1], B. Chen[1], M. Möller[3], M. Gerritsma[2], R. de Breuker[1]

[1] TU Delft, Aerospace Structures and Materials
[2] TU Delft, Flow Physics and Technology
[3] TU Delft, Applied Mathematics

Introduction

Data-driven models been have used to predict composite failure by learning from a relatively small number of numerical simulations and later generalizing to unseen input (e.g. loading) conditions.

Even though most machine learning models are trained on classical computers, quantum computers can also learn from data. In fact, operations on quantum bits are continuous and can be tuned in a hybrid quantum-classical optimization loop. Since the model is a quantum circuit, it is evaluated on quantum hardware, while the parameters are updated classically.

Thanks to the properties of quantum mechanics, quantum models proved able to outperform classical machine learning models when learning specific datasets [1]. Therefore, we can ask whether quantum circuits can be trained to predict composite failure more accurately or more efficiently than classical machine learning models.
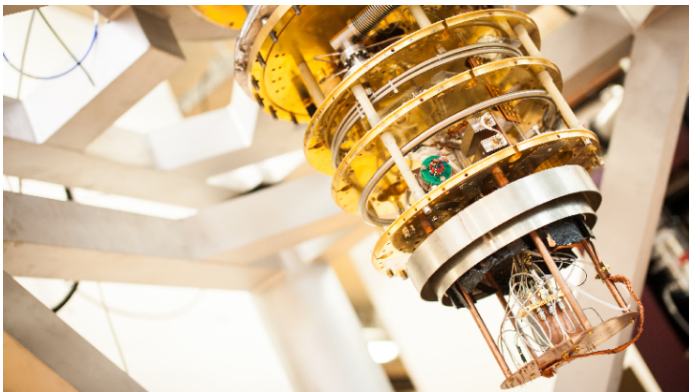
Figure 1: A quantum computer from QuTech.

Quantum neural networks (QNNs)

Amplitude and phase operations on quantum bits (qubits) are continuous. Therefore they are suitable for

- data encoding: change of the probability of the measurement,

$$p_i(0) = \cos^2\left(\frac{\tilde{\varepsilon}_i}{2}\right) \qquad (1)$$

  If $\tilde{\varepsilon}_i \in [0, \pi]$, the encoding is unique.

- parameter learning: tunable change of probability and entanglement.

Training is hybrid.

- Quantum step: model evaluation.
- Classical step: loss calculation and parameters update.
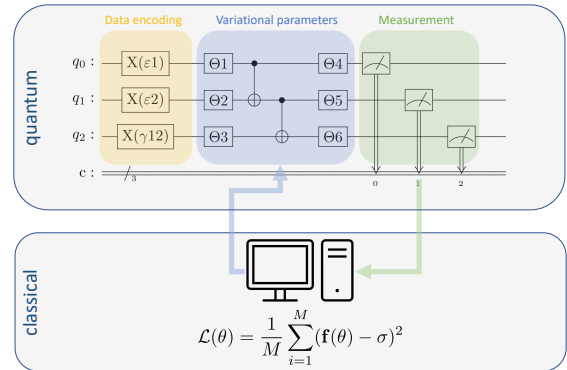
Figure 2: Hybrid training loop of quantum neural networks

Results

Deep neural network (DNN) and QNN models were trained with finite element simulations results and tested on unseen load cases.
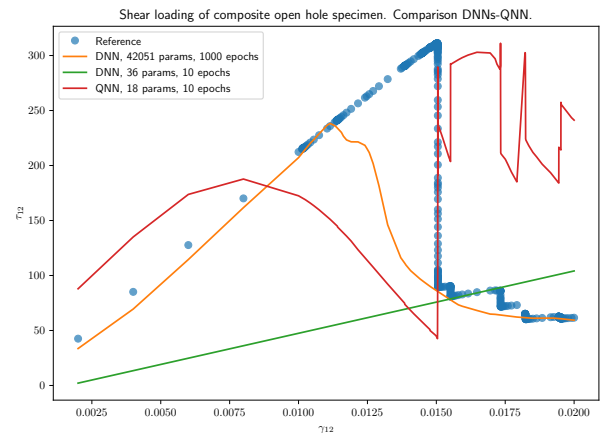
Figure 3: Comparison between DNNs and QNNs.

With few parameters and after only 10 epochs, the QNN learned the curve's peak stress and corresponding strain with better precision than a complex DNN.

	DNN	QNN
err($\tau_{12,max}$)	23.4%	7.0%

Table 1: Peak shear stress prediction errors for classical and quantum model.

References

[1] Havlicek *et al.*. Supervised learning with quantum-enhanced feature spaces. Nature. 2019.

TUDelft

PhD progress

| 1 | 2 | 3 | 4 |

Simple and Efficient GPU accelerated Topology Optimization

E.A. Träff[1], N. Aage[1],
O. Sigmund[1], M. Langelaar[2], F. van Keulen[2]
[1] Technical University of Denmark
[2] SOM, PME, Delft University of Technology

Introduction

Topology optimization is a promising design optimization method, but has a high computational cost. This work presents several approaches to implement GPU-accelerated topology optimization, enabling the solution of large-scale problems with a single GPU.

Optimization formulation

The conventional minimum linear elastic compliance problem with a volume constraint and density filter is used. The structures are optimized using the optionality criteria method.

$$\underset{\mathbf{x}\in\mathbb{R}^{n_e}}{\text{minimize}} \quad \mathbf{u}^\top \mathbf{f}$$

subject to:

state equation $\quad \mathbf{K}\mathbf{u} = \mathbf{f}$

volume $\quad \dfrac{V}{V_{\text{domain}}} \leq V^*$
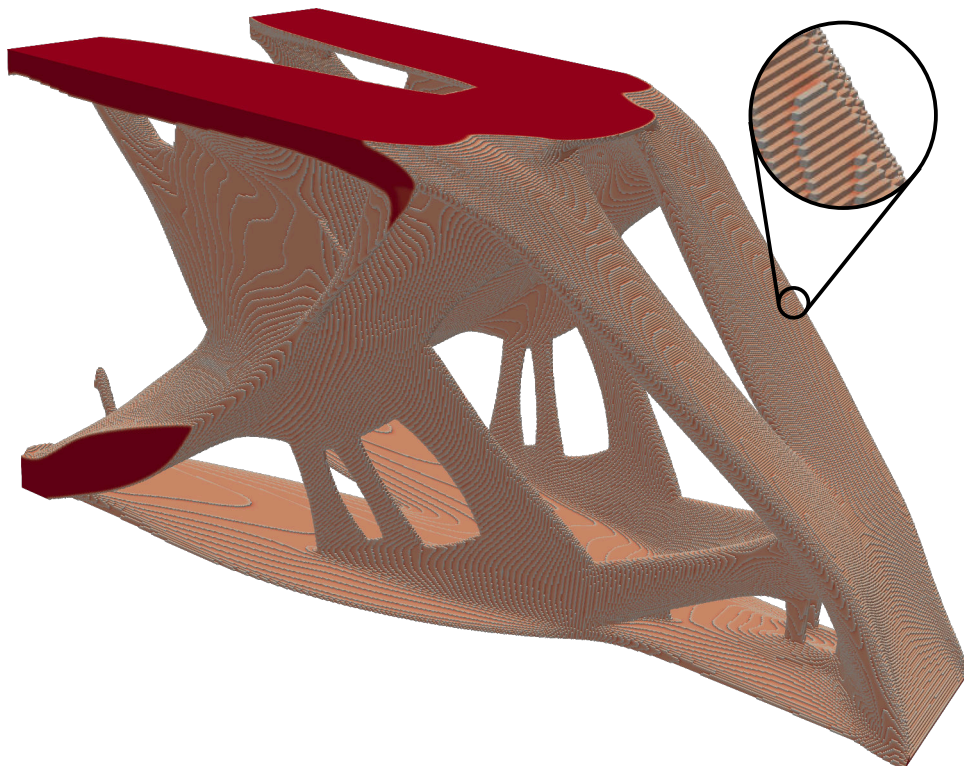
OpenMP

Enables hardware acceleration using GPUs. Moving of data and implementation of kernels is done by adding annotations to programs.

```
1  double val = 0.0;
2  #pragma omp target teams distribute
       parallel for reduction(+ : val)
       map(always,tofrom: val)
3    for (uint_fast32_t i = 0; i < n; i++)
4      val += a[i] * b[i];
```

Futhark

A functional programming language for GPU acceleration. The language is designed to guarantee compilation to efficient GPU-kernels.

```
1  def innerProduct [n] (a :[n]f64) (b
       :[n]f64) =
2    reduce (+) 0 (map2 (*) a b)
```

Computational efficiency

The example shown in Figure 1 is computed using the Futhark implementation on a Nvidia A100 GPU. The example ran for 100 design iterations in approximately 2 hours, compared to 9 hours on two 24 core Intel Xeon processors, or an estimated 27 hours on a high-end desktop.
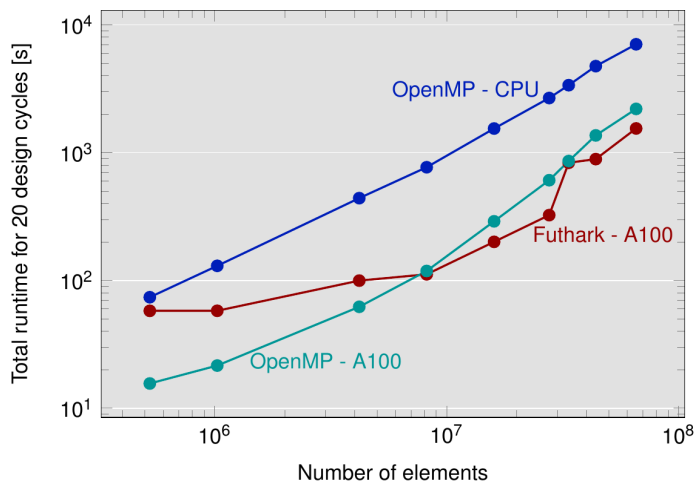
Vibratory pile installation in layered soil media: numerical modelling and field tests

A. Tsetas[1], A. Tsouvalas[1], A.V. Metrikine[1]

[1] Faculty of Civil Engineering and Geosciences
Delft University of Technology

Introduction

Presently, over 80% of the existing **offshore wind** turbines (OWTs) in Europe are founded on **monopiles**. These foundations are commonly installed by impact hammering, albeit more environmentally friendly **installation** methods are increasingly adopted, e.g. vibratory pile driving.

A new technology – **Gentle Driving of Piles (GDP)** – has been proposed by TU Delft and successfully tested at Maasvlakte II. The development of a numerical **model** for the analysis of **vibration-based** installation methods is the present objective.
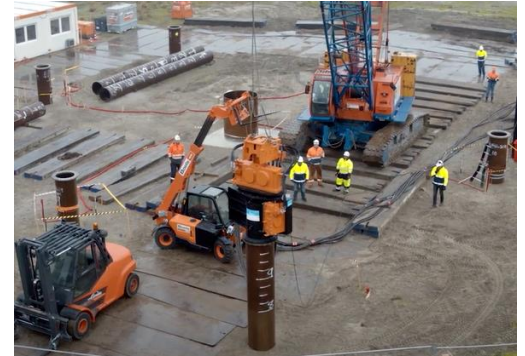
Figure 1: GDP test site

A non-linear pile-soil model for vibratory pile installation

A **non-linear** three-dimensional **pile-soil** model is formulated to analyze vibratory installation, comprised by:

1) a linear elastic thin cylindrical **shell** (pile)
2) a linear elastic layered **half-space** (soil)
3) a history-dependent frictional pile-soil **interface**
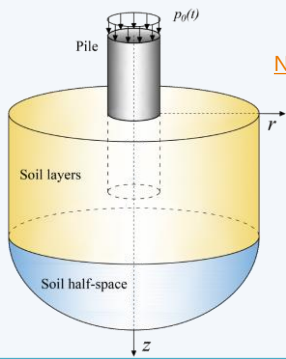
Non-linear pile-soil model

SAFE cylindrical shell

Layered soil medium with PMLs

SAFE EoM

$$\mathbf{I}_{p,0} \frac{\partial^2 \mathbf{u}_{p,0}}{\partial t^2} + \mathbf{L}_{p,0} \mathbf{u}_{p,0} = \mathbf{p}_{p,0}$$
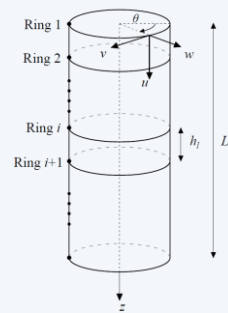
TLM-PMLs EoM

$$\begin{bmatrix} \widehat{\mathbf{u}}_{r,n} \\ \widehat{\mathbf{u}}_{z,n} \end{bmatrix} = \begin{bmatrix} \mathbf{\Phi}_r \mathbf{D}_R \mathbf{\Phi}_r^T & k \mathbf{\Phi}_r \mathbf{K}_R^{-1} \mathbf{D}_R \mathbf{\Phi}_z^T \\ \frac{1}{k} \mathbf{\Phi}_z \mathbf{D}_R \mathbf{K}_R \mathbf{\Phi}_r^T & \mathbf{\Phi}_z \mathbf{D}_R \mathbf{\Phi}_z^T \end{bmatrix} \begin{bmatrix} \widehat{\mathbf{p}}_{r,n} \\ \widehat{\mathbf{p}}_{z,n} \end{bmatrix}$$
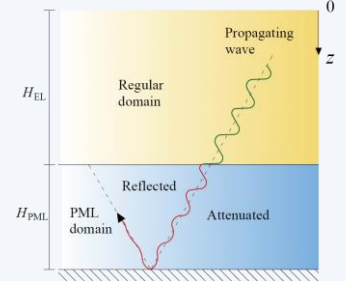
AFT Harmonic Balance Method

$$\mathbf{r} = \begin{bmatrix} \mathbf{r}_c \\ \mathbf{r}_t \\ \mathbf{r}_q \end{bmatrix} \qquad \mathbf{R}_F = \frac{1}{T} \int_0^T \mathbf{r} \mathbf{h}\, dt.$$

Numerical results
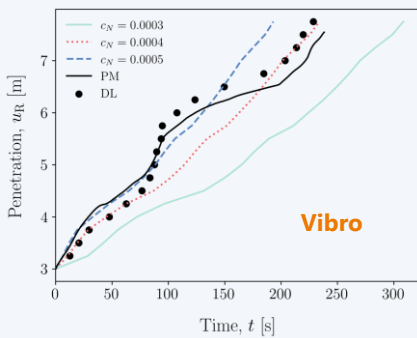
Vibro
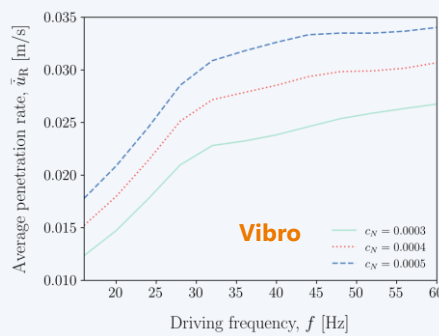
Vibro
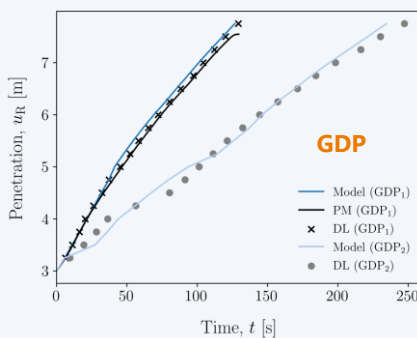
Vibro

GDP
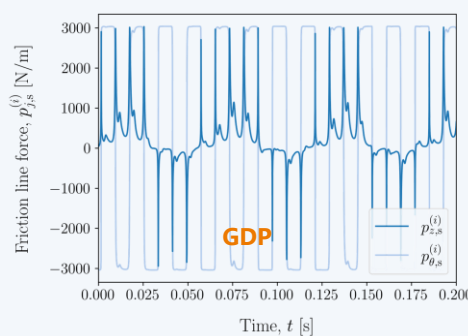
GDP
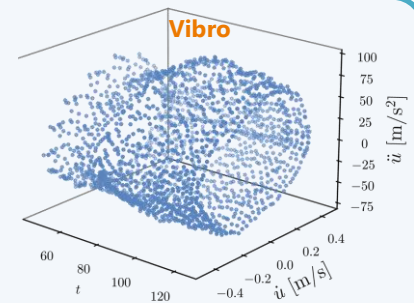
Conclusions

- A **unified model** has been developed to analyze both **vibro** and **GDP** methods.
- **Quasi-periodicity** emerges in pile driving due to slow **modulation** of harmonics.
- A **cyclic memory** mechanism for **friction reduction** is suitable for pile installation.
- **GDP** main mechanism is the substantial **friction** reduction in the vertical direction.

Phononic structures to mitigate crosstalk in clamp-on ultrasonic flowmeters

Sabiju Valiya Valappil, Fred van Keulen,
Hans Goosen, Alejandro M. Aragón
*Department of Precision and Microsystems Engineering,
Delft University of Technology*

Introduction

Clamp-on ultrasonic flowmeters suffer from measurement issues due to crosstalk between waves traveling through the pipe wall and signals through the measuring fluid.

(a)

(b)

Figure 1: (a) photograph of a clamp-on ultrasonic flowmeter, (b) Sectional view showing different signal and noise paths.

Figure 2: (a) PnC's PUC, (b) PnC wavguide, (c) PnC embedded wedge, (d) band structure, and (e) transmissibility relation.

Phononic crystals for wave steering

Phononic crystals (PnCs) are artificial materials possessing band gaps (BGs) – acoustic/elastic waves attenuate – due to Bragg scattering. PnCs with partial BGs can be used for wave steering without distorting the wavefront.

Crosstalk reduction via PnC-embedded wedges

Aligning PnCs in required orientation, we minimize the crosstalk generation, improving signal to crosstalk level.

Figure 3: Time-domain analysis of clamp-on system with partial BG PnC showing crosstalk reduction at the receiver.

Conclusion

A PnC with partial BG is incorporated into the wedge section of the clamp-on ultrasonic flowmeter that reduced waves in the pipe wall, improving the signal to crosstalk level.

References

[1] J Xu and J Tang, Tunable prism based on piezoelectric metamaterial for acoustic beam steering, APL, 2017.

PhD progress
1 2 3 4

Experiments vs Simulations: Episode IV - A New Hope

T. Vermeij[1], J. Wijnen[1], R.H.J. Peerlings[1], M.G.D. Geers[1], J.P.M. Hoefnagels[1]

[1]Eindhoven University of Technology

Problem

Comparison between (regular) deformation experiments & simulations @ microscale is problematic (in e.g. Dual-Phase (DP) Steels)

- **Unknown 3D subsurface microstructure**
→ assumptions for 3D required → Quantitative comparison (of strain fields) is impossible

Solution Strategy

Create thin specimens, aiming for through-thickness "Quasi-2D" microstructures

- **Background of poster is 500 μm area of DP steel specimen with < 5 μm thickness**

Characterization, *in-situ* SEM-DIC testing, data alignment, 3D modelling (Job Wijnen), quantitative comparison

Results

Experiments

Simulations

EBSD

Front   Rear   **Thickness**

Martensite
Ferrite
Martensite

3D mesh
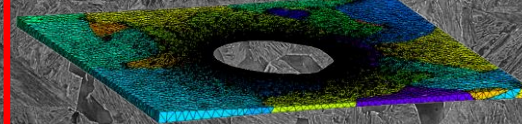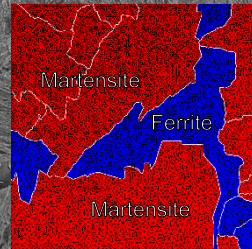
SEM-DIC Strain map
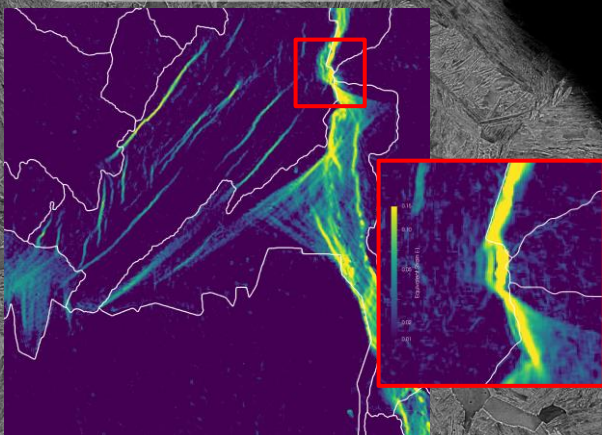
Simulated Strain maps

Regular CP
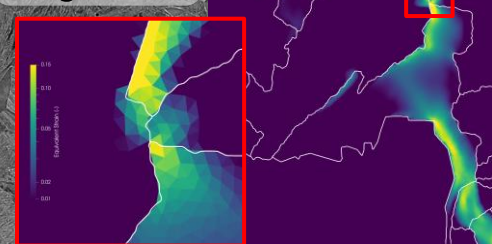
Modified Martensite CP
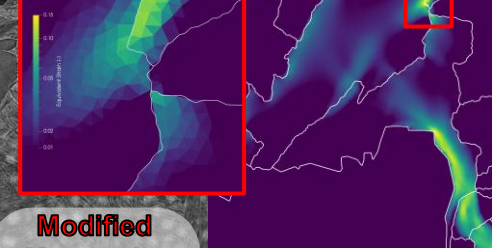
Conclusions

Direct Experimental/Numerical comparison possible through dedicated experiments and simulations

- **A New Hope** for improvement and validation of advanced models of metals

More advanced "Discrete" model: see poster of Job Wijnen

Understanding the hygro-expansion magnitude of freely and restrained dried handsheets

Niels Vonk, Ron Peerlings, Marc Geers, Johan Hoefnagels

Mechanics of materials
Eindhoven University of Technology
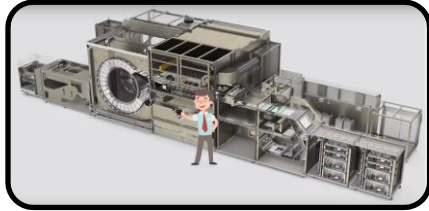
Paper fluting

- Paper unwanted **out-of-plane deformations** after printing (**fluting**).
- Driven by paper's complex **microstructure** down to the **single fiber level**.
- **Hygro-expansion** (Moisture-induced dimensional change) magnitude has a **one-to-one relation** to the severity of the **out-of-plane deformations**.

- The **drying procedure** of paper **affects** the **hygro-expansion**.
- **Freely dried** paper exhibits a **larger hygro-expansion** than **restrained dried** paper sheet

What are the mechanisms driving this difference?

- Approach: test if the **fibers** also exhibit the **hygro-expansion difference**.

10 μm

1 cm

Optical Profilometer

Objective

ΔRH
ΔT

fiber

Climate chamber

Condensation droplets

Wetting period

1 2 3 4

t [h]
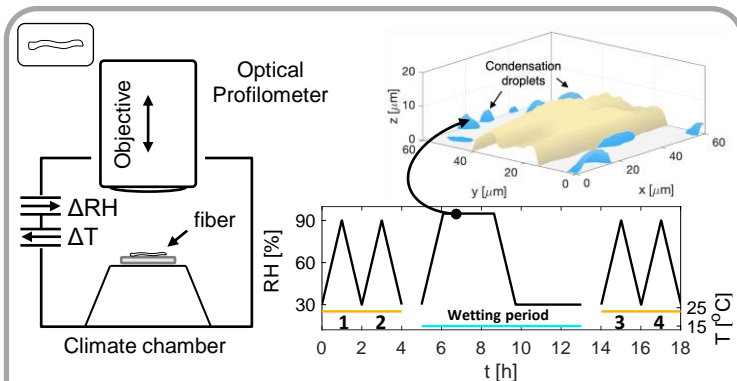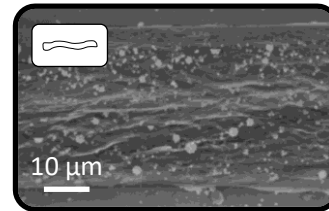
- The **fiber hygro-expansion** is characterized using a novel dedicated full-field methodology based on **Global Digital Height Correlation**.
- Each fiber is subjected to an relative humidity (RH) trajectory of: 2x 30 – 90 – 30 (cycle 1-2), 30 – 95 – 30, and 2x 30 – 90 – 30 (cycle 3-4). The temperature (T) is lowered during the wetting period → Condensation
- To see if a **restrained dried** fiber can **transform** into a **freely dried** fiber

[1] N.H. Vonk et al. *Cellulose* 2020, 27, 6777-6792.   [2] N.H. Vonk et al. *NPPRJ* 2021, 36, 61-74.

GDIC

Strain [-]

Relative Humidity [%]

— Constrained dried
— Freely dried
· RH

Time [hrs]

1 cm
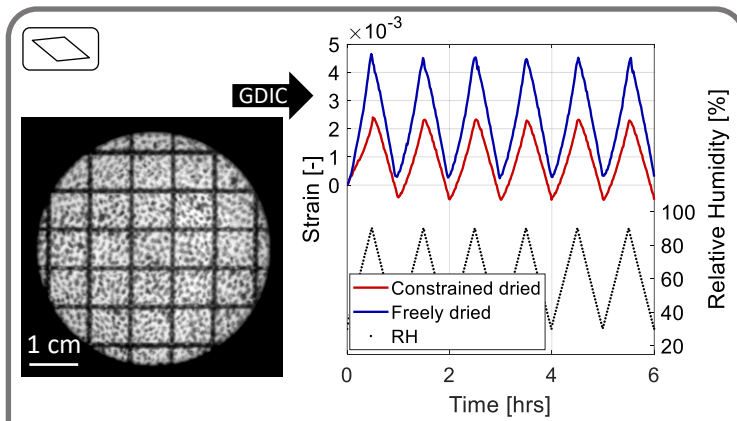
- **Sheet-scale hygro-expansion** measurements using **global digital image correlation** (GDIC) with minimized out-of-plane deformation.
- **Freely dried** paper indeed exhibits a **larger hygro-expansivity** than **restrained dried** paper

---

Freely dried   **Restrained dried**

$\Delta \epsilon_{ll}$ [-]

$\Delta \epsilon_{tt}$ [-]

$\Delta \epsilon_{lt}$ [-]

1 2   1 2
Cycle

θ [°]

$\Delta \epsilon_1$ [-]

$\Delta \epsilon_2$ [-]
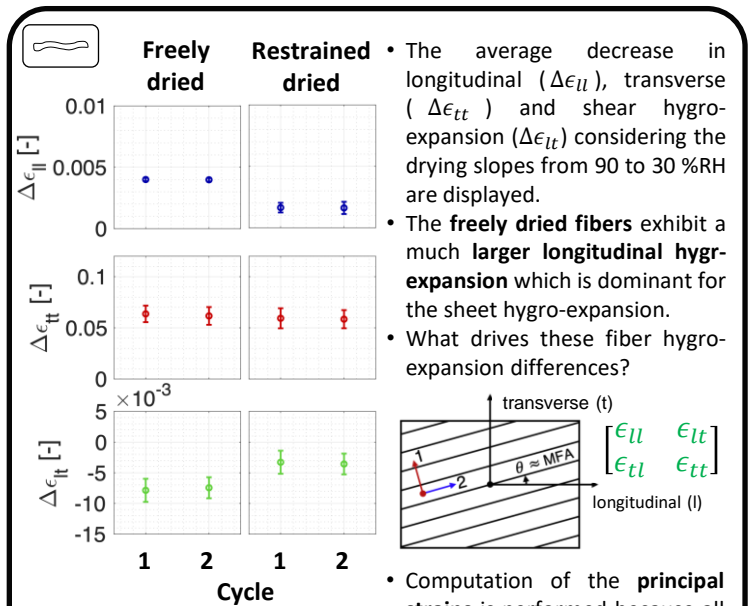
- The average decrease in longitudinal ($\Delta \epsilon_{ll}$), transverse ($\Delta \epsilon_{tt}$) and shear hygro-expansion ($\Delta \epsilon_{lt}$) considering the drying slopes from 90 to 30 %RH are displayed.
- The **freely dried fibers** exhibit a much **larger longitudinal hygr-expansion** which is dominant for the sheet hygro-expansion.
- What drives these fiber hygro-expansion differences?

transverse (t)

$\begin{bmatrix} \epsilon_{ll} & \epsilon_{lt} \\ \epsilon_{tl} & \epsilon_{tt} \end{bmatrix}$

$\theta \approx$ MFA

longitudinal (l)
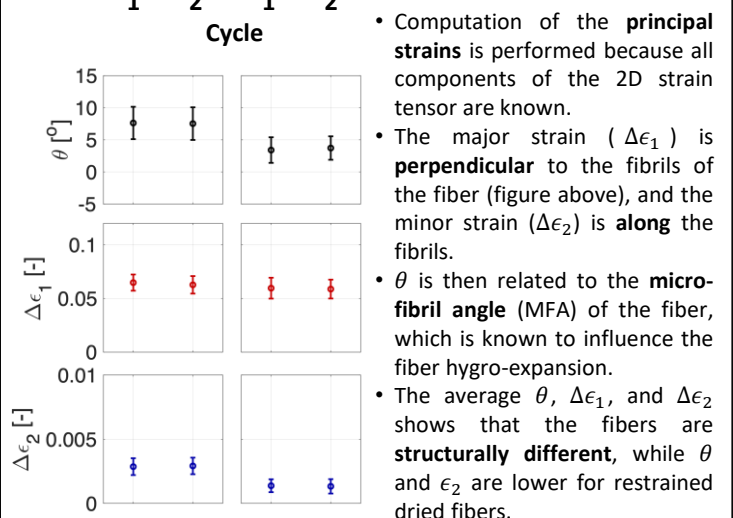
- Computation of the **principal strains** is performed because all components of the 2D strain tensor are known.
- The major strain ($\Delta \epsilon_1$) is **perpendicular** to the fibrils of the fiber (figure above), and the minor strain ($\Delta \epsilon_2$) is **along** the fibrils.
- θ is then related to the **micro-fibril angle** (MFA) of the fiber, which is known to influence the fiber hygro-expansion.
- The average θ, $\Delta \epsilon_1$, and $\Delta \epsilon_2$ shows that the fibers are **structurally different**, while θ and ϵ_2 are lower for restrained dried fibers.

The fiber hygro-expansion is different!

[3] N.H. Vonk et al. 17th fundamental research symposium 2022

Canon
CANON PRODUCTION PRINTING

PhD progress
1 2 3 4

TU/e

NWO
Nederlandse Organisatie voor Wetenschappelijk Onderzoek

Additive manufacturing of concrete: a dynamic analysis

Karlijn van Voorthuizen, M.I. Abdul Rasheed, J.P. Schilder, B. Rosić

Chair of Applied Mechanics & Data Analysis, University of Twente

Introduction

3D printing of concrete provides a greater design freedom compared to traditional methods such as casting. Currently, the printing process is limited by the interlayer time, which influences the interlayer strength. On-site manufacturing of large products with the desired interlayer time can thus be achieved by printing with multiple mobile manipulators instead of one stationary robot. To ensure precision and good part quality, the motion of the end-effector must not deviate from the desired trajectory (e.g. due to undesired vibrations caused by the pumping system). Therefore, the end-effector motion must be modelled and further assimilated with sensing data to improve the quality and predictability of the concrete 3D printing process.

Research aim

Modelling of the mobile manipulators in combination with the transportation of the non-homogeneous concrete from the reservoir to the nozzle, to enable the analysis and prediction of the end-effector motion.
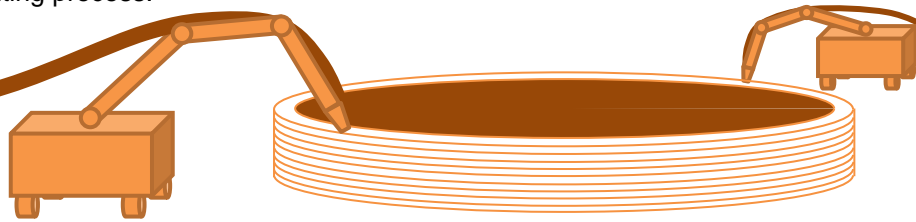
Floating frame of reference formulation

The movement of the manipulators consists of large (non-linear) rotations and small elastic deformation, which can be modelled by the floating frame of reference formulation:

- Rigid body motion is described as global floating frame coordinates $\{r_j^{OO}, R_j^O\}$.
- Elastic displacement is described locally as a set of orthogonal mode shapes which can be reduced.

By transforming the equations of motion to global interface coordinates (Eq. below), complex kinematic constraints are simplified. However, the transformation matrices (T_j and T_B) strongly depend on the definition of the floating frame. Therefore, these are further investigated.

$$\begin{bmatrix} \delta q_j^{OO} \\ \delta q_B^{jj} \end{bmatrix} = \begin{bmatrix} [R_j^O] T_j [\bar{R}_O^j] \\ T_B [\bar{R}_O^j] \end{bmatrix} \delta q_B^{OO} \quad \text{with} \quad T_B = 1 - \Phi_{rig,B} T_j$$

P_O - Origin
P_j - Floating frame
P_i - Material point
$[\cdot]_m^{kl}$ - Vector from l to m expressed in k
R_l^k - Rotation matrix from k to l
$\Phi_{rig,B}$ - Rigid body modes in the boundary nodes
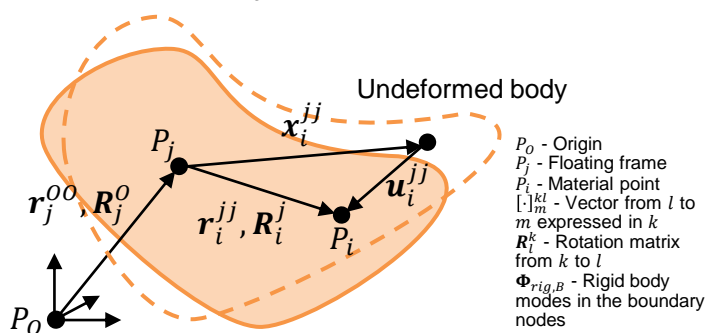
Reference conditions

In this work, four different reference conditions are considered: defining the floating frame as

- attached to one interface coordinate [1] : $\delta q_j^{OO} = \delta q_{B_i}^{OO}$;
- a weighted average of the interface coordinates [2]: $\delta q_j^{OO} = \sum_i \alpha_i \delta q_{B_i}^{OO}$;
- attached to the node in the center of mass of the undeformed body [3]: $\Phi_{CB,j} \delta q_B^{jj} = 0$;
- co-rotational [4]: $\delta r_j^{OO} = \delta r_{B_1}^{OO}$ and $\left(R_j^O\right)_x = \frac{r_{B_2}^{OO} - r_{B_1}^{OO}}{\left|r_{B_2}^{OO} - r_{B_1}^{OO}\right|}$.

By applying the reference conditions as kinematic constraints to a general system of equations, the relation between the methods is examined.

Interface node   **Weighted average**

Center of mass   **Co-rotational**
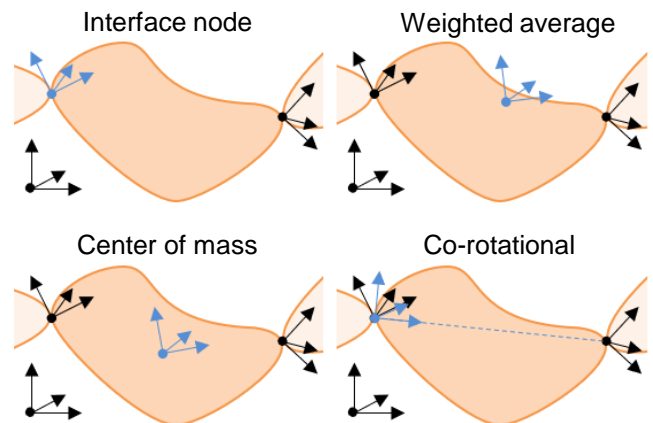
Take away

To model the mobile manipulators using the floating frame of reference formulation, a definition of the floating frame must be selected. To do so, differences between the formulations will be examined.

Contact information

✉ k.l.vanvoorthuizen@utwente.nl
in www.linkedin.com/in/karlijn-van-voorthuizen

References

[1] A. Cardona and M. Géradin. A superelement formulation for mechanism analysis. Computer Methods in Applied Mechanics and Engineering, 100(1):1–29, 1992.
[2] Alberto Cardona. Superelements modelling in flexible multibody dynamics. Multibody System Dynamics, 4:245–266, 08 2000.
[3] Marcel Ellenbroek and Jurnan Schilder. On the use of absolute interface coordinates in the floating frame of reference formulation for flexible multibody dynamics. Multibody System Dynamics, 43, 07 2018.
[4] M.A. Crisfield. A consistent co-rotational formulation for non-linear, three-dimensional, beam-elements. Computer Methods in Applied Mechanics and Engineering, 81(2):131–150, 1990.

UNIVERSITY OF TWENTE.

PhD progress

| 1 | 2 | 3 | 4 |

Gaussian Process Simulation of Nonlinear History Dependent Material Model

D.Wadadar[1], I.B.C.M. Rocha[1], F.P. van der Meer[1]

[1] Applied Mechanics, Delft University of Technology

Introduction

Owing to extreme computational effort associated with computing a nested micromodel at every macroscopic integration point, concurrent multi-scale analysis, though powerful and accurate, becomes restrictive and lacks general applicability. A fast and efficient reduced order framework is required to replace the high-fidelity micromodels.

Reduced Order Model: GP

Our goal is to create an efficent surrogate model based on Gaussian Process (GP) that can replace the nested micomodel.
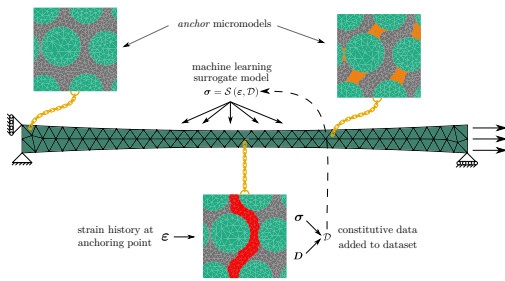
Figure 1: Online Adaptive Reduction Framework, Rocha et al.(2020)

GP: Unloading Problem

The problem of using a traditional GP based model for this purpose is that it assumes a unique mapping between stress and strain which is inaccurate for unloading scenarios.
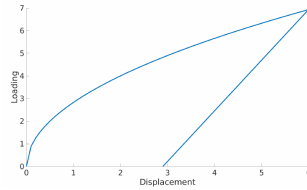
Figure: Input Loading-Unloading Curve
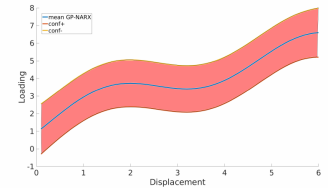
Figure: Standard GP prediction

Figure 2: The GP-based surrogate fails to capture unloading

Non-Linear State Space Model: GP-SSM

Integrating GP within a state-space model (GP-SSM) allows for a more accurate approximation of the solution for highly nonlinear non-monotonic load paths including unloading-reloading behavior.The main algorithm uses Variational Inference which leads to a tractable approximate posterior over nonlinear dynamical systems.
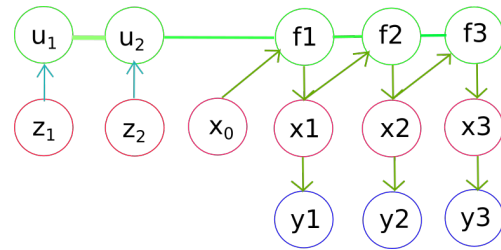
Figure 3: Graph Model for GP-SSM

Learning in GP-SSM
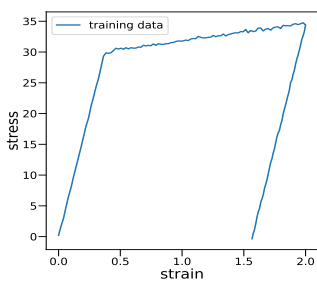
Figure 4: Training curve
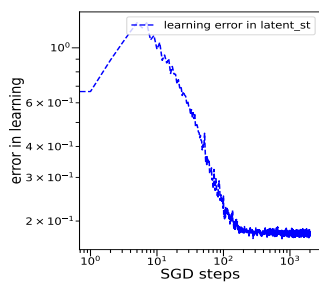
Figure 5: Convergence in learning-error
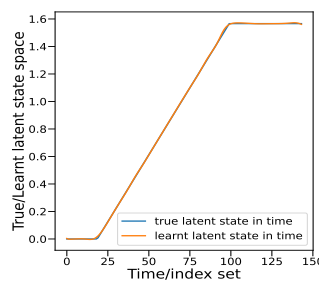
Figure 6: Multi-step ahead latent state prediction
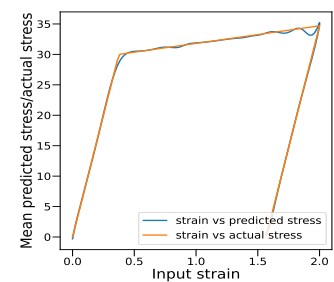
Figure 7: Multi-step ahead stress prediction

Forecasting in GP-SSM
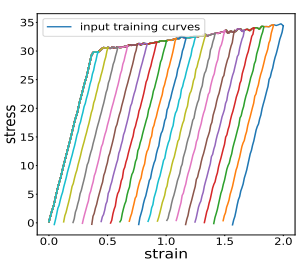
Figure 8: Training curves
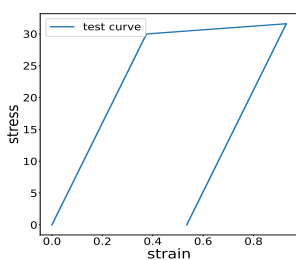
Figure 9: Test curve
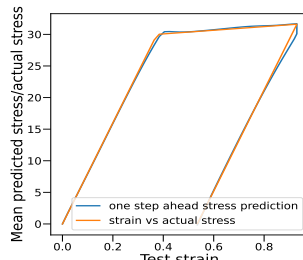
Figure 10: One-step ahead stress prediction
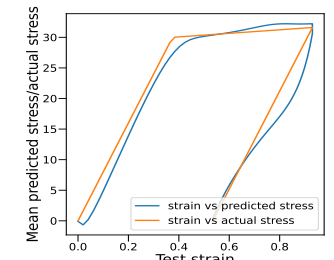
Figure 11: Multi-step ahead stress prediction

PhD progress

| 1 | 2 | 3 | 4 |

Computational Fluid Dynamics of Flows Around Rigid Cylinders: a Comparative Study

C. Wang[1], A.E.P Veldman[2] , E J. Stamhuis[3], B. Jayawardhana[4], A.I. Vakis[1]

[1]CMME-ENTEG-FSE, University of Groningen
[2]CMNM-BI-FSE, University of Groningen
[3]Biomimetics-ESIRG-FSE, University of Groningen
[4]DTPA-ENTEG-FSE, University of Groningen

Introduction

Ocean Grazer (OG) is a novel hybrid renewable energy device combining adaptable Wave Energy Converter (WEC) technology with on-site energy storage and wind turbines. As a component of the mooring system between the WEC and the storage system, cables play an important role in the device, as shown in Fig. 1 [1].

Vortex induced vibrations (VIVs), shown in Fig.2, are generated by flows around subsea cables and may cause damaging vibrations of structures, potentially leading to decreased energy harvesting efficiency and even fatigue damage.

Computational fluid dynamics (CFD) is one of the most common methods used for establishing reliable models to understand and predict VIV behavior and, together with suitable experimental validation, is the main tool used in this project.

Background

Fig. 2 von Karman street [2]

The Reynolds number (Re) helps predict flow patterns in different fluid flow situations. A high Re flow will increase the vortex shedding frequency and the hydrodynamic force on cables, and generally increase the amplitude and frequency of the cable VIV. The Re for the studied cable connections is in the so-called 'drag crisis' regime, which makes CFD calculations especially challenging.

Model setup
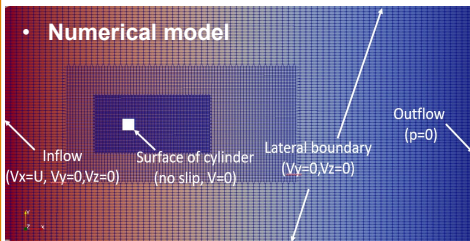
- **Numerical model**

Fig. 3 Domain of 2D numerical model

Firstly, a series of 2D simulations of flow around a fixed square cylinder under different Re have been performed to verify the reliability of CFD in VIVs.

- **Experimental model**

To validate the CFD simulations, experiments using Particle Image Velocimetry (PIV) were carried out with a circular cylinder at varying Re.
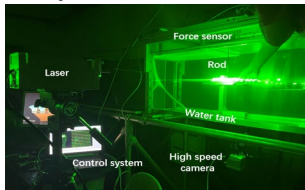
Fig. 4 PIV experiments setup*

*The experiments were conducted in the lab of Biomimetics group | Energy and Sustainability Research Institute Groningen

Fig. 1 Sketch of the OG-WEC system [1]

Results and discussion

To evaluate the results, the drag and lift coefficients, as well as the Strouhal number (St) were calculated for different low to moderate Re, as shown in Fig. 4.
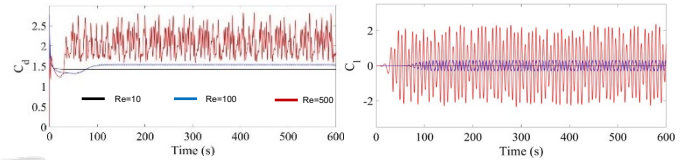
Fig. 4 Drag & lift coefficient of 3 different Re

At high Re, oscillations dominate the flow while, at low Re the oscillations are dampened by the viscous fluid.
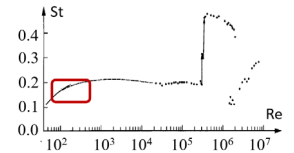
Fig. 5 St for a smooth cylinder [3]
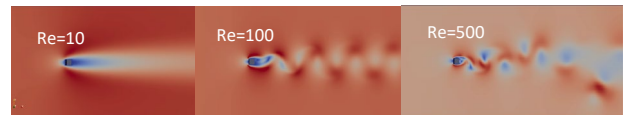
Fig. 6 Velocity at Re10, 100, 500 predicted by simulations

With the emergence of flow developing around a cylinder, at Re=10, there was no oscillation while, at Re=100, the oscillation was dominated by a single frequency. At Re=500 more frequencies were present, marking the start of a gradual transition from laminar to turbulent flow.
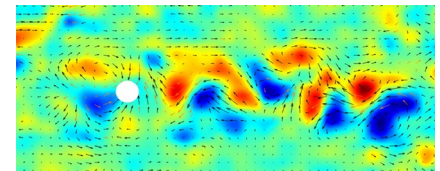
Fig. 7 Velocity at Re500 given by experiments

Preliminary experimental results showed a similar velocity distribution to that from the CFD simulation.

Further work

- Perform numerical simulations with circular cylinder at higher Re
- Set up numerical models to simulate flow around a flexible cable
- Use experimental methods to investigate the characteristics of multiple cables, to understand how the VIVs influence other cables and the efficiency of energy harvesting

References

[1] Wei Y., Bechlenberg A., Van Rooij M., Jayawardhana B., Vakis A.I. Modelling of a wave energy converter array with a nonlinear power take-off system in the frequency domain. Applied Ocean Research 90, 101824 (2019).
[2] Lacaze, L., A. Paci, E. Cid, S. Cazin, O. Eiff, J. G. Esler, E. R. Johnson et al. "Theodore von Kármán, Aerodynamics." (1963).
[3] Sumer, B. Mutlu. Hydrodynamics around cylindrical strucures. Vol. 26. World scientific, 2006.

PhD progress
1 2 3 4

Auto-Adapting Multi-Element Polynomial Chaos Expansion

B.P. van de Weg[1,2], Prof. B. Rosic[2]

[1]*Volkswagen AG*

[2]*Applied Mechanics and Data Analysis, Faculty of Engineering Technology, University of Twente*

Introduction

The use of real time surrogate models in optimization has become an appealing alternative to the straightforward use of finite element method (FEM). The main purpose of the surrogate-model is thus to learn the correlation between given response FEM data samples to the corresponding parameter set (Fig. 1).
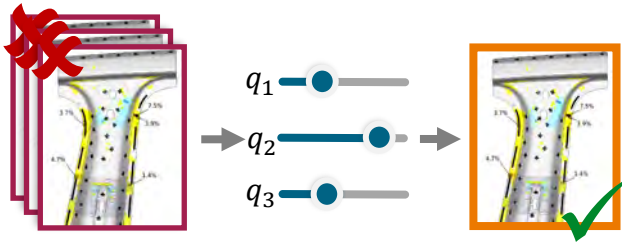
Figure 1. Interactive optimization using a surrogate model.

In this work we propose a novel nonlinear **Automatic Relevance Determination** (ARD) [1] scheme used to estimate the nonlinear surrogate model obtained by combining Multi-Element **Polynomial Chaos Expansion** (PCE) [2,3,4] (Fig. 2), **Proper Orthogonal Decomposition** (POD), and a **Long short-term Memory** (LSTM) neural network [1]. The proposed scheme automatically finds the weights by the use of L1-induced priors in identifying weight relevance. We propose domain separation to describe the time, spatial and stochastic domain in a robust and generally applicable sense.
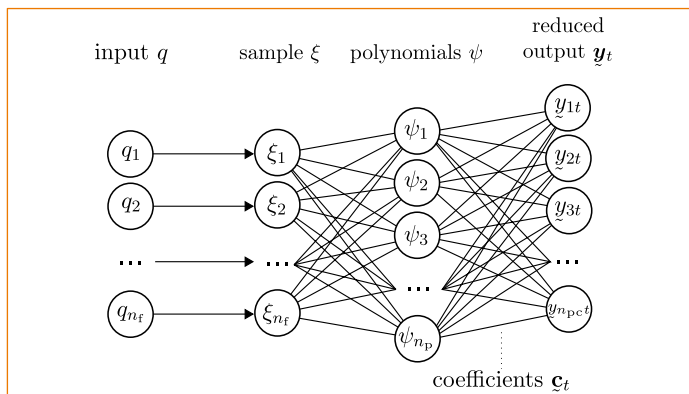
Figure 2. ARD-PCE framework overview, adapted from [2].

Objectives

- Minimize optimization time.
- Separate & sparse domain representation
- Minimize required user knowledge on surrogate architectures.
- General applicability auto-adapting surrogate framework
- Quantify the predictive uncertainty.

Approach

A generally applicable auto-adapting framework is developed that separates domains by (Fig. 3):

- **Spatial**: Proper Orthogonal Decomposition (POD) [5];
- **Stochastic**: ARD Polynomial Chaos Expansion (PCE) [2];
- **Time**: ARD Long Short-Term Memory (LSTM) neural network [1];

dependence.
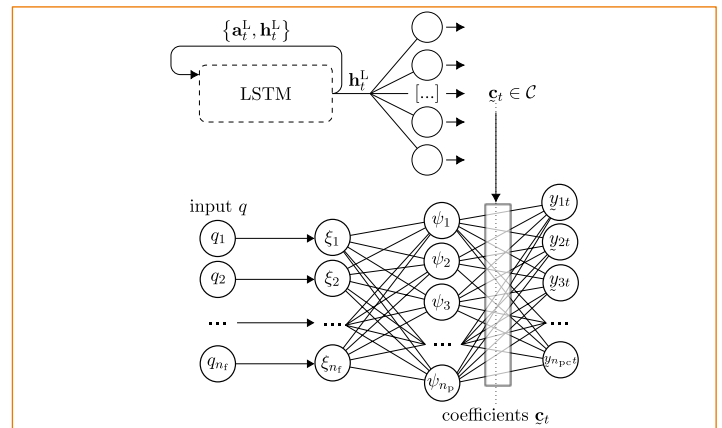
Figure 3. Domain separation overview: ARD-POD-PCE-LSTM, adapted from [2].

Sparse learning

① Transform the weight matrix $\mathbf{w}$ to a stochastic form:
$$\mathbf{w}(c) \rightarrow \mathbf{w}\big(p(\mu, \sigma)\big) = p(\mathbf{w}|\mathbf{y})$$

② For nonlinear models, define local target $\mathbf{s}$ from $\mathbf{y} := \sigma(\mathbf{s})$ for any continuous nonlinear function $\sigma(\cdot)$ and perform Bayesian inference on $\mathbf{s}$:
$$p(\mathbf{w}|\mathbf{s}) = \frac{p(\mathbf{s}|\mathbf{w})\, p(\mathbf{w})}{P(\mathbf{s})}$$
Where $\mathbf{s}$ is obtained by point estimation (stochastic gradient approach).

③ Obtain weights $\mathbf{w}$ by ARD in every iteration of the stochastic gradient approach.

④ Introduce sparsity in $\mathbf{w}$ using a hyperprior:
$$p(\mathbf{w}, \boldsymbol{\alpha}) = N(\mathbf{0}, \boldsymbol{\alpha}^{-1})G(\boldsymbol{\alpha})$$

References

[1] B.P. van de Weg, L. Greve and B. Rosic, Long short-term relevance learning, arXiv:2106.12694, 2021.
[2] B.P. van de Weg, L. Greve and B. Rosic, Sparse low-rank approximation for nonlinear bifurcating deformations [in progress]
[3] X. Dongbin, Numerical Methods for Stochastic Computations: A Spectral Method Approach, Princeton university press, 2010.
[4] O. P. Le Maître, O. M. Knio (Eds.), Spectral Methods for Uncertainty Quantification, Scientific Computation, Springer Netherlands, Dordrecht, 2010.
[5] K. Kunisch, S. Volkwein, Galerkin proper orthogonal decomposition methods for a general equation in fluid dynamics, SIAM Journal on Numerical analysis 40 (2) (2002) 492–515.

Isogeometric Analysis of an Electromechanical Bi-Ventricular Heart Model

R. Willems[1], C.V. Verhoosel[1], O. van der Sluis[1,2]

[1]*Eindhoven University of Technology*
[2]*Philips research*

Motivation and objective

Computer simulations provide information that can be used by clinicians to support decision-making (Computational-model-based decision support = COMBAT) regarding the treatment of **Ventricular Tachycardias** (VTs). It is the goal of this **COMBAT-VT** (*combatvt.nl*) subproject to develop efficient and robust models that can be integrated into the clinical workflow.

Simulation workflow

Our simulation framework combines the **Isogeometric Analysis** (IGA) simulation paradigm [1] with image recognition techniques to obtain **patient-specific** computer models (Fig. 1 & 2). Simulations will be performed directly on a Non-Uniform Rational B-Spline (NURBS) bi-ventricular geometry. Computational costs are improved because of the limited number of control points that quantify the geometry.

NURBS template
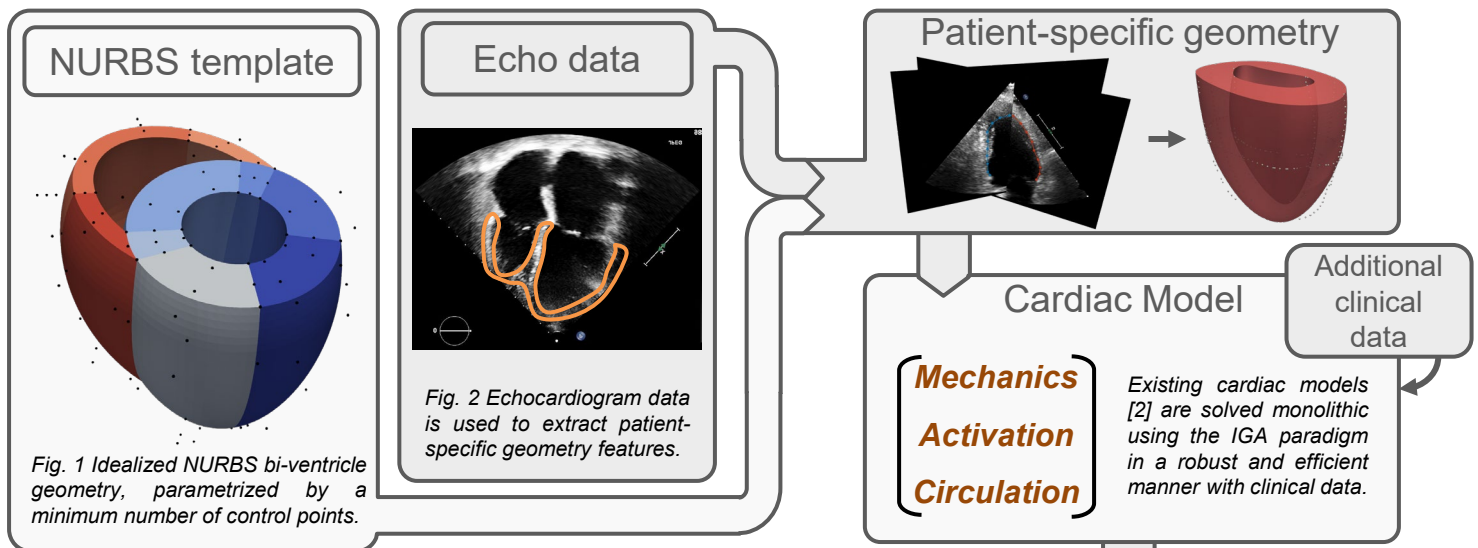
Fig. 1 Idealized NURBS bi-ventricle geometry, parametrized by a minimum number of control points.

Echo data

Fig. 2 Echocardiogram data is used to extract patient-specific geometry features.

Patient-specific geometry

Cardiac Model

Mechanics
Activation
Circulation

Additional clinical data

Existing cardiac models [2] are solved monolithic using the IGA paradigm in a robust and efficient manner with clinical data.

Results

Left-ventricle validation
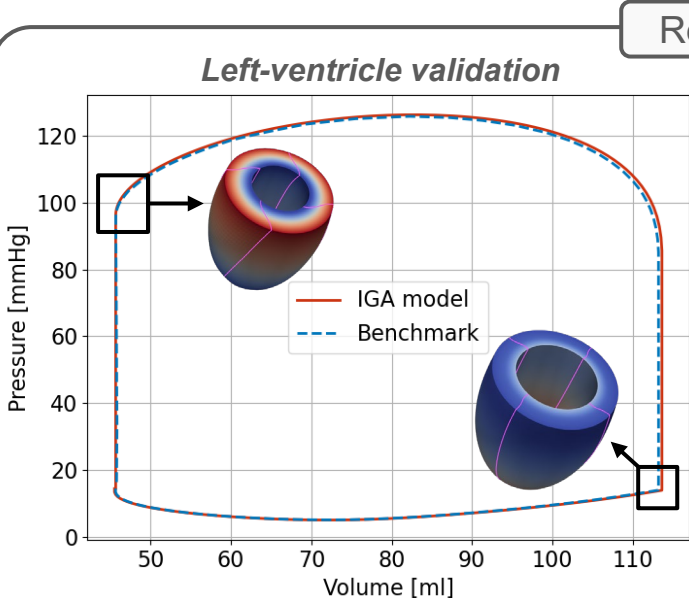
Fig. 3 Left-ventricle pressure-volume comparison between the developed IGA model (5000 degrees of freedom) and external (FEA) benchmark results (469 734 degrees of freedom) [2].

Fast geometry variations
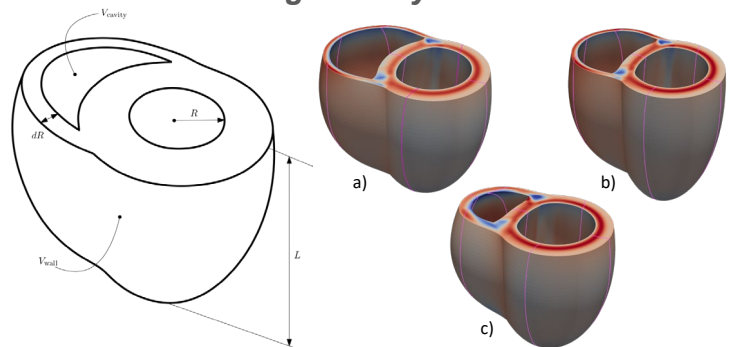
Project outlook

IGA has the potential to yield robust geometry and analysis models in the considered scenario of sparse input data. Future project steps focus on the automation of image-based geometry reconstruction, while extending the model functionality, validation (Fig. 3), and **clinical integration**. Attention will be given to parameter sensitivity and uncertainty quantification, which is essential for **VT prediction**.

VT Prediction

References

[1] Hughes, T. J. R. et al. (2005). *Isogeometric analysis: CAD, finite elements, NURBS, exact geometry and mesh refinement,* Comput. Methods in Appl. Mech. Eng., 194.39, 4135 - 4195.
[2] Bovendeerd, P. H. M. et al. (2009). *Determinants of left ventricular shear strain. Am J Physiol Heart Circ Physiol.* 297(3):H1058-68.

PhD progress
| 1 | 2 | 3 | 4 |

From particles to continuous fields:
Upscaling towards micropolar theory based on structure and rotation

M. Winkelmann[1], S. Luding[1], S. Papanicolopulos[2],
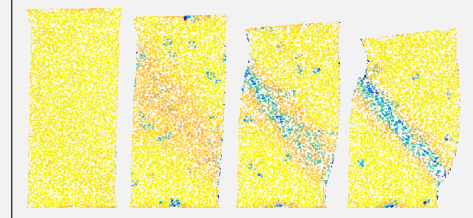V. Magnanimo[1], T. Weinhart[1,3], M. Sousani[4]
[1] *University of Twente,* [2] *University of Edinburgh*
[3] *MercuryLab,* [4] *EDEM Altair*

Motivation

- **Granular materials** are the second-most processed material in the world
- Particles are **discrete**, but **continuum fields** are needed for large applications

- Shear bands are based on **particle rotations** [1]; cannot be described with classic continuum theory
- **Micropolar theory** can represent microstructure and rotation of particles on continuum scale

Theoretical background

How to detect micropolar behaviour?

classic continuum   micropolar theory
$$\sigma = \sigma^\mathsf{T} \qquad\qquad \sigma \neq \sigma^\mathsf{T}$$

$$\Rightarrow \mathrm{skw}\,\sigma = \sigma - \sigma^\mathsf{T} \neq \mathbf{0}$$

What is causing skew-symmetric stress on particle level?
Tangential contact forces can cause skew-symmetric stress through resistance against sliding, rolling and torsion. Proof? See here [2]:

$$\sigma = \underbrace{\sum_{i,j} \mathbf{f}_{ij} \otimes \mathbf{l}_{ij}\Phi(\mathbf{r}, \mathbf{r}_i\mathbf{r}_{ij})}_{\text{contact stress}} - \underbrace{\sum_i m_i \mathbf{v}'_i \otimes \mathbf{v}'_i\Phi(\mathbf{r}, \mathbf{r}_i)}_{\text{kinetic stress}}$$

$$\Rightarrow \textbf{skew-symmetric} \qquad \Rightarrow \text{symmetric}$$

$$\mathbf{f} = \mathbf{f}^{\text{normal}} + \mathbf{f}^{\text{tangential}}$$
sliding, rolling, torsion

How are sliding, rolling and torsion exactly influencing the stress? Parameter study!

Preliminary results: Chute flow

stress ratio over the flow height
contact model: normal + sliding, $H = 10$
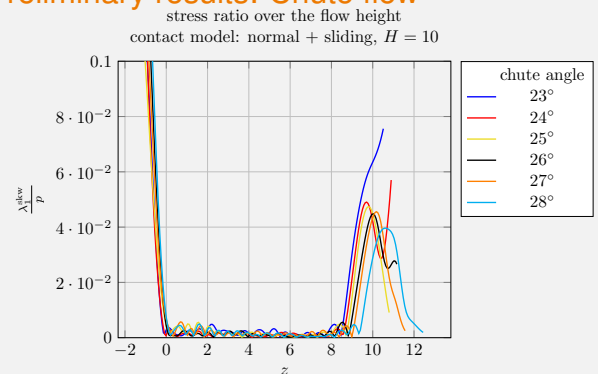
- Independent from chute angle and filling height
- Skew-symmetric stress only outside the flow
  $\Rightarrow$ Influence of sliding negligible
- Study on rolling and torsion ongoing

Challenges

- How does rolling resistance effect the flow and (couple) stress?
- In what other situations does micropolar behaviour gets activated?
- How to evaluate skew-symmetric stress?
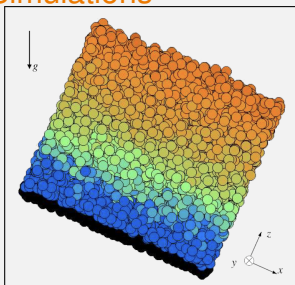- How to show that in a real lab experiment?

Simulations

chute flow [2]

cartesian shear cell [3]

Outlook

1. Study on micropolar behaviour
2. Implement new micropolar fields
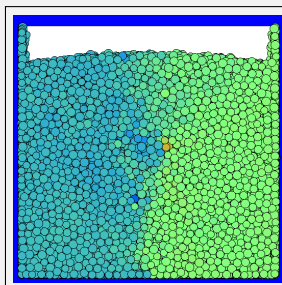3. Study non-spherical particles
4. Application to shear bands

References

[1] R. Kawamoto, **2018**, J Mech Phys Solids, 111:372–392.
[2] T. Weinhart *et al.*, **2012**, Granular Matter, 14:531–552.
[3] S. Roy *et al.*, **2018**, Physical Review E, 98, 052906.

UNIVERSITY OF TWENTE.   THE UNIVERSITY of EDINBURGH   **Mercury**Lab   PhD progress 1 2 3 4   ALTAIR   tusail

Effect of strain hardening on the bending capacity of welded I-section high-strength steel beams

W.J. Wong, C.L. Walters

Department of Maritime and Transport Technology
Delft University of Technology

Introduction

High-strength steel beams are known to have less plastic rotation capacity R (Eq. (1); Fig. 1) than beams with lower yield strengths. This has been related to the decreased strain-hardening ability of high-strength steels [1]. Various rules and standards for steel structures therefore stipulate maximum limits on the allowable yield-to-tensile strength (σ_y/σ_u) ratio of the steel, which indirectly acts as a measure of strain hardening. While the literature suggests that there is an interdependence between rotation capacity, yield strength, strain hardening ability and cross-sectional slenderness [1], the presently prescribed limits on σ_y/σ_u (e.g. 0.91, 0.94 or 0.95) are typically constant for a given material even when used in different situations. This computational study [2] investigates how the rotation capacity is dependent on the aforementioned parameters simultaneously and how better rules could hence be formulated.

Method

Finite element parametric studies accounting for material and geometrical nonlinearities, residual stresses from welding (Fig. 2) and geometrical imperfections (Fig. 3 left) were performed. Material parameters σ_y and σ_y/σ_u and geometric parameters B, H, t_f, and t_w (Fig. 2) were varied, and the effects on the rotation capacity R (Eq. (1); Fig. 1) were plotted with relation to the flange, web and overall cross-sectional slendernesses ($\lambda_f, \lambda_w, \lambda_p$ respectively). The results were used to make comparisons against existing limits in the IACS UR I Requirements for Polar Class [3].

$$R = \theta_{rot}/\theta_{pl} - 1 \qquad (1)$$
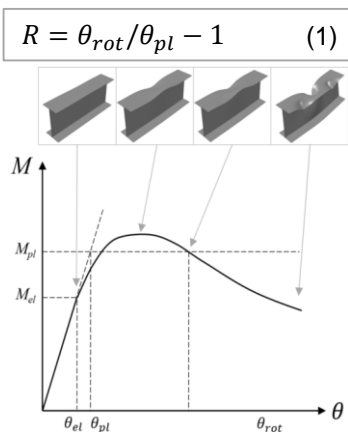
Fig. 1: Moment-rotation curve.
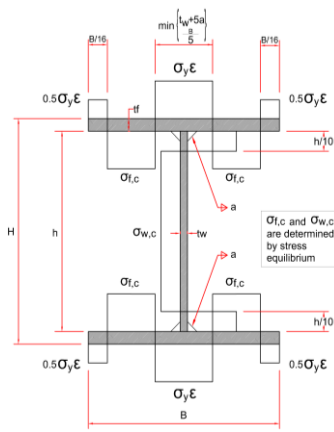
Fig. 2: Residual stress [4].
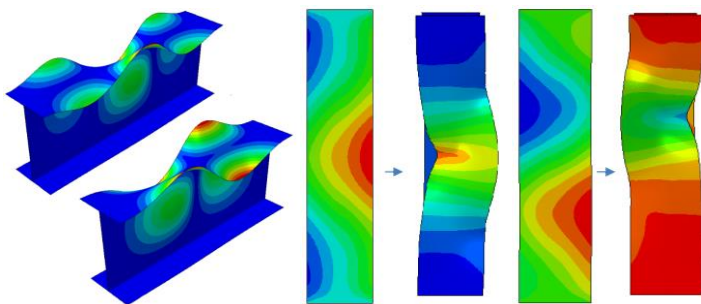
Fig. 3: Linear elastic buckling shapes (left) and plastic buckling shapes (right).
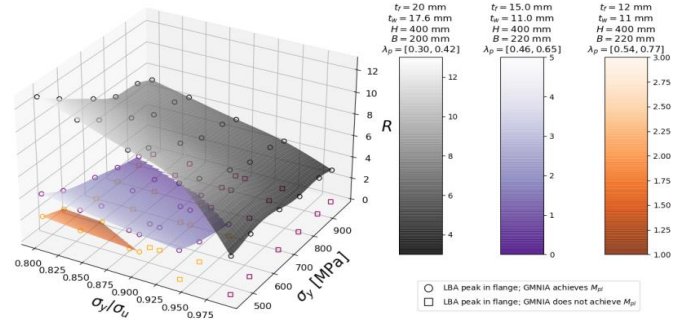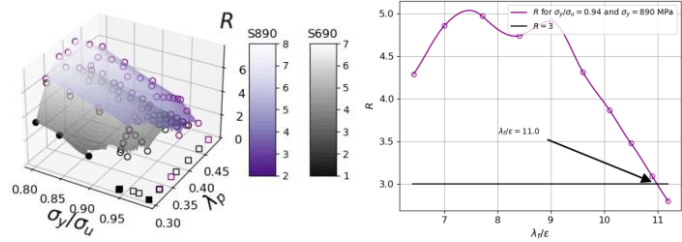
Results

Fig. 4: R against σ_y and σ_y/σ_u.

Fig. 5: R-σ_y/σ_u-λ plot for $t_f = 20$ mm; $t_w = 17.6$ mm; $\lambda_w = 40.0\varepsilon$.

Figs. 4 and 5 show the interdependence between R, σ_y, σ_y/σ_u, overall cross-section slenderness λ_p and flange slenderness λ_f/ε, where $\varepsilon = \sqrt{235 \text{ MPa}/\sigma_y}$, $\lambda_f = (B - t_w)/(2t_f)$ (Fig. 2) $\lambda_p = \sqrt{M_{el}/M_{cr}}$, with M_{el} being the elastic moment and M_{cr} the linear elastic buckling moment. Furthermore, the results suggest that the changes in the trend relating R and λ_f (Fig. 5; right) correlate to changes in the buckling mechanism (Fig. 3; right). The key conclusions are summarized below.

Conclusions

1. A holistic determination of the safety of steel beams with high σ_y/σ_u would depend on desired rotation and specific geometries due to the interdependence between R, σ_y, σ_y/σ_u and λ.

2. For a fixed σ_y/σ_u ratio, cross-sectional slenderness and lateral-torsional buckling slenderness, a higher σ_y leads to higher rotation capacities. This suggests that introducing cross-sectional slenderness limits that are dependent on both the σ_y and σ_y/σ_u, instead of a constant σ_y/σ_u limit could be beneficial.

3. The trend between the rotation capacity and the cross-sectional slenderness depends on the relative slendernesses of the web and the flange and whether the buckling is web- or flange-dominated. Increasing the flange stockiness by decreasing the flange width for a beam that is experiencing web-dominated buckling does not help to increase the rotation capacities but instead decreases it.

4. Future work: Hinge-line analysis of appropriate collapse mechanisms should be used to corroborate these findings.

References

[1] Pavlovic M, Veljkovic M. (2017) In: *Proceedings of the Institution of Civil Engineers 170 SB11:825-840.*
[2] Wong WJ, Walters CL. (2022) Accepted conference submission. (The effect of strain hardening on the bending capacity of high-strength welded I-section beams.) *International Conference on Ships and Offshore Structures (ICSOS) 2022* .
[3] IACS (International Association of Classification Societies). (2019) *IACS UR I Requirements concerning polar class.*
[4] Schaper L, Tankova T, Simões da Silva L, Knobloch M. (2022) *Journal of Constructional Steel Research.188.*

PhD progress
1 | 2 | 3 | 4

Space-time Topology Optimization Considering Material Anisotropy

Kai Wu[1], Weiming Wang[2], Fred van Keulen[1], Jun Wu[1]

[1]Delft University of Technology, Netherlands
[2]Dalian University of Technology, China

Introduction

Topology optimization (TO) is now widely adopted in structural design for additive manufacturing (AM). Specifically, space-time TO[2] was proposed to optimize structural layout and fabrication sequence simultaneously.

Manufacturing induced material anisotropy is common to see in AM, *e.g.*, stainless steel produced by wire and arc additive manufacturing (WAAM). Its Young's modulus depends on material deposition direction (Fig. 1).

In this paper, we incorporate elastic anisotropy into space-time TO, which is a natural extension since the material deposition direction is dependent on the fabrication process.
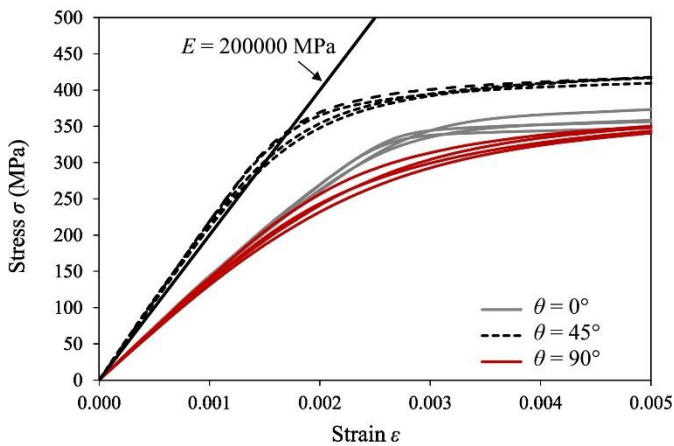
Figure 1: Elastic anisotropy of stainless steel in WAAM[1]

Optimization model

Space-time TO employs a density field ρ to represent the structural layout, and a time field t to encode the fabrication sequence, as can be seen in Fig. 2.

The material deposition direction θ is orthogonal to the gradient of the time field t pointwise.
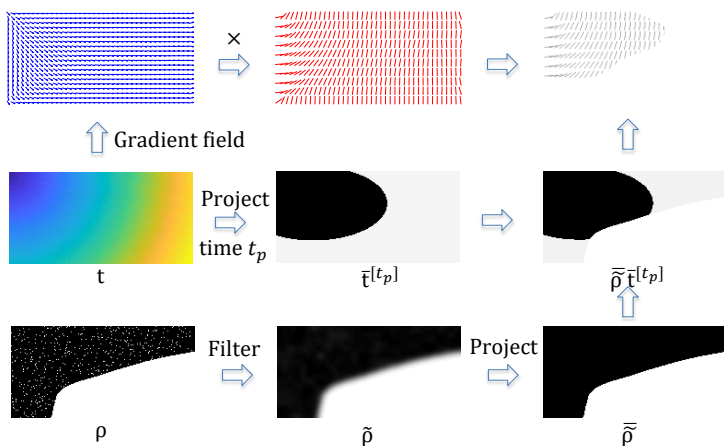
Figure 2: Illustration of space-time TO considering material anisotropy

Numerical example

The optimization result of a cantilever beam is shown in Fig. 3. The gradient of the optimized time field and the optimized material orientation are orthogonal with each other pointwise. The structural stiffness is improved by 26.0%, compared to that fabricated in planar sequence.
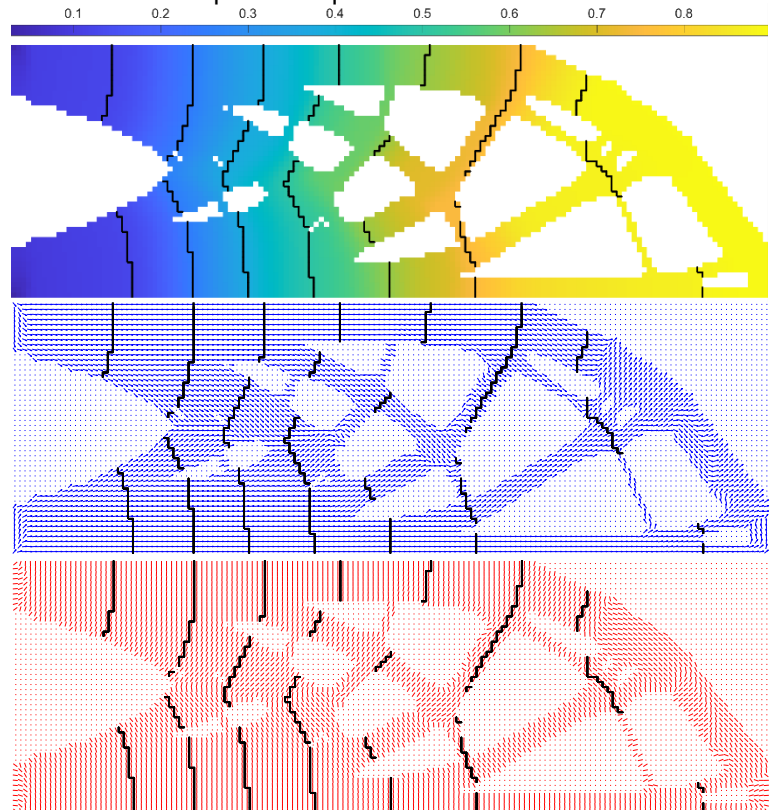
Figure 3: Upper: optimized structural layout and fabrication sequence, Middle: gradient of the optimized time field, Lower: material deposition orientation

Conclusions

1. Material elastic anisotropy can be derived directly from the time field in space-time TO.
2. By taking advantage of elastic anisotropy, structural stiffness during and after fabrication can be improved.

Future work

1. Derive the continuous tool-path automatically.
2. Incorporate strength anisotropy into space-time TO.

References

[1] Pinelopi Kyvelou, Harry Slack, Dafni Daskalaki Mountanou, M. Ahmer Wadee, T. Ben Britton, Craig Buchanan, Leroy Gardner. (2020). Mechanical and microstructural testing of wire and arc additively manufactured sheet material. Materials & Design 192, 108675.
[2] Wang, Weiming, Munro, Dirk, Wang, Charlie C. L., van Keulen, Fred, Wu, Jun. (2020). Space-time topology optimization for additive manufacturing. Structural and Multidisciplinary Optimization, 61(1), 1-18.

TUDelft

PhD progress
1 2 3 4

Quantum and machine learning methods for stacking retrieval of laminated composite materials

Arne Wulff, Boyang Chen

*Aerospace Structures and Materials,
Delft University of Technology*

The lay-up optimization problem

A common approach for the design of **composite laminates** is the use of **lamination parameters**, which allow to optimize towards the desired material characteristics in a two-step approach: First a gradient-based continous optimization of the lamination parameters, followed by finding a stacking sequence that approximates the obtained set of parameters (Fig. 1). This **stacking sequence retrieval** is a combinatorial problem, which is generally hard and usually the bottleneck of this procedure. However, emerging fields like **quantum computing** and **machine learning** might have the potential to accelerate this process.

Quantum computing and machine learning methods

There are various approaches that might show promise in solving combinatorial optimization problems. These different approaches can be viewed separately, but there are also intersections where the different methods might profit from each other when used conjointly (Fig. 2). A selection:

Variational algorithms are the most widely studied algorithms for near-term quantum (NISQ) devices [2]. The problem is encoded as a Hamiltonian on the qubits, such that the ground state corresponds to the solution of the problem. A parameterization of the state space with a parameterized quantum circuit then allows the minimization of the energy expectation value.

Quadratic unconstraint binary optimization aim to minimize problems of the form [3]

$$\min_{x} x^T Q x, \qquad x \in \{0,1\}^n$$

where Q is a symmetric matrix. A QUBO is equivalent to an Ising-model and can therefore by solved on a quantum annealer. It also has applications in QAOA.

Matrix product states and **tensor network states** can restrict the number of variables that are needed to describe a state. They have shown to be a powerful tool in finding the ground state of large many-body systems with classical computation. These methods might also be applicable for combinatorial problems [4].

Quantum random walks and **quantum genetic algorithms** are believed to show speed-ups over their classical counterparts. Since the stacking retrieval is traditionally done with genetic algorithms, these methods should also be considered [5].

Machine learning methods might gain some speed-up from quantum computing, but many aspects in quantum computing, such at algorithm design, qubit routing and resource reduction might also benefit from classical machine learning methods. Machine learning should thus be considered when investigating the other approaches.
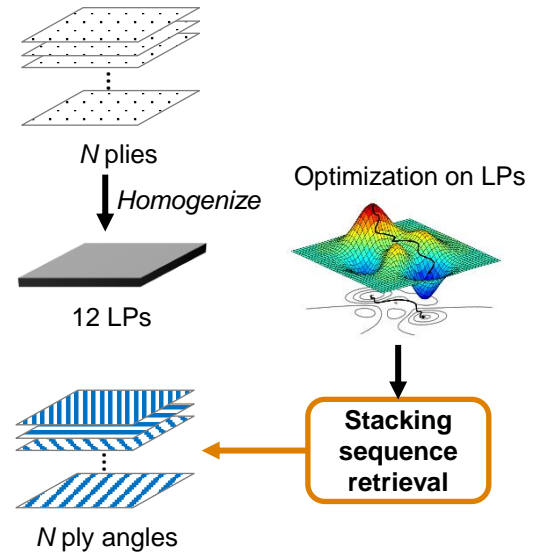

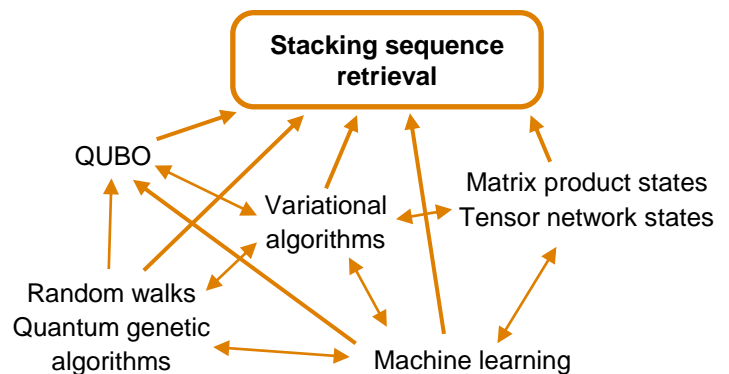Figure 1: Laminate optimization using lamination parameters.

Figure 2: Stacking retrieval might benefit from different methods in quantum computing and machine learning.

References

[1] S.W.Tsai, H.T.Hahn, *Introduction to composite material*s, Technomic Pub. (1980)

[2] K.Bharti *et al.*, *Noisy intermediate-scale quantum algorithms*, Rev. Mod. Phys. **94**, 015004 (2022)

[3] G.Kochenberger et al., *The unconstrained binary quadratic programming problem: a survey*, J. Comb. Optim. **28**, 58–81 (2014)

[4] T.Hao *et al.*, *A quantum-inspired tensor network method for constrained combinatorial optimization problems*, arXiv:2203.15246 (2022)

[5] A.Ambainis, *Quantum walks and their algorithmic applications*, Int. J. Quantum Inf. **1** (4), 507–518

Multiscale Extended Finite Element Method for the Simulation of Cracks Propagation in Fractured Geological Formations

Fanxiang Xu[1], Hadi Hajibeygi[2], Lambertus J. Sluys[1]

[1] Department of Materials, Mechanics, Management & Design, TUD
[2] Department of Geoscience & Engineering, TUD

Challenges

Underground formations are often highly fractured. When the in-situ stress state changes, these fractures may slide and propagate which can lead to disastrous consequences (Fig.1). An efficient and accurate numerical method to simulate complicated fracture networks is essential in order to prevent risks.
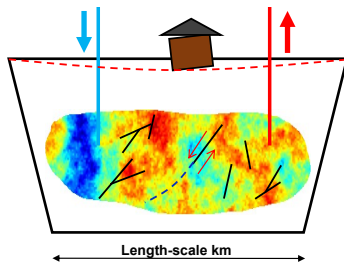
Figure 1: Subsidence as a result operation in fractured formation.

MS-XFEM for Fractures Propagation

In MS-XFEM, the displacement on a fine-scale mesh can be approximated using the result computed on a coarse-scale mesh:

$$d_{f,MS} = P \cdot d_c = P \cdot \underbrace{\left(P^T \cdot K_f \cdot P\right)^{-1}}_{K_c} \cdot \underbrace{\left(P^T \cdot f_f\right)}_{f_c} \qquad (1)$$

where, P is the basis function matrix, d_c is the coarse scale mesh result and $d_{f,MS}$ is the approximate fine scale mesh result. The coarse scale stiffness matrix K_c is constructed based on the fine scale stiffness matrix K_f.
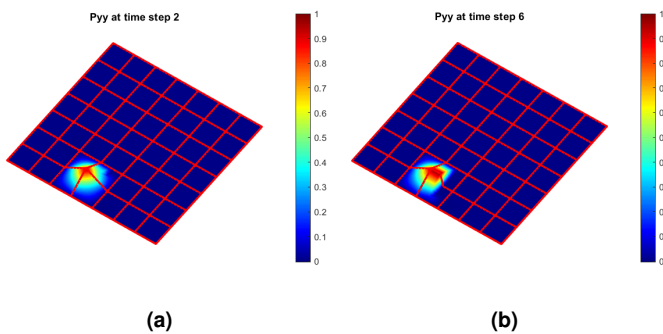
Figure 2: Update of basis functions that captures the propagation of a fracture.

In MS-XFEM, the discontinuities are included in the basis functions. Thus, there are no extra DOFs on coarse scale mesh. When the propagation of fractures occurs, the basis function P is also updated locally to capture this extension (Fig. 2).

An iterative strategy is then used to improve the quality of the final solution to any desired level.

Result

A homogeneous sandstone test case under tensile loading is investigated (Fig. 3). The Young's modulus is $25[GPa]$ and the Poisson's ratio is 0.2. Fracture toughness $k_c = 1.4 \times 10^6 [Pa \cdot m^{-\frac{1}{2}}]$. The size is $10[m] \times 10[m]$. The fine scale mesh is 49×49 and the Coarse scale mesh is 7×7. All four fractures have an initial length of $1[m]$. The fracture increment for each fracture is $0.4[m]$. The results with tolerance of $\tau = 10^{-2}$ are compared to the fine scale XFEM results:
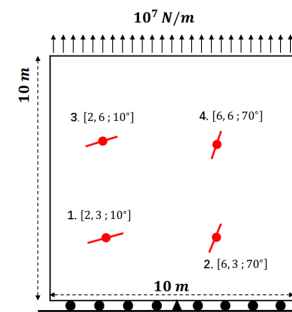

Figure 3: Test case setup.

The comparison between the MS-XFEM results and fine scale XFEM results is good as shown in Fig. 4.
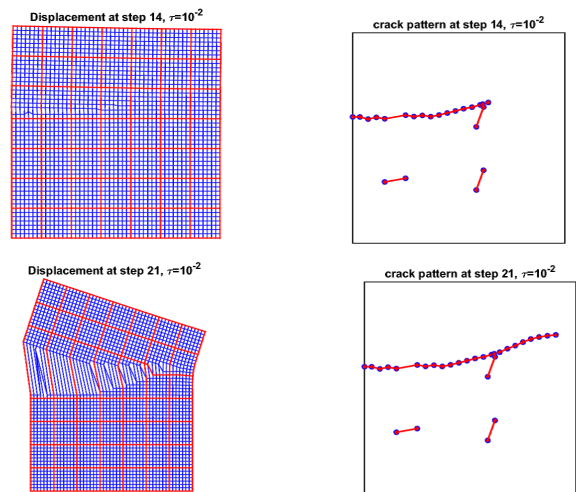

Figure 4: Displacement field and the crack pattern at time step 14 and time step 21. The tolerance used is $\tau = 10^{-2}$.

References

[1] F. Xu, H. Hajibeygi, L.J. Sluys. Iterative Multiscale Extended Finite Element Method (iMS-XFEM) for the Simulation of Multiple Cracks Propagation in Fractured Geological Formations.(In progress)

PhD progress

1 2 3 4

TUDelft

DARSim
Delft Advanced Reservoir Simulation

Implementation of a pyrolysis model in two-way coupled fire-structure simulations

Qingfeng Xu[1], Hèrm Hofmeyer[1], Johan Maljaars[1,2], Ruud A.P. van Herpen[1,3]

[1] Eindhoven University of Technology, Eindhoven
[2] TNO, Delft
[3] Peutz Consulting Engineers, Mook

Introduction

A sandwich panel façade system is a complex structure, which consists of components on different scales (as shown in Fig.1). When it is exposed to fire, currently our simulations can model (a) bolted connections and (b) screw connections using a two-scale method, verified by two experiments. However, (c) the composite core also plays an important role. Therefore, here a modelling approach is presented to predict the thermodynamical and thermomechanical behaviour of structures with composite material under fire, which takes into account the pyrolysis of the composite material and its effects on the overall structure, Fig. 2.
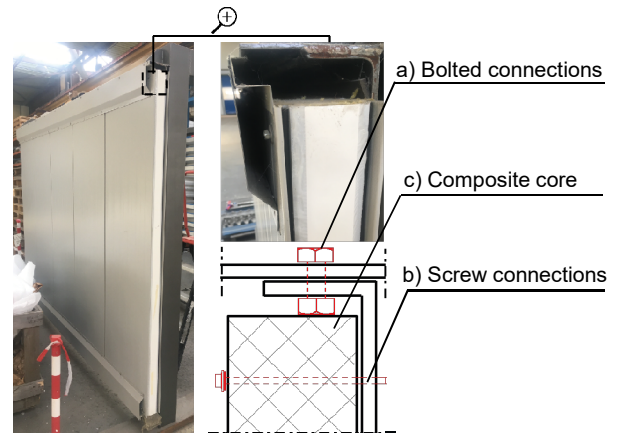
Fig.1 Components in a sandwich panel façade system

a) Bolted connections
c) Composite core
b) Screw connections

Methodology

CFD domain

1800 mm — 5400 mm — 1800 mm
3600 mm
2100 mm
2700 mm
Corridor
Compartment
Width   Burner
Adiabatic Surface Temperature (AST) points
Heat flux q_{total}

FDS (Fire Dynamic Simulator) fire compartment model

FEM domain

Temperature (T) transfer ...

Temperature distribution: composite core
Heat Transfer (HT) analysis **+** Pyrolysis model

FEM domain

T

Applying failure criterion and transferring the failure information

Next load step

Stress distribution – unexposed steel plate
Structural Response (SR) analysis **+** Pyrolysis model

Updated FDS model

etc.

Updated FEM model

Restart simulations with updated models, here failed plates (No. 5, 8, 9, 11) are removed

Fig.2 Overview of the pyrolysis model in a two-way coupled fire-structure simulation

Results and future work

o The pyrolysis reaction absorbs heat, resulting in lower temperatures, and subsequent delayed failures, Fig. 3.

o In a two-way coupled simulation, the effects of pyrolysis are significantly more important than the effects of structural failure on the fire.

❑ More complex thermo-chemical properties should be taken into account: e.g. expansion, viscoelasticity, delamination.

❑ The pyrolysis model should be combined with the modelling of bolt and screw connections, using the two-scale method.

Without pyrolysis model 200 s
With pyrolysis model 260 s

Number of failed plates
Time (s)
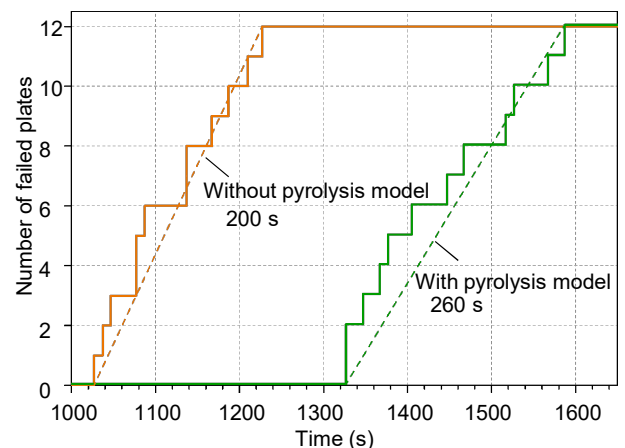
Fig.3 Progressive failure of plates

Nanoindentation creep behavior of supercrystalline nanocomposites

C. Yan[1], B. Bor[2], A. Plunkett[2], B. Domènech[2], G. A. Schneider[2], M.G.D. Geers[1], D. Giuntini[1]

[1]Eindhoven University of Technology
[2]Hamburg University of Technology

Introduction

Supercrystalline nanocomposites (SCNCs) are new materials made of inorganic nanoparticles surface-functionalized with organic ligands and arranged into periodic structures. They have drawn growing attention thanks to their novel superstructures and intriguing functional properties. However, their mechanical behavior is not yet fully explored, and even more poorly understood when it comes to their time-dependent behavior, e.g. creep. Here, creep behavior of ceramic-organic SCNCs is explored with nanoindentation, together with its recoverability and underlying mechanisms, where the interaction between organic ligands plays a key role.

Material
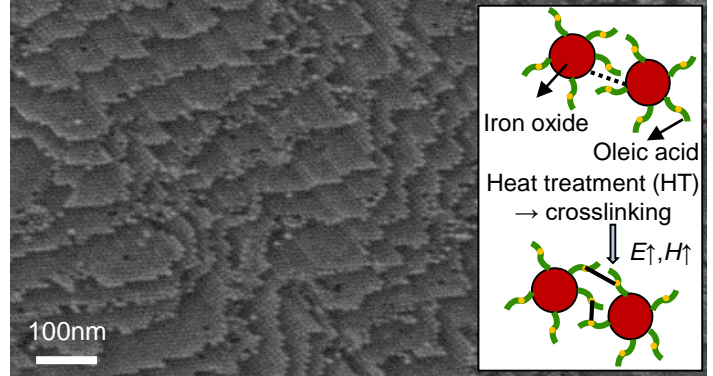
Figure 1: Nanostructure of SCNCs and the inset shows the shift of interaction between ligands induced by heat treatment.

Occurrence of creep and the recoverability
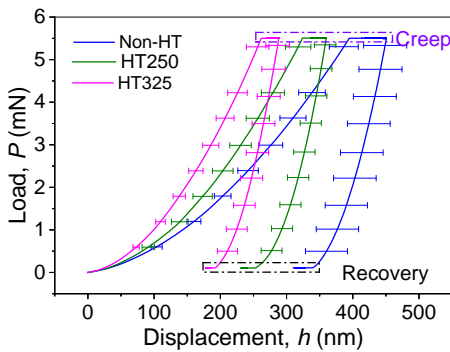
Figure 2: Load-displacement curves. HT250(325) refers to the sample is heat treated under 250(325) ℃.
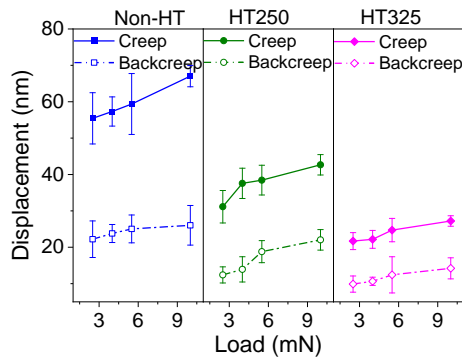
Figure 3: Recovery revealed by nanoindentation (left) and AFM (right).

Recovery during backcreep + Post-indentation recovery (AFM)
< Creep displacement → Viscoelasticity + Viscoplasticity

Creep mechanisms

Stress exponent: $n = \frac{\partial ln\dot{\varepsilon}}{\partial ln\sigma} \sim \frac{\partial ln\dot{\varepsilon}}{\partial lnH}$

Activation volume: $V = 3\sqrt{3}kT \cdot \frac{\partial ln\dot{\varepsilon}}{\partial H}$

$\dot{\varepsilon}$: strain rate;   σ: applied stress;
k: Boltzmann's constant;
T: absolute temperature; H: hardness;

	Stress exponent, n	Activation volume, V (nm^3)
Non-HT	15.80 ± 1.73	0.254 ± 0.016
HT250	19.10 ± 1.33	0.187 ± 0.021
HT325	21.48 ± 0.31	0.126 ± 0.015

❖ $n > 7$ → power-law breakdown → high stress by Berkovich tip;
❖ $V \sim 10^{-5} \boldsymbol{b}^3$ ($\boldsymbol{b}$: Burgers vector) → rearrangement of ligands;

Conclusions

➢ Co-presence of viscoelastic & viscoplastic deformation;
➢ Creep by power-law breakdown is detected.
➢ Extremely small activation volume is rationalized by the rearrangement of ligands.

References

1. A. Dreyer et al. Nat. Mater. 15 (2016) 522–528.
2. D. Giuntini et al. Sci. Adv. 7 (2021) abb6063.

Computational Analysis of Origami Structures for Vibration Isolation

Yuheng Yan, Alejandro M. Aragón

*Department of Precision and Microsystems Engineering,
TU Delft, The Netherlands*

Introduction

Origami structures show vivid mechanical properties while maintaining simple structures. In this work, the origami structures are investigated as acoustic/elastic metamaterials (A/E MMs). The effect of introducing folding is reflected by a origami-inspired corrugated beam structure, and Bragg/Mie scatterings are shown. In addition, the frequency region with no eigenmodes is shown as yet the other mechanism for vibration isolation.

Corrugated beam structure

The geometry of corrugated beam structure is shown in Figure 1, and the band structure as well as transmission spectrum corresponding to different folding angles are shown in Figure 2. The effects of folding on band structure are:

1. if no folding is assigned, wave modes are not coupled and there is no band gaps in the structure (Figure 1(a)),
2. when a slight folding is introduced, wave modes start to couple with each other, and there is "modal band gap" opening between shear and torsional modes (Figure 1(b)),

3. Bragg band gap could exist when folding angle of 50° is assigned (Figure 1(c)),
4. local resonance behavior kicks in when folding angle is 85°, and the largest band gap in Figure 1(d) is a mix of Bragg and local resonance.

Miura-ori structure

The existence of Bragg and local resonance band gaps has already been shown for Miura-ori structure used as A/E MMs[1]. However, the aforementioned mechanisms are for infinite structures. When the condition of infinite periodicity is broken, we have yet the third mechanism for vibration isolation: by the frequency region with no eigenmodes.

Figure 3 shows numerical computations of eigenfrequencies for varying crease stiffness, as well as experimental validation of this frequency region.

Conclusions

Introducing folding to origami-inspired structures could generate modal/complete band gaps, and the three mechanisms for vibration isolation are: Bragg scattering, local resonance and frequency region with no eigenmodes.
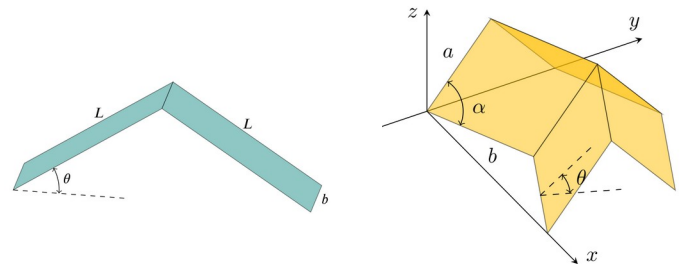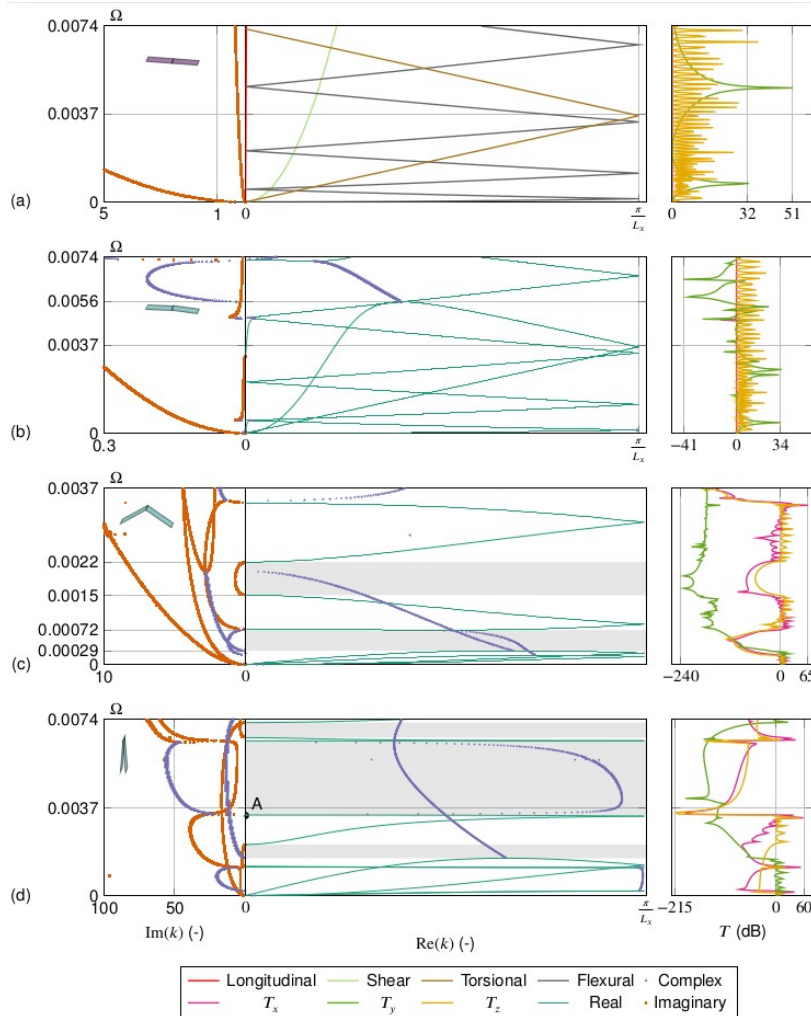
Figure 1: geometries of corrugated beam and Miura-ori unit cells.
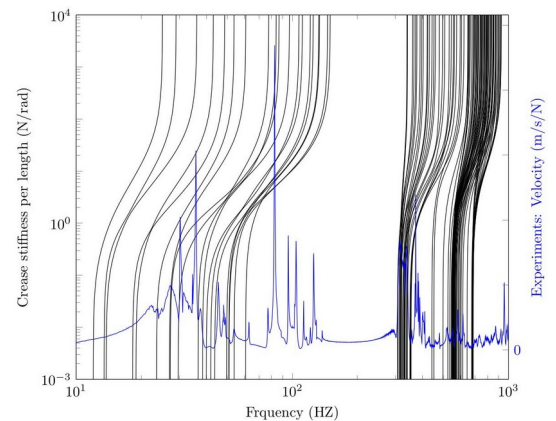
Figure 3: frequency region with no eigenmodes for Miura-ori.

References

[1]. Y. Yan, F. Alijani, A. Aragón. Origami Acoustic/elastic Metamaterials. Submitted for publication.

Figure 2: band structures of corrugated beam for different folding angles

Laser Scanning Strategy Effects on Phase Distribution in Ti–6Al–4V Multi-Laser Powder Bed Fusion Process

Y. Yang[1], F. van Keulen[1], C. Ayas[1]

[1]*Delft University of Technology*

Introduction

- In the emergence of next-generation Laser Powder Bed Fusion (LBPF) systems, there will be equipped with up to eight lasers to melt the metal powder at the same time.
- The multi-laser machines can be viewed as a unique platform to optimally control the temperature field in LPBF process to dictate desirable microstructures.
- The additively manufactured Ti-6Al-4V parts suffer from undesirable α' phase, which leads to a decrease in ductility.

Method

- **Thermal analysis:**

To study the distribution of α' phase and α in the Muti-Laser Powder Bed Fusion (M-LPBF) process, a **semi-analytical method** for fast thermal analysis is adopted (Fig.1), which utilises the superposition of analytical solutions for point heat sources making up a laser line, and complementary fields to enforce boundary conditions [1].
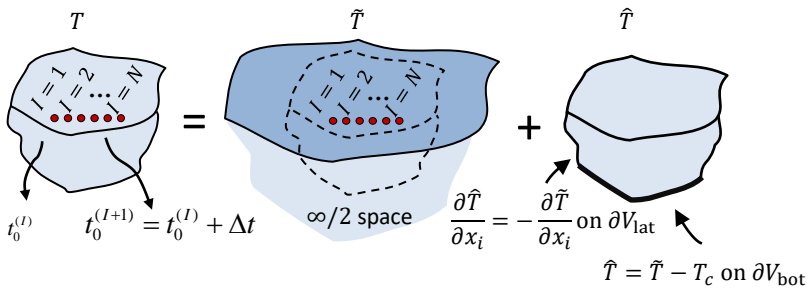
Figure 1: Semi-analytical method

- **Phase calculation:**

Based on the thermal history, a phase transformation framework shown in Fig.2 is introduced to simulate the microstructure evolution in Ti-6Al-4V during additive manufacturing process.

Figure 2: Phase transformation framework

Numerical Example

α phase	α′ phase	α phase	α′ phase
E_v = 41.3J/mm³		E_v = 51.7J/mm³	
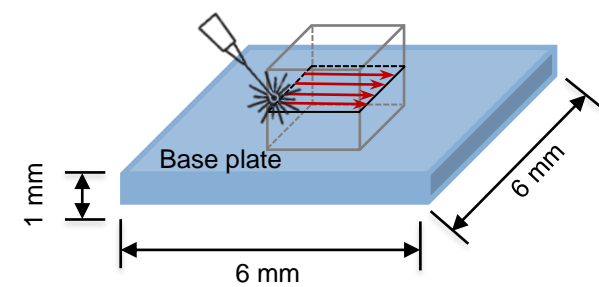
Figure 3 : Single laser and phase in **layer 30**

α phase	α′ phase	α phase	α′ phase
E_v = 41.3J/mm³		E_v = 51.7J/mm³	
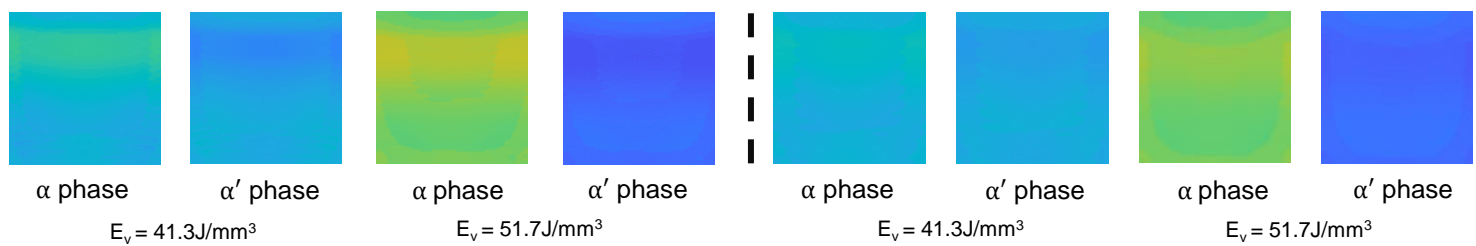
Figure 4 : Multi-laser and phase in **layer 30**

Conclusions

Increasing energy density (E_v) decreases the percentage of phase α', and scanning with multiple lasers simultaneously leads to a more uniform phase distribution.

References

[1] Yang, Y., et al. Additive Manufacturing 21 (2018): 284-297.

PhD progress

| 1 | 2 | 3 | 4 |

Toughening Bio-inspired Ceramics via the Tetragonal-to-Monoclinic Phase Transformation

Jian Zhang, Francesco Aiello, Diletta Giuntini, Mauro Salazar

Eindhoven University of Technology

Introduction

Ceramics are considered as promising materials for multiple functional applications, such as batteries, solar and fuel cells, and thermal engines. However, the inherent brittleness limits the use of ceramics for industrial implementations. Due to the intrinsic brick-and-mortar structure, nacre, consisting of 95 vol.% inorganic plates and 5 vol.% organic matrix, show the significant increase (three orders of magnitude higher) in toughness compared to monolithic aragonite [1]. The tetragonal-to-monoclinic phase transformation [2] that leads to the volume expansion and shear deformation can reduce the stress concentration in the vicinity of the crack tip. Since these two toughening mechanisms occur at different scales, a multiscale methodology is required to incorporate them into ceramics design, refer to Figure 1. This work focuses on introducing the tetragonal-to-monoclinic phase transformation into toughening ceramics at nanoscale.
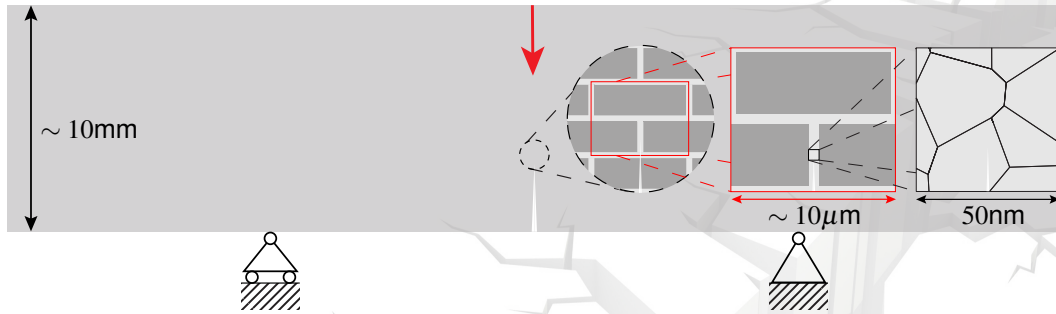
Figure 1. Illustration of the multiscale model including macroscale, microscale and nanoscale structures, where the homogenized, brick-and-mortar and polycrystalline structures are shown at three scales, respectively.

Formulations

The phase field method [3] that uses an order parameter to represent the material states is adopted to capture the phase transformation, crack propagation, and their interactions, which leads to the following formulations:

- Phase transformation

$$\frac{\partial \eta}{\partial t} - L\beta\nabla^2\eta = -L\left(\frac{\partial F_{ch}}{\partial \eta} + \frac{\delta F_{el}}{\delta \eta}\right) \quad (1)$$

η varies from 0 to 1, where 0 and 1 represents the tetragonal and completely monoclinic lattices, respectively; L the kinetic coefficient of phase transformation; β gradient energy coefficient; F_{ch} chemical free energy; F_{el} elastic strain energy.

- Crack propagation

$$\left(\frac{2l_0(1-k)\mathcal{H}}{G_c} + 1\right)\phi - l_0^2\nabla^2\phi = \frac{2l_0(1-k)\mathcal{H}}{G_c} \quad (2)$$

ϕ varies from 0 to 1, where 0 and 1 represents the intact and completely damaged states, respectively; l_0 a parameter that controls the transition region of cracks; k a small value for avoiding singularity; $\mathcal{H}$ a strain-history field; G_c critical energy release rate.

Single grain with phase transformation and fracture

Phase transformation field η with crack propagation
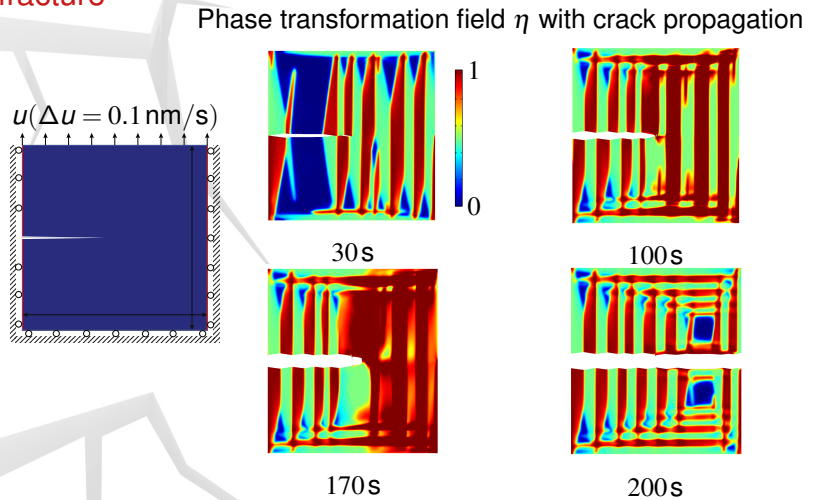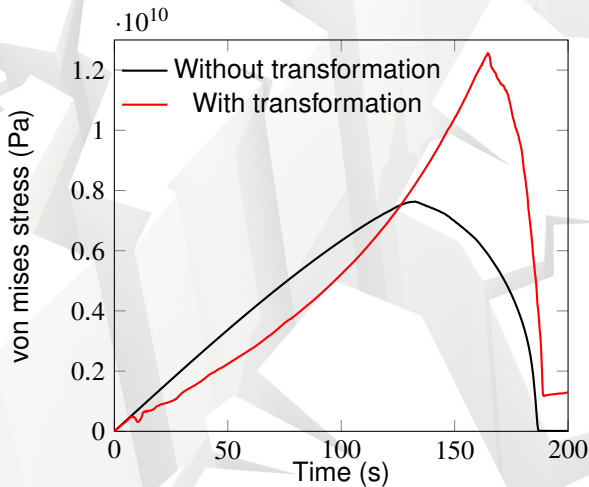

Figure 2. The toughening effect is introduced via considering phase transformaton during crack propagation

References

[1] Sun and Bharat, Rsc Advances (2012)

[2] Hannink *et al.*, Journal of the American Ceramic Society (2000)

[3] Mamivand *et al.*, Computational Materials Science (2013)

Atomistic Fracture in bcc Iron Revealed
by Active Training of Machine Learning Potential

L. Zhang[†], G. Csányi[‡], E. van der Giessen[†] and F. Maresca [†]

lei.zhang@rug.nl
[†] *University of Groningen*
[‡] *University of Cambridge*

Motivation

Fracture is a multiscale process that starts from atomic bond separation to engineering scale (Fig.1). Predictive atomistic model is needed. However, current classical interatomic potentials yield contradicting results (Fig.2)[1].
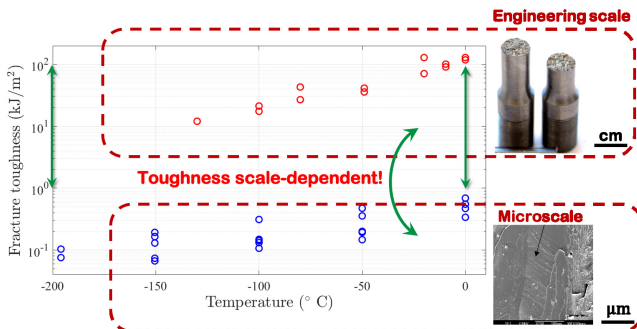

Figure 1: Fracture toughness of ferrite measured at different scale.
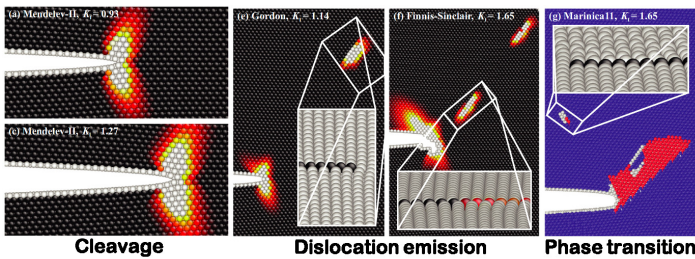
Figure 2: MD simulation of crack-tip using different potentials[1].

Methodology

Development of the machine learning potential

- Database: Density Functional Theory calculations[2]
- Active machine learning framework[3] (Fig.3)
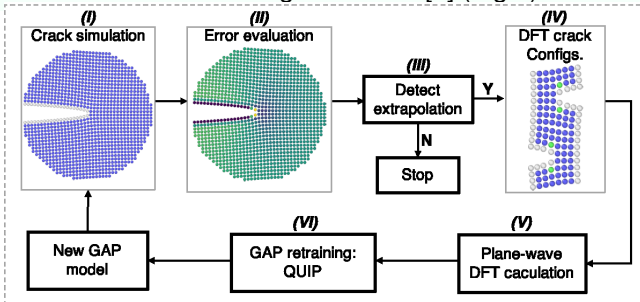
Figure 3: Workflow of the active learning algorithm within Gaussian approximation potential (GAP) framework.

Atomistic simulation

- Edge crack with fixed boundary layer (Fig.4a)
- K-controlled loading scheme (Fig.4b)[4]
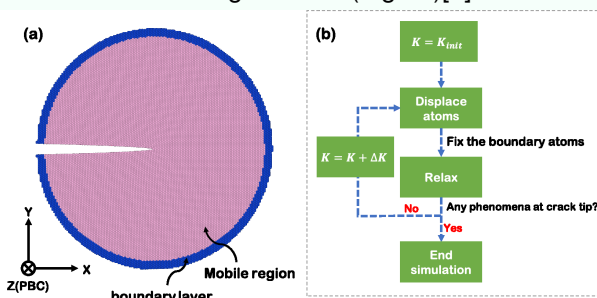
Figure 4: (a) K-test geometry. (b) Incremental loading procedure.

Results

Implementation of active learning

- Trained on crack systems in Fig. 5a and b
- Tested on crack systems in Fig. 5c and d
- Error converged to 8 meV/atom (in 4 iterations)
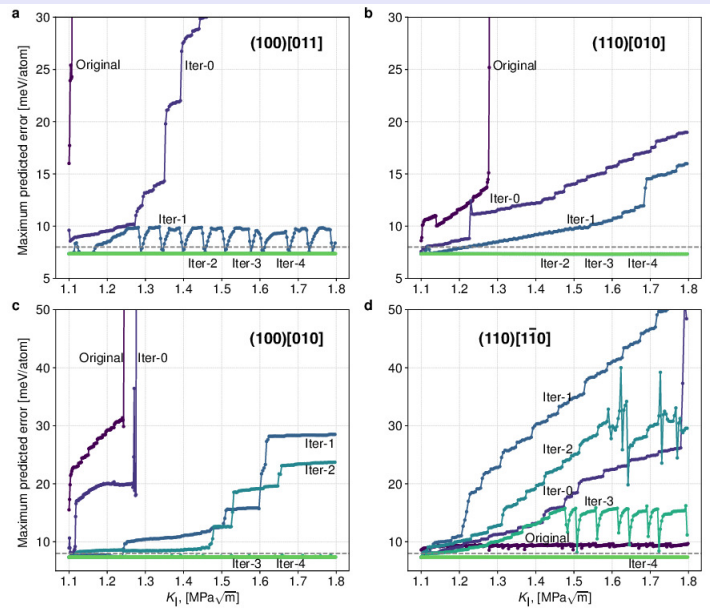
Figure 5: Maximum GAP predicted energy error per atom as functions of K_I for four crack systems[5].

Prediction of fracture mechanisms and K_{Ic}
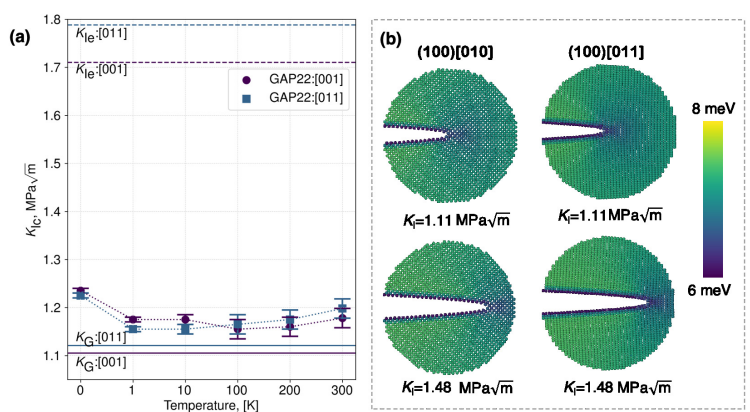
Figure 6: (a)Critical K_I predicted by GAP at different temperatures for (100) crack plane. (b) Atomic snapshots showing the fracture mechanism. Atoms are coloured according to GAP predicted error.

Discussion and Conclusion

- An active learning framework is provided
- Cleavage is the controlling mechanism at T=0K (Fig.6)
- Upscaling is needed for comparison with experiment (the topic of our current research)

References

[1] J. Moller and E. Bitzek, *Modelling Simul. Mater. Sci. Eng.*(2014).
[2] D. Dragoni *et al.*, *2018, Phys. Rev. Mater.* (2018).
[3] A. Bartók *et al.*, *Phys. Rev. Lett.* (2010).
[4] P. Andric, PhD THESIS, EPFL, 2019.
[5] L. Zhang *et al.*, *arXiv preprint arXiv:2208.0591*, (2022).

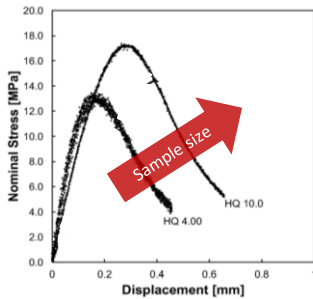# Size effect on the mechanical properties of 3D printing

X. Zhang[1], M. Lesueur[1]

[1]Delft University of Technology
Computational Mechanics Group, 3MD

Does size effect exist?

Fig. 1. Mechanical testing of different-size samples. Taken from Bell (2018)[1].

Additive manufacturing is undoubtedly a revolution in numerous disciplines including mechanical engineering. Yet fundamental aspects of mechanical characterization remain uncertain, such as size effect.
Bell (2018)[1] found out that:
➢ Larger sample size = larger strength
However, **same printing parameters** were used for every sample per bundle.

Taking into account printing parameters

➢ Fused Deposition Modelling parameters determine the internal structure (figure 2).
➢ There exists an internal length scale, correlated to the filament and airgap size.
➢ Airgaps are known to weaken porous material.
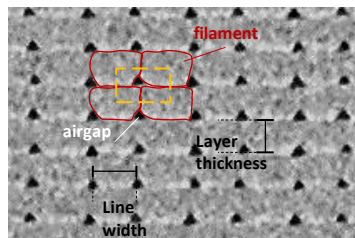
Fig. 2. μ-CT scan image of internal structure of 3D-printed material

Controlling internal length

Size effect has to be assessed when all internal lengths are properly scaled:
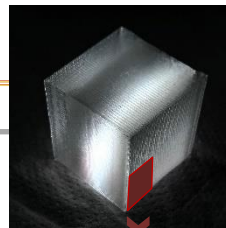➢ How to change filament size without changing internal structure?
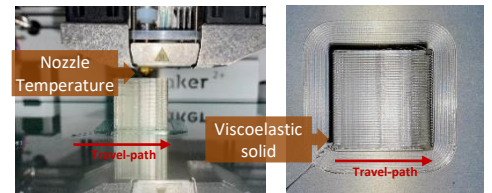
Fig. 3. Printing features related to temperature:

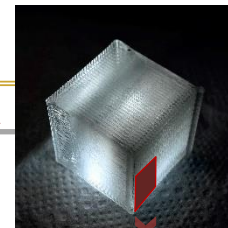Temperature determines each layer's cross-sectional shape via viscosity *[2]*.

➢ When modelling extruded filament as viscoelastic solid *[3]*, we find a critical temperature above which the extruded filament liquefies.
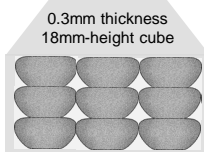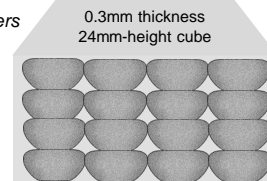
Experimental design
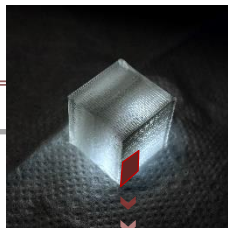
Flow rate τ

$$\tau \cdot A_{nozzle} = v_{print} \cdot A_{filament}$$

0.3mm thickness
18mm-height cube

Printing parameters
• Scale (x,y,z)
• Print speed
• Travel speed

Scale sample size

0.3mm thickness
24mm-height cube

Printing parameters
• Layer thickness
• Line width

Scale internal length

0.4mm thickness
24mm-height cube
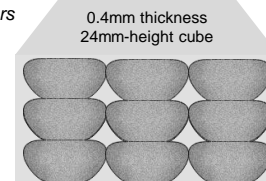
The thermal properties of filament is **neglectable.**

τ = for each cube

Results with rigorous scaling

Strength increases with increasing ratio of sample size to layer thickness:

➢ Bell (2018)[1] results are verified

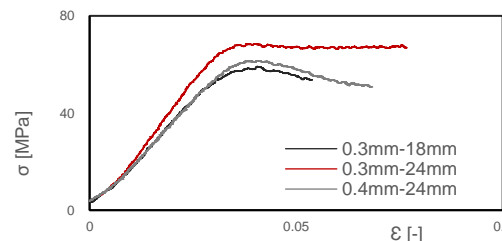Strength is equal for different sample size with rigorous scaling of internal structure.

Fig. 4. Strain-stress curves of samples under uniaxial compression

0.3mm-18mm (reference)
σ: 50.1MPa
E: 1950MPa

0.3mm-24mm
σ: 56.4MPa → **12.6% error**
E: 2317MPa → **18.8% error**

0.4mm-24mm
σ: 51.7MPa → **3.2% error**
E: 1887MPa → **3.2% error**

Discussion/future work

Size effects on mechanical properties of 3D printing **vanishes** when sample size is scaled down along with the filament size.

Using homogenization theory, we will upscale for the strength of 3D printed materials modelled as a periodic porous unit cell (composed of filament and airgap)
➢ Combined with this work, the objective is to find scaling laws between printing parameters and 3D-printed material strength
➢ Provide design guidelines for manufacturing

References

[1] Bell, D., & Siegmund, T. (2018). 3D-printed polymers exhibit a strength size effect. Additive Manufacturing, 21, 658-665.
[2] Lei, M., et al. (2022). Numerical Simulation and Experimental Study the Effects of Process Parameters on Filament Morphology and Mechanical Properties of FDM 3D Printed PLA/GNPs Nanocomposite. Polymers, 14(15), 3081.
[3] Duty, C., et al. (2018). What makes a material printable? A viscoelastic model for extrusion-based 3D printing of polymers. Journal of Manufacturing Processes, 35, 526-537.

TUDelft Delft University of Technology

PhD progress
| 1 | 2 | 3 | 4 |

DASML

Stevin Laboratory
Micro2Macro

Programmable Shape-morphing of Rose-shaped Mechanical Metamaterials

Z. Zhang, A. O. Krushynska

Meta Mechanics group, CMME, ENTEG, FSE, University of Groningen

1. Rose-shaped Mechanical Metamaterial

Introduction

Mechanical metamaterials can obtain shape morphing functionality by programming their microstructrues (Fig. 1). For instance, auxetic and conventional mechanical materials can be combined to program the shape morphing behavior under loading. We proposed so-called rose-shaped mechanical metamaterial that can be used in the programmable design of shape morphing.
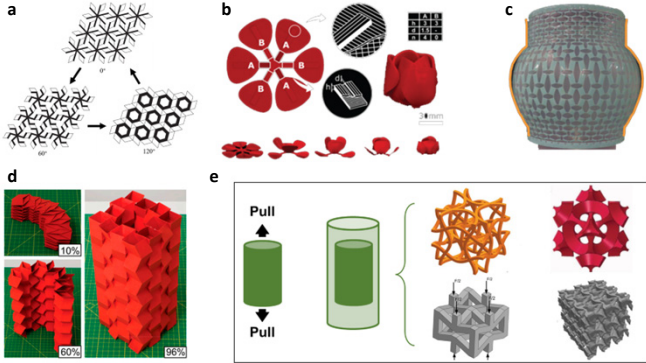
Figure 1: Mechanical metamaterials with programmable potential [1]: **a** dilational, **b** shape-memory, **c** kirigami, **d** origami, and **e** auxetic materials.

Geometry Design

Rose-shaped mechanical metamaterial is formed by four-leaved rose curves joined by four straight connecting ligaments (Fig. 2a). The shape of a rose curve is governed by an analytical expression with parameters a and n. As shape control parameter n increases, the rose curve changes from a star-like shape ($n=1.3$) to a close-to-circle shape ($n=30$).

Mechanical Properties

✓ Large range of Poisson's ratio governed by a single parameter n
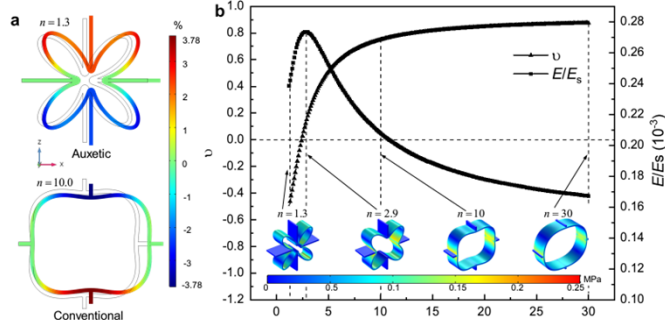✓ Smooth shape without sharp edges to reduce stress concentration

Figure 2: The basic mechanical properties of rose-shaped unit cells. **a** The displacement field in z direction under tensile loading, **b** the geometries and corresponding mechanical properties as n increases. [2]

2. Programmable Shape Morphing

Design strategies

Auxetic and conventional rose-shaped unit cells can be combined to program the shape morphing behavior of flat structures under tensile loading by designing their arrangement.
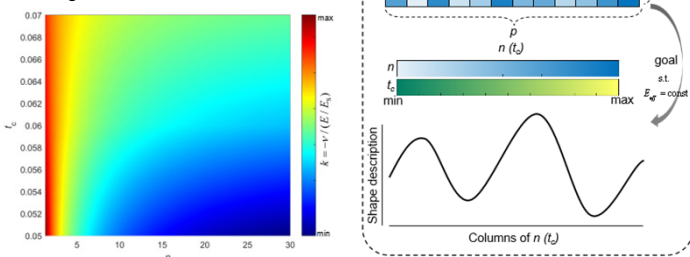

Figure 3: Programmable design space and general strategy schematics. [2,3]
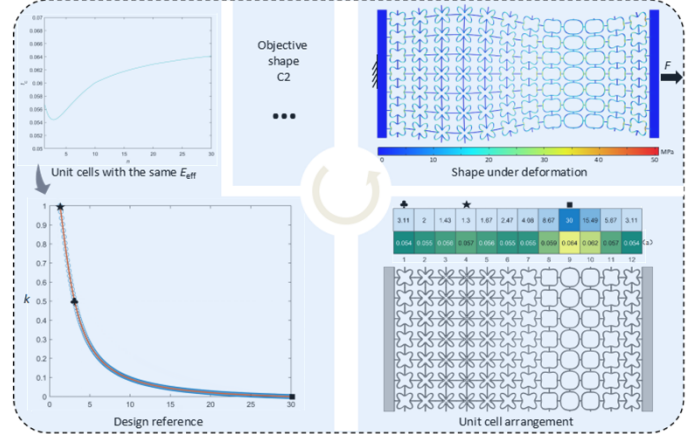
Design Example

Figure 4: An example for the programmable design procedure of flat structures. [2]
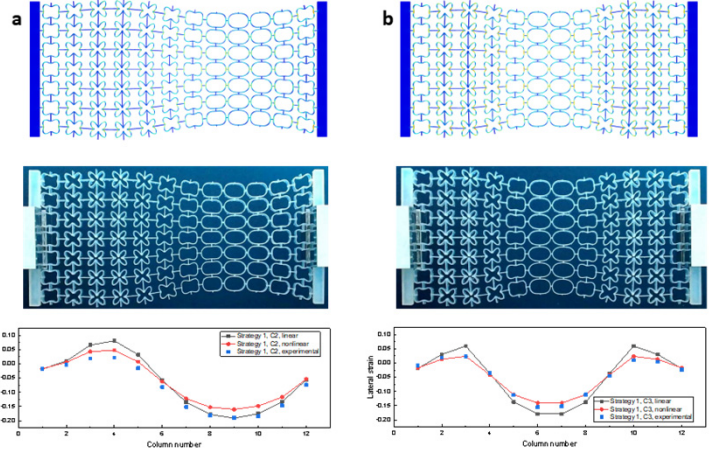
Experimental Validation

Figure 5: Simulation and experimental results of designed structures. [2]

3. Conclusion and Outlook

We have proposed a rose-shaped mechanical metamaterial with tailorable and large-range Poisson's ratio, and conducted the programmable design of shape morphing behavior driven by tensile loading. We also extended the design to 3D unit cells (Fig. 6). The metamaterial has great potential in practical applications like medical stents, scaffolds, and soft robotic grippers.
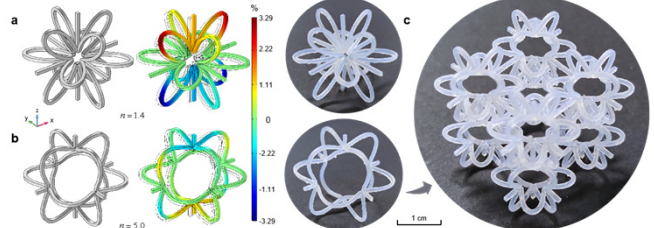

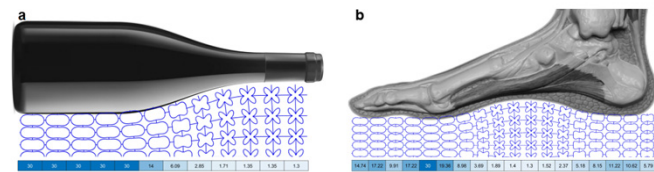Figure 6: 3D rose unit cells with tailorable Poisson's ratio. [2]

Figure 7: Possible application scenarios of programmed flat structures. [2]

Reference

[1] A. Zadpoor. Mater. Horiz. 3(5):371–81, 2016.
[2] Z. Zhang, et al., APL Materials, 2022
[3] Z. Zhang, et al., submitted.

PhD progress
1 2 3 4

university of groningen

CmME

Multi-material topology optimization with crisp material interfaces

J.M. van der Zwet, C. Ayas, M. Langelaar

Delft University of Technology

1. Introduction

Incorporating multiple materials in a design can greatly improve its performance as combinations of different material properties allow for more design freedom, where topology optimization can be an effective tool to generate these designs. In topology optimization each finite element is assigned a virtual density value, which serve as optimization variables. For multi-material topology optimization discrete material optimization (DMO) [1] is very promising, but the conventional filtering method causes undesirable behaviour at the material interface.

3. Interface detection

The proposed filter achieves crisp material interfaces, which enables both detection and penalization at these interfaces. Figure 2 shows the blind spot of conventional interface detection and how the proposed method fixes it.

Figure 2: (left) input test case for detecting interfaces; (middle) Sobel filter interface detection; (right) Proposed interface detection.

2. Filter for crisp material interfaces

The proposed filter works by first defining a total material phase and performing the filter operation on it, after which the filtered total material field is separated again, this approach is compared to the conventional approach in Figure 1.
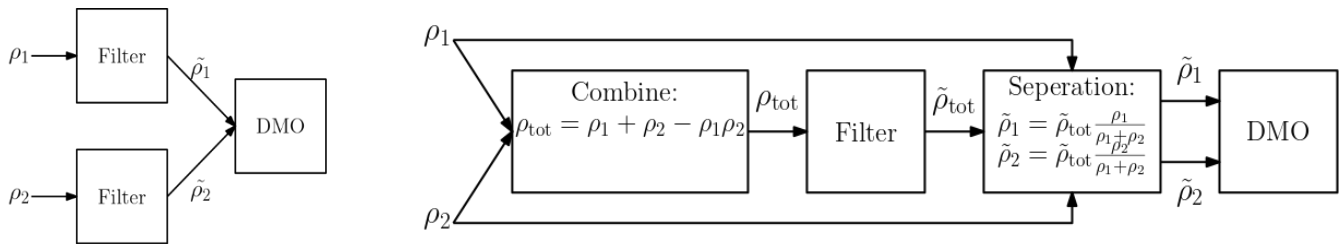

Figure 1: schematic representation of the conventional and proposed filtering approach.

4. Results

The proposed filter can be applied to any multi-material topology optimization case. Figure 3 shows a cantilever optimized for maximum stiffness with the different filtering approaches.
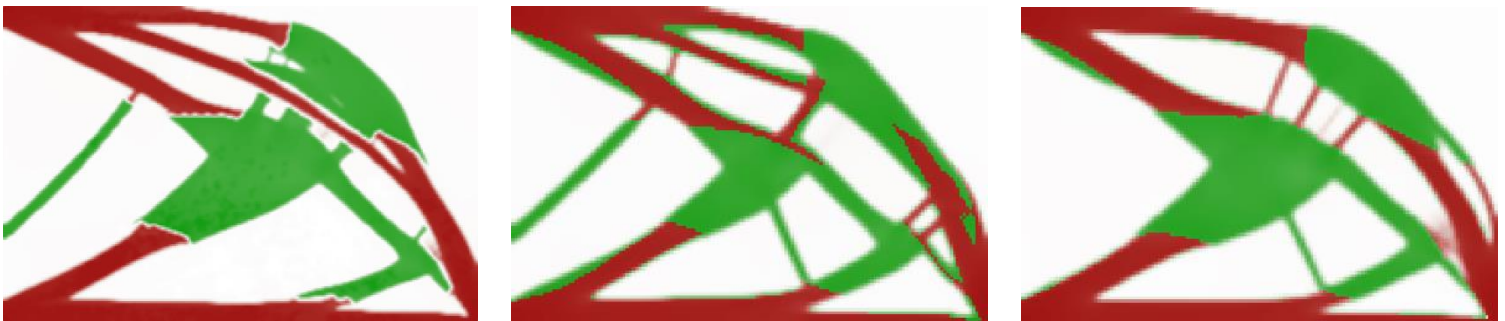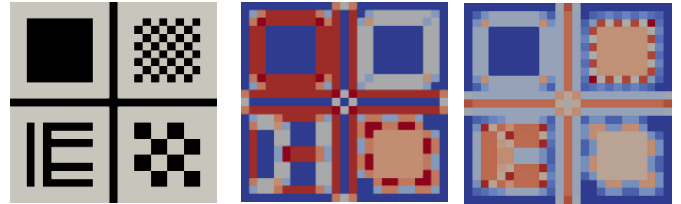

Figure 3: results for a cantilever problem, where red denotes stiff material and green compliant material. Using the conventional filter and the proposed filter with and without interface penalization

5. Conclusion

- The proposed filter achieves crisp material interfaces
- Interface detection can be improved using a new detection scheme
- Penalization on detected interfaces can be used to limit undesirable trapped material

References

[1] E. Lund and J. Stegmann, "On structural optimization of composite shell structures using a discrete constitutive parametrization", *Wind Energy*, 2005

PhD progress

| 1 | 2 | 3 | 4 |

Graduate School on Engineering Mechanics
c/o Eindhoven University of Technology

PO Box 513, building Gemini-Zuid 4.133
5600 MB Eindhoven NL
Tel.: +31 40 2478306
Fax: +31 40 2447355
E-mail: Engineering.Mechanics@tue.nl
http://www.em.tue.nl